

อิทธิพลของความร้อนต่อมลทินแร่เส้นไหมในแซปไฟร์จากจังหวัดจันทบุรี



นายทัศนรา ศรีปุ่นจัน

จุฬาลงกรณ์มหาวิทยาลัย
CHULALONGKORN UNIVERSITY

วิทยานิพนธ์นี้เป็นส่วนหนึ่งของการศึกษาตามหลักสูตรปริญญาวิทยาศาสตรมหาบัณฑิต

สาขาวิชาธรณีวิทยา ภาควิชาธรณีวิทยา

คณะวิทยาศาสตร์ จุฬาลงกรณ์มหาวิทยาลัย

บทคัดย่อและแฟ้มข้อมูลฉบับเต็มของวิทยานิพนธ์ตั้งแต่ปีการศึกษา 2554 ที่ให้บริการในคลังปัญญาจุฬาฯ (CUIR)

ปีการศึกษา 2556

เป็นแฟ้มข้อมูลของนิสิตที่ส่งมาขึ้นทะเบียนวิทยานิพนธ์ที่ส่งมาทางบัณฑิตวิทยาลัย

The abstract and full text of theses from the academic year 2011 in Chulalongkorn University Intellectual Repository (CUIR) are the thesis authors' files submitted through the University Graduate School.

INFLUENCE OF HEAT TO SILKY-MINERAL INCLUSION IN SAPPHIRE FROM CHANGWAT
CHANTHABURI

Mr. Tasnara Sripoonjan

The logo of Chulalongkorn University, featuring a central emblem with a sunburst and a tiered structure, set against a light background.

จุฬาลงกรณ์มหาวิทยาลัย
CHULALONGKORN UNIVERSITY

A Thesis Submitted in Partial Fulfillment of the Requirements
for the Degree of Master of Science Program in Geology

Department of Geology

Faculty of Science

Chulalongkorn University

Academic Year 2013

Copyright of Chulalongkorn University

Thesis Title	INFLUENCE OF HEAT TO SILKY-MINERAL INCLUSION IN SAPPHIRE FROM CHANGWAT CHANTHABURI
By	Mr. Tasnara Sripoonjan
Field of Study	Geology
Thesis Advisor	Associate Professor Chakkaphan Sutthirat, Ph.D.
Thesis Co-Advisor	Bhuwadol Wanthanachaisaeng, Dr.rer.nat.

Accepted by the Faculty of Science, Chulalongkorn University in Partial
Fulfillment of the Requirements for the Master's Degree

.....Dean of the Faculty of Science
(Professor Supot Hannongbua, Dr.rer.nat.)

THESIS COMMITTEE

.....Chairman
(Associate Professor Montri Choowong, Ph.D.)

.....Thesis Advisor
(Associate Professor Chakkaphan Sutthirat, Ph.D.)

.....Thesis Co-Advisor
(Bhuwadol Wanthanachaisaeng, Dr.rer.nat.)

.....Examiner
(Associate Professor Visut Pisutha-Arnon, Ph.D.)

.....External Examiner
(Somruedee Satitkune, Dr.rer.nat.)

ทัศนรา ศรีปุ่นจัน : อิทธิพลของความร้อนต่อมลทินแร่เส้นไหมในแซปไฟร์จากจังหวัดจันทบุรี. (INFLUENCE OF HEAT TO SILKY-MINERAL INCLUSION IN SAPPHIRE FROM CHANGWAT CHANTHABURI) อ.ที่ปรึกษาวิทยานิพนธ์หลัก: รศ. ดร. จักรพันธ์ สุทธิรัตน์, อ.ที่ปรึกษาวิทยานิพนธ์ร่วม: ดร. ภูวดล วรรณชะชัยแสง, 159 หน้า.

พลอยแซปไฟร์ที่บดแสงสีน้ำตาลเป็นพลอยที่มีความต้องการในตลาดที่ต่ำ พลอยสีที่บดเหล่านี้มีอิทธิพลมาจากมลทินแร่เส้นไหมจำนวนมากในเนื้อพลอย ซึ่งแร่เส้นไหมเหล่านี้สามารถสร้างปรากฏการณ์พิเศษตารในพลอยแซปไฟร์สาแทรก การศึกษานี้เลือกใช้ตัวอย่างแซปไฟร์ที่มีมลทินแร่เส้นไหมมากจากแหล่งบางกะจะ จังหวัดจันทบุรี ตัวอย่างถูกแบ่งออกเป็น 3 กลุ่ม ได้แก่ กลุ่มที่มีมลทินแร่เส้นไหมน้อย กลุ่มที่มีมลทินแร่เส้นไหมปานกลางและกลุ่มที่มีมลทินแร่เส้นไหมมาก จากการศึกษาแซปไฟร์ที่มีมลทินแร่เส้นไหมมาก ด้วยกล้องจุลทรรศน์อัญมณี พบมลทินแร่เส้นไหมหนาแน่นมากในตัวอย่างจากกลุ่มที่มีมลทินแร่เส้นไหมปานกลางและกลุ่มที่มีมลทินแร่เส้นไหมมาก การศึกษาชนิดของมลทินแร่เส้นไหมด้วยเทคนิครามานสเปกโทรสโกปี และองค์ประกอบทางเคมีด้วยเทคนิคอีพีเอ็มเอ ทั้งสองเทคนิคบ่งชี้ว่าแร่เส้นไหมดังกล่าวเป็นแร่ฮีมาไทต์ ภายหลังจากนำตัวอย่างไปเผาปรับปรุงคุณภาพที่อุณหภูมิ 1650 องศาเซลเซียสเป็นเวลา 3 ชั่วโมง พบว่าตัวอย่างมีความใสสะอาดขึ้นอย่างเห็นได้ชัด ลักษณะเนื้อในบริเวณที่มีเส้นไหมจำนวนมาก จากสีเทาน้ำตาลเปลี่ยนเป็นสีน้ำเงินชัดเจน พบว่าแถบการดูดกลืนแสงในช่วงเหนือม่วง-มองเห็น-ใต้แดงใกล้ที่ตำแหน่งประมาณ 900 นาโนเมตรซึ่งเกี่ยวข้องกับการเกิดสีน้ำเงินอันเนื่องมาจาก Fe^{2+}/Fe^{3+} IVCT แสดงการดูดกลืนอย่างรุนแรง บ่งชี้การเปลี่ยนแปลงของสีหลังจากการเผา

จุฬาลงกรณ์มหาวิทยาลัย
CHULALONGKORN UNIVERSITY

ภาควิชา ธรณีวิทยา

สาขาวิชา ธรณีวิทยา

ปีการศึกษา 2556

ลายมือชื่อนิสิต

ลายมือชื่อ อ.ที่ปรึกษาวิทยานิพนธ์หลัก

ลายมือชื่อ อ.ที่ปรึกษาวิทยานิพนธ์ร่วม

5472182123 : MAJOR GEOLOGY

KEYWORDS: HEAT TREATMENT / CORUNDUM / SAPPHIRE / SILKY INCLUSIONS /
CHANTHABURI / BANG KACHA

TASNARA SRIPOONJAN: INFLUENCE OF HEAT TO SILKY-MINERAL INCLUSION
IN SAPPHIRE FROM CHANGWAT CHANTHABURI. ADVISOR: ASSOC. PROF.
CHAKKAPHAN SUTTHIRAT, Ph.D., CO-ADVISOR: BHUWADOL
WANTHANACHAISAEANG, Dr.rer.nat., 159 pp.

Opaque sapphires with brownish color have low demand in the gems market. These opaque sapphire contains by abundant silky inclusions. These inclusions may produce special phenomenon of asterism in star sapphire. Sapphires with silky inclusion from Bang Kacha area, Changwat Chanthaburi were sampled for this study. Samples were divided into three groups consisting of minor silky inclusions; moderate silky inclusions and abundant silky inclusions. Large amount of silky inclusions features can be observed in moderate silky inclusions and abundant silky inclusions groups under gemological microscope. These inclusions were identified by Raman microscope and were also analyzed chemically using EPMA. The results from both techniques indicate that the mineral inclusions are hematite. Transparency of the samples were improved after heat treatment at 1650 °C for 3 hours. Zones of silky inclusions with grey-brown color were turned to blue after heating. The UV-Vis-NIR spectrum of heated samples showed strong absorption at about 900 nm due to Fe^{2+}/Fe^{3+} IVCT which conclusively indicated main color-causing of blue.

จุฬาลงกรณ์มหาวิทยาลัย
CHULALONGKORN UNIVERSITY

Department: Geology

Field of Study: Geology

Academic Year: 2013

Student's Signature

Advisor's Signature

Co-Advisor's Signature

ACKNOWLEDGEMENTS

First of all, the author would like to express his sincere gratitude and deepest appreciation to my thesis advisor, Associate Professor Dr. Chakkaphan Sutthirat and Dr. Bhuwadol Wanthanachaisaeng for their invaluable suggestion, supervision, forbearance and encouragement throughout the completion of this thesis. This thesis would never be successfully completed without the excellent advice and pioneering spirit from them. Thanks are also extended to Associate Professor Dr. Montri Choowong, Associate Professor Dr. Visut Pisutha-Arnond and Dr. Somruedee Satitkune for comments during thesis examination.

The author sincerely appreciates the Department of Geology, Faculty of Science, Chulalongkorn University for providing sample preparation, electric furnace and Electron Probe Micro Analy (EPMA). The Gem and Jewelry Institute of Thailand (GIT) under the director ship of Mrs. Wilawan Atichat provided basic equipments and advanced instruments, i.e., Gemological Microscope, Raman Microscope Spectrometer, Fourier Transform Infrared Spectrometer (FTIR), UV-Vis-NIR Spectrophotometer and Laser Ablation Inductively Coupled Plasma-Mass Spectrometry (LA-ICP-MS). The author is very grateful to staffs of the GIT-GTL e.g., Mr. Thanong Leelawatanasuk, Miss Namrawee Susawee and Miss Sasipim Pumpeng for their assistances. Furthermore, I would like to thank Miss Sopit Poompuang who assisted in the EPMA analysis. Some financial support for this research has been provided by GIT research projects.

Special thanks must go to my wonderful beloved family for their perpetual encouragement, cheerful moral and financial support. I am profoundly grateful to Miss Yenruedee Lhongsomboon for her kind assistance, social support, cordiality, attention and encouragement.

Finally, Special thanks are also delivered to friends and colleagues at both Chulalongkorn University and Burapha University that have everlasting friendship and many people who are not named here for various kinds of help.

CONTENTS

	Page
THAI ABSTRACT	iv
ENGLISH ABSTRACT	v
ACKNOWLEDGEMENTS	vi
CONTENTS	vii
LIST OF TABLES	ix
LIST OF FIGURES	x
CHAPTER I	1
INTRODUCTION.....	1
1.1 General Statement	1
1.2 Objectives.....	2
1.3 Scope of work.....	2
1.4 Methodology.....	2
CHAPTER II.....	15
LITERATURE REVIEWS.....	15
2.1 Corundum.....	15
2.2 Causes of Color	16
2.3 Heat Treatment.....	20
2.4 Bang Kacha Corundum Deposits in Chanthaburi.....	22
2.5 Gem Varieties in Bang Kacha Deposits.....	26
CHAPTER III.....	28
PHYSICAL AND GEMOLOGICAL PROPERTIES	28
3.1 Introduction.....	28
3.2 Physical Properties.....	31
3.3 Internal Characteristics.....	32
3.4 UV-Vis-NIR Spectra	38
3.5 Fourier Transform Infrared Spectra	42
CHAPTER IV	45

	Page
HEATING EXPERIMENT	45
4.1 Heating Cycle	45
4.2 Color and Clarity	46
4.3 Alterations of Inclusions	51
4.4 UV-Vis-NIR Spectra	59
4.5 Fourier Transform Infrared Spectra	64
CHAPTER V	68
MINERAL CHEMISTRY OF SILKY INCLUSIONS AND EFFECT TO COLOR OF HOST SAPPHIRE	68
5.1 Mineral Chemistry	68
5.2 Dissolution by Heating	70
5.3 Trace Element and Color Causing	73
CHAPTER VI	82
DISCUSSION AND CONCLUSIONS	82
6.1 Silky Inclusions Characterization	83
6.2 Reaction between Silky Inclusions and Sapphire Host	86
6.3 Conclusions	91
6.4 Suggestions for further study	92
REFERENCES	93
APPENDICES	97
VITA.....	159

LIST OF TABLES

	Page
3.1 Showing summarized physical properties of sapphire from Bang Kacha deposit, Changwat Chanthaburi.....	32
5.1 Representative EPMA analyses of silky inclusions in sapphire and hematite from alluvial deposits in Bang Kacha Gem field, Chanthaburi.....	70
5.2 EPMA profile analysis (spots as shown in Figure 5.2) revealing changes of FeO _{total} and TiO ₂ (wt%) along a silky inclusion in sapphire sample (Sample C6) after heating experiments.....	72
5.3 Trace element contents of representative analyses of Bang Kacha sapphire samples obtained by LA-ICP-MS reported as ppm unit.....	74
5.4 Recalculated atom mole ppm (amp) of trace elements in representative Bang Kacha sapphire samples.....	75
5.5 Atomic proportions (atom mole ppm, amp) based on 60 oxygen atom along different color zones.....	79

LIST OF FIGURES

	Page
1.1 Basic gem equipments; including 1. Refractometer, 2. Ultraviolet fluorescence, 3. Dichroscope, 4. Hydrostatic balance, and 6. Gemological microscope.....	4
1.2 Rayleigh and Raman bands of Stokes and anti-Stokes line of some matter excited with the Argon ion (514 nm).....	5
1.3 Renishaw Raman inVia microscope based at the GIT.....	6
1.4 JEOL Electron Probe Micro-Analyzer (EPMA) model JXA 8100 based at Department of Geology, Chulalongkorn University.....	7
1.5 PerkinElmer UV-Vis-NIR Spectrophotometer (Model LAMBDA 950) at the GIT	9
1.6 Thermo Scientific Fourier Transform Infrared (FTIR) Spectrometer (Model Nicolet 6700) at the GIT.....	10
1.7 Linn electric furnace (model HT1800 Plus VAC Bottom Loader) base at the Department of Geology, Faculty of Science, Chulalongkorn University.....	11
1.8 Laser Ablation Inductively-Coupled-Plasma Mass Spectrometry (LA-ICP-MS)based at The Gem and Jewelry Institute of Thailand.....	13
1.9 Flowchart showing methodology of this study.....	14
2.1 Figure 2.1 Three different views of the corundum structure. The top illustration shows structure looking down the c axis whereas below view is perpendicular to the c axis. The right diagram is perspective view (after Nassau, 1983).....	16
2.2 (a): Two adjacent octahedral sites in corundum structure, containing Fe ²⁺ and Ti ⁴⁺ in blue sapphire (b): Energy transitions from the ground state to an excited state in blue sapphire, so-called intervalence charge transfer (IVCT) (Nassau, 2001).....	18
2.3 The dichroic o-ray and e-ray absorption spectra of blue sapphire. (1) from Fe ²⁺ /Ti ⁴⁺ charge transfer, and band (2) from Fe ²⁺ /Fe ³⁺ charge transfer (Burns, 1993).....	18

	Page
2.4 Coloration of natural gem corundum (Bunnag, 2008).....	20
2.5 Geological map of the western part of Chanthaburi showing location of sapphire deposits (modified after Vichit, 1992).....	23
2.6 Traditional pit mining.....	25
2.7 Open cast mining.....	25
2.8 Varieties of sapphires from Bang Kacha deposit, Changwat Chanthaburi.....	26
2.9 The large quantities of Star sapphire from Bang Kacha deposit, Changwat Chanthaburi.....	27
3.1 Illustration of crystal habits in some sapphire samples from Changwat Chanthaburi.....	28
3.2 Sapphires with minor silky inclusions before heating experiment (A).....	29
3.3 Sapphire with moderate silky inclusions before heating experiment (B).....	30
3.4 Sapphire with abundant silky inclusions before heating experiment (C).....	31
3.5 Abundant silky inclusions orienting along the growth structure and basal pinacoid perpendicular to the c-axis (sample C7).....	34
3.6 Silky inclusions in sample A5 oriented in three directions along crystallographic direction.....	34
3.7 Silky inclusions in sample B8 in sapphire with moderate silky inclusions group show three directions orientation along crystallographic direction.....	35
3.8 Photomicrograph with high magnification (using combination of reflected and transmitted lights) showing irregular lamellae feature of silky inclusions orientated along crystallographic directions in sample C9; indication of subsolidus exsolution of the sapphire host.....	35
3.9 Raman spectrum of a represent silky inclusions of sample in sapphire with abundant silky inclusions group compared with hematite, magnetite and black spinel patterns collected from alluvial deposits around the Bang Kacha deposit.....	36
3.10 Minute particles or white dusts in sample C6.....	37
3.11 Negative crystals in sample B4.....	37
3.12 UV-Vis-NIR spectra of unheated sapphire with minor silky inclusions (A4).....	39

	Page
3.13 UV-Vis-NIR spectra of unheated sapphire with minor silky inclusions (A7).....	39
3.14 UV-Vis-NIR spectra of unheated sapphire with moderate silky inclusions (B1)	40
3.15 UV-Vis-NIR spectra of unheated sapphire with moderate silky inclusions (B7)	40
3.16 UV-Vis-NIR spectra of unheated sapphire with abundant silky inclusions (C4)	41
3.17 UV-Vis-NIR spectra of unheated sapphire with abundant silky inclusions (C5)	41
3.18 FTIR spectra of unheated sapphires with minor silky inclusions (Group A)....	43
3.19 FTIR spectra of unheated sapphires with moderate silky inclusions (Group B)	43
3.20 FTIR spectra of unheated sapphires with moderate silky inclusions (Group B)	44
3.21 FTIR spectra of unheated sapphires with abundant silky inclusions (Group C)	44
4.1 Color and clarity appearances of sapphires with minor silky inclusions (Group A) before heating (left) and after heating at 1650 °C (right).....	47
4.2 Color and clarity appearances of sapphires with moderate silky inclusions (Group B) before heating (left) and after heating at 1650 °C (right).....	48
4.3 Color and clarity appearances of more sapphire samples with moderate silky inclusions (Group B) before heating (left) and after heating at 1650 °C (right).....	49
4.4 Color and clarity appearances of sapphires with abundant silky inclusion (Group C) before heating (left) and after heating at 1650 °C (right).....	50
4.5 Comparison of sapphire sample between before heat treatment (left) and after heat treatment at 1650 °C (right) which silky inclusions appear to have dissolved into sapphire host lead to development of blue color and clarity (Sample B7).....	52
4.6 Silky inclusions were altered from brown to blue after heating at 1650 °C. These inclusions partly disappeared and produced intense blue color concentrations after heating (Sample B3).....	53

	Page
4.7 After heating at 1650 °C, silky inclusions were partly dissolved and altered from brown to blue. Intense blue color can be observed around silky zone (Sample B4).....	54
4.8 Silky inclusions before and after heating at 1650 °C, they were partly dissolved and altered from brown to blue (Sample B16).....	55
4.9 Silky inclusions before and after heating at 1650 °C, they were dissolved and altered from brown to blue (Sample C6).....	56
4.10 Silky inclusions with 60°/120° intersecting angles in sapphire sample with minor silky inclusion were partially dissolved to dot-like pattern after heating at 1650 °C (A10).....	57
4.11 A large hematite mineral inclusion which identified by Raman spectroscopy was partially melted and then became obviously residue in cracks of host sapphire. Its luster was lost and turned to blackish appearance (C4).....	58
4.12 The subsurface fingerprints were appeared and developed expansively after heating at temperature 1650 °C in representative samples such as in B1.....	58
4.13 A) Typical UV-Vis-NIR absorption spectra (o-ray) of sapphires in minor silky inclusions (A4) before and after heating at 1650 °C. B) The remaining spectrum after subtraction of heated stone's spectrum from original spectrum.....	60
4.14 A) Typical UV-Vis-NIR absorption spectra (o-ray) of sapphires in moderate silky inclusions (B1) before and after heating at 1650 °C. B) The remaining spectrum after subtraction of heated stone's spectrum from original spectrum.....	61
4.15 A) Typical UV-Vis-NIR absorption spectra (o-ray) of sapphires in abundant silky inclusions (C4) before and after heating at 1650 °C. B) The remaining spectrum after subtraction of heated stone's spectrum from original spectrum.....	62
4.16 A) Representative of sample in group B (B6) were lost blue shade after heating under ambient air due to reduction of charge transfer process with Fe ²⁺ -Ti ⁴⁺ pairs. B) The remaining spectrum after subtraction of heated stone's spectrum from original spectrum.....	63
4.17 FTIR spectra of sapphire with minor silky inclusions (A6) before and after heating at 1650 °C under ambient air.....	66

	Page
4.19 FTIR spectra of sapphire with moderate silky inclusions (B16) before and after heating at 1650 °C under ambient air.....	66
4.18 FTIR spectra of sapphire with moderate silky inclusions (B3) before and after heating at 1650 °C under ambient air.....	67
4.20 FTIR spectra of sapphire with abundant silky inclusions (C6) before and after heating at 1650 °C under ambient air.....	67
5.1 Back Scatter Electron Image (BSI) showing bright tiny silky inclusions with approximately length of $\leq 10 \mu\text{m}$ in sapphire from Bang Kacha gem field, Chanthaburi.....	69
5.2 Secondary Electron Image (SEI) showing multi-analytical spots on the profiles (elongation and perpendicular) on a tiny silky inclusion in sapphire sample (C6) of abundant silky inclusions group (Group C). Left image was taken before heating and right image show altered feature of the same silky inclusion after heating.....	71
5.3 Profiles of FeO and TiO ₂ comparing before and after heating (wt%) in sample C6.....	72
5.4 Histogram showing averages and standard deviation (ppm) of typical trace elements analyzed by LA-ICP-MS.....	76
5.5 Histogram showing averages and standard deviation (amp) of typical trace elements recalculated based on 60 oxygen atoms.....	76
5.6 Analytical spots on dark blue zones after heating at 1650 °C in samples C9 (left) and sample B5 (right).....	77
5.7 Analytical spots 1 and 2 on light blue zone and spot 3 on greenish blue zone in sample B3 (left). Analytical spots 1 and 3 on light blue zone and spot 2 on greenish blue zones in sample B12 (right). All color zones appeared after heating at 1650 °C.....	77
5.8 Analytical spot 1 on greenish blue zone, spot 2 on light blue zone and spot 3 on bluish yellow zone in sample B4 (left). Analytical spot 1 on bluish yellow zone, spot 2 on dark blue zone and spot 3 on light blue zone in sample B6 (right). These color zones appeared heating at 1650 °C.....	78
5.9 Statistical plots (mean \pm SD) showing means and bars of standard deviation of trace analyses (in atom mole ppm recalculated based on 60 oxygen atoms) of different color zones after heating at 1650 °C.....	80

	Page
6.1 Binary phase diagram of $\text{Al}_2\text{O}_3\text{-Fe}_2\text{O}_3$ system displaying solvus curves of hematite-corundum exsolution (Feenstra et al., 2005) and chemical plots of sapphire host and silky inclusions under this study.....	85
6.2 Color and clarity appearances of a sapphire sample before (left) and after heating (right) and three different color zones (points 1 to 3) selected for quantitative trace element analyses.....	88
6.3 Composition of some treated sapphire discussed in text plotted on the triangular diagram proposed by Häger (2001) which clustered at the only Fe apex shows blue coloring.....	89
6.4 Plots of Mg-Ti after heat treatment analyzed by LA-ICP-MS of sapphire samples for Bang Kacha deposits, Chanthaburi.....	90

CHAPTER I

INTRODUCTION

1.1 General Statement

Thailand is one of the most world famous gem suppliers, especially corundum (ruby and sapphire) and an important jewelry trading center. Moreover, Thailand has also its own indigenous source of ruby and sapphire trend in several localities, such as Kanchanaburi in the west and Chanthaburi and Trat in the east. These gemstones are found in association with basaltic rocks. They generally contain rather high Fe content (Vichit, 1992; Somboon, 2006). As a result, Fe-rich content may cause dark tone color and low transparency to opaque of these stones. Silky inclusions, exsolved particles, are often found in the corundum from this area as well as basaltic-type corundum throughout the world. The silky inclusions usually cause phenomena in the stone such as asterism.

Rough corundums are not normally admiring. The proper color, shape, luster and transparency can be improved after cutting and polishing to a facet gem. Moreover, many of them also need treatment for quality improvement. The stone without any treatment will be referred as “untreated” or “unheated” gemstones; however, over 95 percent of gem corundums in the world market have undergone treatment particularly for improvements of clarity and color. Among various processes of treatment, heating method is the most popular and acceptable process.

Sapphires from Bang Kacha deposit which are blue/green, yellow/green, and dark blue colors are mostly required by heaters because they can be heat treated with light element such as beryllium (from an external source) turning into rich, intense and stable yellow sapphires. This heating process is currently well-known and has been generally accepted in the gem industry for many years (Themelis, 1992; Pisutha-arnond et al., 2004 and 2006; Somboon, 2006). Recently, those sapphires are rarer than previous times. Therefore, the six-ray black star sapphire and another low quality opaque stones in this source, which had low market demand, became an important raw material for traders to do the beryllium heat treatment.

1.2 Objectives

The main objective of this research is to study the physical and chemical properties and to investigate the change silky inclusions in sapphire from Changwat Chanthaburi by heat treatment experiment. The study is intended to compare their characteristics such as color, absorption spectra, internal characteristics, and chemical composition between unheated and heated stones at temperature 1650 °C. In addition, the aims of this study are also to understand its physical and chemical changes after heating. Finally, this study could be used as guidelines to enhance the sapphire with abundance of silk by heat treatment.

1.3 Scope of work

The scope of this work will be limited to the study of sapphire samples containing silky inclusion are from Bang kacha deposits, Changwat Chanthaburi that will be subjected to simple heating under a controlled atmosphere without chemical flux.

1.4 Methodology

The method of study was consequently designed to reach the objectives (Figure 1.9). Details of each step are described below.

Literature Survey: previous works related to this study were carried initially to receive background information including nature of corundum, typical properties of sapphire, sapphire heat treatment which they are reported in Chapter II. Subsequently, experiments were designed accordingly. Moreover, crucial information was discussed with results of this study in some aspects.

Samples Collection: All corundum samples from Bang Kacha, Changwat Chanthaburi were collected directly from the local miners which detailed description of the area is also reported in Chapter II. Subsequently, these samples, most euhedral crystals, were selected particularly based on their shape and transparency.

Samples Preparation: Each rough sample was marked its c-axis observed directly from the crystal form and also using a polariscope before cutting and surface polishing perpendicular to the c-axis. The polished samples were then used for further investigation and analyses.

Physical and Optical Properties: All polished samples were weighed and photographed. The basic physical and optical properties were measured initially to confirm the properties of corundum. These basic properties include refractive indices (RI) and specific gravity (SG). Colors under daylight lamp and fluorescent colors under long wave ultraviolet light (LWUV, 365 nm) and short wave ultraviolet light (SWUV, 254 nm) were also observed. Moreover, pleochroism was also observed. These basic equipment were shown in Figures 1.1. All basic gem equipment used for measurement and observation include refractometer, hydrostatic balance, calcite dichroscope, ultraviolet lamps both long wave (LW) and short wave (SW) and gemological microscope. They are based at the Gem Testing Laboratory of the Gem and Jewelry Institute of Thailand (GIT-GTL) (see Figure 1.2).

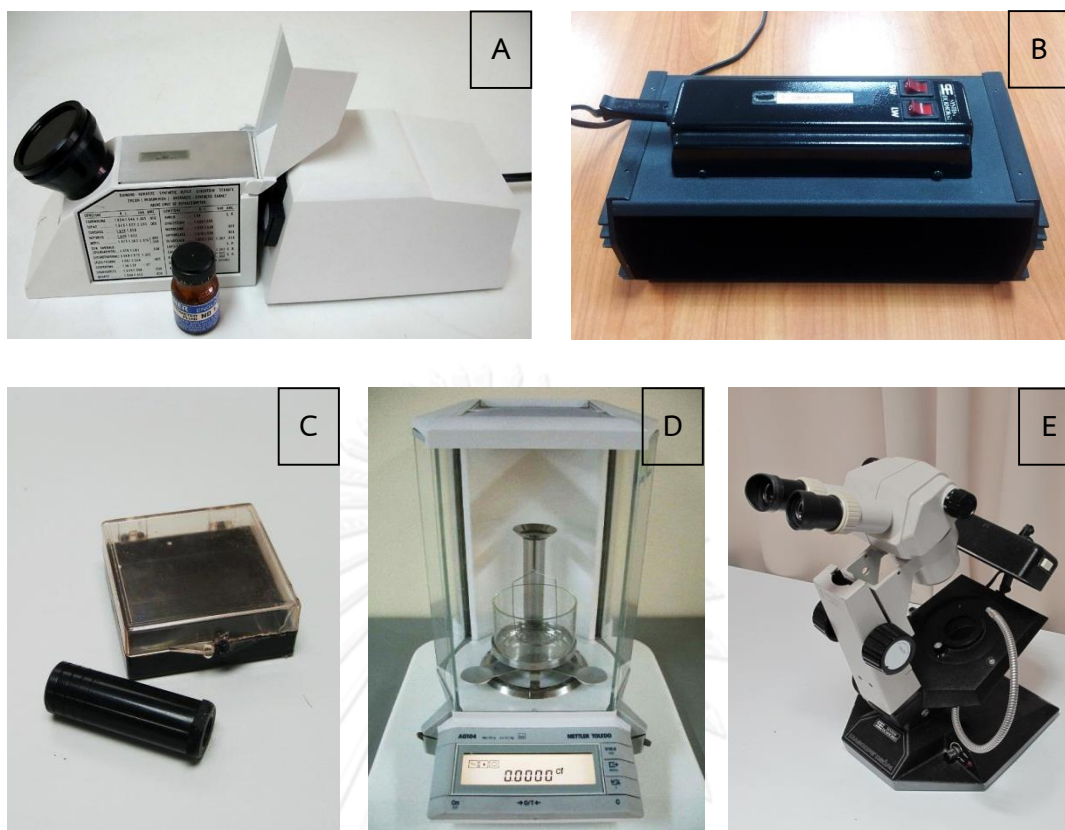


Figure 1.1 Basic gem equipments, based at the Gem and Jewelry Institute of Thailand (GIT) used in this study, including: a) refractometer; b) hydrostatic balance; c) calcite dichroscope; d) ultraviolet lamps; e) gemological microscope.

Internal Features: Internal features were observed firstly under microscope before taking photos. Mineral inclusions exposed close to the samples' surface were subsequently identified using Laser Raman Spectroscopy. Raman spectroscopy is a vibrational spectroscopy based upon the Raman Effect described as the scattering of light from a gas, liquid or solid with a shift in wavelength from the monochromatic incident radiation. When a sample was irradiated with a monochromatic light, not only the exciting frequency is observed (Rayleigh scattering (ν_0), elastic light scattering with no change in energy) but also some weaker bands (certain loss of energy of a material due to molecule vibration) shifted in energy from the Rayleigh line are detected. These weaker bands can be found on both sides of the Rayleigh and the scattering lines are called Stokes and anti-Stokes (Figure 1.2). Stokes is the lower frequency shift ($\nu_0 - \nu_i$) and anti-Stokes is the higher frequency shift ($\nu_0 + \nu_i$) from the incident wavelength. The intensity of Stokes bands is much stronger than the anti-Stokes bands, which is usually used to determine the molecule vibration bond of the materials used the

experiment. Consequently, Raman microscope became to be the equipment for identify mineral inclusions in this study (Figure 1.3).

Internal characteristics of 39 sapphire samples from Bang Kacha deposit, Changwat Chanthaburi were observed under gemological microscope and photos of important internal characteristics were taken. Alterations of internal features were again observed after heat treatment for comparison. Silky inclusions were additionally identified by the Renishaw inVia Raman microscopes based at the Gem and Jewelry Institute of Thailand (GIT). Not all of the mineral inclusions, however, were able to distinguish clearly due to the depth and scale of inclusions. If they were too deep or too small, the signal would be too weak for identification. So the best results were obtained when mineral inclusions are exposed or very close to the sample's surface.

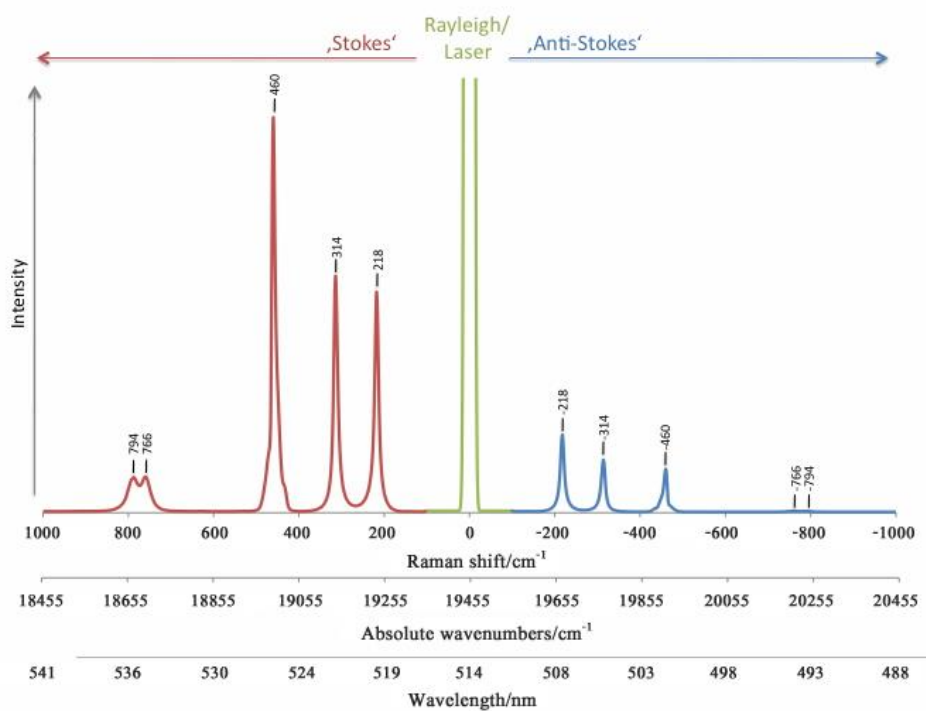


Figure 1.2 Rayleigh and Raman bands of Stokes and anti-Stokes line of some matter excited with the Argon ion (514 nm) (Wanthachaisaeng, 2007).



Figure 1.3 Renishaw Raman inVia microscope based at the GIT

In addition, Electron Probe Micro-Analyzer (EPMA) was engaged to analyze silky inclusions. Quantitative spot analyses of some selective elements were carried out for comparison of composition change after heating. Electron microprobe analysis (EMPA) is a technique for chemically analysis small selected areas of solid samples, in which X-rays are excited by a focused electron beam. The X-ray spectrum contains lines characteristic of the elements present; hence a qualitative analysis is easy to obtain by identifying the lines from their wavelengths (or photon energies). By comparing their intensities with those emitted from standard samples (pure elements or compounds of known composition) it is also possible to determine the concentration of the elements quantitatively. Accuracy approaching $\pm 1\%$ (relative) is obtainable and detection limits down to tens of parts per million (by weight) can be attained. Under normal conditions, spatial resolution is limited to about $1 \mu\text{m}$ by the spreading of the beam within the sample. The spatial distributions of specific elements can be recorded in the form of line profiles or two-dimensional 'maps', which are commonly displayed using a 'false' color scale to represent elemental concentrations (Reed, 2005).

Electron probe microanalysis with wavelength dispersive X-ray fluorescent spectrometry (EPMA-WDS) provides detailed information on the chemical composition. Quantitative determination can be obtained on elements with an atomic number greater than five (boron) to ninety-two (uranium) to detectable limits in the order of

10 ppm. The process is non-destructive; however, the mineral samples have to be prepared as polished sections. Analysis of sample mounts requires carbon coating on good polished surface. Carbon coating provides a conduction path of the probe current and prevents electron charging.

Accordingly from previous study, only three elements (including Al, Ti, Fe) were selected for analyses on silky inclusions. Thirty polished samples were selected for quantitative analysis using a JEOL Electron Probe Micro-Analyzer (EPMA) model JXA 8100 equipped with WDXRF system at Department of Geology, Faculty of Science, Chulalongkorn University (Figure 1.4). Condition for analysis was set at 15 kV and 2.4×10^{-8} A with different counting times for each element. The LTD crystal in spectrometer 1 was selected to analyze for oxygen. Standard was internal standard. The TAP crystal in spectrometer 2 was selected to analyze Al, corundum was used as standard for Al. The PET crystal in spectrometer 3 was engaged for Ti, standard for Ti was rutile. The LiF in spectrometer 4 was applied for Fe, Fayalite was used as standard for Fe. The detection limit of EPMA analysis for most trace elements is about 0.05 weight %.



Figure 1.4 JEOL Electron Probe Micro-Analyzer (EPMA) model JXA 8100 based at Department of Geology, Chulalongkorn University

Absorption Spectroscopy: Absorption spectra were obtained from Ultraviolet-Visible-Near Infrared (UV-VIS-NIR) spectrophotometer and Fourier Transform Infrared (FTIR) spectrophotometer. The UV-VIS-NIR absorption patterns can indicate causes of color in the samples both before and after heat treatment; besides, they sometimes assist identification of geographic origin. In this study, absorption spectra of UV-VIS-NIR and FTIR were analyzed for all polished unheated samples. In addition, some samples selected for heat treatment were reanalyzed again after heating for comparison.

UV-Vis-NIR Spectrophotometer contains a monochromatic light source generating wavelengths over the range of ultraviolet (UV), visible light (Vis) and near infrared (NIR). Absorption spectra are detected with the photocell and then signal is transferred to display on the monitor. This instrument has double beams. A beam of light is switched between a reference path and a sample path, which are re-combined at the detector, which thus compares the two beams. The signal from the reference path is subtracted from that of the sample path to give a spectrum of the sample. UV-Vis-NIR absorption spectrum may be related to electron transitions of trace elements or other structural defects in sapphires (Burn, 1993). For this study, the absorption spectra in UV-Vis-NIR region samples were measured using PerkinElmer UV-Vis-NIR Spectrophotometer, model LAMBDA 950 (Figure 1.5) based at the Gem and Jewelry Institute of Thailand (GIT).

As basis of the molecular structure and chromophoric elements contained in structure, spectroscopic methods are applied to investigate corundum samples and their colors. The absorption spectra over UV-Vis-NIR range and transmission spectra covering near to far infrared region of 39 samples were observed before heating and after heating.



Figure 1.5 PerkinElmer UV-Vis-NIR Spectrophotometer (Model LAMBDA 950) at the GIT

Fourier Transform Infrared (FTIR) spectrometer can be used for recording the absorption or transmission spectra in the range of near to far infrared. The infrared spectra give information about the structures and specific bonding in mineral specimen. The transition responsible for IR band is related to molecular vibrations (stretching or bending of bonds) (Field et al., 2002). The infrared absorption is caused by structural vibration determined by bond lengths and bond angles between atoms (Yan et al., 1995). Measuring of transmission spectra in mid infrared range ($400\text{-}4000\text{ cm}^{-1}$) was carried out using Thermo Scientific FTIR spectrometer (model Nicolet-6700) based at the Gem and Jewelry Institute of Thailand (GIT) (Figure 1.6)

Thirty-nine polished samples were examined in the near – to mid – infrared spectral region. Each sample was placed in the cell holder. Single IR beam was allowed to pass through the sample to detector. The infrared spectrum of corundum is dominated by absorption resulting from Al-O stretch frequencies (Smith, 1995).



Figure 1.6 Thermo Scientific Fourier Transform Infrared (FTIR) Spectrometer (Model Nicolet 6700) at the GIT

Experimental Heat Treatment: was carried out to get additional information that would be useful for the gem industry. The experiment was set using optimum conditions that have been reported by previous researchers which peak temperature was set at 1650°C. Three hours for soaking time at highest temperature under ambient air (oxidizing atmosphere). Three group of sapphires (totally 39 samples) were inspected for their physical and optical properties before heating experiment. Selective samples for the experiments were considered from their absorption spectra and mineral chemistry. All cleaned samples were subsequently placed into alumina crucible for heating via Linn electrical furnace (model HT1800 PlusVAC Bottom Loader) (Figure 1.7) at Department of Geology, Faculty of Science, Chulalongkorn University. The furnace consists of a heating chamber attached with bottom-side sample loader. U-shaped rods of molybdenum disilicide (MoSi_2) are used as heat elements. A pair of heating is hung on the top of chamber. Heating steps and soaking temperatures are automatically controlled using preset programs. The atmosphere in chamber is free without controlled throughout the heating and cooling processes. Maximum temperature was set and planned to heat the all groups of sample. Alterations of

properties and internal characteristics between before and after heat treatment are present in this chapter.



Figure 1.7 Linn electric furnace (model HT1800 PlusVAC Bottom Loader) base at the Department of Geology, Faculty of Science, Chulalongkorn University.

Trace Element Analysis: trace elements (i.e., Be, Mg, Ti, Cr, V, Fe and Ga) of selected sapphire samples were analyzed using a Laser Ablation-Inductively Coupled Plasma-Mass Spectrometer (LA-ICP-MS). These trace elements are very useful for origin determination as well as understanding the color causing of host stones. Laser Ablation-Inductively Coupled Plasma-Mass Spectrometry (LA-ICP-MS) (Figure 1.8) is used to analyses sample in solid state with least sample preparation. The technique is extremely sensitive, multi-element, and capable of detecting trace concentration of almost all elements from Li to U with a wide analytical dynamic range from ppt to ppm level. It is an extremely effective means of investigating the distribution of light elements. However, the determination of element ratios by LA-ICP-MS is based on the comparison of the ratios measured for an external standard with well-known isotopes ratios.

Quantitative results of isotopes for eight trace elements (Be⁹, Mg²⁴, Ti⁴⁷, V⁵¹, Cr⁵³, Mn⁵⁵, Fe⁵⁶ and Ga⁷¹) were obtained through calibration of relative element sensitivities using internal standards NIST-610 and 612 multi-element glasses and pure Al₂O₃, and the external standard Nevada basalt BNV-1. The contents are reported as µg/g or ppm by weight. The detection limits vary from analysis to analysis and are typically less than 1 ppm for Be, V and Ga; less than 4 ppm for Mg, Ti and Mn; less than 13 ppm for Cr and less than 80 ppm for Fe. Descriptions of LA-ICP-MS instrumentation were described below following.

ICP-MS

Model:	Agilent 7500CS
Forward power:	1200 W
Mass analyzer:	Quadrupole

Laser-Ablation

Model:	New Wave Research UP213
Wavelength:	213 nm (Nd:YAG)
Energy distribution:	Homogenized – flat beam, aperture imaged
Energy density:	0.3 J cm ⁻²
Repetition rate:	5 Hz
Nominal spot size diameter:	55 µm (standard and sample)
Analysis duration:	153 sec. (65 sec background, 88 sec signal)



Figure 1.8 Laser Ablation-Inductively Coupled Plasma-Mass Spectrometry (LA-ICP-MS) based at The Gem and Jewelry Institute of Thailand.

Discussion and Conclusion: Finally, discussion on crucial aspects including identification of silky inclusions and guideline for treatment on these sapphires. These discussions reach all objectives using all data obtained from the research in combination with literature. These are included in the last chapter of this report.

Final Report: research report is written and submitted to full fill requirement of MSc program in Geology of Chulalongkorn University. In addition, a few publications are preparing for international journals.

CHULALONGKORN UNIVERSITY

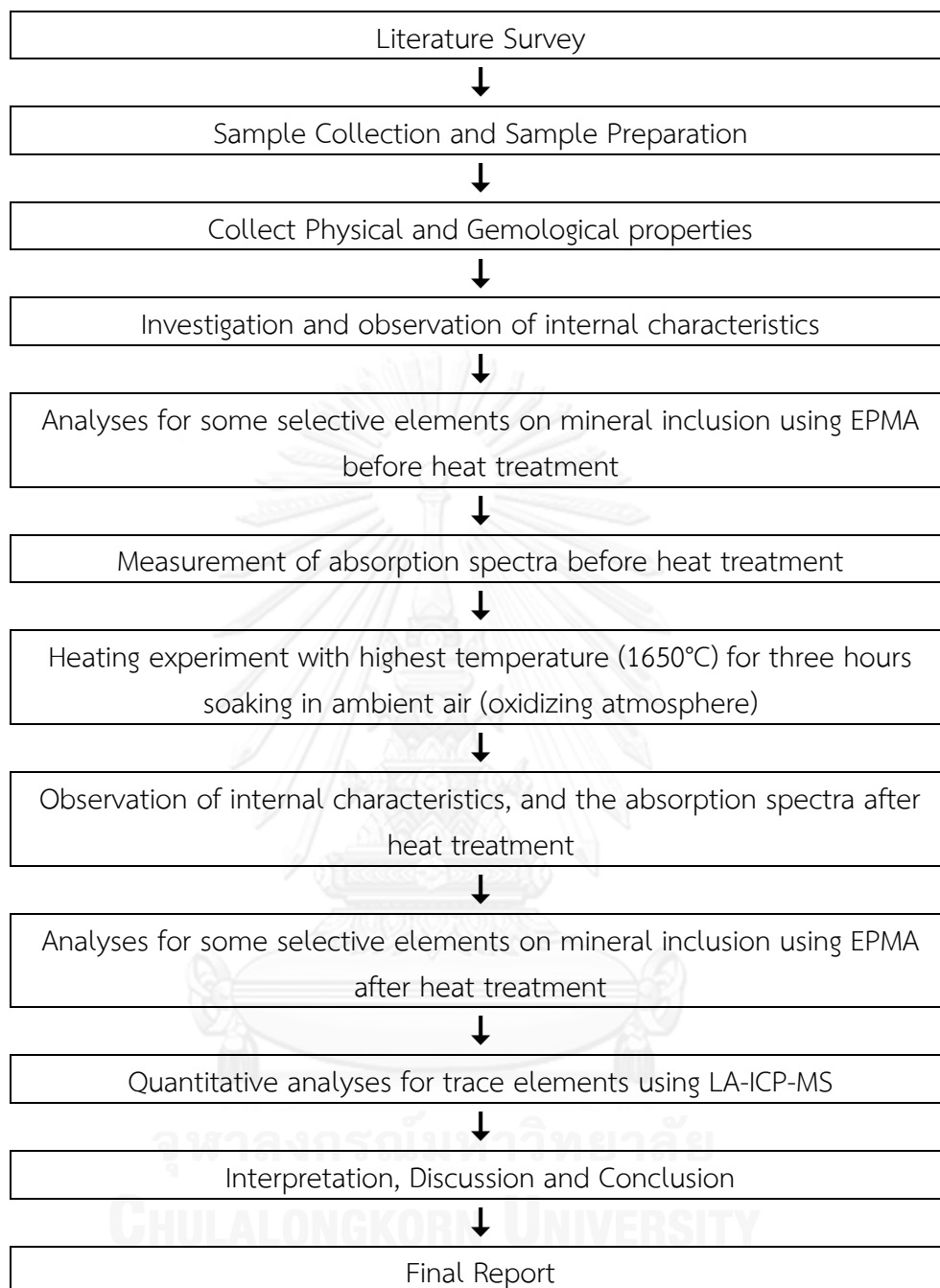


Figure 1.9 Schematic diagram showing methodology of this project study.

CHAPTER II

LITERATURE REVIEWS

2.1 Corundum

Chemically, corundum consists of a ratio of two aluminum atoms and three oxygen atoms or aluminium oxide (Al_2O_3). In its purest form, corundum is colorless. When corundums contain traces of color causing elements known as chromophores, some colors are produced. Moreover, other non-color causing elements may also be bare in corundum. As such, corundum is an allochromatic mineral, owing its color to one or more chromophoric transition metal elements that can absorb selective ranges of visible light. Corundum can be separated into two main varieties, ruby and sapphire. Rubies have red color caused by chromium (Cr^{3+}) in crystal structure whereas sapphire is other colors such as blue, yellow, green, pink, orange, violet and other colors as combination mainly of yellow/blue/red. Iron (Fe^{2+}) and titanium (Ti^{4+}) typically cause blue color whereas yellow are usually influenced by iron (Fe^{3+}) and/or color centers (crystal defect) (Themelis, 1992).

Arrangement of Al^{3+} ions and substituted cations along vertical section of corundum structure is shown in Figure 2.1. Aluminium ions (Al^{3+}) commonly fill in the distorted octahedral site between the oxygen layers. Groups of three oxygen ions form a common face of two neighboring octahedra and thus the groups are linked to a pair of Al ions. It exhibits a three folds rotational symmetry around c axis that is perpendicular to the plane of oxygen ions (Nassau, 2001).

In natural corundum, presence of varying amount of Cr^{3+} causes the range of color from pink (< 0.01 wt% oxide) to red (≥ 0.01 wt% oxide). The intensity of red is a factor of Cr^{3+} concentrations. Blue is due to Fe^{2+} and Ti^{4+} or Fe^{3+} , while yellow is due to Fe^{3+} and/or color center. Other colors are due to the combination of the principal colors (red, blue and yellow). Heat treatment may improve the color by changing oxidation states of these coloring elements, Fe and Ti in particular. However, not all of the stones can be successfully treated.

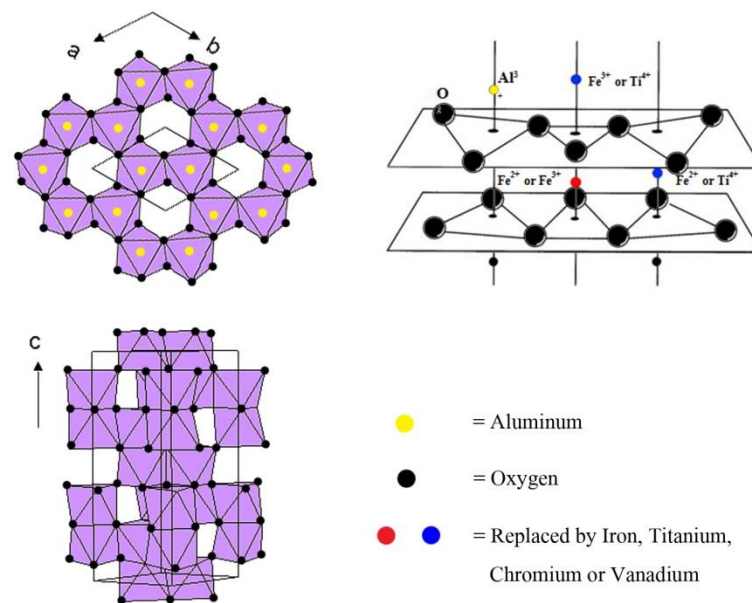


Figure 2.1 Three different views of the corundum structure. The top illustration shows structure looking down the c axis whereas below view is perpendicular to the c axis. The right diagram is perspective view (after Nassau, 1983)

2.2 Causes of Color

Many researchers (e.g., Ferguson and Fielding, 1972; Nassau, 1978; 2001; Fritsch and Rossman, 1987; Nassau and Valent, 1987; Themelis, 1992; Hughes, 1997; Emmett et al., 2003; Bunnag, 2008) suggested that causes of color in gemstones can be explained by crystal field theory, charge transfer or molecular orbital theory, band theory and optical phenomena. Regarding to corundums, their colors can be caused significantly by three theories.

Crystal Field Theory: describes the interaction of surrounding anions on the orbital energy level of a transition metal ion. This theory explains electronic transition involving electrons in the *d*-orbital of the first row transition metal ions (i.e., Ti, V, Cr, Mn, Fe, Co, Ni, Cu, and Zn). Corundum may contain dispersed transition ions, particularly Cr³⁺ with unpaired electrons (1s² 2s² 2p⁶ 3s² 3p⁶ 3d³) substituting aluminium ions, the main composition in its structure. Three unpaired electrons in 3d shell can then absorb visible light selectively to produce red color emission for ruby.

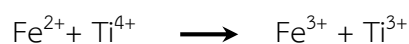
Metal-Metal Charge Transfer: Intervalence Charge Transfer (IVCT) may involve displacement of electron density between metal ions of different oxidation states. The cation pair or cluster must share edges or faces of coordination polyhedral. When a $3d$ electron is transferred between neighboring cations in adjacent coordination sites, there are momentary changes of valences during the lifetime of the electron transition (10^{-15} s). This process is called intervalence charge transfer (IVCT). Although, concentration of these pairs is relatively low, appreciable absorption can be produced strongly. Two general types of charge transfer processes can be recognized; which are depending on whether the same element (homonuclear) or two different elements (heteronuclear) involved in the electron transfer.

Homonuclear IVCT involves ions of the same metal with two different oxidation states occupying adjacent octahedral sites. In corundum, iron can exist crucially in two forms, i.e., Fe^{2+} and Fe^{3+} . An electron of Fe^{2+} ion in one site may transfer to Fe^{3+} ion in another site:



The pair on the right-hand side of the above reaction has presumably higher energy. This process absorbs energy from the spectrum in the near infrared region; consequently, this may cause dark blue color in sapphire (e.g. basaltic sapphire).

Heteronuclear IVCT involves different transition metal cations. In corundum structure, iron and titanium ions may substitute Al^{3+} at two adjacent face shared octahedral (Figure 2.2), in the lower or ground state the two cations exist as Fe^{2+} and Ti^{4+} . Visible light can excite an electron of Fe^{2+} and transfer to Ti^{4+} then these ions turn to Fe^{3+} and Ti^{3+} , accordingly.



The pair on right-hand side of the reaction has higher energy than that of the left-hand side for about 2 eV and absorbs energy of yellow and red light. When the excitation stops and the energy is released, in form of heat, the reaction would reverse ($\text{Fe}^{3+} + \text{Ti}^{3+} \rightarrow \text{Fe}^{2+} + \text{Ti}^{4+}$). The absorption band, during excitation, is broad banding from 562 nm to 704 nm with centered at 588 nm in visible region. Therefore, blue color in sapphire is then produced by this mechanism.

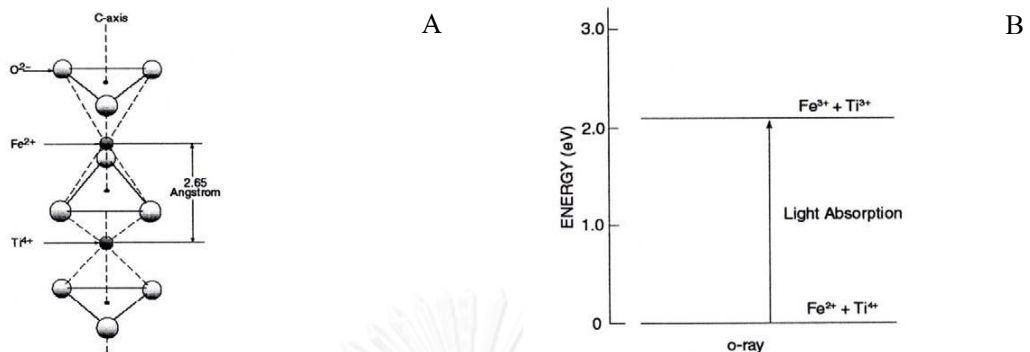


Figure 2.2 (a) Two adjacent octahedral sites in corundum structure, containing Fe^{2+} and Ti^{4+} in blue sapphire. (b) Energy transitions from the ground state to an excited state in blue sapphire, so-called intervalence charge transfer (IVCT) (Nassau, 2001).

Blue color in corundum due to $\text{Fe}^{2+}/\text{Ti}^{4+}$ IVCT has very high value of molar absorptivity (ϵ); therefore, intense blue can be produced from even a low concentration of Fe^{2+} and Ti^{4+} with broad absorption band from 550 to 700 nm (Figure 2.3). On the other hand, blue by $\text{Fe}^{2+}/\text{Fe}^{3+}$ IVCT usually associated with basaltic occurrences which contain high iron concentration may yield strong absorption band with approximately peak at 900 nm (Figure 2.3).

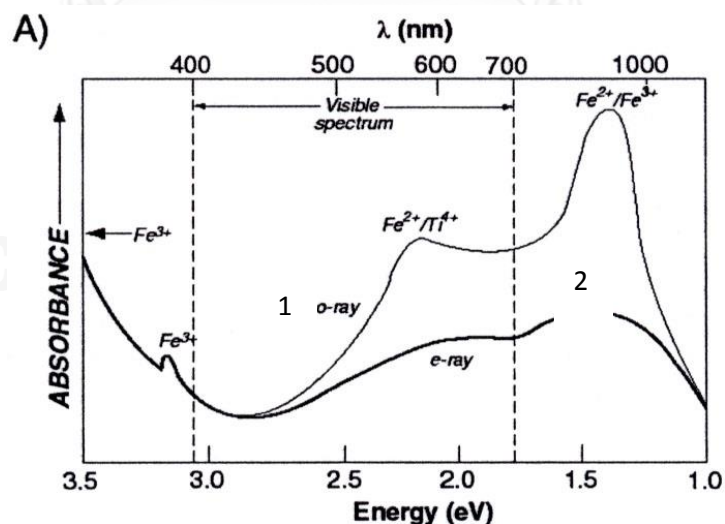


Figure 2.3 The dichroic o-ray and e-ray absorption spectra of a blue sapphire resulted by absorptions of $\text{Fe}^{2+}/\text{Ti}^{4+}$ charge transfer and $\text{Fe}^{2+}/\text{Fe}^{3+}$ charge transfer (Burns, 1993).

Color Centre: is a general term for defect in crystal that may be caused by the unpaired electron which produces color by light absorption while being promoted into

excited states. Under certain circumstances the electron can be located on a non-transition element impurity ion and/or at color centers. This can be the crucial cause of yellow color in sapphire (Nassau, 1978).

The most important defect which is the cause of color in mineral is F-centre (F derived from Farbe: German word for color). Various color centers are known in both natural and synthetic corundums. Physicists subdivide these color centers into anion defect center (related to oxygen vacancies) or electron color center and cation defect center (related to aluminum vacancies) or hole color center.

As mentioned above, major colors of corundum are red, yellow and blue which Cr^{3+} may produce pale pink to deep red related to increasing of Cr concentration (Emmett et al., 2003). Fe^{3+} , $\text{Fe}^{3+}\text{-Fe}^{3+}$ pairs and/or color centers potentially produce yellow whereas $\text{Fe}^{2+}\text{-Ti}^{4+}$ and/or $\text{Fe}^{2+}\text{-Fe}^{3+}$ pairs may yield blue. Consequently, the other colors can be combination of these main colors (see Figure 2.4)

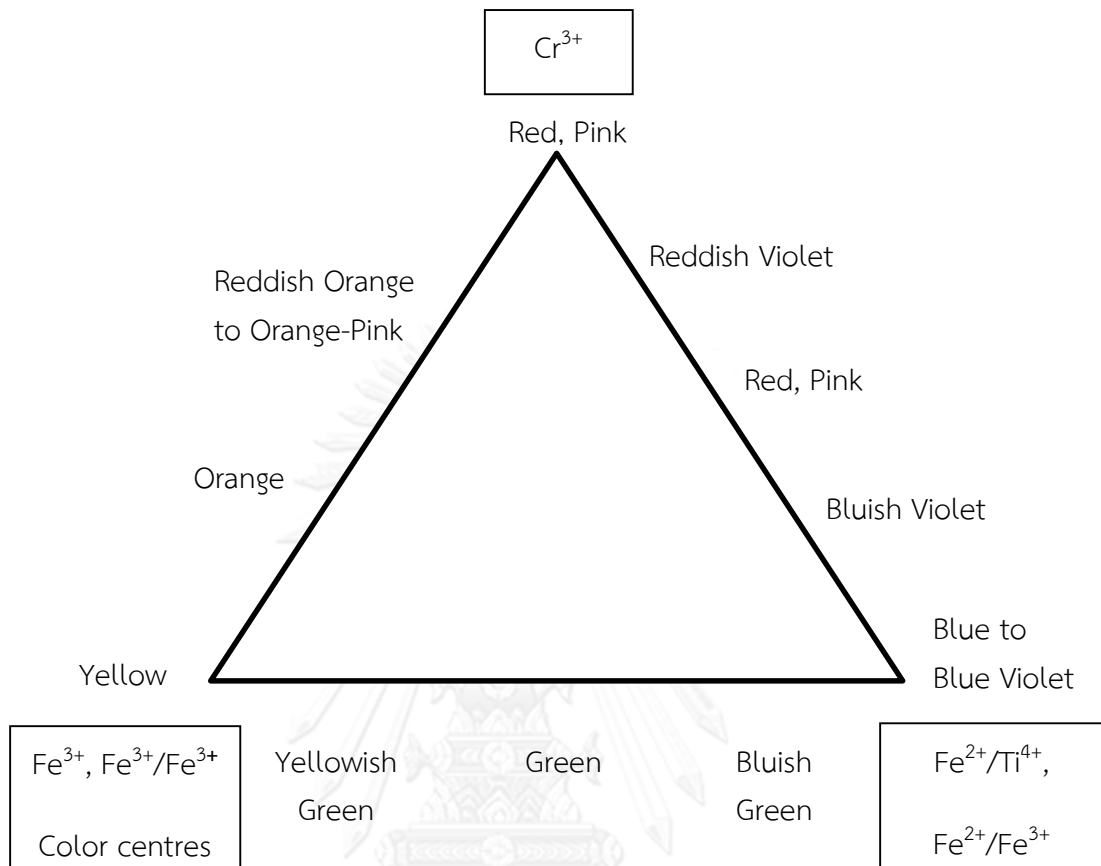


Figure 2.4 Various coloration of natural gem corundum (Bunnag, 2008).

2.3 Heat Treatment

Gemstone enhancement was initially practiced in Greece and Rome period before the Christian era (Nassau, 1994). Consequently, heat treatment of ruby and sapphire is one of the most common techniques which are still in used today to enhance their qualities particularly color, clarity and also asterism . Because natural ruby and sapphire with proper color and good clarity are very rare which have led to very expensive price of high gem quality stones. Heat treatment processes have also been developed on the basis of balancing trace chemistry in the crystal lattice. For example, the blue color of sapphire depends iron (Fe) and titanium (Ti) presences and their valence states, particularly ferrous (Fe^{2+}), ferric (Fe^{3+}), titanous (Ti^{3+}) and titanic (Ti^{4+}); hence, high temperature heating with oxidizing/reducing should develop the proper colors. In the nature, both Fe and Ti may be formed as chemical impurities or mineral inclusions in corundum based on crystallization environment, e.g.,

temperature, pressure, atmosphere and cooling rate. Therefore, reheating with proper condition may lead to better quality blue color of sapphire.

The most important factors for the heat treatment of corundum suggested by Nassau (1994) are composed of highest temperature, soaking time at the highest temperature, heating rate, cooling rate, chemical nature of heating atmosphere and atmospheric pressure. Examples of heat treatments for gem corundums are reported below.

Themelis (1992) developed transparency in opaque milky, silky stones from Thailand to semi-transparent sapphires by heat-treated at over 1750 °C in oxidizing atmosphere for 1 hour.

Nassau (1994) reported that to remove asterism or silk caused by TiO_2 in corundum, it is necessary to reheat the specimen above 1600 °C and wait sufficiently long for the TiO_2 to diffuse away from needles, lose oxygen by reaction and dissolve in Al_2O_3 mostly as Ti_2O_3 . The material is then cooled relatively rapidly so that the time for oxygen in-diffusion and needle growth below about 1600 °C is not available. In the same way, silky, milky, hazy or whitish sapphires in which the imperfections are derived from titanium can be modified their clarity.

Kyi et al. (1998) reported the heat treatment of geuda-like (milky or contain abundant silk) sapphires from Mogok under reducing atmospheres for 2 hours, step heating temperature from 1200 °C, 1300 °C, 1400 °C, 1500 °C, 1600 °C and 1700 °C. After heating temperature from 1200 °C the milky sapphire turned to transparent or translucent colorless stones with the exception of very light blue milky sapphire with zonal structure turned white. Repetition of the experiment to 1300 °C and 1400 °C caused no further dramatic changes in the sapphires. At the temperature of 1500 °C, the heating period was much longer than for the treatments described above, some milky sapphires change to medium blue at 1500 °C. When the temperature was raised to 1600 °C and the heating period further extended, the color dramatically changed from medium blue to more beautiful blue. When the temperature was increased to 1700 °C with longer period of heating than heating at 1600 °C, the beautiful blue sapphire turned to medium blue.

Read (1999) heat treated geuda sapphires (milky-colored translucent sapphire) in timed steps through 1200 °C to about 1700 °C in an oxygen free atmosphere, a process which was taken up to 30 hours, the titanium dissolved in the alumina and produced transparent blue stone.

Pisutha-Arnond et al. (2004; 2006) explained beryllium-diffusion treatment method of natural blue/green sapphires in gem market. Color mechanism of these treated stones is involved by Fe, Ti, Mg and Be. LA-ICP-MS profile analyses were carried out on their treated surfaces; the results have confirmed that divalent Be acts essentially in the same way as that of Mg which is stabilizer of color centers yielding stable yellow of sapphire.

Themelis (2010) reported the heat treatment process to remove asterism, silk, cloudiness and dust for Thai black star sapphires from Bang Kacha deposit by heating at 1830 °C in a reducing atmosphere for 85 minutes.

2.4 Bang Kacha Corundum Deposits in Chanthaburi

Thailand has long been known as a crucial supplier of gemstones and become one of the world's color stone centers. An estimated 70% of the world's high-quality gem sapphires come from Thailand; however, most of these stones have been imported from many places throughout the world, particularly from East African countries. Recently, the country's indigenous sapphires are supplied mainly from Chanthaburi deposits around Khao Wua, Khao Phloi Waen and Ban Bang Kacha; although, corundum deposits in Thailand have also been found in the northern, northeastern and west-central parts of the country (Vichit, 1992).

Geologic setting of Thai corundum deposits is typically associated with alkali basalts. Rubies and sapphires are found as a product of weathering and erosion within or nearby basaltic terrains but gem corundums in fresh basaltic rocks are extremely rare. Most of gemstones in the country are found as secondary deposits, i.e., alluvial placer and residue soil. Chanthaburi region can be divided into two mining zones. The first zone lies to the west, near the town of Chanthaburi (Figure 2.5) which has been known for production of blue, blue-green and yellow sapphires as well as black star sapphire. The second zone is along boundary between Chanthaburi and Trat Provinces in which ruby and sapphire have been discovered (Vichit, 1992).

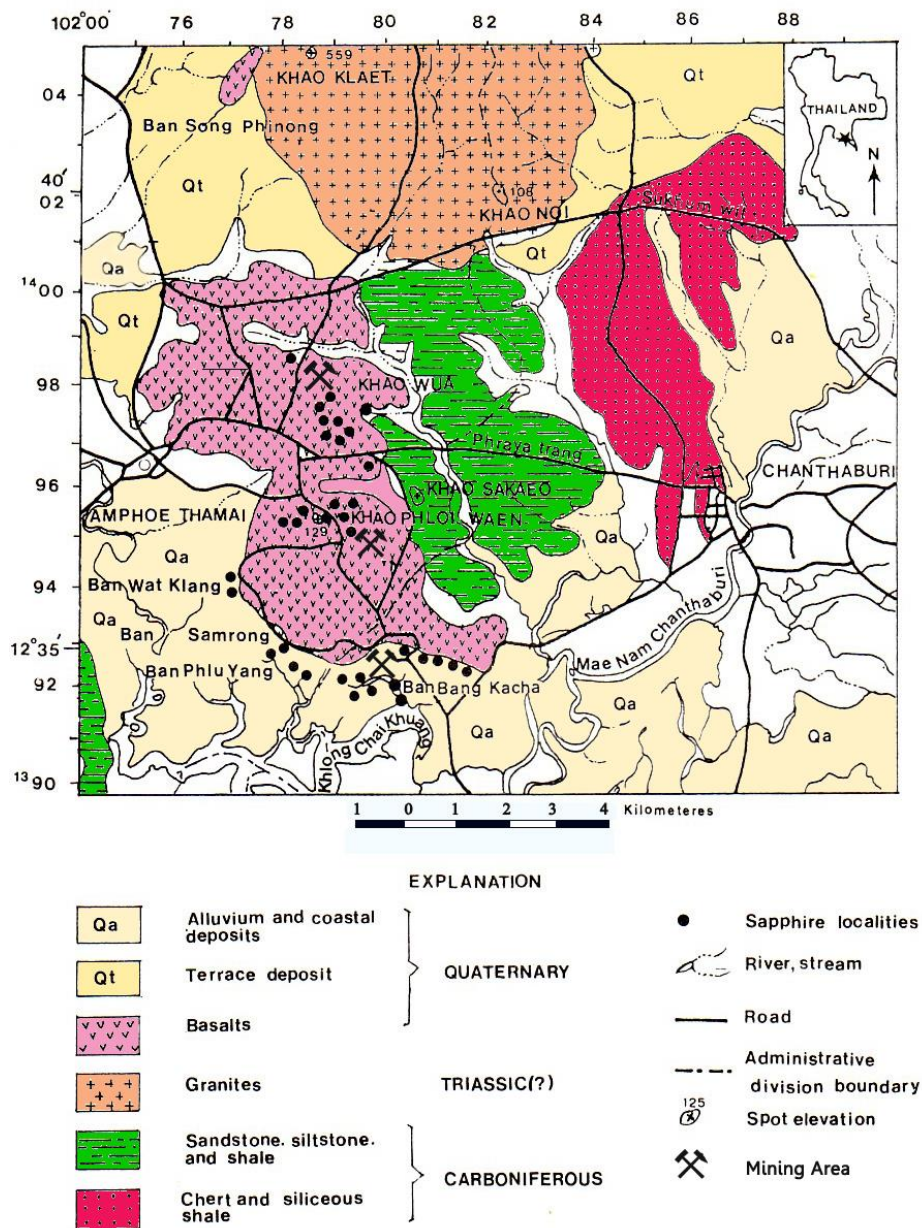


Figure 2.5 Geological map of the western zone of Chanthaburi showing locations of sapphire deposits (after Vichit, 1992).

The western Chanthaburi zone is one of the oldest and best-known sapphire deposits in Thailand. It is located approximately six kilometers to the west of Chanthaburi (Figure 2.5). The gem deposits situate around Khao Wua, Khao Phloi Waen and Ban Bang Kacha (this study area). Recently, there are only a few mines still operating in some particular areas. Khao Wua and Khao Phloi Waen are small volcanic

hills with heights about 85 meters and 129 meters above mean sea level, respectively. Ban Bang Kacha is situated approximately 3 kilometers southeast of Khao Phloi Waen at the southeastern margin of the basalt terrain which is Quaternary basalts covering an area of approximately 3 x 7 square kilometers. The basalt in Khao Phloi Waen yields K-Ar age of 0.44 ± 0.11 million years (Barr and Macdonald, 1981). Sutthirat et al. (1994) reported an Ar/Ar age of 3.0 ± 0.19 million years of basalt sample from Khao Wua. These basalts are strongly alkali and identified as basanitoid or nephelinite (Vichit, 1992; Barr and Macdonal, 1981).

Sapphires are found at relatively shallow depths of deeply weathered basaltic rocks in the vicinity of Khao Wua and Khao Phloi Waen and at about 3 to 8 meters depth in the surrounding areas. At least two sapphire-bearing layers at average depths of about 3 to 4 and 6 to 7 meters, respectively, have been discovered. The thickness of sapphire-bearing layer are averaged between 30 cm to 1 m. Associated minerals are typically pyropic garnet, pyroxene, phlogopite. Its grain size varies from a fraction of cm to 6 cm in diameter (Vichit, 1992).

Sapphire mines at Ban Bang Kacha, are in swampy area. The working areas are around 1 to 1.5 km from the edge of the basalt flows. The average depth to paydirt, locally called as “kra sa”, is about 2 to 4 m. The paydirt is about 10 to 80 cm thick. Pyroxene is the most abundant mineral associated with sapphire in the paydirt. Red garnet and zircon are comparatively rare.

In this area, sapphires have various colors such as blue, green, and yellow or combination of these colors. Star sapphires are also common whereas color-change sapphire occurs rarely. Among these sapphires, yellow variety is the rarest and small stones which they are accounted approximately ten percent. Big rough stone is usually smaller than ten carats in weight. On the other hand, star and green sapphires are found easier than the blue and yellow sapphires. The mining methods used in Bang Kacha vary widely, from traditional hand dug pits (Figure 2.6) to open cast mining with machinery (Figure 2.7). Open cast mining produces the highest yield but the financial costs are relatively high. Occasionally, smaller pits are still found recently around Bang Kacha, particularly in the private lands.



Figure 2.6 Traditional pitting in gem mining area of Bang Kacha.

Open cast mining usually operate seasonally because huge amount of water is demanded for soil washing and dressing processes. Therefore, during the rainy season between May and September is the proper period for mining.



Figure 2.7 Open cast mining with heavy machineries in Bang Kacha gem deposit.

2.5 Gem Varieties in Bang Kacha Deposits

There are a variety of gems found in Bang Kacha deposit but sapphires (Figure 2.8) are the most important group. Dark red pyrope garnets and zircons are also found but their quantity and quality are low. The most famous gem in this area is golden yellow sapphire. Before beryllium treatment was initially applied to sapphires by the end of 2001, high quality blue sapphires and whisky yellow sapphires from Bang Kacha were demanded in the market; however, both varieties are relatively less abundant. On the other hand, green sapphires are also found with significant quantity with dark tone in general; their prices were lower than former varieties. There are, however, some unearthed, very fine, grass-green sapphires from Bang Kacha, sometimes weighing over ten carats. Sapphires with a color combination of golden and green, producing a very pleasing virgin olive oil color. These stones are quite rare and expensive.



Figure 2.8 Varieties of sapphires from Bang Kacha deposit, Chanthaburi.

Moreover, star and opaque sapphires are also found with fairly large quantity (Figure 2.9). The star effect is a result of intersecting needle or silk inclusions which their high amount may make the host stone distinctively black. Twelve rayed stars are sometimes seen when there is a combination of hematite and other mineral (may be rutile) (Hughes, 1990 and 1997). The star sapphires are occasionally found with a golden body color. These gems are very rare and highly prized in the local markets.



Figure 2.9 Large quantities of star and opaque sapphire from Bang Kacha deposit, Chanthaburi.

Saminpanya (2001) investigated exsolved ‘needles’ and ‘silk’ inclusions in star sapphire from Bang Kacha and subsequently reported that these inclusions are not pure rutile or hematite as stated similarly by Hughes (1997) and Weibel and Wessicken (1981). It is more likely a mineral of ilmenite-hematite solid solution series, ilmenite or spinel which can produce the asterism and/or chatoyancy in Thai sapphire. The sample of Bang Kacha star sapphire contains high Fe dispersed throughout the grain whereas titanium mainly concentrates in the area full with exsolved needles and silks.

The so-called “silk”, composed of very fine, usually short needle epitaxially intergrown with the basal plane of the host sapphire, whereas the “needle” is a thin, usually long, elongated crystal that could be looked like a tiny rod (Gübelin and Koivula, 1997).

High temperature heat treatment of green sapphires with beryllium can turn their color to bright yellow. The same result was seen in green sapphires from Bang Kacha, Changwat Chanthaburi.

CHAPTER III

PHYSICAL AND GEMOLOGICAL PROPERTIES

3.1 Introduction

Thirty nine samples of sapphire with abundant silky inclusions from Bang Kacha deposit in Chanthaburi province were selected for this study. The samples have various sizes from 3 to 13 millimeters and weights range from 0.2 to 5.0 carats. Most of them are transparent to semi-transparent. Some samples show a well crystal habit as tabular hexagonal (see Figure 3.1). They were subsequently cut and polished surface perpendicular to c-axis before further investigation.

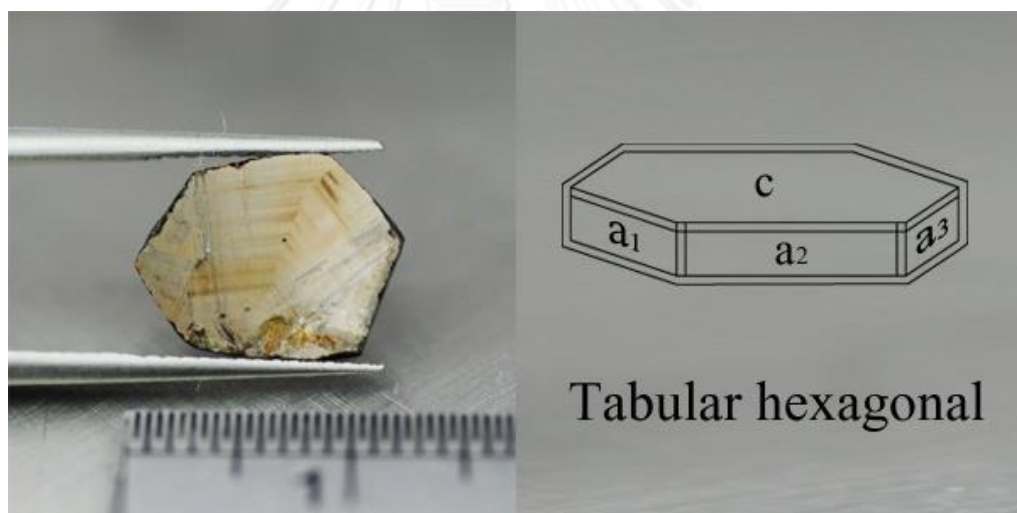


Figure 3.1 A sapphire samples from Bang Kacha Deposits, Chanthaburi showing a well hexagonal crystal habit.

Sapphire samples were distinguished, based on the abundance of silky inclusions, into 3 groups which are labeled as group A, group B, and group C. Group A includes sapphires with minor silky inclusions having green to light bluish green body color whereas group B is green to greenish blue body color samples with moderate silky inclusions. On the other hand, C group refers to sapphires with abundant silky inclusions having greyish brown body color. They were photographed under standard daylight 6500K by digital camera which images were displayed in Figures 3.2 -3.4.

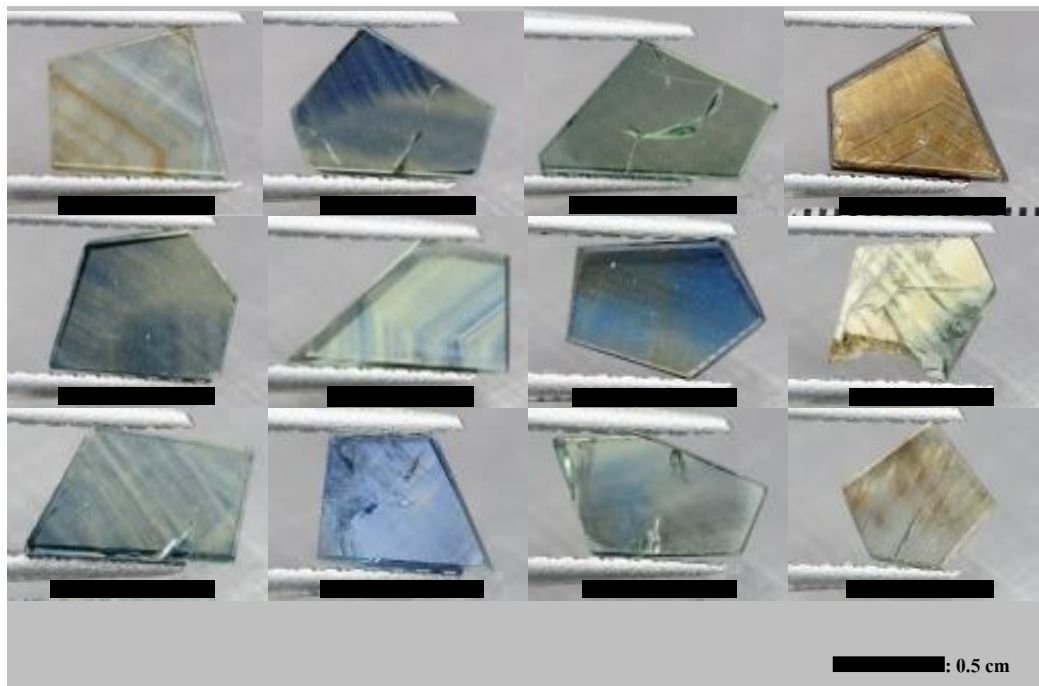


Figure 3.2 Sapphire samples with minor silky inclusions (Group A) before heating experiment.

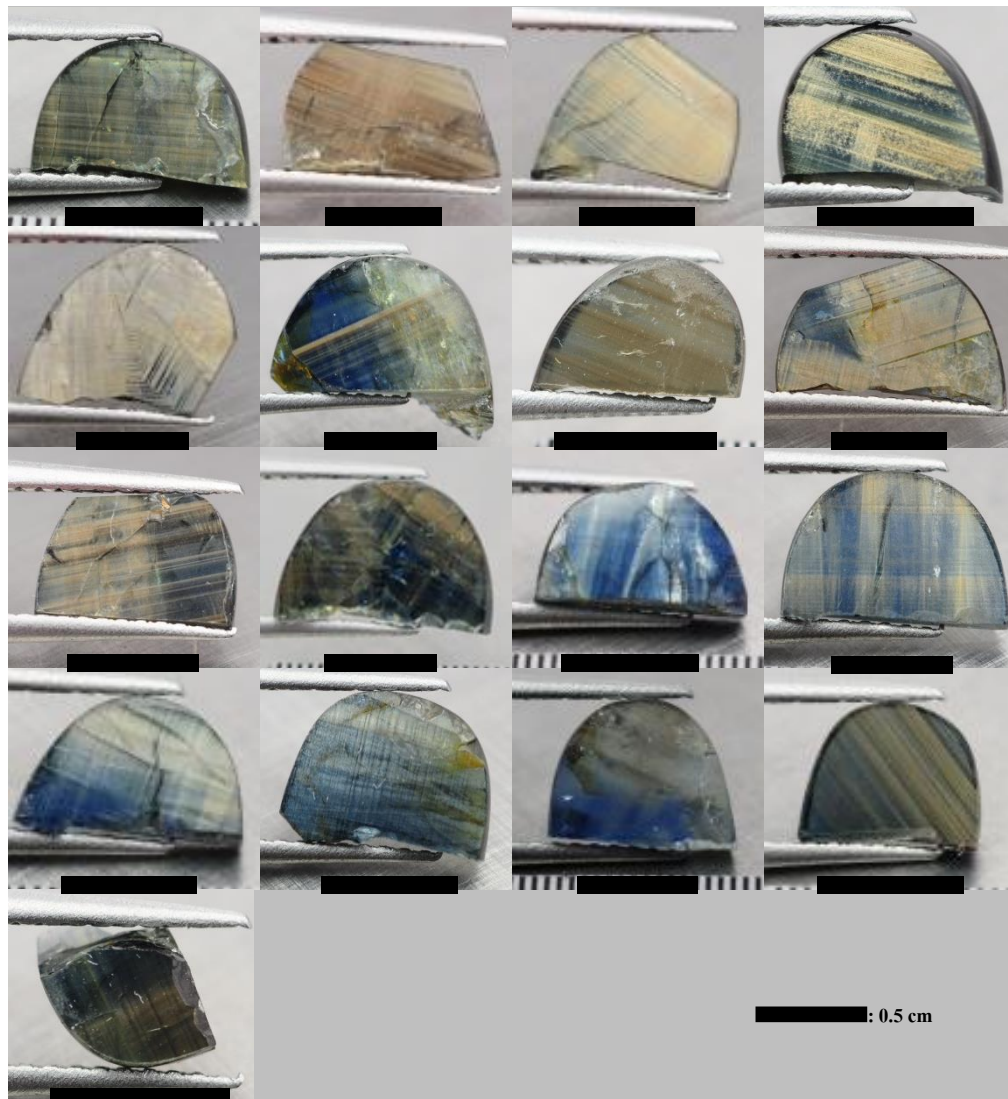


Figure 3.3 Sapphire samples with moderate silky inclusions (Group B) before heating experiment.

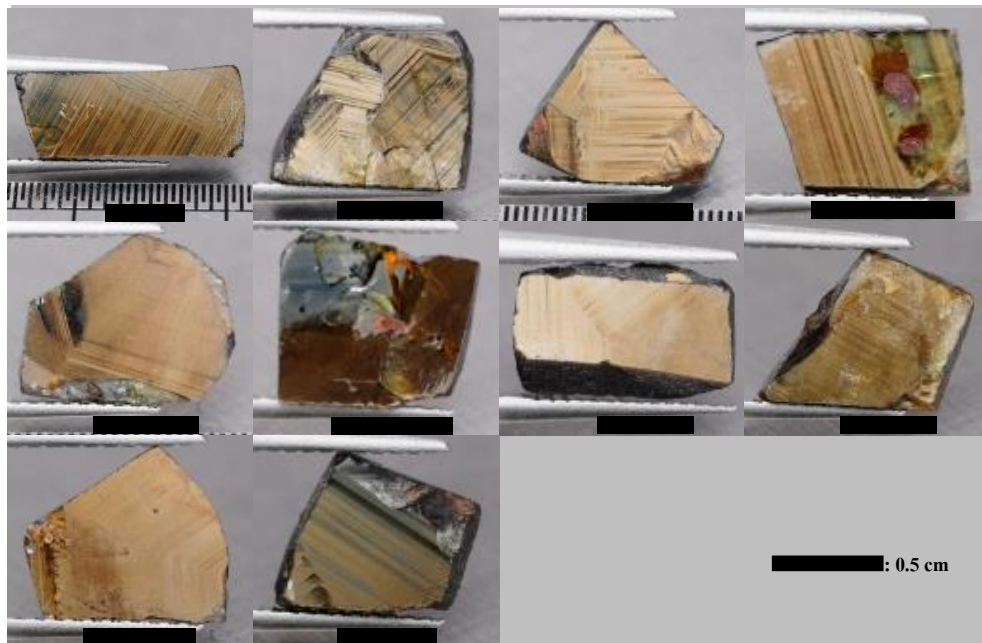


Figure 3.4 Sapphire samples with abundant silky inclusions (Group C) before heating experiment.

3.2 Physical Properties

In general, physical properties of all samples fall within typical range of corundum. The refractive indices (RI) are 1.759 - 1.767 for ordinary ray (n_o) and 1.770 - 1.776 for extraordinary ray (n_e) with birefringences range between 0.006 and 0.013. Specific gravity (SG) ranges approximately 3.80 - 4.06. The physical properties of those samples are summarized in Table 3.1 and more details are reported in Appendix A1.

Table 3.1 Summary of physical properties of sapphire samples from Bang Kacha Deposit, Chanthaburi.

Sample Group	SG	RI		Birefringence	Fluorescence		Pleochroism
		n_o	n_e		SWUV	LWUV	
A	3.80 -	1.772 -	1.762 -	0.007 -	Inert	Inert	light Blue/light Green - Blue/Green
	3.96	1.776	1.767	0.012			
B	3.92 -	1.771 -	1.761 -	0.006 -	Inert	Inert	light Blue/light Yellow - Blue/Green
	4.07	1.774	1.765	0.013			
C	3.82 -	1.770 -	1.759 -	0.008 -	Inert	Inert	Brown/Brown
	4.05	1.775	1.763	0.012			

3.3 Internal Characteristics

Investigation of mineral inclusions in 39 sapphire samples usually yield resemble results. The first group (Group A, sapphire samples with minor silky inclusions), typically contains a little amount of silky inclusions (Figure 3.2). The second group (Group B, sapphire samples with moderate silky inclusions) also presents generally silky inclusions with more abundance than the group A (see Figure 3.3). The last group (Group C, sapphire samples with abundant silky inclusions) usually has opaque appearance which is caused by a large amount of silky inclusions. They usually show grey to brown color influenced by these silky inclusions (see Figure 3.4). The group C usually shows that abundant silky inclusions appear to orient perpendicular to the c-axis along the growth pattern and planes of basal pinacoid (see Figure 3.5). Three direction orientation of silky inclusions along crystallographic direction is clearly observed in groups A and B (Figures 3.6 and 3.7). Moreover, some samples, particular in Group C, reveal irregular lamellae feature of the silky inclusions under high magnified microscope using combined light sources of transmission and reflection (Figure 3.8). this significant feature seems to indicate exsolution of these silky inclusions from the sapphire host under subsolidus condition (Hughes, 1997; Turnock and Eugster, 1962).

Identification of these tiny inclusions is rather difficult because they are smaller than the beam spot of laser used for Raman Spectroscope. This is the most crucial limitation of this study. Most spectra are usually influenced by spectrum of the sapphire host. However, some crucial associated minerals such as hematite, magnetite

and black spinel from the alluvial gem deposits surrounding the Bang Kacha area were also collected and analyzed using Raman spectroscopy for reference and comparison to the patterns of these tiny inclusions.

Better Raman spectra are usually obtained from the bigger silky inclusions, particularly found in the sapphire with abundant silky inclusions group (Group C) (Figure 3.8). These silky inclusions yielded significant peak positions at 213, 293, 413, 492, 590, 638, 810, and 1302 cm^{-1} which is closely comparable to the pattern of alluvial hematite (Figure 3.9). On the other hand, alluvial magnetite yielded peak positions at 300, 557 and 672 cm^{-1} and alluvial black spinel gave peak positions at 277, 611, 702, and 746 cm^{-1} (see also Figure 3.9). Although, pattern of these silky inclusions are closely related to alluvial hematite as mentioned above some peaks slightly shift to patterns of magnetite and black spinel. Therefore, composition of magnetite and spinel may occur in these sapphire; Electron Probe Micro-Analyzer was then applied to analyze some of these silky inclusions which will be reported in Chapter 5.

Other internal features in some sapphire samples contain fingerprints, fracture, minute particles and negative crystals (see Figures 3.10 - 3.11).

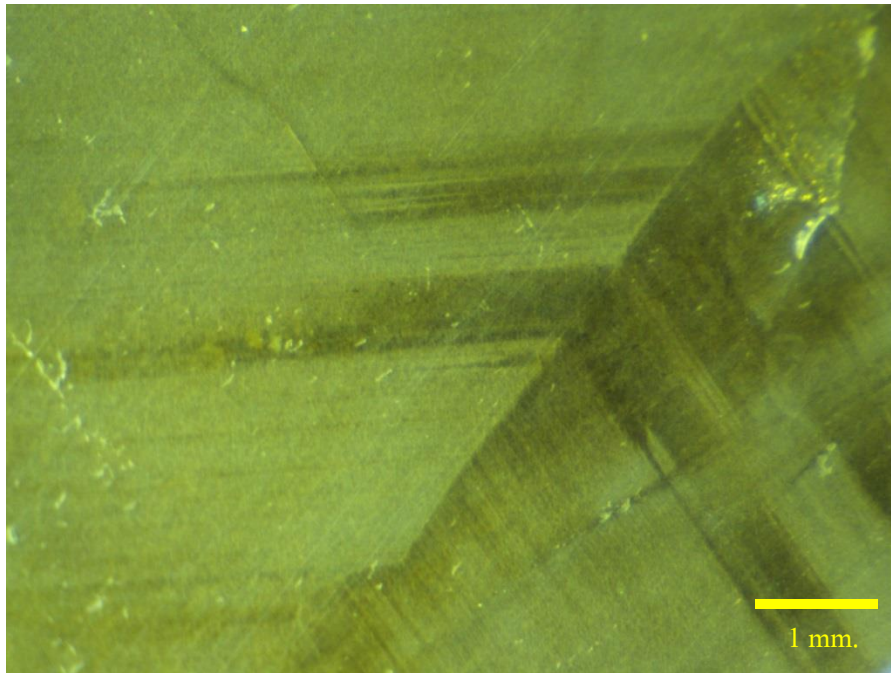


Figure 3.5 Abundant silky inclusions orientating along the growth structure and basal pinacoid perpendicular to the c-axis (sample C7).

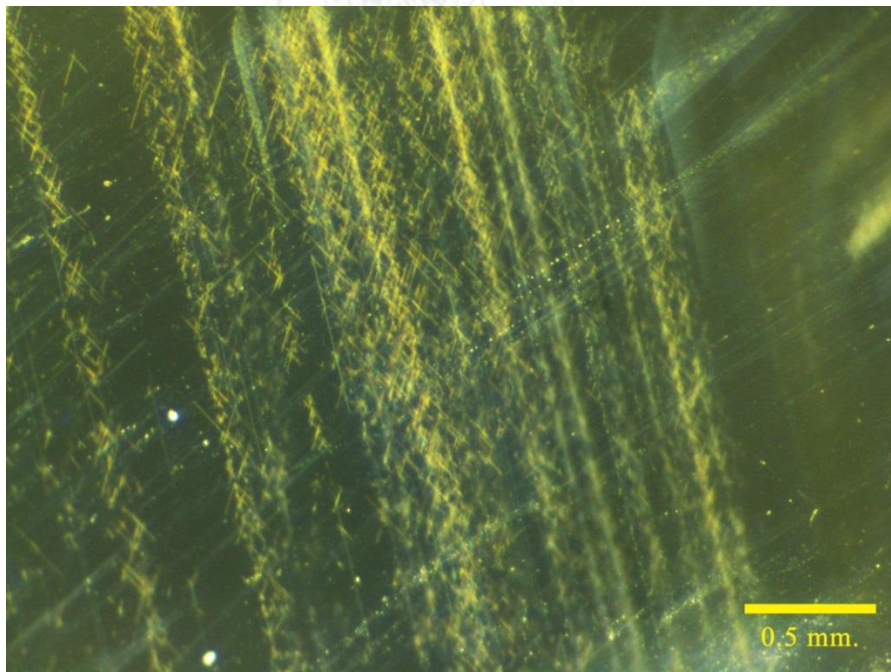


Figure 3.6 Silky inclusions in sample A5 oriented in three directions along crystallographic direction.

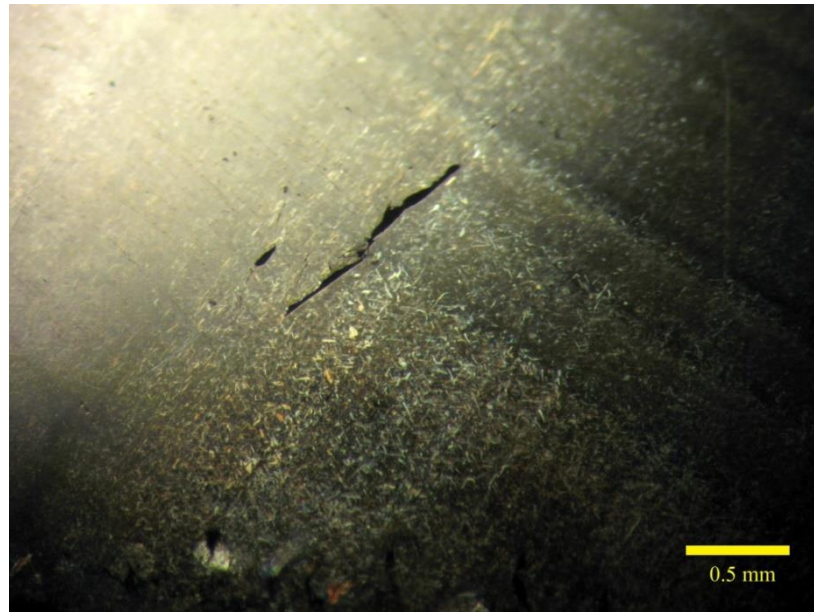


Figure 3.7 Silky inclusions in sample B8 in sapphire with moderate silky inclusion group showing three directions orientation along crystallographic direction.



Figure 3.8 Photomicrograph with high magnification (using combination of reflected and transmitted lights) showing irregular lamellae feature of silky inclusions orientated along crystallographic directions in sample C9; indication of subsolidus exsolution of the sapphire host.

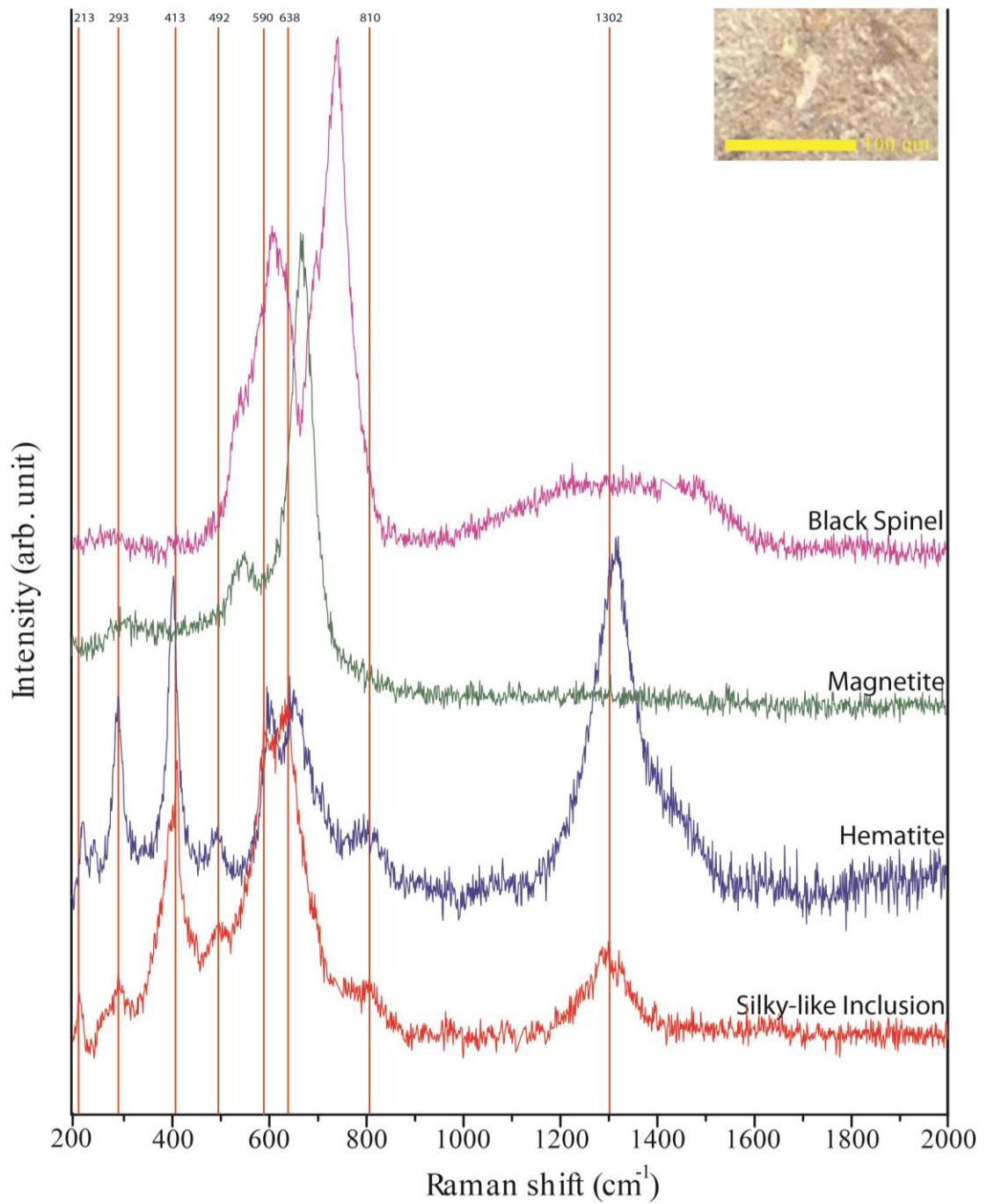


Figure 3.9 Raman spectrum of a represent silky inclusion of sapphire sample with abundant silk inclusion group compared with hematite, magnetite and black spinel patterns collected from alluvial deposits around the Bang Kacha deposit.

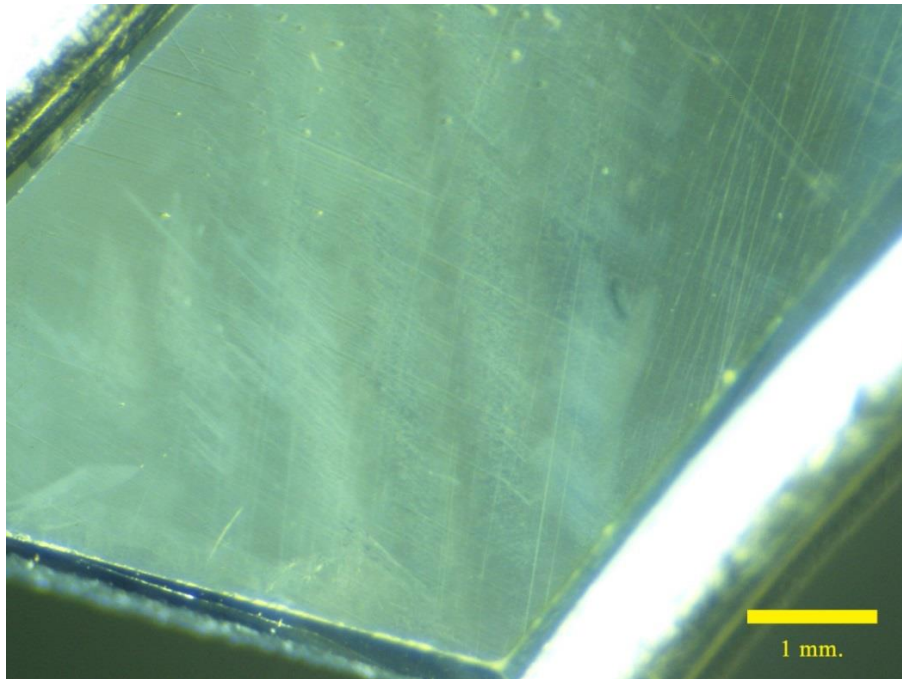


Figure 3.10 Minute particles or white dusts in sample C6.

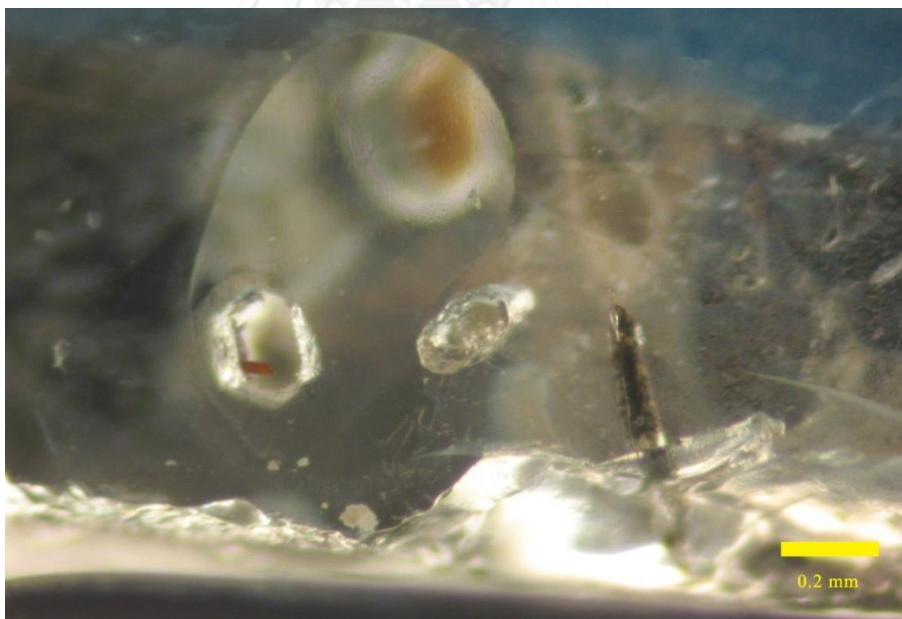


Figure 3.11 Negative crystals in sample B4.

3.4 UV-Vis-NIR Spectra

Oriented samples were fixed in the middle of black plate with 2-2.5 mm diameter slit and placed into the cell holder. Each sample was measured twice, perpendicular to c-axis for ordinary ray (o-ray) and parallel to c-axis for extraordinary ray (e-ray). Some samples (e.g., B2, B4, B8, B11, B13, B14, B15 in the group of minor silky inclusions, and C1 to C10 in the group of abundant silky inclusions) could not obtain extraordinary ray due to their thickness and abundant inclusion. The absorption spectra were examined in a range between 250 and 1500 nanometers (nm) with 2 nm spectral resolution. This section will be showed only o-ray spectrum covering most probable transition of causes of color. All selective absorption spectra were collected in Appendix B.

Typical UV-Vis-NIR spectra of unheated sapphires in all groups are displayed in Figures 3.12 to 3.17. All absorptions are related to transition metal ions which are the cause of colors in corundum (e.g., Fe^{2+} , Fe^{3+} and Ti^{4+}). All sapphire samples with silky inclusions usually show $\text{Fe}^{3+}/\text{Fe}^{3+}$ pairs absorption peaks at 378 and 450 nm, Fe^{3+} absorption peaks at 387 nm, low intensity of $\text{Fe}^{2+}/\text{Ti}^{4+}$ IVCT absorption band with highest absorbance at about 560 nm and $\text{Fe}^{2+}/\text{Fe}^{3+}$ IVCT absorption band at about 910 nm. Typical samples have yellowish green and greenish blue which may be caused by the combination of Fe^{3+} , $\text{Fe}^{2+}/\text{Ti}^{4+}$ IVCT and $\text{Fe}^{2+}/\text{Fe}^{3+}$ IVCT.

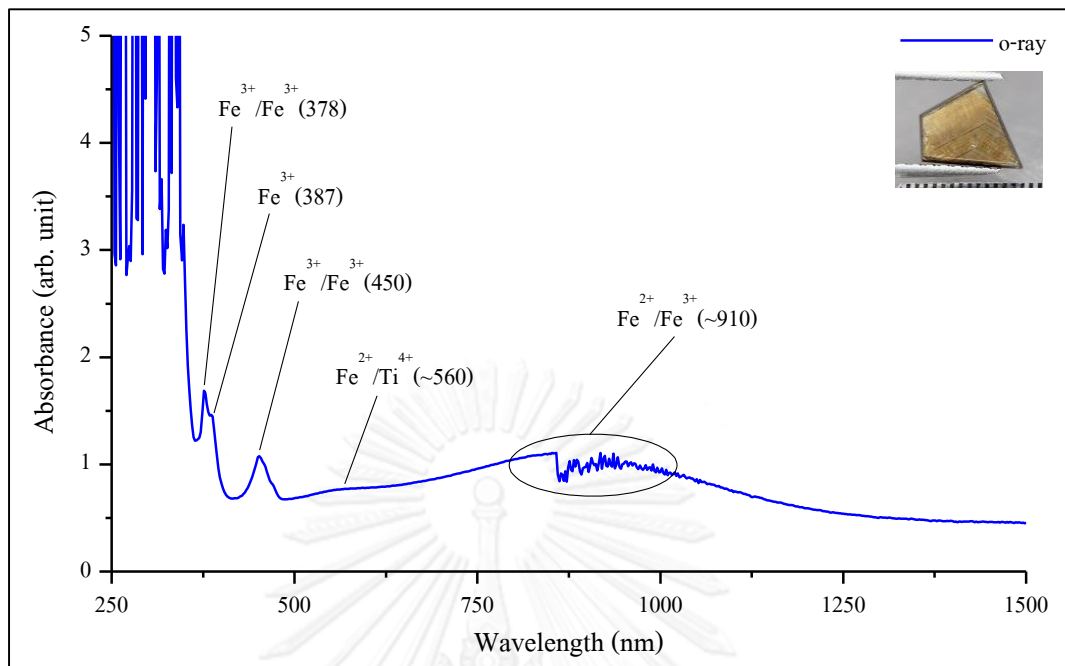


Figure 3.12 UV-Vis-NIR spectra of unheated sapphire with minor silky inclusions (A4).

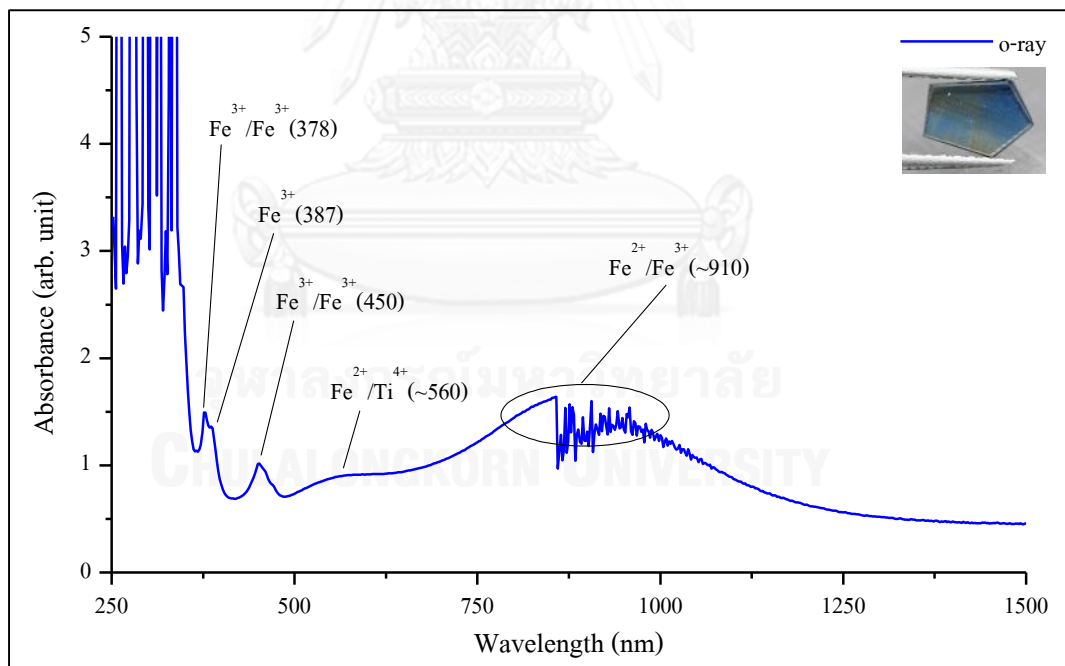


Figure 3.13 UV-Vis-NIR spectra of unheated sapphire with minor silky inclusions (A7).

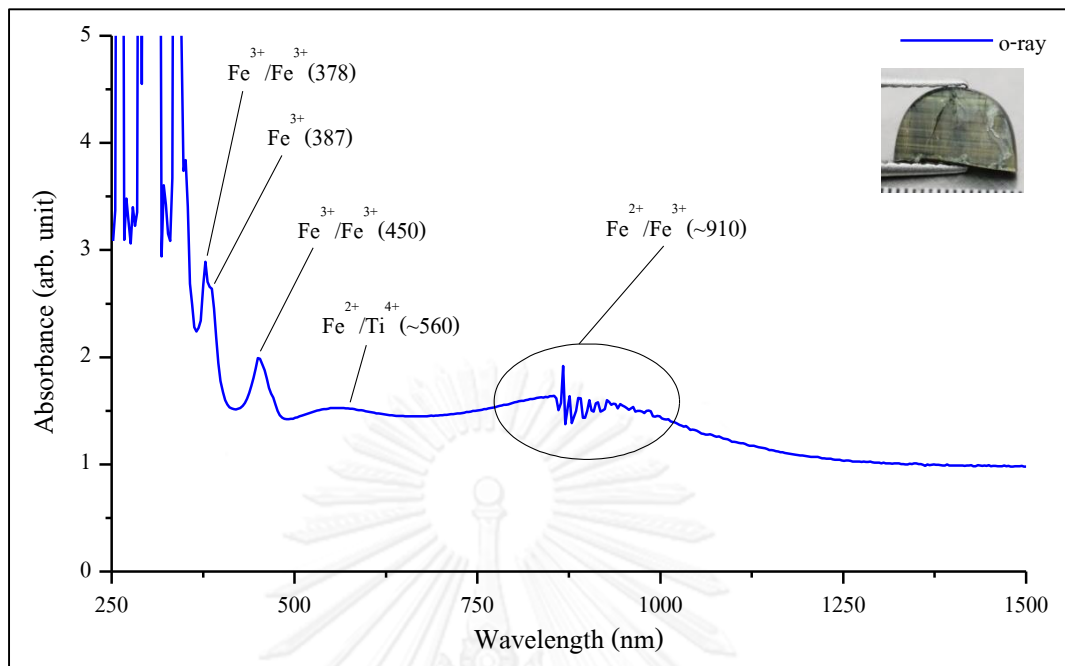


Figure 3.14 UV-Vis-NIR spectra of unheated sapphire with moderate silky inclusions (B1).

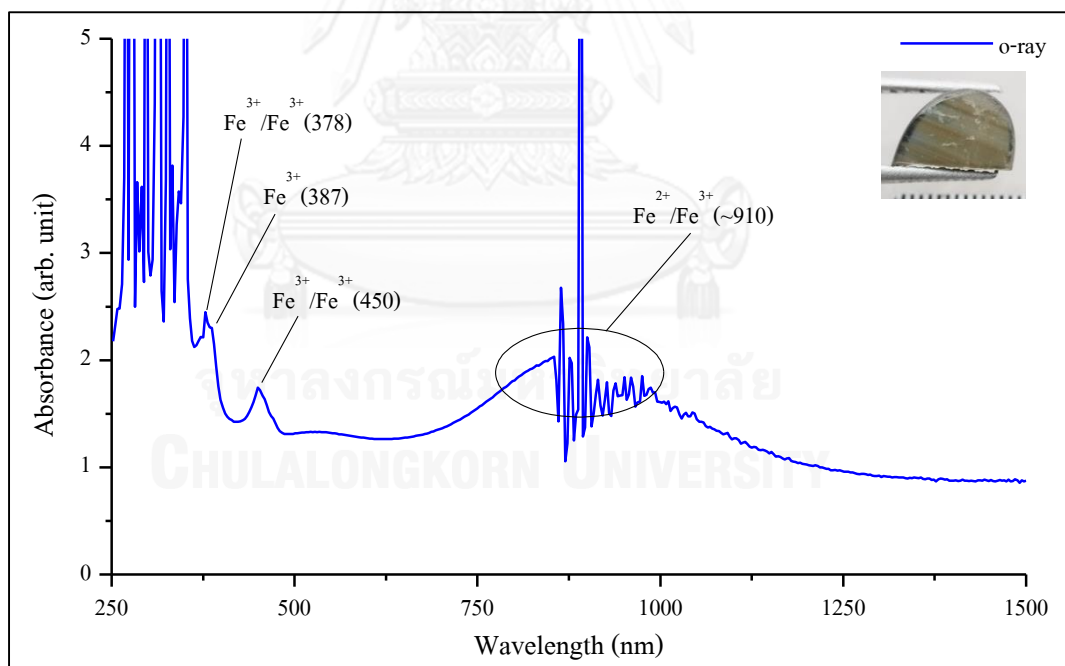


Figure 3.15 UV-Vis-NIR spectra of unheated sapphire with moderate silky inclusions (B7).

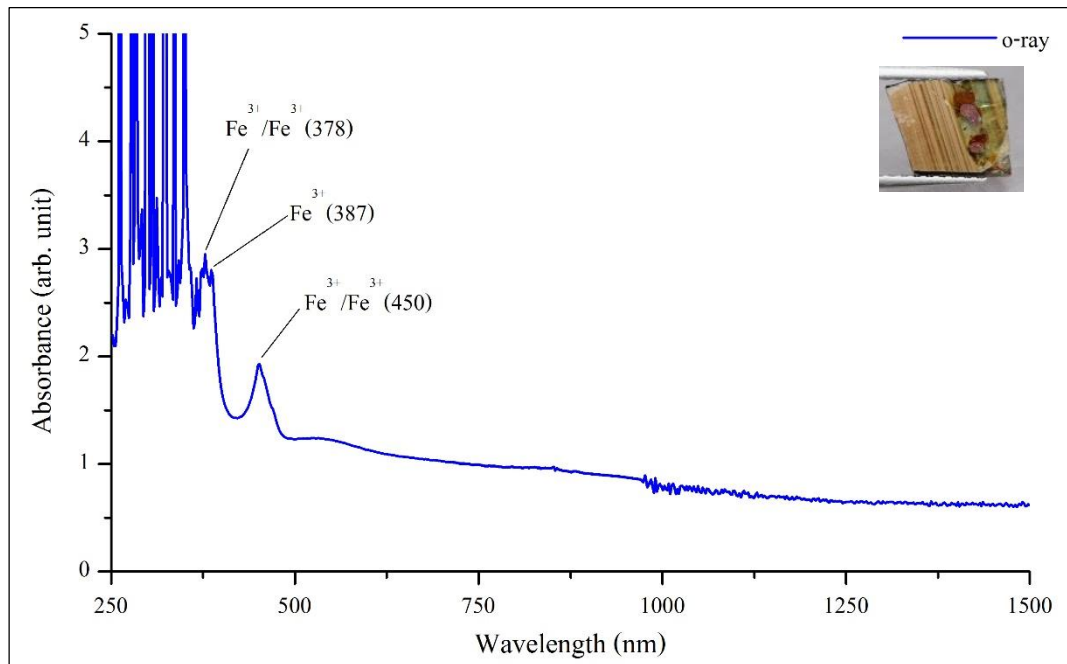


Figure 3.16 UV-Vis-NIR spectra of unheated sapphire with abundant silky inclusions (C4).

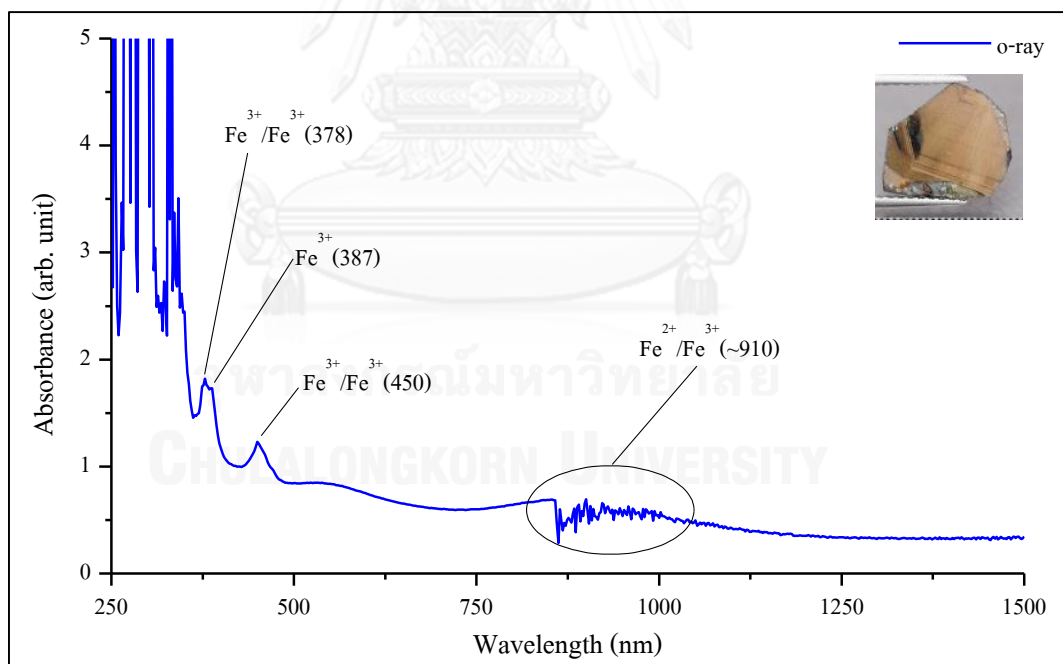


Figure 3.17 UV-Vis-NIR spectra of unheated sapphire with abundant silky inclusions (C5).

3.5 Fourier Transform Infrared Spectra

FTIR spectra revealed as transmittance of sapphires before heating are displayed in Figures 3.18 to 3.21. All sapphire groups appear to have similar pattern. In general, almost complete absorption below wavenumber 1500 cm^{-1} which is typical spectrum of corundum. Their spectra also show peaks at $3900\text{-}3400\text{ cm}^{-1}$ due to moisture (H_2O), $2924\text{-}2919\text{ cm}^{-1}$ and $2853\text{-}2848\text{ cm}^{-1}$ due to C-H stretching, $2364\text{-}2359\text{ cm}^{-1}$ and $2345\text{-}2339\text{ cm}^{-1}$ due to CO_2 (as described by Smith, 1995). The moisture and CO_2 appear to be influenced by ambient air in the sample chamber or in open fracture whereas the C-H stretching is likely contamination of organic substance on sapphires surface. Inverting of CO_2 peak may be caused by lower CO_2 content during measurement than the background measurement (Volynet et al., 1969; 1972). In addition, some samples show peaks at 3695 and 3625 cm^{-1} due to kaolinite mineral phases which commonly encountered in basaltic-related sapphire as form of soil particle. The presence of these minerals phases indicates that the sample is not subject to heat treatment (Beran and Rossman, 2006; Thirangoon, 2009)

Sapphire samples with minor silk inclusions usually show very small peaks at about 3309 cm^{-1} (e.g., A2, A6, A9, and A11). All samples show peaks at $3900\text{-}3400\text{ cm}^{-1}$, $2924\text{-}2919\text{ cm}^{-1}$ and $2853\text{-}2848\text{ cm}^{-1}$, $2364\text{-}2359\text{ cm}^{-1}$ and $2345\text{-}2339\text{ cm}^{-1}$ (Figure 3.18).

Most samples (e.g., B1, B5, B6, B8, B9, B10, B12, B14, B15, B16 and B17) in moderate silky inclusions group also show small peaks at about 3309 cm^{-1} . Moreover, some samples (e.g., B5, B11, B12, B13 and B14) show broad band between $3400\text{-}3300\text{ cm}^{-1}$. Only one sample (B17) in this group shows sharp peaks around 3691 , 3648 and 3619 cm^{-1} related to Kaolinite group mineral (Beran and Rossman, 2006). All samples show peaks at $3900\text{-}3400\text{ cm}^{-1}$, $2924\text{-}2919$ and $2853\text{-}2848\text{ cm}^{-1}$, $2364\text{-}2359\text{ cm}^{-1}$ and $2345\text{-}2339\text{ cm}^{-1}$ (Figure 3.19 and 3.20).

Sapphire samples with abundant silky inclusions which are mostly opaque; consequently, infrared transmission is poorly obtained from these samples. Only one sample in this group (C2) presents small peak at about 3309 cm^{-1} . Many samples (e.g., C2, C3, C4, C6, and C8) show sharp peaks around 3691 , 3648 and 3619 cm^{-1}

(Beran and Rossman, 2006). Most samples in this group show peaks at 3900-3400 cm^{-1} , 2924-2919 and 2853-2848 cm^{-1} , 2364-2359 and 2345-2339 cm^{-1} (Figure 3.21).

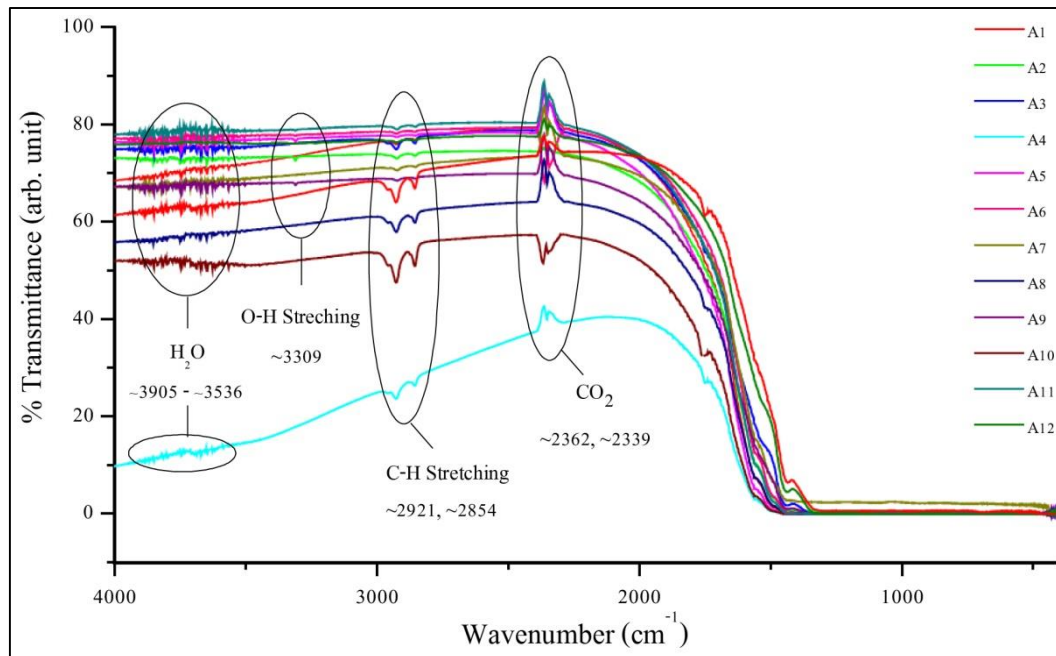


Figure 3.18 FTIR spectra of unheated sapphires with minor silky inclusions (Group A).

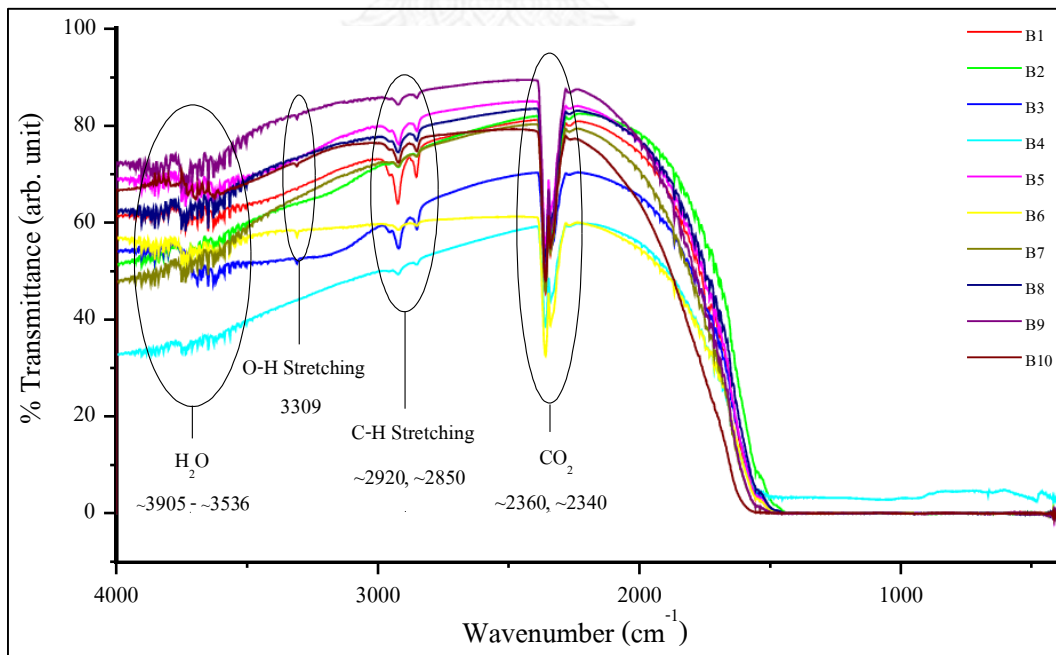


Figure 3.19 FTIR spectra of unheated sapphires with moderate silky inclusions (Group B).

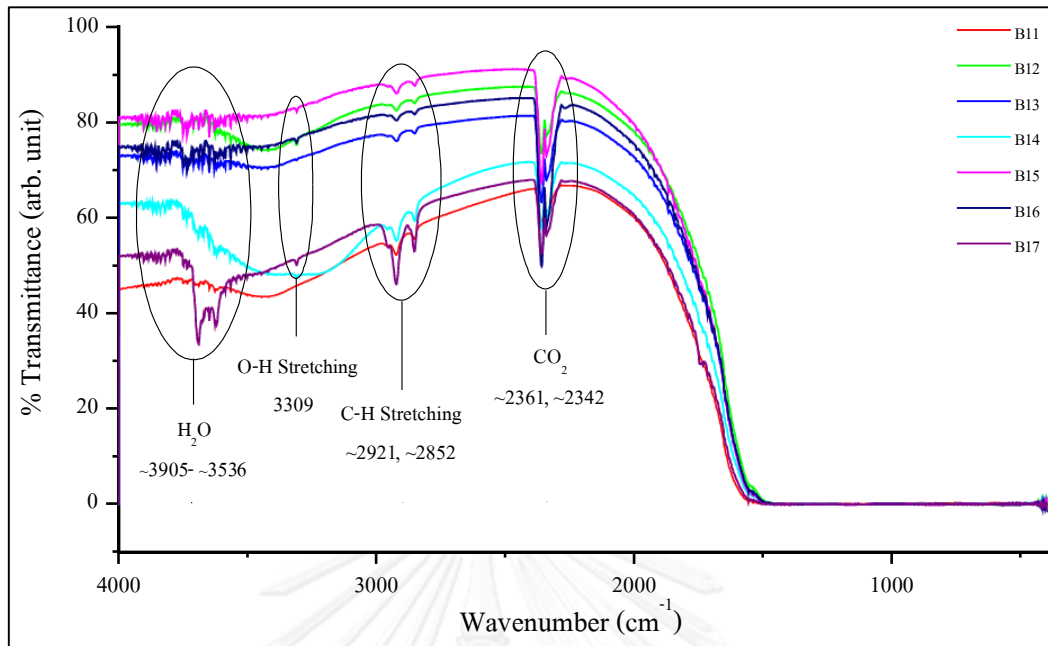


Figure 3.20 FTIR spectra of unheated sapphires with moderate silky inclusions (Group B) (continue).

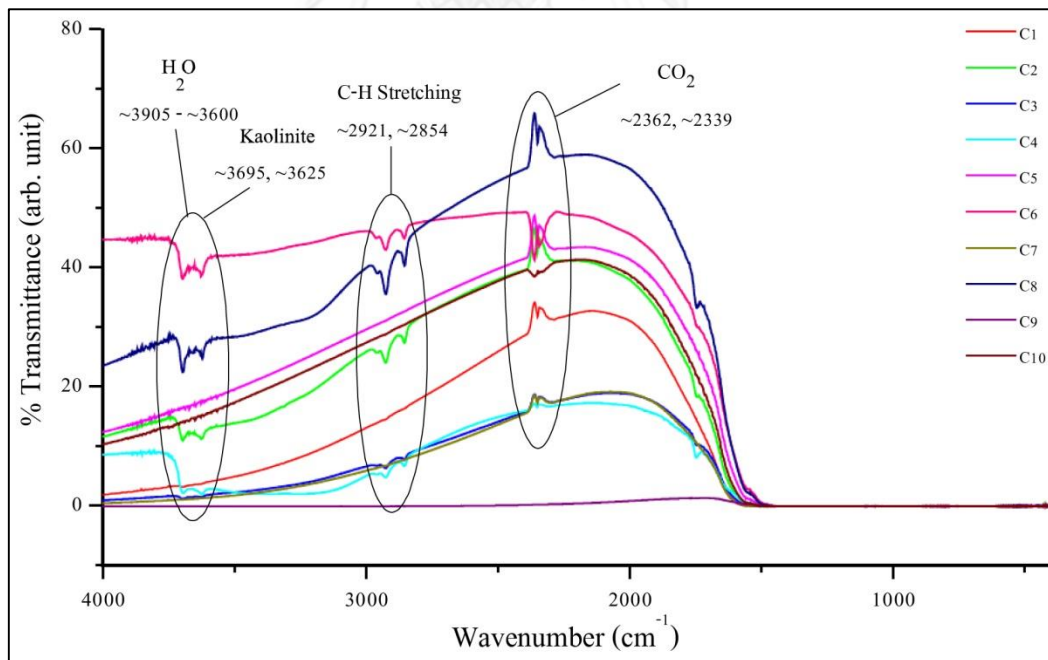


Figure 3.21 FTIR spectra of unheated sapphires with abundant silky inclusions (Group C).

CHAPTER IV

HEATING EXPERIMENT

4.1 Heating Cycle

The experimental heat treatment was set based on optimum condition as previously reported (e.g., Themelis, 1992; Häger, 2001; Pattamalai, 2002; Sakkaravej, 2004; Lomthong, 2004; Pisutha-Arnond, 2006a and b; Somboon, 2006). Successive segments (i.e., heating up, soaking and cooling down) were set prior to heating process, automatically. Cleaned samples were heated at maximum temperatures of 1650 °C for 3 hours soaking time, period of heating at maximum temperature, within an ambient air (oxidizing atmosphere). Heat-up segment was started from room temperature to maximum temperature at about 4 °C/minute. The cooling rate was programmed at approximately 3-4 °C/minute. The cooling segment was started at the end of soaking segment until reaching approximately 1000 °C: then, sapphires samples were taken out from the furnace for rapid quenching to room temperature. Alterations of color, clarity as well as other external and internal appearances were observed after heating experiment which all results are reposted herein this chapter.

4.2 Color and Clarity

The experimental results of all samples in each group are shown in Figures 4.1 to 4.4, respectively. Alterations of color and clarity after heating at 1650 °C can be compared with original appearances in detail below.

Sapphires with Minor Silky Inclusions (Group A): color appearances of light green to light bluish green samples with zones of brown silky inclusion before and after heating at 1650 °C are displayed in Figure 4.1. Most samples with zones of grey-brown silky inclusions (e.g., samples A1, A2, A3, A5, A6, A7, A8 and A9) were turned to blue after heating. On the other hand, some samples without silky inclusions zone (e.g., A2, A10, A11, and A12) appeared to lose blue shade but yellow shade was produced after heating. However, clarity of all samples was improved.

Sapphires with Moderate Silky Inclusions (Groups B): color appearances of green to greenish blue samples with zones of grey-brown silky inclusions before and after heating at 1650 °C are displayed in Figures 4.2 and 4.3. All the samples were turned to blue, particularly along their grey-brown silky inclusions zone, after heating. However, some samples (e.g., B6) were lost blue shade and changed to green shade after heating. Clarity of all samples was improved.

Sapphires with Abundant Silky Inclusions (Group C): color appearances of grey-brown samples with abundant silky inclusions before and after heating at 1650 °C are displayed in Figure 4.4. All the samples containing abundant grey-brown silky inclusions were turned to blue-deep blue after heating; although, their clarities were slightly improved.

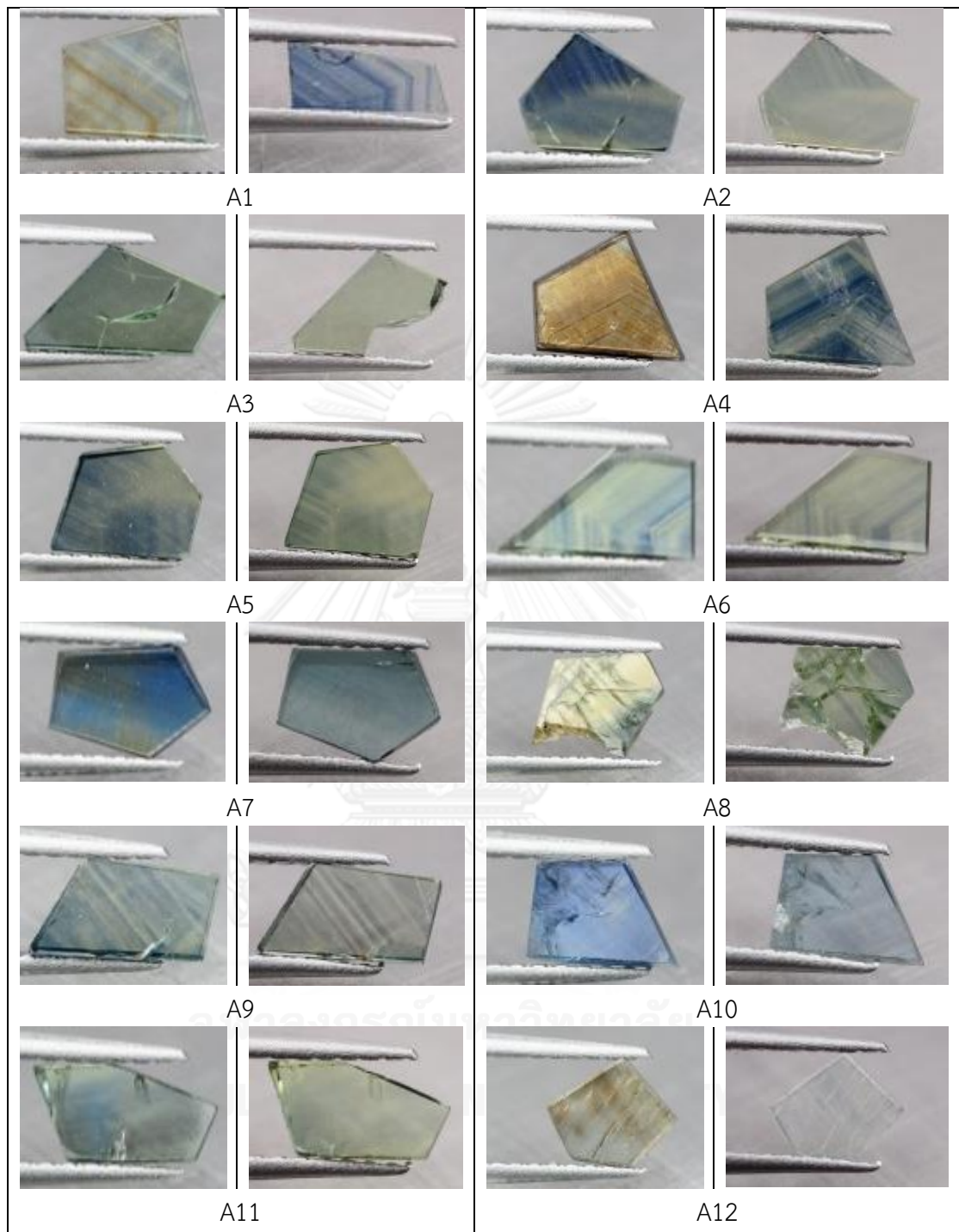


Figure 4.1 Color and clarity appearances of sapphires with minor silky inclusions (Group A) before heating (left) and after heating at 1650 °C (right).

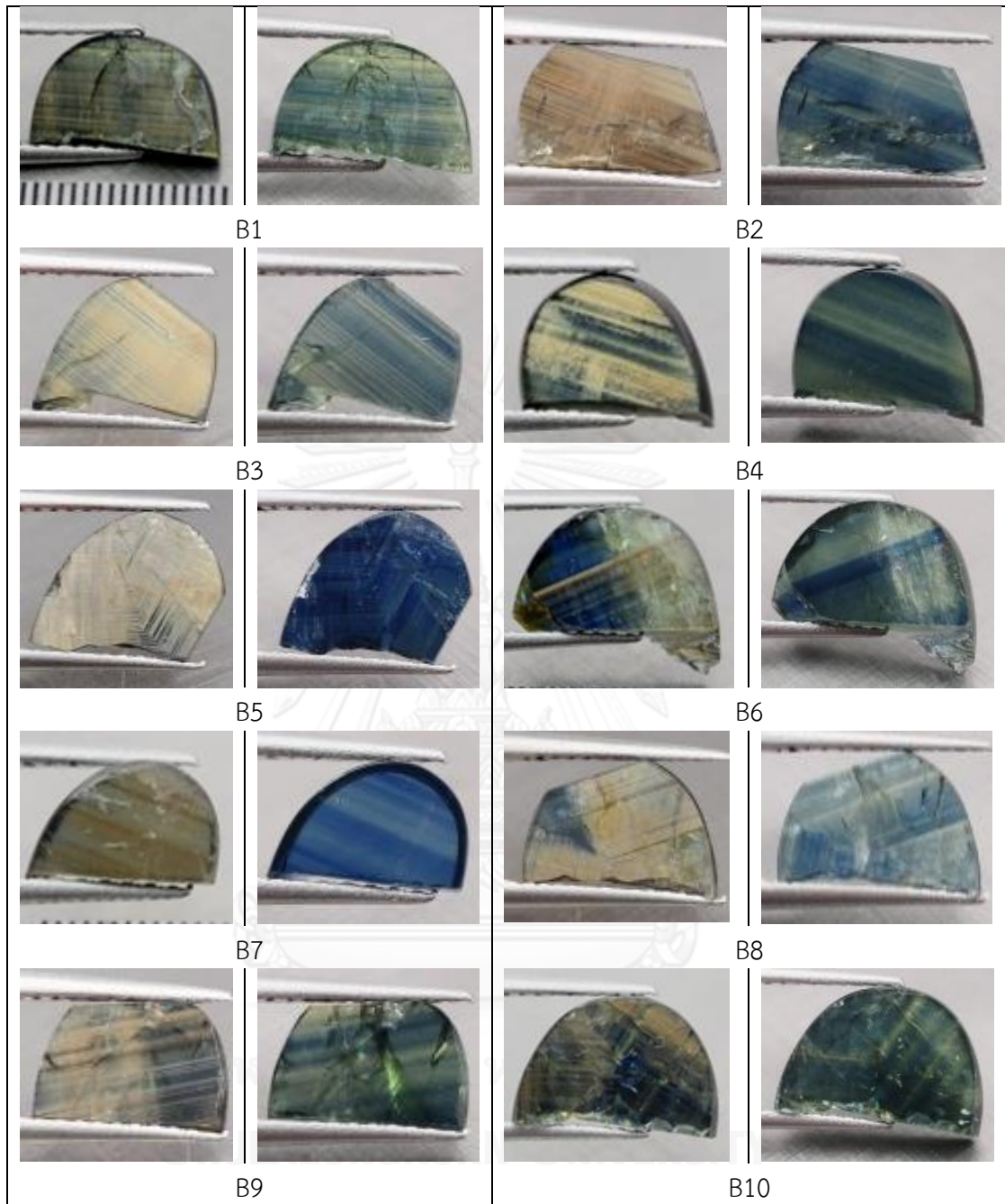


Figure 4.2 Color and clarity appearances of sapphires with moderate silky inclusions (Group B) before heating (left) and after heating at 1650 °C (right).

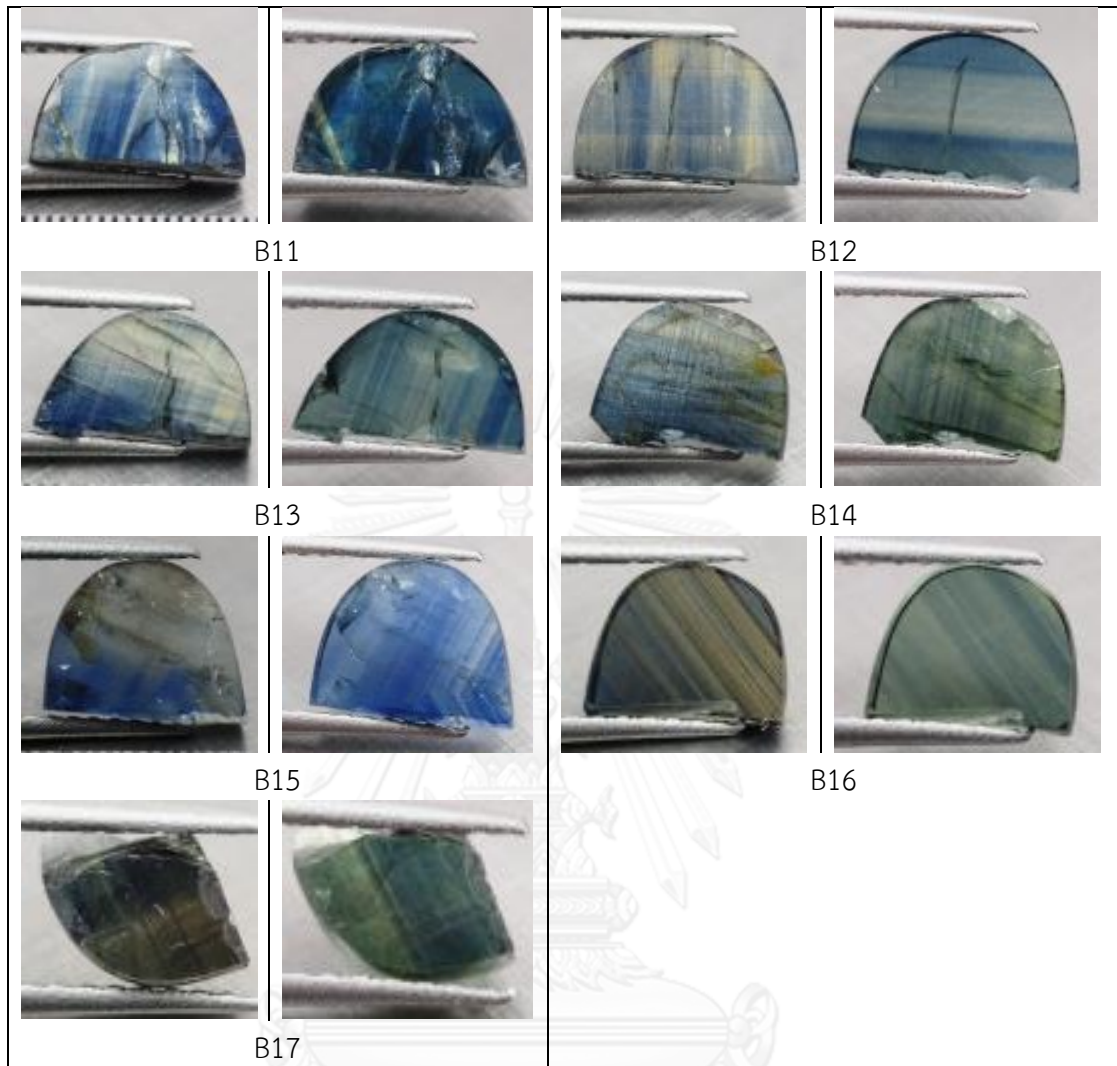


Figure 4.3 Color and clarity appearances of more sapphire samples with moderate silky inclusions (Group B) before heating (left) and after heating at 1650 °C (right).

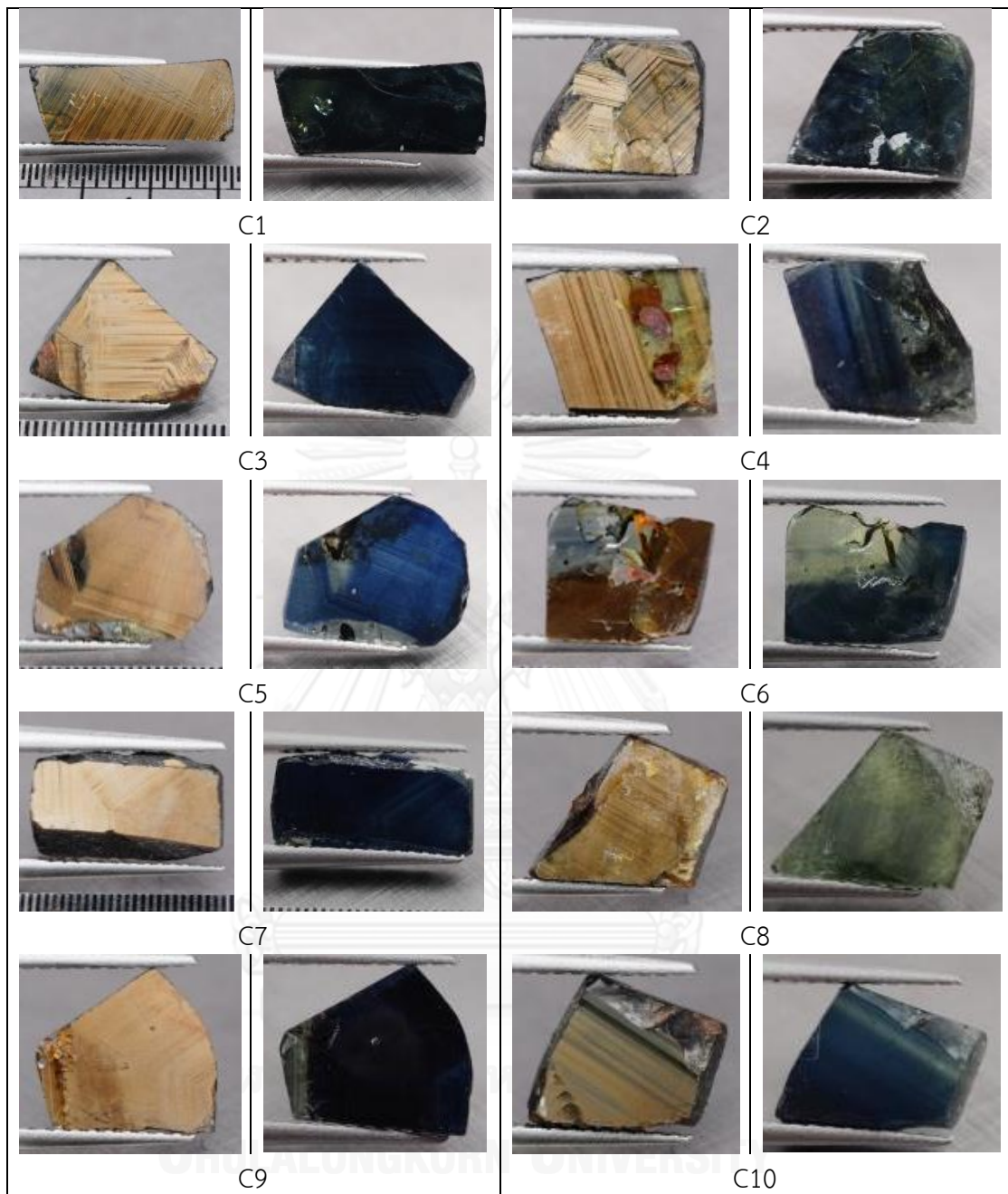


Figure 4.4 Color and clarity appearances of sapphires with abundant silky inclusion (Group C) before heating (left) and after heating at 1650 °C (right).

4.3 Alterations of Inclusions

Exsolved Silky Inclusions: are usually brown or gray. High temperature heat treatment appears to dissolve partially or completely some particles of these silky inclusions which are often incorporated chemically into the sapphire host causing internal diffusion. Consequently, some of these inclusions produced intense color surrounding their grains, so called blue bleeding (Figures 4.5 - 4.9). In addition, some sample displayed pattern of dot-like minute dissolved particles (Figures 4.10). The temperature 1650 °C may imply the ranges of dissolution temperature or eutectic temperature between silky inclusions and Al₂O₃ host as reported by Muan & Gee (1955); Feenstra et al. (2005).

A hematite inclusion is usually found in sapphire sample with abundant silky inclusions group. It appears to be altered at 1650 °C and it may be dissociated, decomposed and partially melted at this temperature. It lose luster and turned to blackish residue in cracks of host sapphire (Figure 4.11).

Fluid-healed fractures or fingerprints were commonly found in all groups of the host sapphire. However, they are unclearly observed due to abundant silky inclusions. Fingerprints turned to be developed and expanded after heating at 1650 °C in some samples (see Figure 4.12).

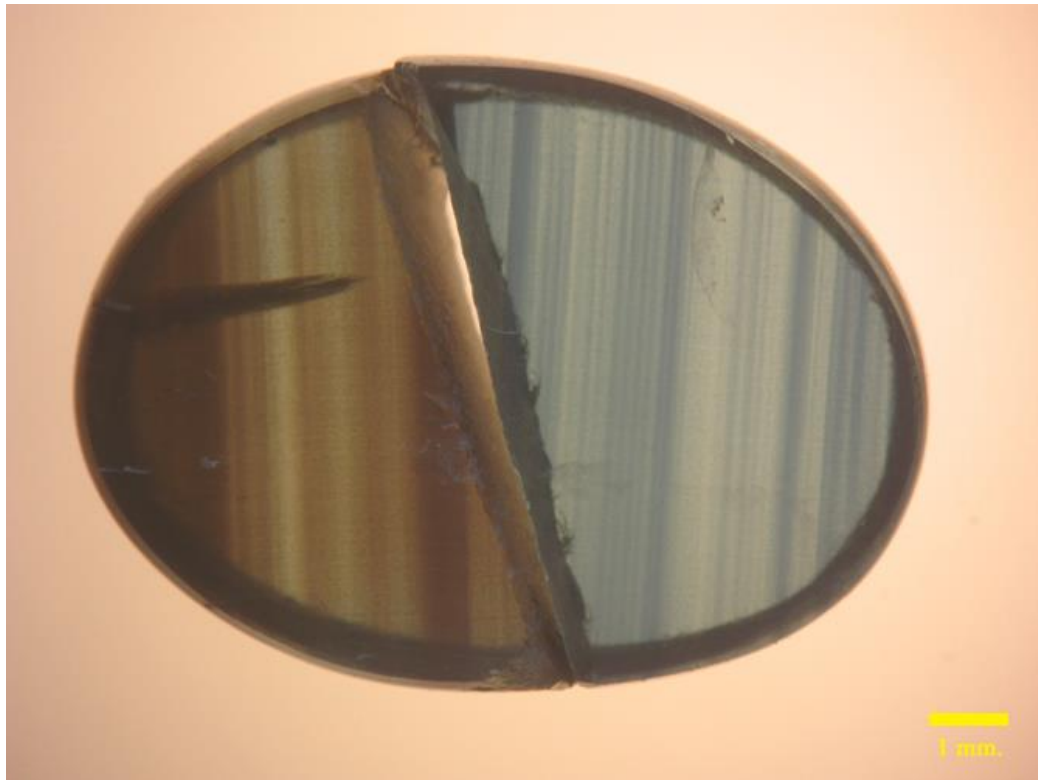
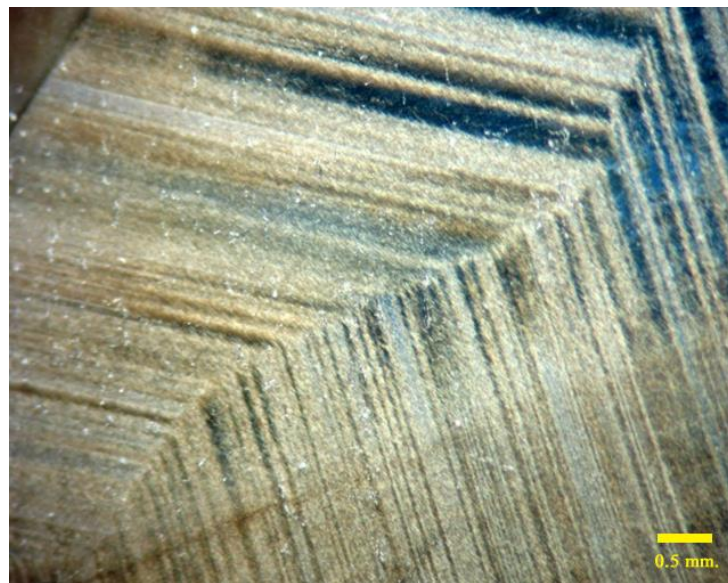


Figure 4.5 Comparison of sapphire sample between before heat treatment (left) and after heat treatment at 1650 °C (right) which silky inclusions appear to have dissolved into sapphire host lead to development of blue color and clarity (Sample B7).

Unheated



Heated at 1650 °C

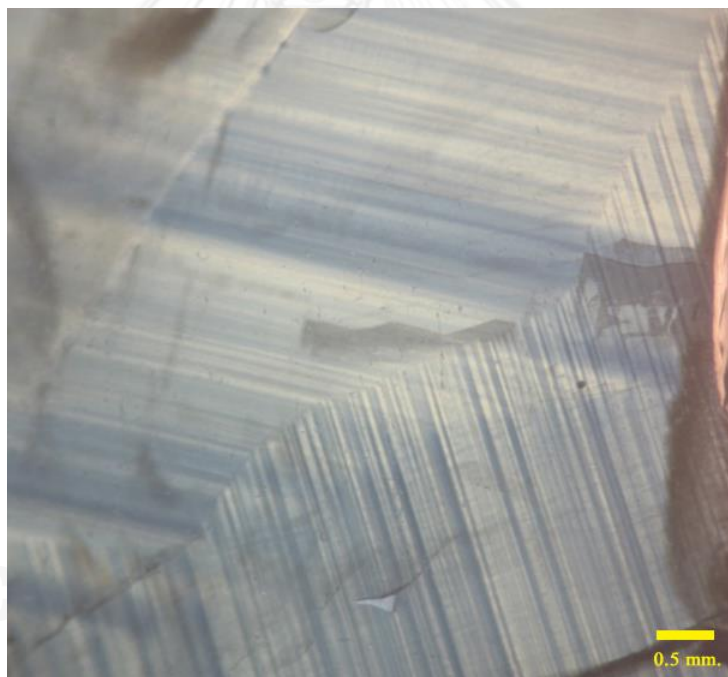
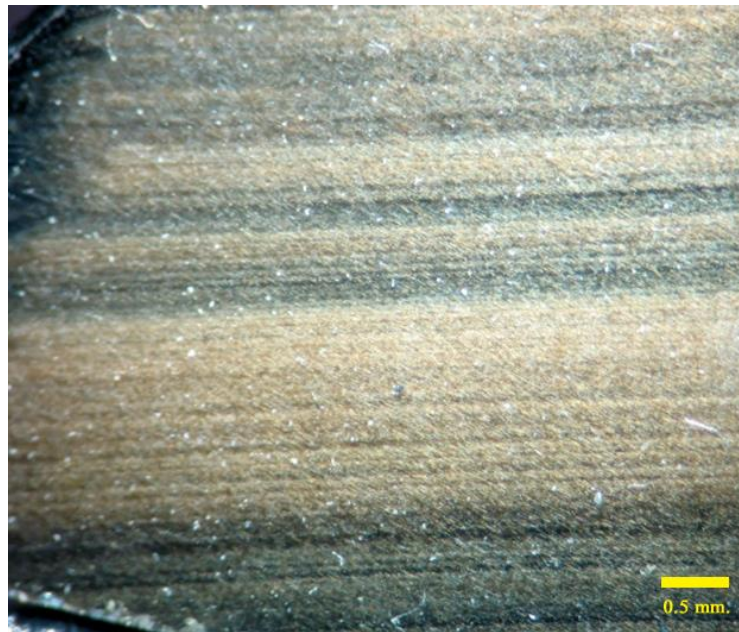


Figure 4.6 Silky inclusions were altered from brown to blue after heating at 1650 °C. These inclusions partly disappeared and produced intense blue color concentrations after heating (Sample B3).

Unheated



Heated at 1650 °C

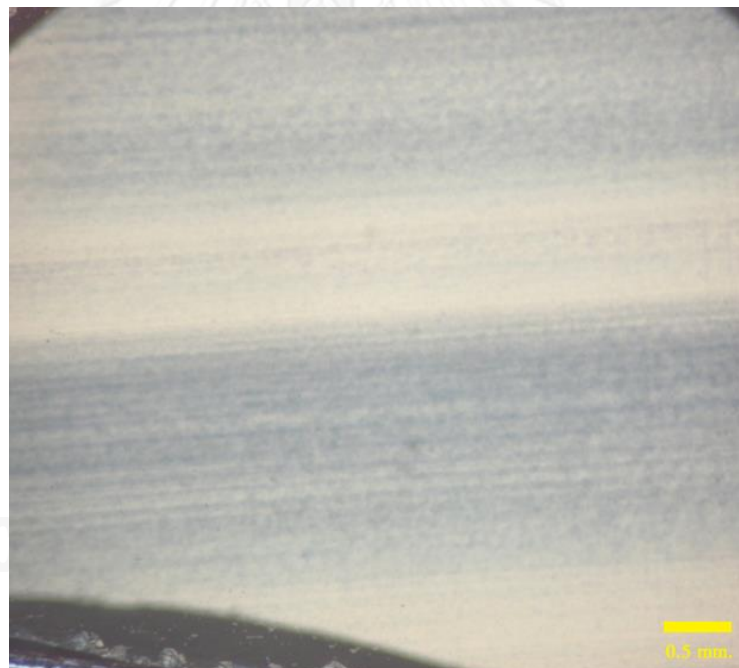


Figure 4.7 After heating at 1650 °C, silky inclusions were partly dissolved and altered from brown to blue. Intense blue color can be observed around silky zone (Sample B4).

Unheated



Heated at 1650 °C

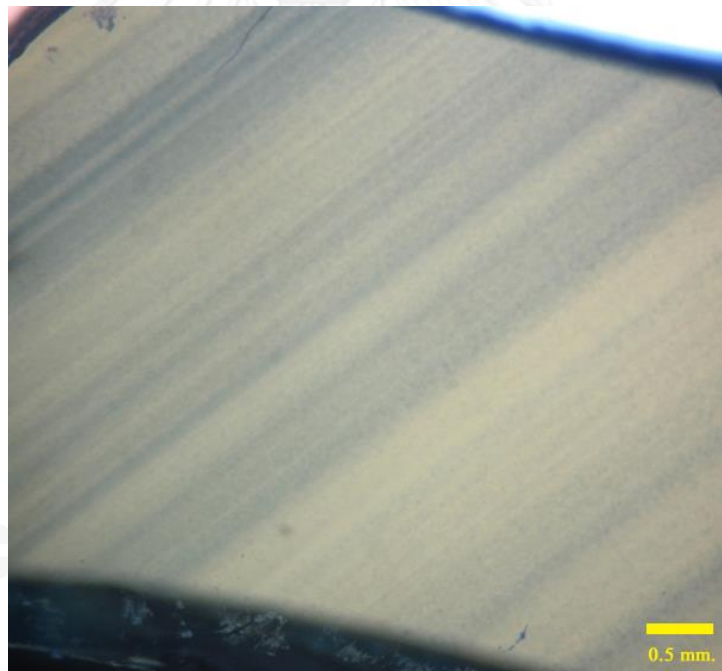


Figure 4.8 Silky inclusions before and after heating at 1650 °C, they were partly dissolved and altered from brown to blue (Sample B16).

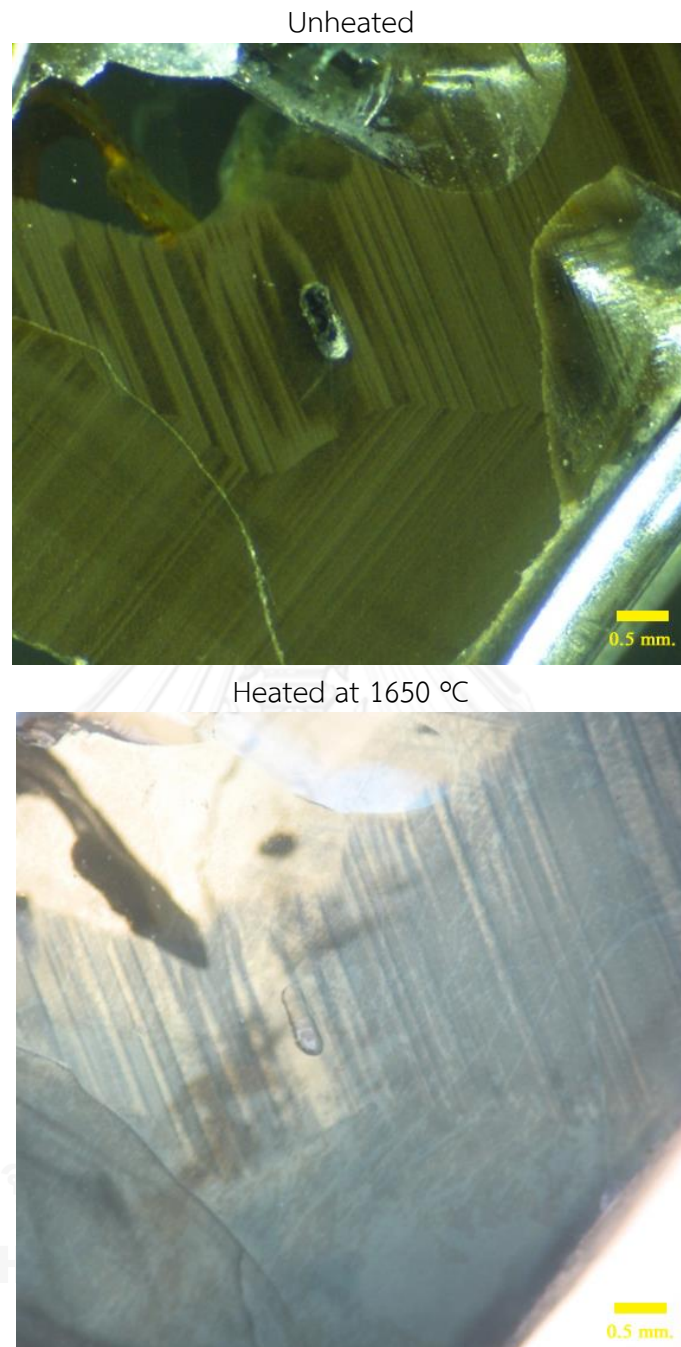


Figure 4.9 Silky inclusions before and after heating at 1650 °C, they were dissolved and altered from brown to blue (Sample C6).

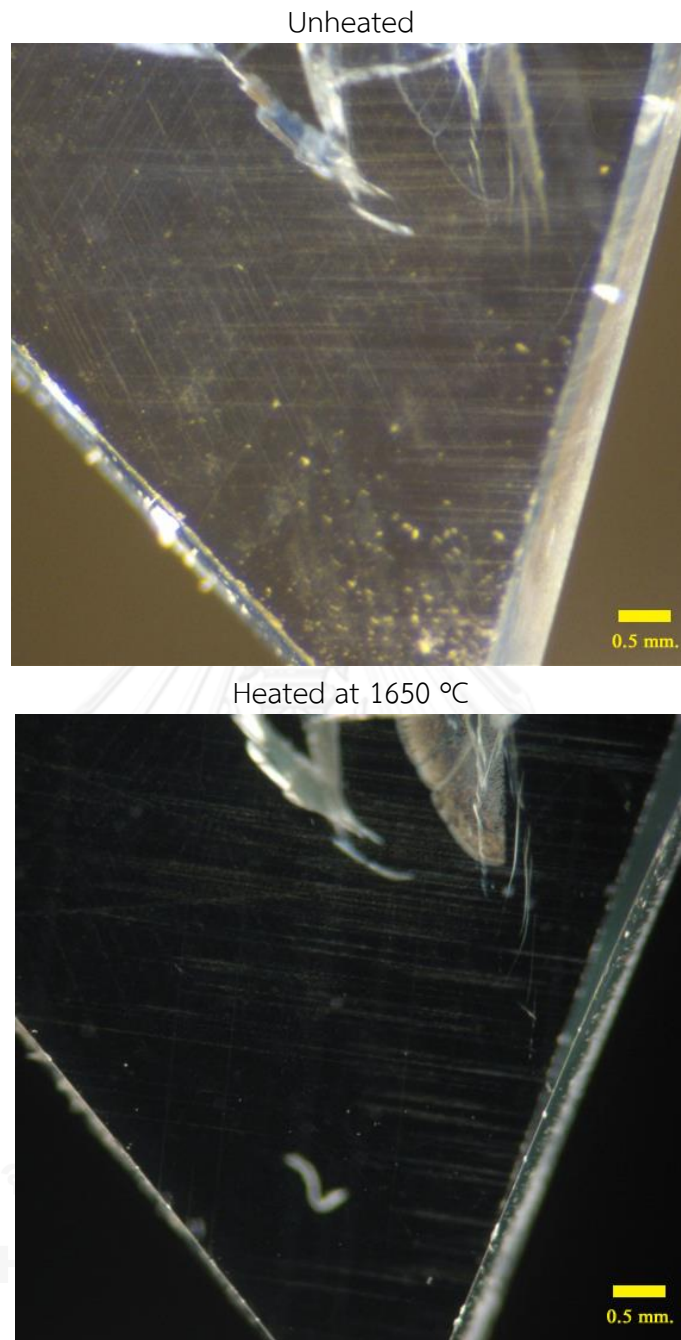


Figure 4.10 The long needle inclusions with $60^\circ/120^\circ$ intersecting angles in sapphire sample with minor silky inclusion were partially dissolved to dot-like pattern after heating at 1650 °C (A10).

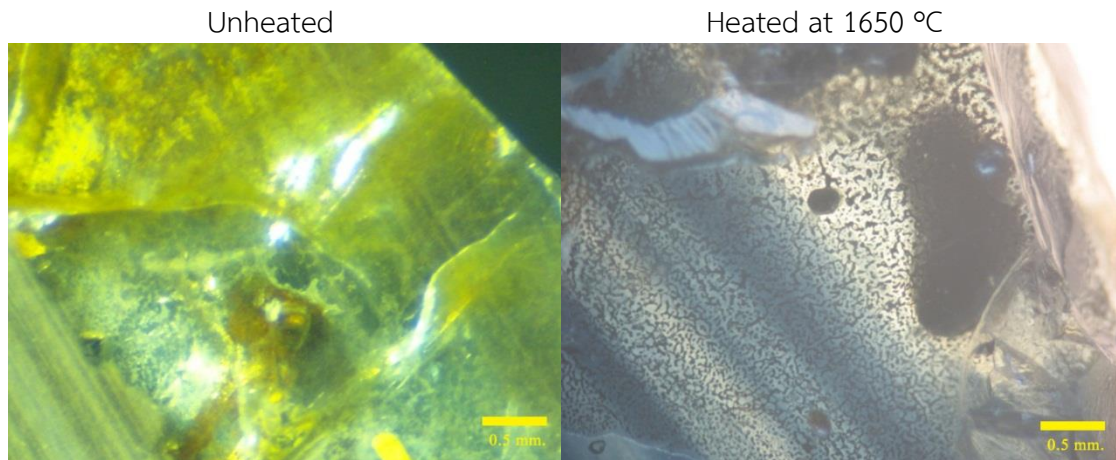


Figure 4.11 A large hematite mineral inclusion which identified by Raman spectroscopy was partially melted and then became obviously residue in cracks of host sapphire. Its luster was lost and turned to blackish appearance (C4).

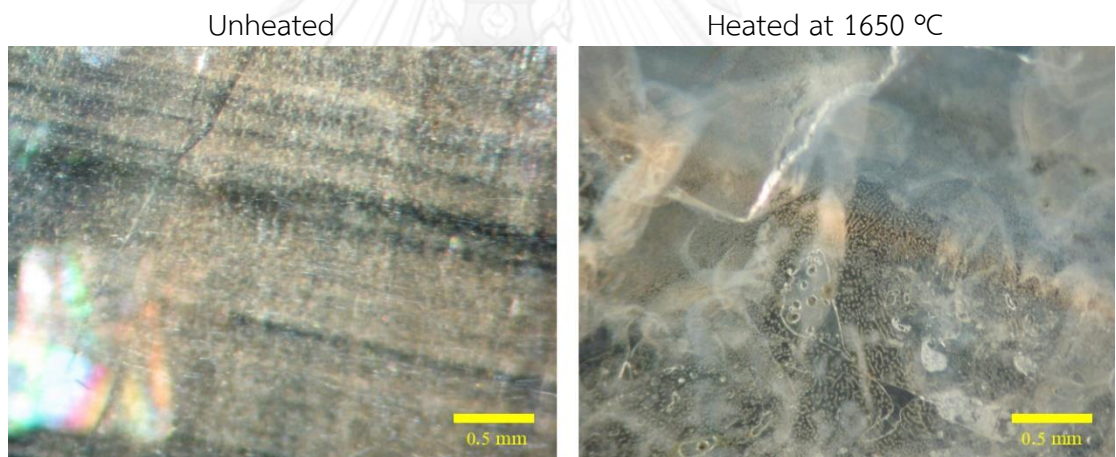


Figure 4.12 The subsurface fingerprints were appeared and developed expansively after heating at temperature 1650 °C in representative samples such as in B1.

4.4 UV-Vis-NIR Spectra

Absorption spectrum in the ranges of ultraviolet (UV), visible light (Vis) and near infrared (NIR), mainly direct effect to the color appearances of sapphires as well as those of other gemstones, was analyzed both before and after heating. It is expected to give important information on the causes of colors and changes after heating. Some selected spectra are displayed in Figures 4.13 to 4.16 and more samples are collected in Appendix III. The absorption spectra of sample before and after heating at 1650 °C were compared in the same diagram; however, these spectra are somehow different in the baseline levels caused by a slightly different condition during measurement. Consequently, spectrum subtraction was therefore considered to present different absorptions between before and after heating of the stone. Spectrum of sample after heating was subtracted by initial absorption spectrum of the same stone. The remaining peak in the positive zone indicates that absorption was increased after heating whereas reverse peak located in the negative zone apparently reflect reduction of the absorption after heating.

The UV-Vis-NIR spectra (o-rays) of initial samples in all groups showed absorption peaks due to Fe^{3+} at 450, 388 and 377 nm which are normally present in the high iron-containing sapphires. In addition, some samples containing blue zones or patches present absorption bands due to $\text{Fe}^{2+}/\text{Ti}^{4+}$ and $\text{Fe}^{2+}/\text{Fe}^{3+}$ intervalence charge transfers (IVCT) with the maxima about 565 nm and 910 nm, respectively. As the color of most samples was obviously changed after heat treatment, the residue spectra after subtraction usually show the shifted absorption line. Grey-brown zones of silky inclusions in unheated sapphires were obviously turned to intense blue zone after heating at 1650 °C. As the results, there were clearly changed in absorption pattern (mostly up direction) which indicate the cause of color changed due to $\text{Fe}^{2+}/\text{Ti}^{4+}$ IVCT incorporated with $\text{Fe}^{2+}/\text{Fe}^{3+}$ IVCT at about 565 nm and 910 nm, respectively (Burn, 1993; Häger, 2001; Somboon, 2006). The remaining spectra after subtraction show board band of $\text{Fe}^{2+}/\text{Fe}^{3+}$ IVCT at about 900 nm (Figures 4.13b to 4.16b). Moreover, some sapphire samples in Group A (e.g., A2, A10, A11, and A12) and sample B6 of Group B were lost blue body color after heating due to changing of ferrous (Fe^{2+}) to ferric (Fe^{3+}) by heating under ambient air (oxidizing atmosphere). This causes reduction of ferrous iron (Fe^{2+}); consequently, $\text{Fe}^{2+}-\text{Ti}^{4+}$ IVCT, the main cause of blue coloring in sapphire is destroyed (Figures 4.16).

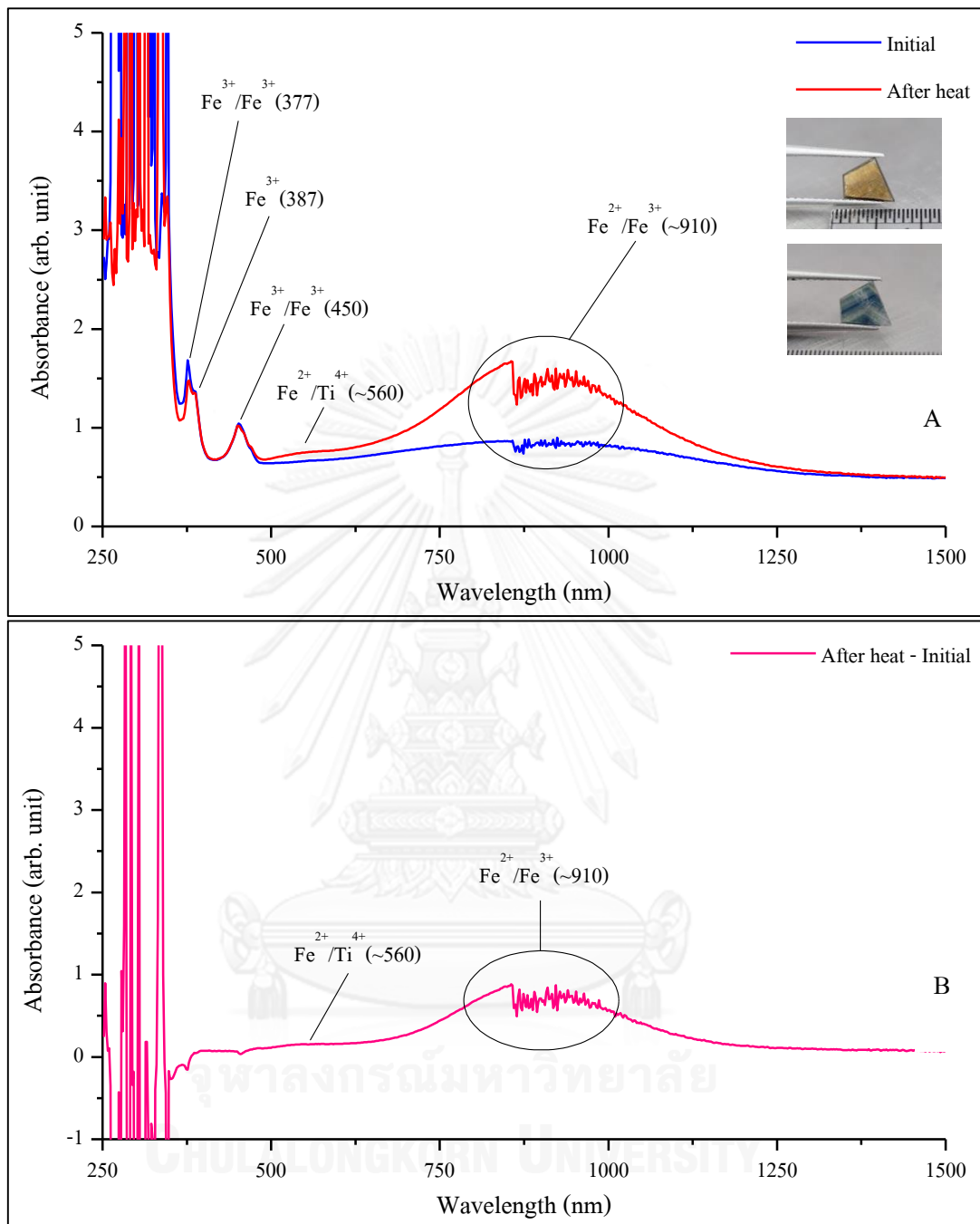


Figure 4.13 A) Typical UV-Vis-NIR absorption spectra (o-ray) of sapphires in minor silky inclusions (A4) before and after heating at 1650 °C. B) The remaining spectrum after subtraction of heated stone's spectrum from original spectrum.

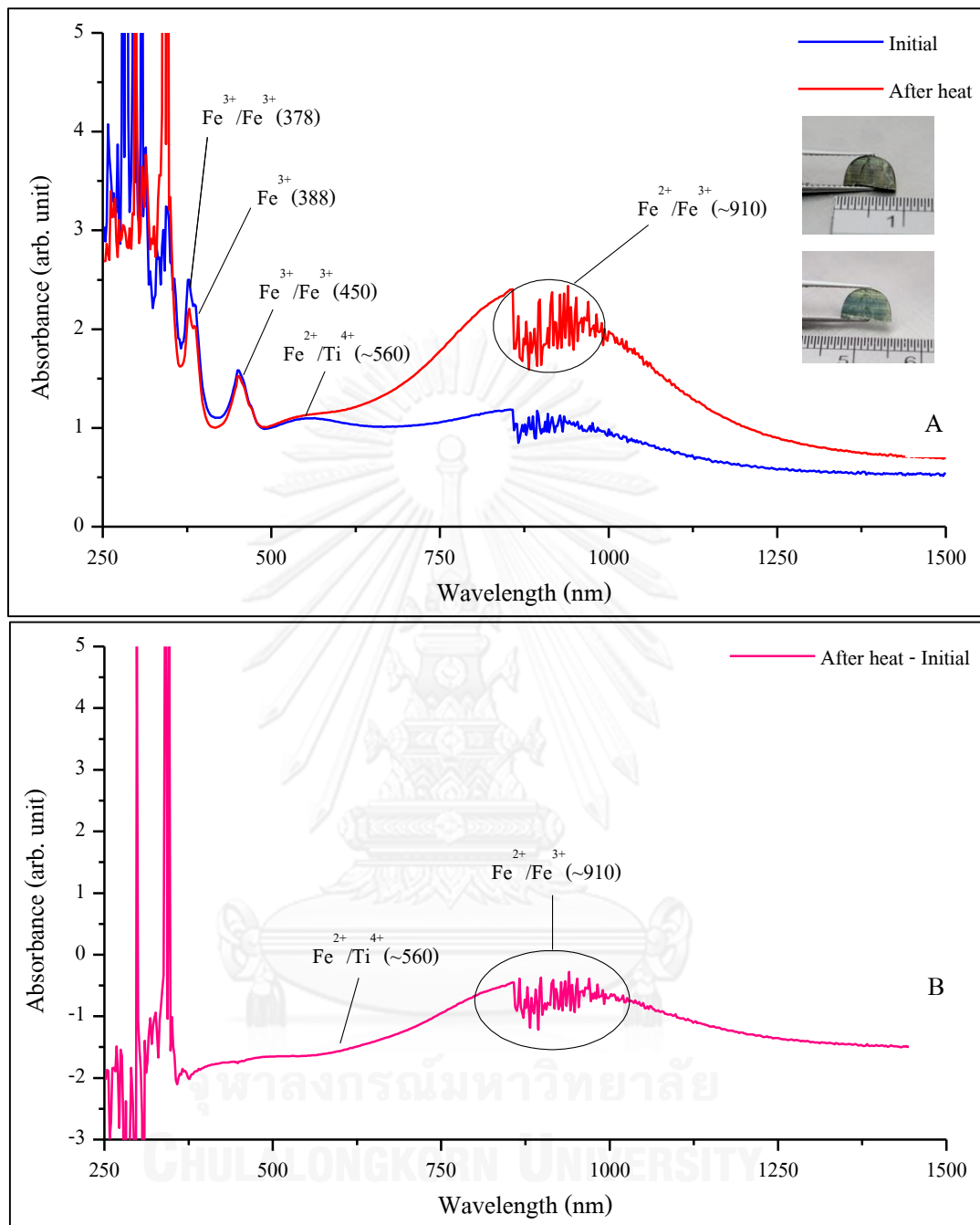


Figure 4.14 A) Typical UV-Vis-NIR absorption spectra (o-ray) of sapphires in moderate silky inclusions (B1) before and after heating at 1650 °C. B) The remaining spectrum after subtraction of heated stone's spectrum from original spectrum.

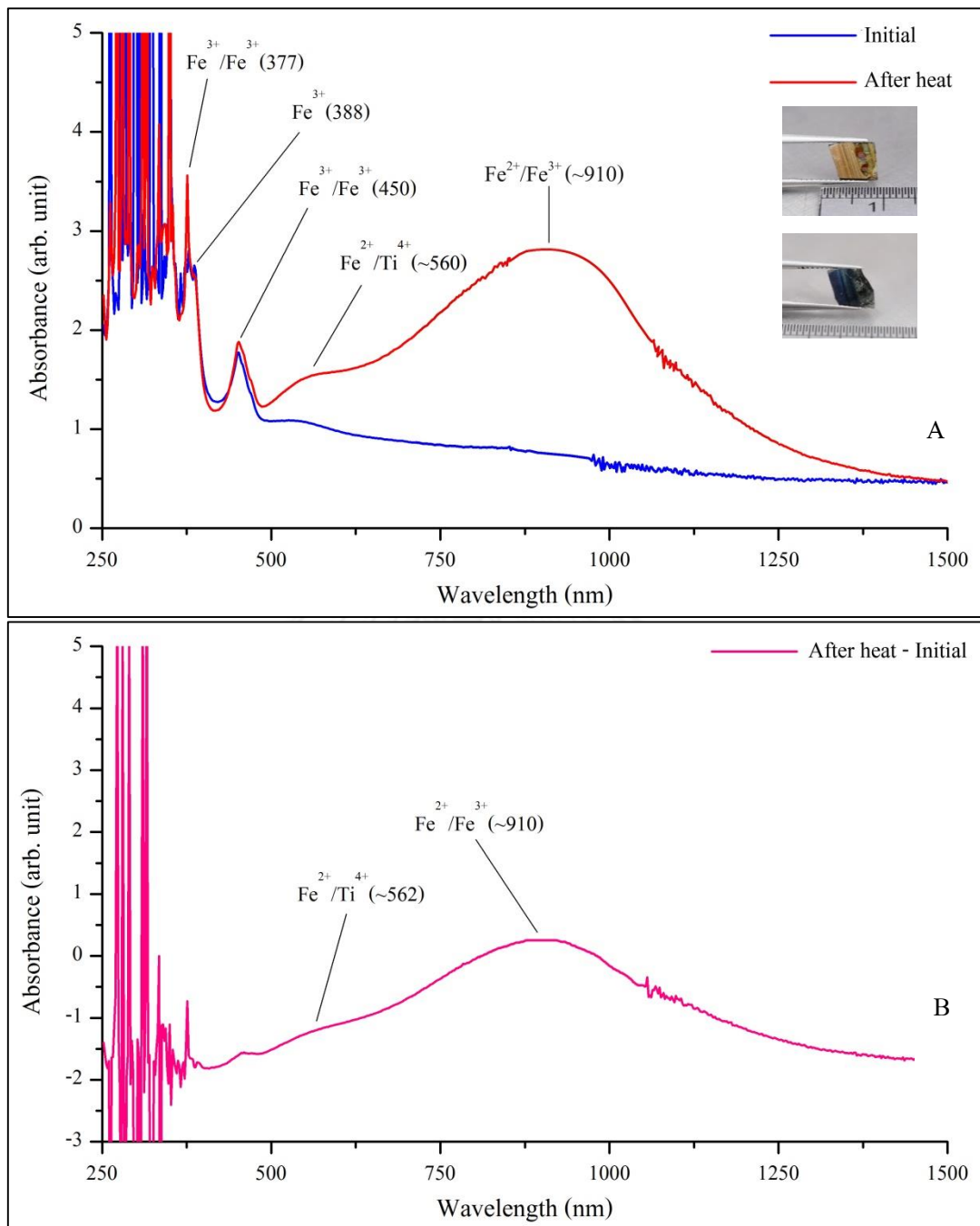


Figure 4.15 A) Typical UV-Vis-NIR absorption spectra (o-ray) of sapphires in abundant silky inclusions (C4) before and after heating at 1650 °C. B) The remaining spectrum after subtraction of heated stone's spectrum from original spectrum.

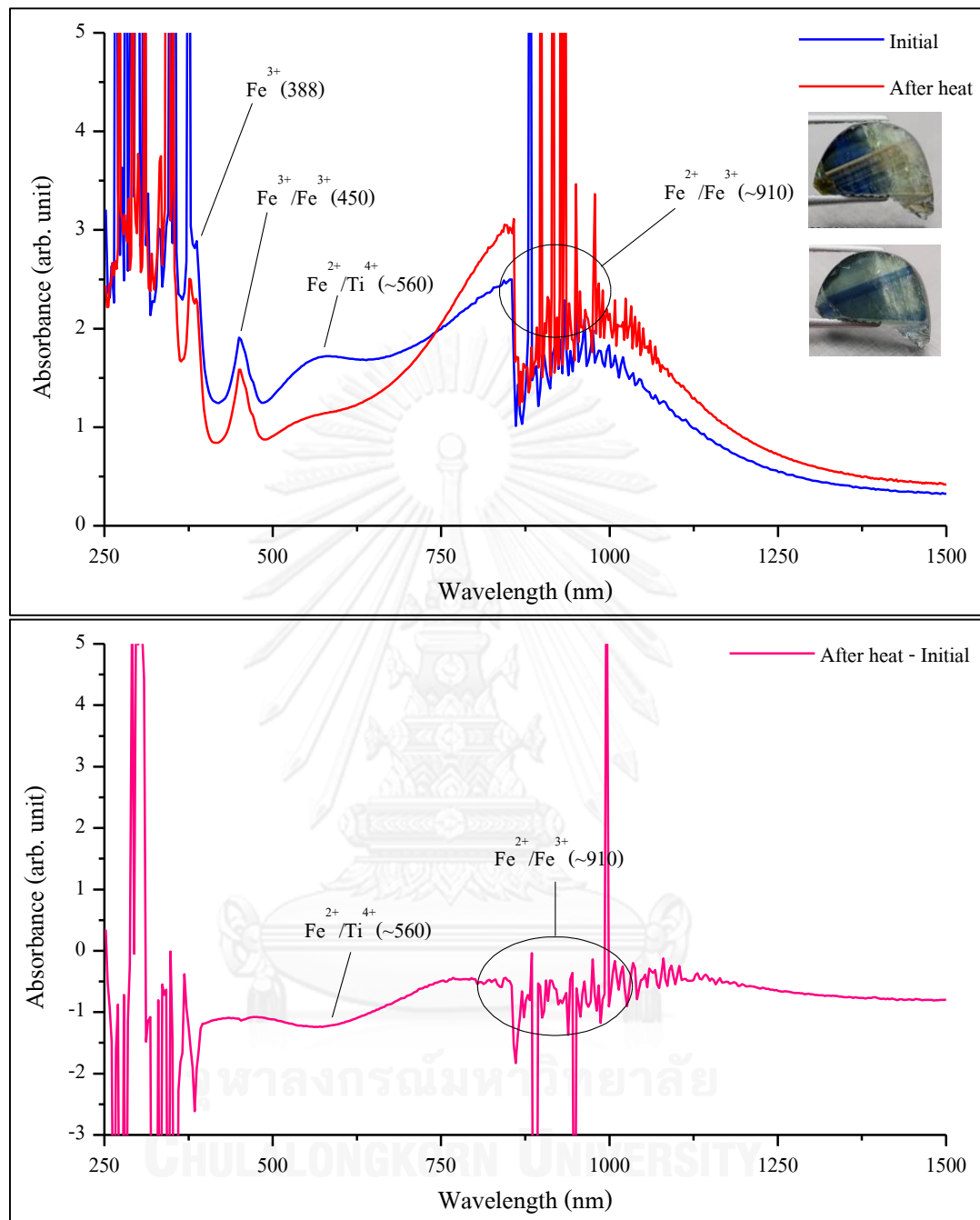


Figure 4.16 A) Representative of sample in group B (B6) were lost blue shade after heating under ambient air due to reduction of charge transfer process with $\text{Fe}^{2+}\text{-Ti}^{4+}$ pairs. B) The remaining spectrum after subtraction of heated stone's spectrum from original spectrum.

4.5 Fourier Transform Infrared Spectra

The incorporation of hydrogen in corundum has been a topic of study by many researchers (e.g., Volynets et al., 1969; 1972; Smith, 1995; Yan, 1995; Pattamalai, 2002; Sakkaravej, 2004; Beran and Rossman, 2006). Most of previous works reported that the structural bonding and stretching of OH groups in corundum has been recorded in both synthetic and natural corundum. The OH absorption peak was much more typically recorded in blue sapphire from basaltic source than ruby and sapphire from metamorphic source. The absorption peak of the OH stretching of hydrothermal synthetic corundum was stronger than natural and other synthetic corundums. Volynets et al. (1972) reported that hydrogen atoms are typically incorporated within the structure of corundum as a charge compensation mechanism. They may be bound to various trace transitional metal ions, occupying interstitial sites between two oxygen atoms (O^{2-}) or may also be trapped by cation vacancies. Systematic measurements were taken place for all samples before and after heating.

Representative FTIR spectra of sapphire samples before and after heating are shown in Figures 4.17 to 4.20 whereas all FTIR spectra collected in this study are displayed in Appendix II. They show crucially the same pattern. After heating, the H_2O absorption peaks are decreased or disappeared probably due to losing water in open fractures or moisture on the surface. Most samples do not show OH absorption peak at 3309 cm^{-1} or broad band between 3200 cm^{-1} to 3400 cm^{-1} before heating and after heating (Figure 4.17). The very small OH absorption peak or broad band present in some samples (e.g., A2, B3, B6, B9, B10, B12, B14, B15, B16, B17) before heating and they were eliminated after heating. For examples, sapphire with moderate silky inclusions (B3) initially showed a weak OH absorption peak at 3309 cm^{-1} ; after heating at $1650\text{ }^\circ\text{C}$ for 3 hours, the grey-brown color zones were turned to blue, OH peak was disappeared (Figure 4.18). The OH peak of sapphire with moderate silky inclusions (B16) disappeared after heating at $1650\text{ }^\circ\text{C}$ (Figures 4.18 and 4.19). Other patterns of H_2O at $3900 - 3400\text{ cm}^{-1}$, pattern of C-H stretching at about 2920 and 2850 cm^{-1} , and patterns of CO_2 at about 2360 and 2340 cm^{-1} are possibly influenced by contamination. For examples, peaks of H_2O and CO_2 may be involved by vapor and air surrounding the sample whereas C-H stretching peaks may indicate organic oil film coated on the samples' surface. The kaolinite peaks at 3695 and 3625 may also be disappeared due to decomposing by heat treatment (Figure 4.20).

In addition, it should be notified that OH-stretching peak at about 3309 cm^{-1} is the most crucial for consideration of high temperature treatment in sapphire which is related to metamorphic occurrences. It may be used to indicate heat treatment of metamorphic sapphire but it is not the case for all basaltic sapphires under this study.



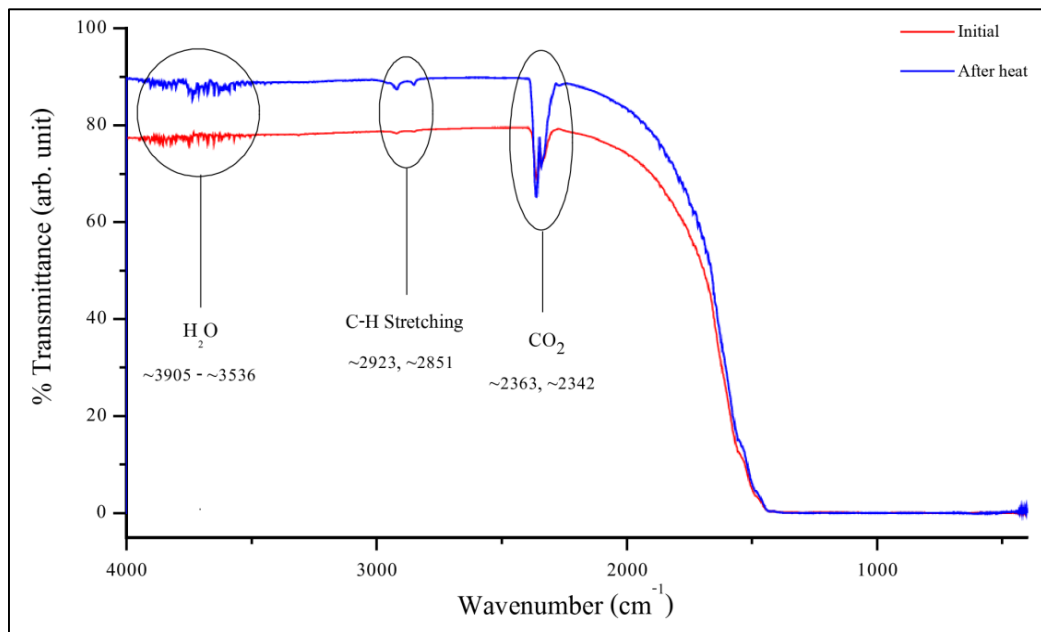


Figure 4.17 FTIR spectra of sapphire with minor silky inclusions (A6) before and after heating at 1650 °C under ambient air.

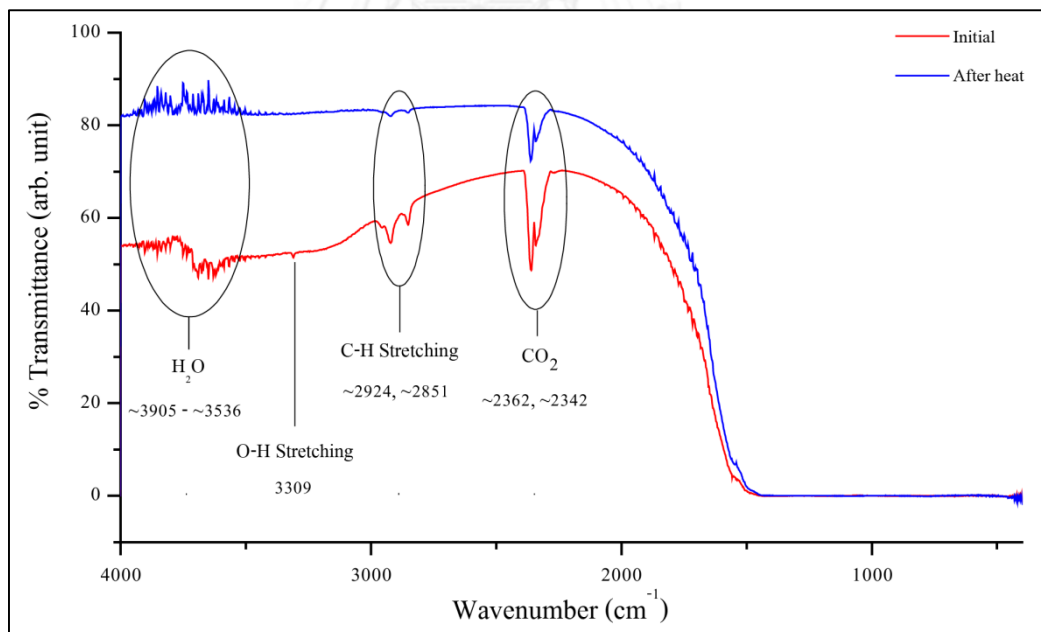


Figure 4.18 FTIR spectra of sapphire with moderate silky inclusions (B3) before and after heating at 1650 °C under ambient air.

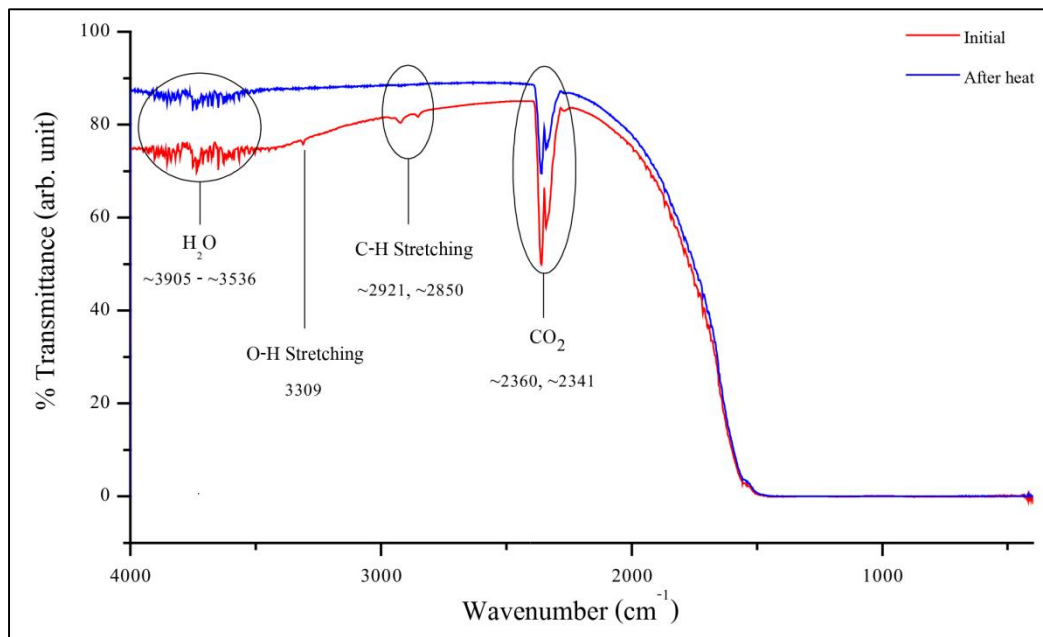


Figure 4.19 FTIR spectra of sapphire with moderate silky inclusions (B16) before and after heating at 1650 °C under ambient air.

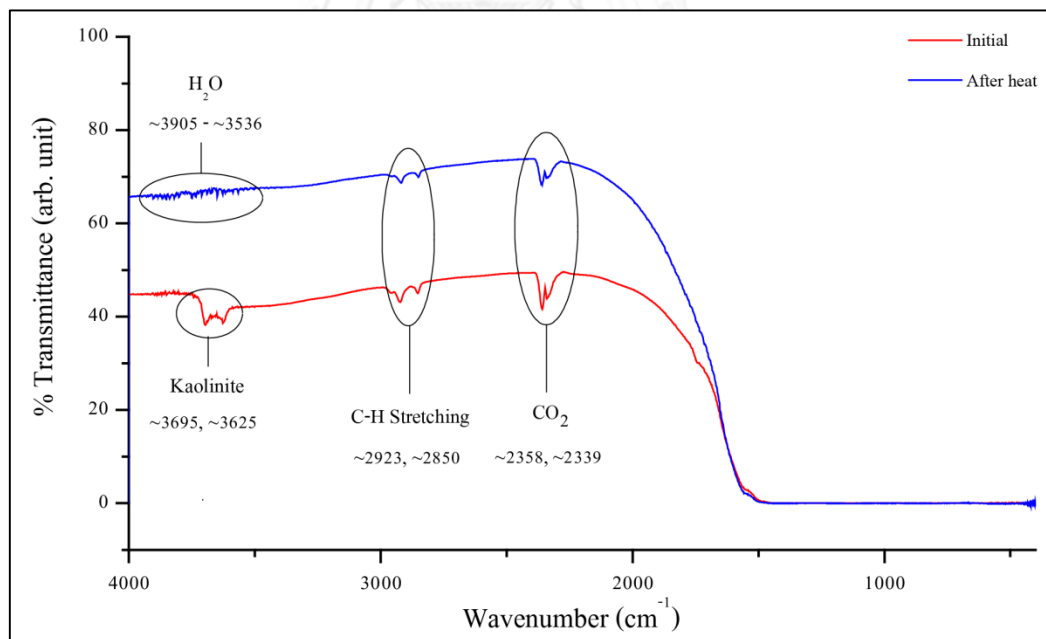


Figure 4.20 FTIR spectra of sapphire with abundant silky inclusions (C6) before and after heating at 1650 °C under ambient air.

CHAPTER V

MINERAL CHEMISTRY OF SILKY INCLUSIONS AND EFFECT TO COLOR OF HOST SAPPHIRE

5.1 Mineral Chemistry

Silky inclusions are usually tiny approximately 1-10 μm (Figure 5.1). They usually embed in the host sapphire samples. Therefore, these samples need to be cut and polished until they expose onto the surface. As reported in the previous chapter, the silky inclusions was identified as hematite using Raman spectroscope. In addition, chemical compositions of these inclusions were also performed by EPMA-WDS and reported herein this chapter. Before quantitative analysis was designed, these inclusions were scanned qualitatively for major and minor elements. Consequently, Al_2O_3 , FeO and TiO_2 were then indicated as major composition. Saminpanya (2001) also reported similarly significant elements consisting of iron and titanium found in silky inclusions in sapphire form the same area. Therefore, these three elements (i.e., Al, Fe and Ti) were selected and set up for EPMA analysis.

Representative compositions of a silky inclusions (analyses 1-7 in Table 5.1) contain about 75–76 wt% $\text{FeO}_{\text{total}}$ 11-12 wt% TiO_2 and 2-4 wt% Al_2O_3 . In addition, hematite specimens collected from alluvial deposit in the study area (analyses 8-10 in Table 5.1) were analyzed and consequently yielded major content of about 85-87 wt% $\text{FeO}_{\text{total}}$ with minor contents of about 3-5 wt% Al_2O_3 and 3-4 wt% TiO_2 . Recalculated cations based on 3 oxygen atoms were then carried out as well as $\text{Fe}^{2+}/\text{Fe}^{3+}$ was also estimated using equation of Droop (1987). Although quality of these analyses are not very good as presented by low total wt% oxides these may be affected by polished surface of analytical spot. Moreover, high contents of iron (both Fe^{2+} and Fe^{3+}) directly impact low total content of wt% oxide. However, cation contents clearly indicate major component of hematite with minor components of spinel and rutile. Higher rutile component present in silky inclusions; on the other hand, higher spinel component are recognized in alluvial hematite samples.

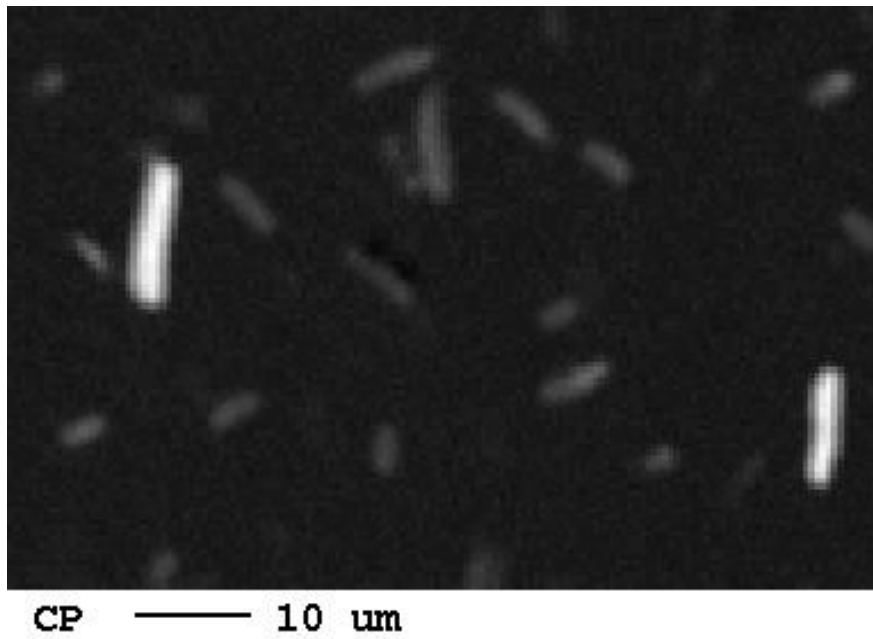


Figure 5.1 Back Scatter Electron Image (BSI) showing bright tiny silky inclusions with approximately length of $\leq 10 \mu\text{m}$ in sapphire from Bang Kacha gem field, Chanthaburi.

Table 5.1 Representative EPMA analyses of silky inclusions in sapphire and hematite from alluvial deposits in Bang Kacha Gem field, Chanthaburi.

Analysis	silky inclusion with main hematite composition						alluvial hematite			
	1	2	3	4	5	6	7	8	9	10
Sample	C9-5-5	C9-8-5	C9-11-5	C5-6-5	C5-7-5	C6-3-5	C6-5-5	7-hem-4	9-hem-3	9-hem-2
dAl ₂ O ₃	2.08	3.93	3.43	3.21	2.80	3.83	2.53	3.15	5.58	4.93
FeO _{total}	75.16	75.47	75.42	75.64	75.62	75.85	75.60	86.70	84.80	84.95
TiO ₂	11.98	11.57	11.40	11.21	11.68	11.51	11.92	3.75	2.75	3.79
Total	89.22	90.96	90.25	90.06	90.10	91.20	90.05	93.60	93.14	93.67
Formula 3(O)										
Al	0.087	0.159	0.141	0.132	0.116	0.155	0.104	0.133	0.232	0.204
Fe ³⁺	1.449	1.424	1.440	1.453	1.446	1.430	1.444	1.763	1.731	1.711
Fe ²⁺	0.781	0.741	0.753	0.759	0.766	0.744	0.772	0.835	0.775	0.783
Ti	0.320	0.298	0.298	0.295	0.307	0.297	0.314	0.101	0.073	0.100
Total*	2.637	2.622	2.632	2.639	2.635	2.626	2.634	2.833	2.811	2.798

5.2 Dissolution by Heating

After heating experiment, these silky inclusions appeared to have been destroyed and dissolved into the host sapphire. To prove such chemical dissolution, profile analysis (multiple analytical spots crossing the inclusion grain) using EPMA was then performed before and after heating experiment. Although, profile analyses were performed in many silky inclusions, only a few profiles yielded good results. This is actually caused by very tiny size of inclusion and natural orientation which are really difficult to be cut and polished properly for EPMA analysis. For example, an analyzed silky sample in sapphire sample C6 of abundant silky inclusions group (Group C) (Figure 5.2) is selected as a representative and reported here. Figure 5.2 shows analytical spots 1, 9, 10 and 13 located in the sapphire host whereas analytical spots 2, 8, 11 and 12 were set on the boundaries between silky inclusion and sapphire host. The other spots (3-7) were analyzed within the silky inclusion. The same positions were analyzed twice, before and after heating experiment (see Figure 5.2). The main blue color-causing elements, iron and titanium are the most concern under this study. The results can be summarized below.

Iron: Along the sapphire host (spots 1, 9, 10 and 13), they initially contained about 1.5-1.7 wt% FeO. After heating experiment, these spots still remain the same FeO contents (see Table 5.2). For analytical spots 2, 8, 11 and 12 located along edge boundary between the silky inclusion and sapphire host, they yielded higher iron contents of about 2.0-2.8 wt%. These area usually present alteration after heating experiment and significantly reduced in iron contents to about 1.4-1.6%. Silky inclusion (spots 3-7) initially contained rather high iron contents (63-76%) but, after heating experiment, they obviously decreased to 0.92-0.98%. This evidence clearly indicates dissolution of iron into sapphire host.

Titanium: Along the sapphire host (spots 1, 9, 10 and 13), titanium contents appear to slightly increased from about $\leq 0.02\%$ to $\leq 0.03\%$ wt% after heating experiment. Along the altered zone (spots 2, 8, 11, and 12) after heating, titanium contents also appeared to be changed (about from 0.16 to 0.18%). However, analyses within silky inclusion (spots 3, 4, 5, 6 and 7) initially contained high titanium contents (about 9-12%) which dramatically reduced to about 1-4% after heating experiment (see Table 5.2). These results may represent low diffusion rate of titanium which slowly moved and diffused internally. Some selected analyses were displayed in Table 5.2.

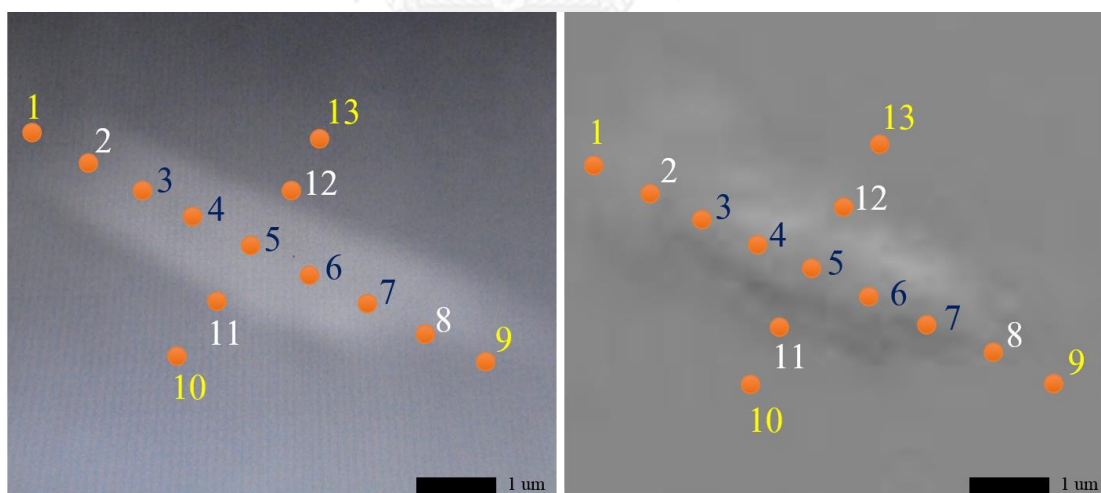


Figure 5.2 Secondary Electron Image (SEI) showing multi-analytical spots on the profiles (elongation and perpendicular) on a tiny silky inclusion in sapphire sample (C6) of abundant silky inclusions group (Group C). Left image was taken before heating and right image show altered feature of the same silky inclusion after heating.

Table 5.2 EPMA profile analysis (spots as shown in Figure 5.2) revealing changes of $\text{FeO}_{\text{total}}$ and TiO_2 (wt%) along a silky inclusion in sapphire sample (Sample C6) after heating experiments.

Analytical Spots		FeO (wt%)		TiO ₂ (wt%)	
		Initial	After heating	Initial	After heating
Sapphire host	1	1.53	1.48	0.02	0.04
Edge boundary	2	1.99	1.41	0.14	0.16
Silky inclusion Rim ← Core → Rim	3	62.94	0.97	9.48	1.05
	4	74.83	0.95	10.37	3.68
	5	75.60	0.95	11.92	4.31
	6	73.46	0.98	10.20	3.24
	7	63.13	0.92	9.60	1.45
Edge boundary	8	2.19	1.57	0.16	0.18
Sapphire host	9	1.50	1.41	0.01	0.02
	10	1.47	1.52	0.02	0.02
Edge boundary	11	2.76	1.51	0.15	0.16
	12	2.06	1.45	0.22	0.22
Sapphire host	13	1.63	1.53	0.01	0.02

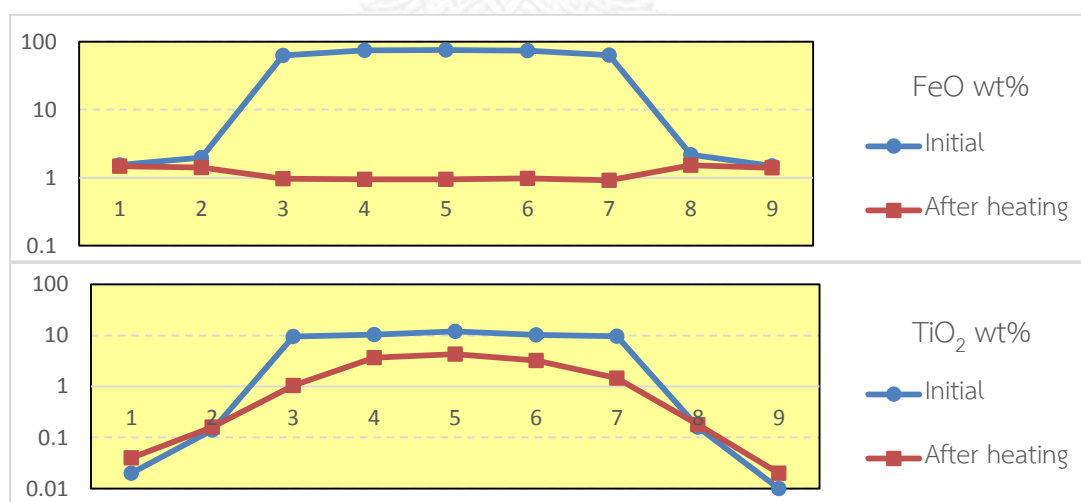


Figure 5.3 Profiles of FeO and TiO₂ comparing before and after heating (wt%) in sample C6.

5.3 Trace Element and Color Causing

Selected samples were taken for subsequent trace analyses using Laser Ablation-Inductively Coupled Plasma-Mass Spectrometry (LA-ICP-MS). Trace element contents were recalculated as atom mole ppm (abbreviated as amp) and normalized into 40 atoms of cation which correspond to 60 atoms of oxygen in Al_2O_3 structure. Six representative sapphires were analyzed for the most important trace elements. Most sapphire samples show uneven color features formed as color zoning along the basal planes after heat treatment (see Figures 5.6, 5.7 and 5.8). Three analytical spots in each sample were selected based on different color zones for analysis. Interaction between crucial elements and color causing after heating can be investigated.

In general, the most important chromophore of sapphires in this study was Fe which yielded an average of about 9707 ppm. Another chromophore was Ti which yielded an average of 71 ppm. Mg concentrations were consistently low with an average of about 15 ppm. Ga values were consistently high (average 141 ppm) whereas V and Cr were rather low (averages of 3 and 8, respectively). In particular, Cr in many samples even yielded lower than the detection limit. Be was below the detection limit in all analyses. All the results were summarized in Figure 5.4 and Table 5.3.

Based on atomic proportions to 60 oxygen atoms, all sapphire samples usually contain high averages of Ti, Mg and Ga about 30 amp, 12 amp and 40.91 amp, respectively. On the other hand low averages of V and Cr are about 1.36 and 1.44 amp, respectively.

Table 5.3 Trace element contents of representative analyses of Bang Kacha sapphire samples obtained by LA-ICP-MS reported as ppm unit.

No.	Spot	Be	Mg	Ti	V	Cr	Fe	Ga
C9	#1	<0.85	25.20	167.68	2.22	<2.67	16193.03	162.08
	#2	<0.88	30.30	232.20	2.37	8.76	15104.75	159.25
	#3	<0.91	28.26	210.10	2.90	<2.85	15458.53	166.86
B3	#1	<0.94	10.65	29.27	1.91	<2.82	8607.88	119.52
	#2	<0.98	13.14	46.43	2.09	<3.05	8876.35	120.62
	#3	<0.86	10.46	31.97	2.24	2.94	8422.73	116.52
B4	#1	<0.91	10.36	25.43	1.07	3.26	9841.90	113.26
	#2	<0.92	10.39	31.15	0.95	<2.65	10167.90	119.85
	#3	<0.82	12.37	22.98	0.92	<2.63	9748.99	117.47
B6	#1	<0.73	9.86	16.18	7.58	4.21	6553.27	154.66
	#2	<0.82	12.46	96.73	6.37	<2.65	7946.34	152.24
	#3	<0.74	5.99	26.77	6.81	<2.43	7069.50	154.10
B12	#1	<0.83	13.20	57.19	5.99	3.85	8039.06	155.45
	#2	<0.96	12.41	33.33	6.48	6.27	7612.88	160.14
	#3	<0.80	13.46	38.49	6.94	31.92	7675.14	157.71
B5	#1	<0.98	15.50	71.16	1.58	5.26	9441.12	135.31
	#2	<1.06	10.82	57.5	1.33	<3.11	8630.03	131.06
	#3	<0.96	17.01	78.65	1.75	<2.96	9342.18	135.69
Max		bdl	30.30	232.20	7.58	31.92	16193.03	166.86
Min		bdl	5.99	16.18	0.92	2.94	6553.27	113.26
Average		bdl	14.55	70.73	3.42	8.31	9707.31	140.65
S.D.		bdl	6.65	65.55	2.46	7.55	2877.15	19.08

< = below the detection limit (bdl)

Table 5.4 Recalculated atom mole ppm (amp) of trace elements in representative Bang Kacha sapphire samples.

No.	Spot	Be	Mg	Ti	V	Cr	Fe	Ga
C9	#1	bdl	21.03	71.02	0.88	0.00	5879.96	47.14
	#2	bdl	25.28	98.35	0.94	3.42	5484.79	46.32
	#3	bdl	23.58	88.99	1.15	bdl	5613.25	48.53
B3	#1	bdl	8.89	12.40	0.76	bdl	3125.66	34.76
	#2	bdl	10.96	19.66	0.83	bdl	3223.15	35.08
	#3	bdl	8.73	13.54	0.89	1.15	3058.43	33.89
B4	#1	bdl	8.64	10.77	0.43	1.27	3573.76	32.94
	#2	bdl	8.67	13.19	0.38	bdl	3692.13	34.86
	#3	bdl	10.32	9.73	0.37	bdl	3540.02	34.17
B6	#1	bdl	8.23	6.85	3.02	1.64	2379.6	44.98
	#2	bdl	10.40	40.97	2.54	bdl	2885.45	44.28
	#3	bdl	5.00	11.34	2.71	bdl	2567.05	44.82
B12	#1	bdl	11.01	24.22	2.38	1.50	2919.12	45.21
	#2	bdl	10.35	14.12	2.58	2.45	2764.36	46.58
	#3	bdl	11.23	16.30	2.76	12.45	2786.97	45.87
B5	#1	bdl	12.93	30.14	0.63	2.05	3428.23	39.36
	#2	bdl	9.03	24.35	0.53	bdl	3133.71	38.12
	#3	bdl	14.19	33.31	0.70	bdl	3392.3	39.47
	Max	bdl	25.28	98.35	3.02	12.45	5879.96	48.53
	Min	bdl	5.00	6.85	0.37	0.00	2379.60	32.94
	Average	bdl	12.14	29.96	1.36	1.44	3524.89	40.91
	S.D.	bdl	5.55	27.77	0.98	2.94	1044.74	5.55

< = below the detection limit (bdl) of which 0.00 value is used for calculation of atom mole ppm

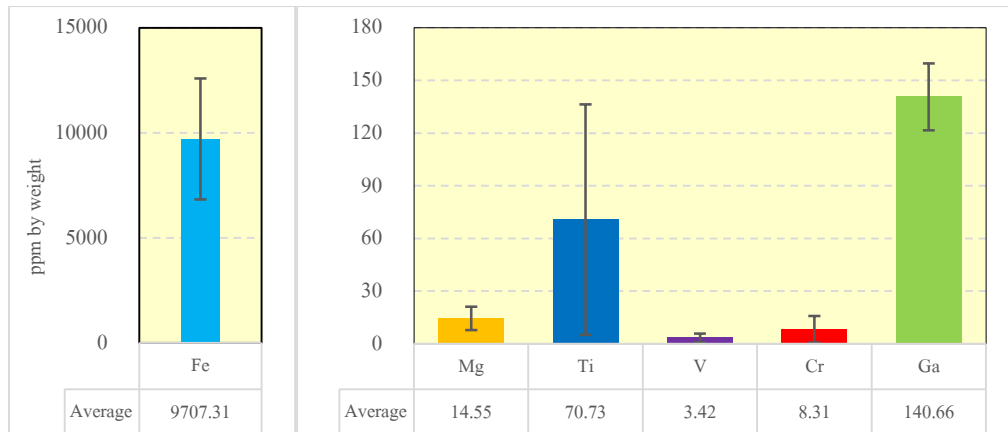


Figure 5.4 Histogram showing averages and standard deviation (ppm) of typical trace elements analyzed by LA-ICP-MS.

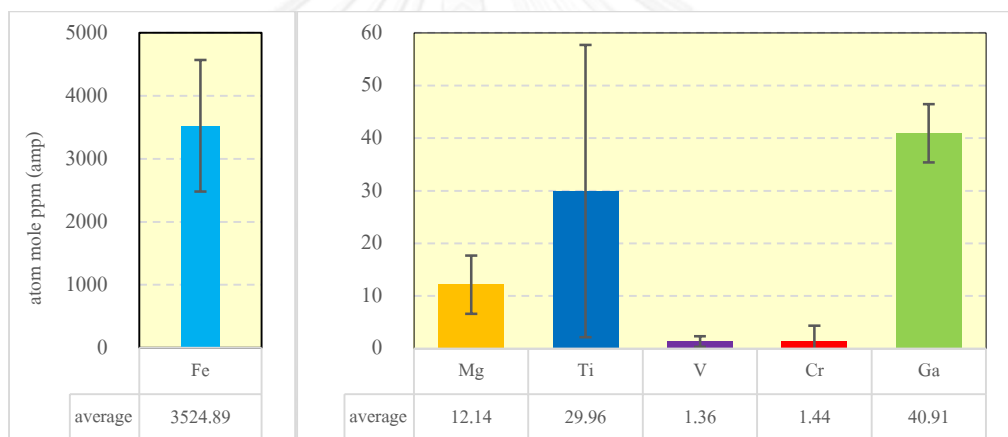


Figure 5.5 Histogram showing averages and standard deviation (amp) of typical trace elements recalculated based on 60 oxygen atoms.

However, Fe and Ti of different color zones in the same samples appeared to have somewhat different values. Therefore, three groups of analyses were divided, based on color appearances, consisting of dark blue (C9 spots 1-3; B6 spot 2; B5 spots 1-3), light blue-greenish blue (B3 spots 1 and 3; B4 spots 1 and 2; B6 spot 3; B12 spots 1-3) and bluish yellow (B4 spot 3; B6 spot 1) (see Figures 5.6-5.8)



Figure. 5.6 Analytical spots on dark blue zones after heating at 1650 °C in samples C9 (left) and sample B5 (right).

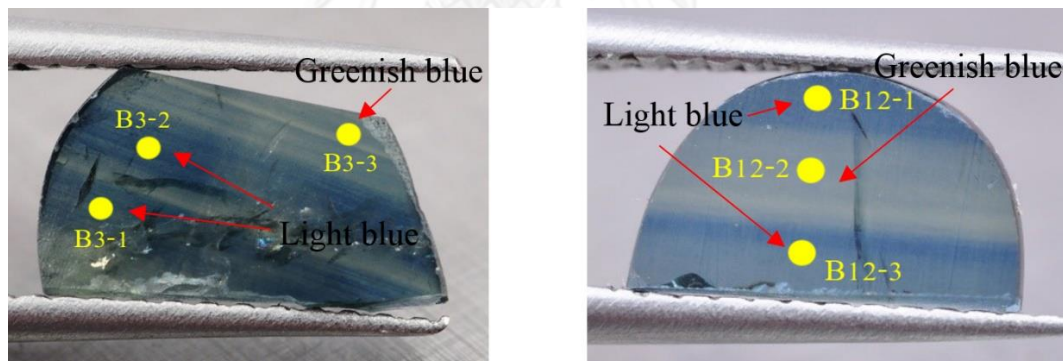


Figure. 5.7 Analytical spots 1 and 2 on light blue zone and spot 3 on greenish blue zone in sample B3 (left). Analytical spots 1 and 3 on light blue zone and spot 2 on greenish blue zones in sample B12 (right). All color zones appeared after heating at 1650 °C.

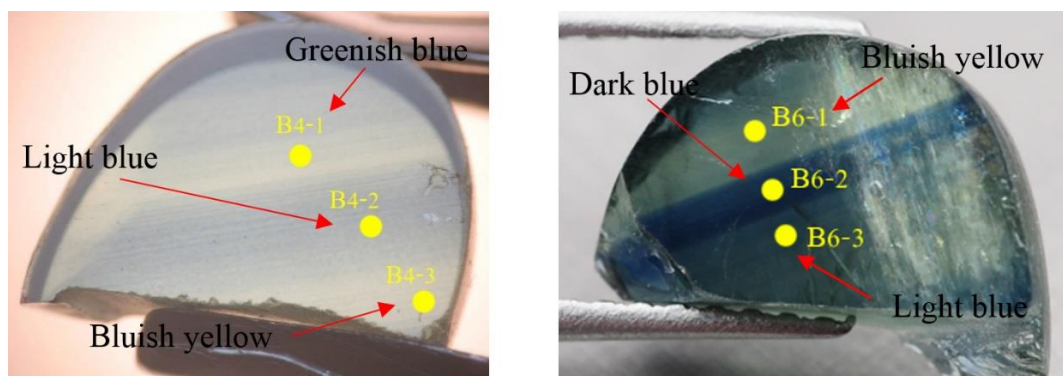


Figure. 5.8 Analytical spot 1 on greenish blue zone, spot 2 on light blue zone and spot 3 on bluish yellow zone in sample B4 (left). Analytical spot 1 on bluish yellow zone, spot 2 on dark blue zone and spot 3 on light blue zone in sample B6 (right). These color zones appeared heating at 1650 °C.

Atom mole ppm (amp) of all analyses reported in Table 5.4 were grouped and sorted by color appearances mentioned previously and summarized in Table 5.5

Table 5.5 Atomic proportions (atom mole ppm, amp) based on 60 oxygen atom along different color zones.

Zones	Spot	Mg	Ti	V	Cr	Fe	Ga
Dark blue zone	C9-1	21.03	71.02	0.88	bdl	5879.96	47.14
	C9-2	25.28	98.35	0.94	3.42	5484.79	46.32
	C9-3	23.58	88.99	1.15	bdl	5613.25	48.53
	B6-2	10.40	40.97	2.54	bdl	2885.45	44.28
	B5-2	9.03	24.35	0.53	bdl	3133.71	38.12
	B5-3	14.19	33.31	0.70	bdl	3392.3	39.47
	B5-1	12.93	30.14	0.63	2.05	3428.23	39.36
	Max	25.28	98.35	2.54	3.42	5879.96	48.53
	Min	9.03	24.35	0.53	bdl	2885.45	38.12
	Average	16.63	55.30	1.05	0.78	4259.67	43.32
S.D.	6.57	30.32	0.69	1.39	1326.54	4.27	
Light blue to Greenish blue zone	B12-1	11.01	24.22	2.38	1.50	2919.12	45.21
	B6-3	5.00	11.34	2.71	bdl	2567.05	44.82
	B3-2	10.96	19.66	0.83	bdl	3223.15	35.08
	B4-2	8.67	13.19	0.38	bdl	3692.13	34.86
	B12-3	11.23	16.30	2.76	12.45	2786.97	45.87
	B3-1	8.89	12.40	0.76	bdl	3125.66	34.76
	B3-3	8.73	13.54	0.89	1.15	3058.43	33.89
	B12-2	10.35	14.12	2.58	2.45	2764.36	46.58
	B4-1	8.64	10.77	0.43	1.27	3573.76	32.94
	Max	11.23	24.22	2.76	12.45	3692.13	46.58
Min	5.00	10.77	0.38	bdl	2567.05	32.94	
Average	9.28	15.06	1.52	3.76	3078.96	39.33	
S.D.	1.84	4.12	0.99	4.37	352.14	5.67	
Bluish yellow zone	B4-3	10.32	9.73	0.37	bdl	3540.02	34.17
	B6-1	8.23	6.85	3.02	1.64	2379.6	44.98
	Max	10.32	9.73	3.02	1.64	3540.02	44.98
	Min	8.23	6.85	0.37	bdl	2379.60	34.17
	Average	9.28	8.29	1.70	0.82	2959.81	39.58
S.D.	1.05	1.44	1.33	0.82	580.21	5.40	

bdl = below the detection limit

Dark blue zone contains of about 2885-5880 amp of Fe, 24-98 amp of Ti, 9-25 amp of Mg, 38-49 amp of Ga, 1-3 amp of V and ≤ 3 amp of Cr. Light blue-greenish blue zone has trace compositions ranging from 2567-3692 amp of Fe, 11-24 amp of Ti, 5-11 amp of Mg, 33-47 amp of Ga, ≤ 3 amp of V and ≤ 12 amp of Cr. Bluish yellow zone obtained wide range of trace elements including about 2380-3540 amp of Fe, 7-10 amp of Ti, 8-10 amp of Mg, 34-45 amp of Ga, ≤ 3 amp of V and ≤ 2 amp.

In comparison, iron (Fe) is the most significant trace element presented as impurity in all sapphire groups. Fe content in dark blue zone (approximately 4260 amp) is higher than those in light blue-greenish blue zone (approximately 3079 amp) and bluish yellow zone (approximately 2960 amp). Ti in dark blue zone is averaged at 55 amp which is higher than averages of 15 amp in light blue-greenish zone, 8 amp in bluish yellow zone. Moreover, Mg content in dark blue zone (average of 17 amp) is also higher than those in light blue-greenish blue and bluish yellow zone (averages of 11 amp). The other trace elements, Ga, V and Cr, are mostly very low which appeared to have no difference. These comparative results were graphically shown as statistic plots in Figure 5.9

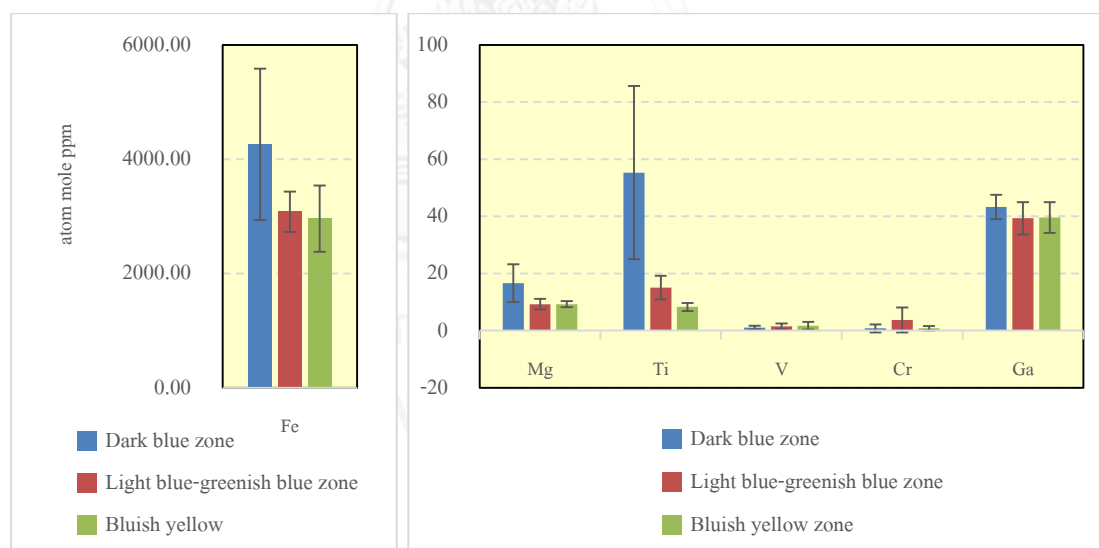


Figure 5.9 Statistical plots (mean \pm SD) showing means and bars of standard deviation of trace analyses (in atom mole ppm recalculated based on 60 oxygen atoms) of different color zones after heating at 1650 °C.

In conclusion, as shown in Table 5.5, the blue coloration after heating is dominated by Fe which is related to basaltic-type sapphire. The interaction between Ti and Mg are relatively cause of colors after heating in these sapphires as well. Moreover, analyses in dark blue and light blue-greenish blue zones show $Ti > Mg$; particularly, Ti/Mg ratios of the dark blue zone are obviously high compared to those in the light blue-greenish blue zones. On the other hand, analyses in bluish yellow zone show $Mg \geq Ti$. These evidences are comparable to the information as previously reported (Häger, 2001) which will be taken into discussion in the next chapter.



CHAPTER VI

DISCUSSION AND CONCLUSIONS

Thailand is one of the world famous gem suppliers, especially corundum both ruby and sapphire, and jewelry trading center. Moreover, Thailand have operated ruby and sapphire mines in several localities; recently, gem mines are found only in Changwat Chanthaburi (the study area). In this area, corundums, particularly sapphires, are found in association with basaltic rocks similar to the other gem fields of the country. These sapphires generally contain rather high Fe content (Sutherland, 1998; Sutthirat, 2001; Vichit, 1992). As a result, Fe-rich content usually causes dark tone color and low transparency to opaque. Silky mineral inclusions appear to be exsolved particles often found in the iron-rich sapphires from this area and other basaltic corundums throughout the world. These silky inclusions may cause asterism phenomena in the stone. Sapphires from Chanthaburi deposits are usually dark blue blue/green, yellow/green and opaque sapphires which they are highly demanded by local gem trader for heat treatment. After heat treatment, these stones can turn into stable intense yellow or blue sapphires. Heating process is currently well known and has been generally accepted in the gem market for many years (Emmett et al., 2003; Pisutha-arnond et al., 2004, 2006). However, gem-quality rough stones from Chanthaburi deposits have been dramatically decreased, only a few mines are still operated in the area. Therefore, black star sapphire and other low quality opaque sapphires with abundant silky inclusions which used to be low demanded have recently become significant raw material for heat treatment. Therefore, this research project was carried out to characterize silky inclusions, the most significant feature occurred in these stones, and to investigate the effect of heat treatment to these stones. Discussion on these aspects are reported and concluded below.

6.1 Silky Inclusions Characterization

The morphological properties of the silky inclusions reveal irregular lamellae shapes under high magnification microscope. They are usually very fine and short grey-brown silk. These silky inclusions oriented along the basal plane $\{0001\}$ parallel to three crystallographic directions $\{10\bar{1}0\}$ with intersection of $60/120^\circ$. They appear flat when viewing by a fiber-optic light; iridescent colors can also be seen due to light interference from these tiny mineral inclusions. Moreover, these tiny silky inclusions may cause star effect in corundum host (Hughes, 1997).

Identification of these micro inclusions is difficult because of their small sizes (average ≤ 5 micrometer). In general based on the Raman technique, the smallest analytical spot should be bigger than 20 micrometers with good quality polished surface. The recorded Raman spectra of these silky inclusions are comparable to the pattern of alluvial hematite (Figure 3.9) as reported in Chapter 3. However, their peak positions are slightly shifted which may be due to the substitution of other ions, particularly titanium and aluminium. In addition, differences pressure condition may be another reason for shifting of Raman spectrum. Shim and Duffy (2002) reported that Raman spectroscopy of Fe_2O_3 shows a Raman shift increasing from 1320 to $\sim 1620 \text{ cm}^{-1}$ at high pressure of 62 GPa. Although, initial sapphire-bearing rocks originated at great depth with high pressure, quick releasing of pressure appear to have taken place during rapid uprising of the basaltic magma after picking up to the surface. Although this may impact Raman shift of these silky inclusions, their chemical composition seems to have more effects. EPMA analyses indicated that these silky inclusions contain significant Fe content with minor contents of Ti and Al. Similar data have also been reported by Saminpanya (2001) for exsolved silks in Thai star sapphires from Bang Kacha, Chanthaburi Province, Thailand whereas impure rutile or hematite inclusions in gem corundum were mentioned by Hughes (1997) and Weibel and Wessicken (1981). Saminpanya also suggested that the exsolved silk was more likely a mineral of the ilmenite-hematite solid-solution series which were major mineral producing asterism effects in black star sapphire. Moon and Phillips (1984) reported similarly that the exsolved phase in Australian black star sapphire was high iron/titanium oxide. These Australian sapphires also relate to basaltic rock same as Thailand (Sutherland and Schwarz, 2001).

The silky inclusions appear to have been exsolved after the host corundum was completely crystallized; therefore, these inclusions should be a secondary phase or slightly post-genetic origin. The exsolved hematite may cause star in sapphire (Gübelin and Koivula, 1997). The exsolution is a separation process during sub-solidus cooling, a solid-solution mineral separates into two distinct crystalline phases; the minor component or solute (Fe_2O_3 in this case) will seclude from solute the main component or solvent (Al_2O_3 in this case). Then the exsolved Fe_2O_3 form hematite, accordingly. At high temperatures, corundum can accommodate more defects in expanded lattice that allow impurities such as iron and titanium to allocate, partly. Gradually cooling down under sub-solidus state, reduction of the defects and lowering of degree of freedom lead to lattice ordering (Reduction of ability to independently move). Consequently, impurities in the solid-solution phase will be eliminated and then precipitated along the weak zones such as cleavages, twinning plains and other crystallographic orientations. Due to the constraints of space in the solid state, impurity atoms are unable to travel large distances; rather than forming large crystals, then they form multitudes of tiny particles scattering around the host crystals. Therefore, the exsolved silky hematite inclusions are often arranged with crystallographic orientations of the host corundum as reported by Hughes, 1997 and Kane et al., 2005.

Occurrences of exsolved hematite inclusions in corundum can be explained by experimental study of Fe-Al solubility in the system corundum-hematite (Feenstra et al., 2005). They reported temperature of exsolution of silky hematite inclusions appear to range between 800 and 1200 °C as present in the binary phase diagram (Figure 6.1). Feenstra et al. (2005) also suggested that physico-chemical condition in the magmatic system must differ considerably from those in experiments imposing 'maximum' Fe solubility in corundum.

In addition, titanium also commonly presents in solid solution within the hematite-ilmenite series. Trace amount of titanium may be embedded in the corundum structure (Morley, 1964). Basta (1953) concluded from experimental studies that, at 800 °C, < 5% TiO_2 can enter into hematite's structure. Izokh et al. (2010) mentioned that Al-Ti hematite inclusion in Dak Nong sapphire, topotactic inclusion, appears to have formed from solid solution immediately after ending of the host sapphire crystallization. Therefore, some rutile (TiO_2) components in silky inclusions may influence the crystal habit shape of some silky inclusions forming needle-like inclusions.

Consequently, heat treatment is a method to drive iron and titanium content into lattice via dissolution process of silky hematite inclusions. The orientation of these exsolved inclusions are restricted by the host structure which sometimes cause asterism (star effect). Therefore, to remove these inclusions in star and opaque sapphires, sample should be heated above 850 °C with sufficiently long enough for hematite inclusions breaking down and dissolving into vacancies of Al_2O_3 (Nassau, 1994) which detailed in the next section. This experimental condition was therefore applied under this research project. In addition, quenching from about 1,000°C to room temperature was performed by taken samples quickly from the furnace into ambient room temperature. As such, colors of most samples have been modified and the clarity was improved as reported in the previous chapter. Discussion on interaction of these impurities, heat treatment and color modification is discussed in the next section.

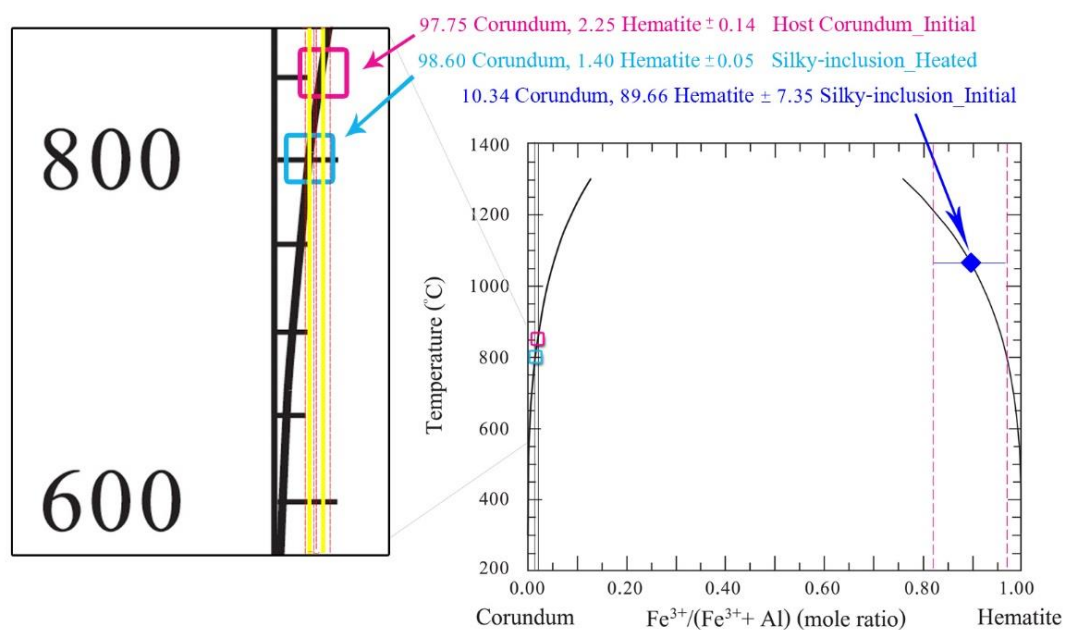


Figure 6.1 Binary phase diagram of Al_2O_3 - Fe_2O_3 system displaying solvus curves of hematite-corundum exsolution (Feenstra et al., 2005) and chemical plots of sapphire host and silky inclusions under this study.

6.2 Reaction between Silky Inclusions and Sapphire Host

Feenstra et al. (2005) suggested that corundum can take up to 20 mole% Fe_2O_3 in its solid solution at 1400 °C and about 10 mole% at 1100 °C at high pressure (see phase diagram in Figure 6.1). Their data also indicate pressure independent reaction. Therefore, silky hematite inclusions may be easily dissolved at 1650 °C as the temperature was applied for heating experiment under this study. As the results, these silky inclusions were mostly decomposed as reported in Chapter 5, their chemical analyses also showed dissolution of Fe and Ti into the sapphire host. These results are conformable to the experiment of Feenstra et al. (2005). Plots of initial chemical compositions of host sapphire and silky inclusions and their composition changes after heating are also carried out in mole proportions of Fe_2O_3 and Al_2O_3 in Figure 6.1. Regarding to initial composition of silky inclusions, their average composition and standard deviation are plotted as blue diamond and parallel isoplates which both isoplates cut the solvus curve at about 800-1200 °C. That indicates temperature range of exsolution from the sapphire host. Chemical compositions of sapphire appear to be changed slightly from initial composition and after heated composition represented by analytical spot of decomposed silky inclusions. Both compositions fall on the solvus curve indicating compatible temperature of about 800-850°C.

Crystal structure of some hematite was related with TiO_2 (Ti^{4+}) and will be formed as tetragonal (Bowles et al., 2011), while the Al_2O_3 crystal structure is hexagonal. Since these structure are incompatible, the TiO_2 rather difficult to be entered and dissolved into the Al_2O_3 . TiO_2 has very low solubility in corundum. On the other hand, the crystal structure of the Fe_2O_3 (Fe^{3+}) is hexagonal, compatible with the Al_2O_3 hexagonal structure, and very soluble in corundum; thus the Fe_2O_3 easily fits into the Al_2O_3 lattice. Therefore, after heat treatment at 1650 °C, iron content presented approximately 1.50 weight% Fe_2O_3 completely soluble in corundum lattice whereas titanium content of about 0.2 weight% TiO_2 was partially dissolved from the silky inclusions into host sapphire. Moreover, the valence states of Fe^{3+} is compatible pairing with Al^{3+} in corundum structure which not entered to the mechanism of charge compensation, while Ti^{4+} has one extra positive charge than the Al^{3+} . When Ti^{4+} were dissolved and incorporated into corundum lattice during dissolution, it must be charge compensated by a divalent ion such as Fe^{2+} , Mg^{2+} , or by an aluminum vacancies for produces the electrical neutral. Consequently, possibility of Fe^{3+} is much higher than Ti^{4+} to be diffused into the lattice. Other previous researchers (e.g., Fritsch, 1987;

Hughes, 1997; Koivula, 1987; Nassau, 1984) also reported similarly that natural inclusions (mainly hematite and rutile) in corundum can be dissolved at high temperature.

Regarding to UV-Vis-NIR absorption spectrum, absorption spectrum after heat greatly usually reveal shifting of $\text{Fe}^{2+}/\text{Fe}^{3+}$ pairs IVCT band around 900 nanometer with combination of minor change of $\text{Fe}^{2+}/\text{Ti}^{4+}$ intervalence charge transfer absorption bands around 570 nanometer. Therefore, decomposition and dissolution of silky inclusions appear to produce intense blue spots, or blue color bleeding surround these tiny inclusions. Dissolved dot particles appear to have remained partially after high temperature heating; consequently, higher transparency has also been improved. Blue bleeding caused by internal diffusion or of chromophoric elements, particularly Fe and Ti, as suggested by Emmett et al., 2003; Koivula, 1987; Nassau, 1981,1984; Perera et al., 1991; Pisutha-arnond et al., 2004; Sakkaravej, 2004; Schmetzer, 1990; Themelis, 1992.

Quantitative analyses of trace elements in sapphire samples after heat were carried out to support the idea suggested above. Representative sapphire sample with abundant silky inclusions was heated at 1650°C in ambient air; after the experiment, the sample turned to clear intense blue in the some particular zones (Figure 6.2). Three points in different color zones were selected and analyzed by LA-ICP-MS as reported in the previous chapter. Significant amounts of Fe with small amounts of Mg and Ti are obviously detected in all points; however, their proportions are slightly different. High Fe contents have been typically detected in sapphires from basaltic sources (e.g., Keller, 1982; Nassau, 1987; Vichit, 1992; Sutherland et al., 1998 and 2001; Pisutha-arnond, 2004; Somboon, 2006) as similar in this case. All the analyses fall close to the Fe apex of ternary Fe-Ti-Mg diagram (suggested by Häger, 1996, 2001). Häger (2001) suggested that the excess Ti after calculation of MgTiO_3 clusters could from color active FeTiO_3 clusters or Fe-Ti intervalence charge transfer mechanism causing blue coloration in sapphire; analytical point 2 which forms deep blue and destruct grey-brown silky inclusions, obviously, after heating yields the highest Ti/Mg ratio. This analysis was plotted very close to the blue area on the diagram. Likewise, point 3 with pale blue after treatment contains slightly higher Ti than Mg which is plotted in colorless area toward blue area on the diagram. On the other hand, point 1 contained slightly higher Mg than Ti showing pale green/yellow may be cause of color by Fe^{3+} spin forbidden transition or stabilized Mg^{2+} trapped color center (Häger, 2001; Pisutha-

arnond et al., 2004). It is plotted in colorless area towards yellow area on the diagram (Figure 6.3).

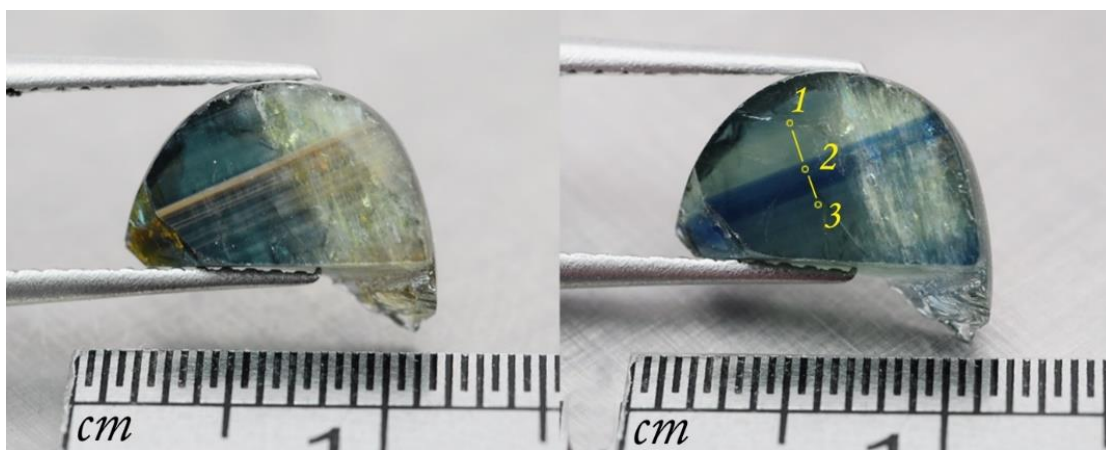


Figure 6.2 Color and clarity appearances of a sapphire sample before (left) and after heating (right) and three different color zones (points 1 to 3) selected for quantitative trace element analyses.

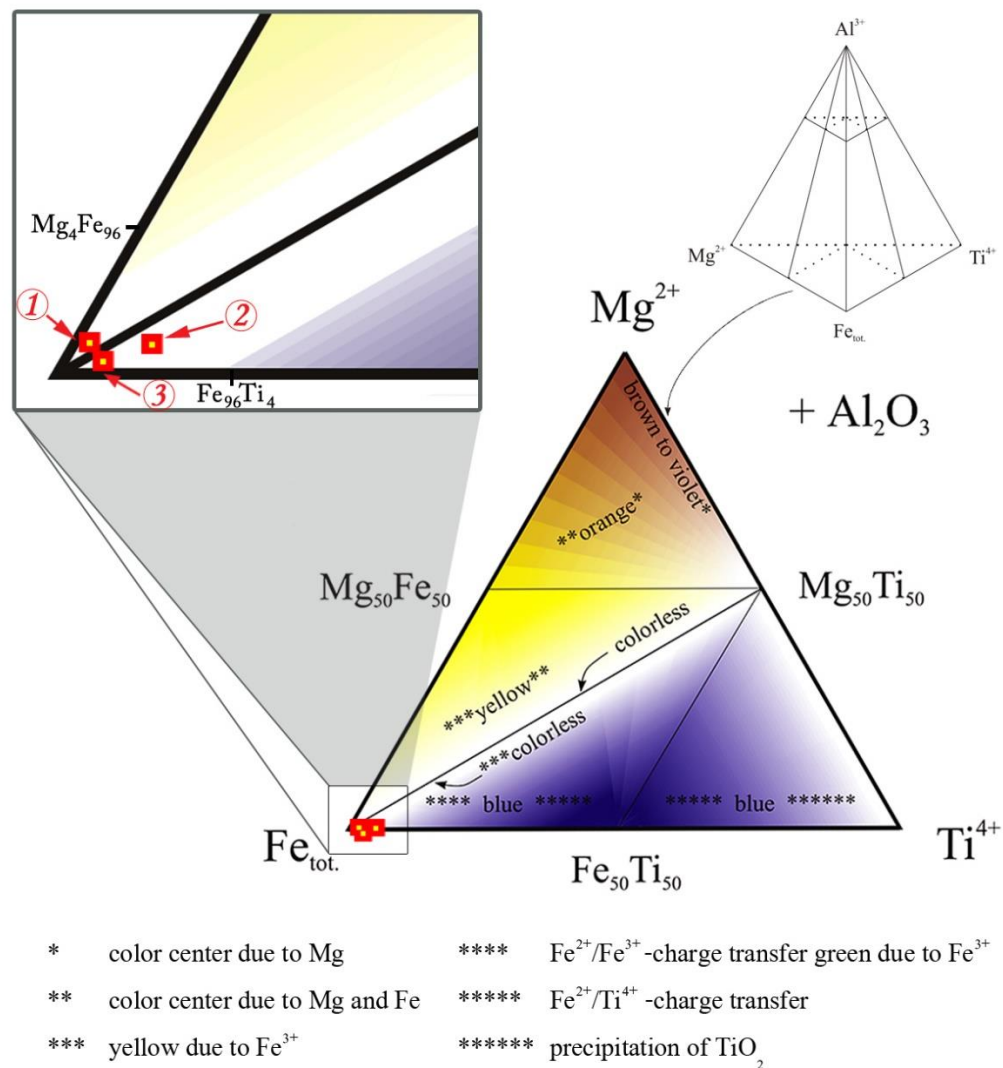


Figure 6.3 Composition of some treated sapphire discussed in text plotted on the triangular diagram proposed by Häger (2001) which clustered at the only Fe apex shows blue coloring

.Intensity of color appearances after high temperature heat treatment are strongly effected by trace elements, particularly Fe. In addition, trace element analyses by LA-ICP-MS show rather high Fe contents ranging between about 2300 and 5900 atom mole ppm, amp. Averages of 2900 amp 3100 amp and 4300 amp were obtained from minor silky inclusions (Group A), moderate silky inclusions (Group B) and abundant silky inclusions (Group C), representatively. Ti and Mg of representative samples (18 pcs.) were analyzed. Their silky inclusions zones usually typically contain $\text{Ti} > \text{Mg}$

whereas silky inclusions free zones reveal $Mg > Ti$. The later cases commonly show green-bluish yellow after heating (Figure 6.4). The best sample for sapphire yielded blue after high temperature heat may be represented by sample B5 (see Figure 6.4). Some samples in group A have lost their blue shade as reported in chapter 4 (again, see Figure 4.1.) which are also plotted over $Mg_{50}Ti_{50}$ composition line (see Figure 6.4) that usually yielded pale green-bluish yellow after high temperature treatment. These trace elements may form only $MgTiO_2$ clusters. There was no excess Ti to form color effective $FeTiO_3$ clusters (Häger, 2001).

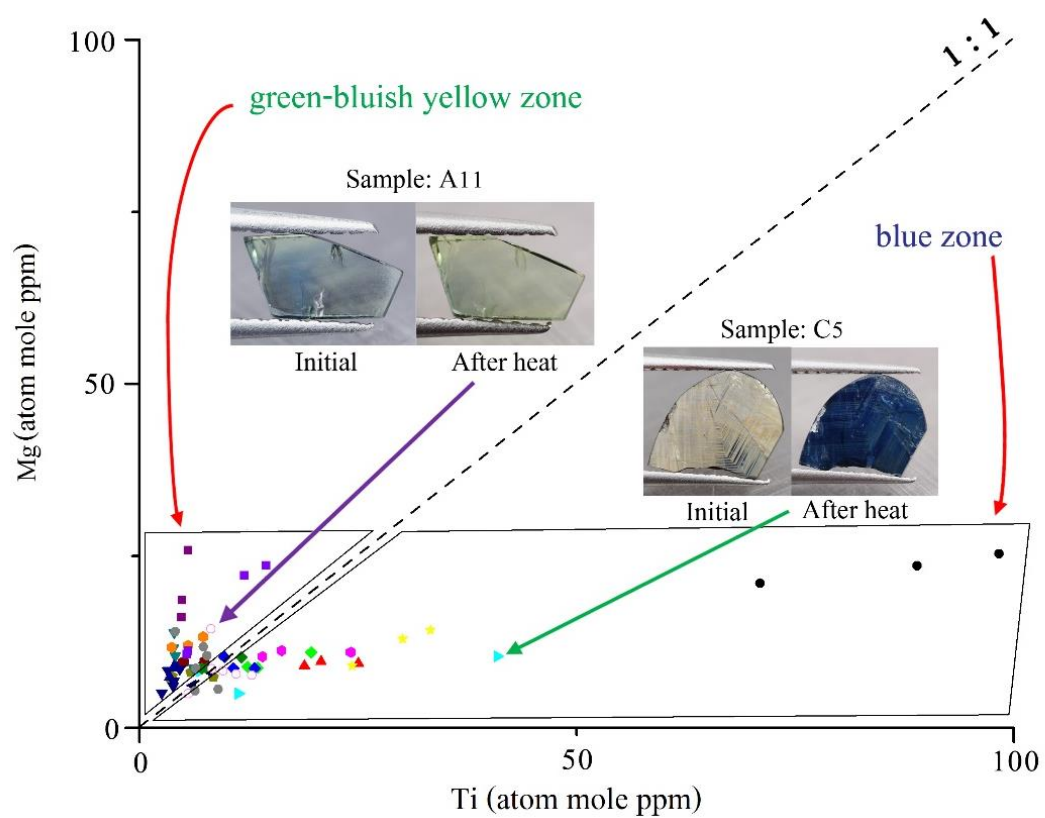


Figure 6.4 Plots of Mg-Ti after heat treatment analyzed by LA-ICP-MS of sapphire samples for Bang Kacha deposits, Chanthaburi.

6.3 Conclusions

1. Silky inclusions found as abundant exsolved phases in opaque sapphires from basaltic deposits from Chanthaburi Province produce greyish brown colors, and usually form on the basal plane $\{0001\}$ and orientated along the crystallographic directions $\{10\bar{1}0\}$. They are very tiny grains with an average size of about $\leq 1\text{-}5\ \mu\text{m}$. Silky inclusions contain significant Fe content with minor contents of Ti and Al. These inclusions may produce special phenomenon of asterism in black star sapphire as usually discovered in Chanthaburi deposit.

2. These inclusions can be dissolved partially or completely after heating at $1650\ \text{°C}$. Blue color and transparency of sapphire samples were improved after heating experiment.

3. Blue color zones were developed from grey-brown zone of silky inclusions after heating at high temperature ($1,650\ \text{°C}$). Iron and titanium of these inclusions appear to be diffused into the sapphire's crystal lattice after heat treatment via internal diffusion process. This result is supported by UV-Vis-NIR absorption spectrum which significantly related with $\text{Fe}^{2+}/\text{Fe}^{3+}$ pairs IVCT to cause blue coloration and also supported with quantitative trace element analyses by LA-ICP-MS.

4. Heating technique can enhance opaque sapphire with abundant silky inclusions from basaltic deposits to be transparent blue sapphire. The most appropriate raw materials for this treatment method should be moderate silky inclusions sapphire group (see Figures 4.2 and 4.3).

6.4 Suggestions for further study

1. The maximum temperature of heat treatment in this study was set up to 1650 °C only. Actually, successive heating should be set up from low temperature to high temperature, e.g., 600, 800, 1000, 1200, 1400, 1600, 1800 °C to monitor the change of silky inclusions. This process could be observed a noticeable differences at various temperatures.

2. The heat treatment condition in this study should be applied and proved to sapphire containing silky inclusions which from other basaltic sources, e.g., Australian sapphires, Vietnamese sapphires. This study could be used as guidelines to enhance the sapphires from the other sources.

3. The sapphires with abundant silky inclusions group have highest iron concentration in among sample groups (see Figure 3.4). In particular, appearance of these sapphires after heating experiment yield very deep blue color. These sapphires should be re-heated up to 1200 °C (peak of exsolution temperature in this study) under oxidizing atmosphere and sufficiently long for completed dissolution. Then, held and cooled down gradually at lower temperature which in the range 700-1200 °C for a long time (800 °C is the lowest indicator for exsolution). In this process, the iron/titanium oxides is precipitated and deposited outside the crystal structure. Subsequent heat treatment may allow some recrystallization of the silky inclusions, forming thin and very fine shapes, which are deposited along the crystallographic direction. If the sapphires was cut to cabochon, this method may be produced the blue star sapphire.

REFERENCES

- Bar, S.M. and Macdonald, A.S. 1981. Geochemistry and Geochronology of Late Cenozoic Basalts of Southeast Asia. Geological Society of America Bulletin. 92(8): 1069-1142.
- Basta, E.Z. 1953. Mineralogical aspects of the system FeO-Fe₂O₃-TiO₂. Doctoral dissertation. University of Bristol.
- Beran, A. and Rossman, G.R. 2006. OH in naturally occurring corundum. European Journal of Mineralogy. 18: 441-447.
- Bowles, J.F.W., Howie, R.A., Vaughan, D.J. and Zussman, J. 2011. Rock-forming Minerals: Non-silicates: oxides, hydroxides and sulphides, 2nd ed, 5A. Great Britain: Geological Society of London.
- Bunnag, N. 2008. Crystal chemistry of coloration in corundum. Doctoral dissertation. Department of Geological Science, Faculty of Science, Chiang Mai University, 406 pp.
- Burns, R.G. 1993. Mineralogical applications of crystal field theory, 2nd ed. Cambridge, Great Britain: Cambridge University Press.
- Cornelis, K., Cornelius, S. and Hurlbut, J. 1998. Manual of Mineralogy, 21st rev. ed. USA: John Wiley & Sons.
- Emmett, J.L., Scarratt, K., McClure, S.F., Moses, T., Douthit, T.R., R., H., Novak, S., Shigley, J.E., Wang, W., Bordelon, O. and Kane, R. 2003. Beryllium diffusion of ruby and sapphire. Gems&Gemology. 39(2): 84-135.
- Feenstras, A., Sämann, S. and Wunder, B. 2005. An experimental study of Fe-Al solubility in the system corundum-hematite up to 40 kbar and 1300 °C. Journal of Petrology. 46(9): 1881-1892.
- Ferguson, J. and Fielding, P.E. 1972. The origins of the colours of natural yellow, blue, and green sapphires. The Australian Journal of Chemistry. 25(7): 1371-1385.
- Fritsch, E. and Rossman, G.R. 1987. An update on color in gems. Part 1: Introduction and colors caused by dispersed metal ions. Gems&Gemology. 23(3): 126-139.
- Gübelin, E.J. and Koivula, I.K. 1997. Photoatlas of inclusions in gemstones 3rd rev. ed. Zürich, Switzerland: ABC Edition.
- Häger, T. 1996. Farbrelevante Wechselwirkungen von Spurenelementen in Korund. Doctoral dissertation. University of Mainz.
- Häger, T. 2001. High temperature treatment of natural corundum. In Hofmeister, W., Dao, N.Q., Quang, V.X. (eds.), Proceeding of the international workshop on material characterization by solid state spectroscopy: The Minerals of Vietnam, Hanoi, Vietnam, 24-37.
- Hughes, R.W. 1997. Ruby & Sapphire. Colorado, USA: RWH Publishing.

- Izane, R.E., Izammerling, R.C., Koivula, I.K., Shigley, J.E. and Fritsch, E. 1990. The identification of blue diffusion-treated sapphire. Gems&Gemology. 26(2): 115-133.
- Kane, R.E., Boehm, E.W., Overlin, S.D., Dirlam, D.M., Koivula, I.K. and Smith, C.P. 2005. A gemological pioneer: Dr. Edward J. Gübelin. Gems&Gemology. 41(4): 298-327.
- Koivula, I.K. 1987. Internal Diffusion. Journal of Gemmology. 20(7-8): 474-477.
- Leelawattanasuk, T., Atichat, W., Sriprasert, B., Pisutha-arnond, V., Wathanakul, P., Sutthirat, C. and Sripoonjan, T. 2012. Some characteristics of blue sapphires from Cameroon. In Proceeding of The 3rd International Gem and Jewelry Conference: GIT2012 Challenging New Era of Gemological World, Bangkok, Thailand, 127-130.
- Lomthong, P. 2004. Characteristics of some corundum from Songea deposits, Tanzania. Master's Thesis. Department of Geology, Faculty of Science, Chulalongkorn University.
- Moon, A.R. and Phillips, M.R. 1984. An electron microscopy study of exsolved phases in natural black Australian sapphire. Micron and Microscopica Acta. 15(3): 143-146.
- Muan, A. and Gee, C.L. 1956. Phase equilibrium studies in the system iron oxide- Al_2O_3 in air and at 1 atm. O_2 pressure. Journal of The American Ceramic Society. 39(6): 207-214.
- Nassau, K. 1978. The origin of color in minerals. American Mineralogist. 63: 219-229.
- Nassau, K. 1981. Heat treating ruby and sapphire: Technical aspects. Gems&Gemology. 17(3): 121-131.
- Nassau, K. 1994. Gemstone Enhancement, 2nd rev ed. Great Britain: Redwood books.
- Nassau, K. 2001. The physics and chemistry of colour: The fifteen causes of colour, 2nd ed. USA: John Wiley&Sons.
- Nassau, K. and Valent, G.K. 1987. The seven types of yellow sapphire and their stability to light. Gems&Gemology. 23(4): 221-231.
- Nickel, E.H. 1958. The composition and microtexture of an ulvöspinel-magnetite intergrowth. Canadian Mineralogist. 6: 113.
- Pattamalai, K. 2002. Heat treatment of some corundum from Madagascar. Master's Thesis. Department of Geology, Faculty of Science, Chulalongkorn University.
- Pisutha-arnond, V., Häger, T., Wathanakul, P. and Atichat, W. 2004. Yellow and brown coloration in beryllium treated sapphires. Journal of Gemmology. 29(2): 77-103.
- Pisutha-arnond, V., Häger, T., Wathanakul, P. and Atichat, W. 2006. The role of Be, Mg, Fe and Ti in causing colour in corundum. Journal of Gemmology. 30(3/4): 131-143.
- Pisutha-arnond, V., Naruedeesombut, N., Chaipaksa, M., Sripoonjan, T., Wanthanachaisaeng, W., Sutthirat, C., Atichat, W., Sriprasert, B., Wathanakul, P. and Leelawattanasuk, T. 2012. Newly Treated Blue Sapphire - a Preliminary Investigation. In

- Proceeding of The 3rd International Gem and Jewelry Conference: GIT2012 Challenging New Era of Gemological World, Bangkok, Thailand, 235-239.
- Reed, S.J.B. 2005. Electron microprobe analysis and scanning electron microscopy in geology, 2nd ed. Great Britain: Cambridge University Press.
- Sakkaravej, S. 2004. Thermal enhancement of some blue sapphires from Madagascar. Master's Thesis. Department of Geology, Faculty of Science, Chulalongkorn University.
- Saminpanya, S. 2001. Ti-Fe mineral inclusions in star sapphire from Thailand. The Australian Gemmologist. 21(3): 125-128.
- Saminpanya, S., Manning, D.A.C., Droop, G.T.R. and Henderson, C.M.B. 2003. Trace elements in Thai gem corundums. Journal of Gemmology. 28(7): 399-415.
- Saminpanya, S. and Sutherland, F.L. 2011. Different origins of Thai area sapphire and ruby, derived from mineral inclusions and co-existing minerals. European Journal of Mineralogy. 23: 683-694.
- Schmetzer, K. and Kiefert, L. 1990. Spectroscopic evidence for heat treatment of blue sapphire from Sri Lanka-additional data. Journal of Gemmology. 22(2): 80-82.
- Smith, C.P. 1995. A contribution to understanding the infrared spectra of rubies from Mong Hsu, Myanmar. Journal of Gemmology. 24(5): 321-335.
- Somboon, C. 2006. Yellow coloration in heat-treated natural sapphires. Master's Thesis. Department of Geology, Faculty of Science, Chulalongkorn University.
- Sripoonjan, T., Pisutha-arnond, V., Atichat, W., Wanthanachaisaeng, W. and Sutthirat, C. 2013. A New Heat Treatment of Opaque Sapphires from Basaltic Deposit in Chanthaburi, Eastern Thailand. In Proceeding of The 10th Anniversary Meeting and First Time in the Southern Hemisphere: AOGS 10th Annual Meeting, Brisbane, Australia,
- Sutherland, F.L. and Schwarz, D. 2001. Origin of gem corundums from basaltic fields. The Australian Gemmologist. 21(1): 30-33.
- Sutherland, F.L., Schwarz, D., Jobbins, E.A., Coenraads, R.R. and Webb, G. 1998. Distinctive gem corundum suites from discrete basalt field: a comparative study of Barrington, Australia, and West Pailin, Cambodia, gemfields. Journal of Gemmology. 24(2): 65-85.
- Sutthirat, C., Charusiri, P., Farrar, E. and Clark, A.H. 1994. New ⁴⁰Ar/³⁹Ar geochronology and characteristics of some Cenozoic basalts in Thailand. In Proceedings of the International Symposium on: Stratigraphic Correlation of Southeast Asia, Bangkok, Thailand, 306-321.
- Sutthirat, C., Pisutha-arnond, V., Hauzenberger, C.A., Atichat, W., Chualaowanich, T., Khamloet, P., Lomthong, P., Saengbuanglam, S., Sripoonjan, T., Nilhud, N., Sriprasert, B. and Wathanakul, P. 2012. Genesis of basaltic corundum-evidence from magmatic and metamorphic assemblages. In Proceeding of The 3rd International Gem and Jewelry

- Conference: GIT2012 Challenging New Era of Gemological World, Bangkok, Thailand, 100-103.
- Themelis, T. 1992. The heat treatment of ruby and sapphire. USA: Word Graphic.
- Thirangoon, K. Ruby and Pink Sapphire from Aappaluttoq, Greenland [Online]. GIA Laboratory, Bangkok, Thailand, 2009. Available from: http://www.giathai.net/pdf/Greenland_Ruby_March_2009.pdf.
- Turnock, A.C. and Eugster, H.P. 1962. Fe-Al oxides: phase relationships below 1000 °C. Journal of Petrology. 3: 533-565.
- Vichit, P. 1992. Gemstones in Thailand. In Proceeding of national conference on Geologic Resource of Thailand: Potential for Future development, Bangkok, Thailand, 124-150.
- Volynets, F.K., Sidorova, E.A. and Stsepuro, N.A. 1972. Oh groups in corundum crystals which were grown with the verneille technique. Journal of Applied Spectroscopy. 17(6): 1626-1628.
- Volynets, F.K., Vorob'ev, V.G. and Sidorova, E.A. 1969. Infrared absorption bands in corundum crystals. Journal of Applied Spectroscopy. 10(6): 665-667.
- Wanthanachaisaeng, W., Bunnag, N., Sutthirat, C., Atichat, W., Ounorn, P., Sripoonjan, T. and Chanmuang, C. 2012. Influence of Be to phase change on the melted surface of high temperature-heated sapphire. In Proceeding of The 3rd International Gem and Jewelry Conference: GIT2012 Challenging New Era of Gemological World, Bangkok, Thailand, 217-219.
- Weibel, M. and Wessicken, R. 1981. Haematit als Einschluss im schwarzen Sternsaphir. Journal of The German Gemological Association. 30: 170-176.
- Yan, G., Jingzhi, L. and Beili, Z. 1995. The infrared microscope and rapid identification of gemstones. Journal of Gemmology. 24(6): 411-414.



APPENDICES

จุฬาลงกรณ์มหาวิทยาลัย
CHULALONGKORN UNIVERSITY



APPENDIX A

Table A.1 Showing the gemological properties of sapphire with silky-mineral inclusion before heating

Table A.2 Showing the gemological properties of sapphire with silky-mineral inclusion after heating

Table A.1 The gemological properties of sapphires with silky-mineral inclusion before heating.

Sample no.	S.G.	R.I.		Birefringence	Fluorescence		Pleochroism
		n_o	n_e		SWUV	LWUV	
A1	3.962	1.764	1.774	0.010	Inert	Inert	light Green/Yellow
A2	3.964	1.764	1.772	0.008	Inert	Inert	light Blue/light Green
A3	3.963	1.764	1.772	0.008	Inert	Inert	Green/Yellow
A4	3.950	1.763	1.773	0.010	Inert	Inert	Yellow/Yellow
A5	3.943	1.767	1.774	0.007	Inert	Inert	light Blue/Green
A6	3.954	1.762	1.773	0.011	Inert	Inert	light Blue/Green
A7	3.973	1.762	1.773	0.011	Inert	Inert	Blue/Green
A8	3.985	1.764	1.772	0.008	Inert	Inert	Green/Yellow
A9	3.849	1.763	1.772	0.009	Inert	Inert	light Green/Yellow
A10	3.805	1.765	1.775	0.010	Inert	Inert	Blue/Green
A11	3.803	1.764	1.776	0.012	Inert	Inert	light Blue/light Green
A12	3.906	1.764	1.772	0.008	Inert	Inert	Yellow/Yellow
B1	3.985	1.762	1.772	0.010	Inert	Inert	light Green/Yellow
B2	3.963	1.764	1.773	0.009	Inert	Inert	light Green/Yellow
B3	3.984	1.762	1.772	0.010	Inert	Inert	light Green/Yellow
B4	3.972	1.764	1.771	0.007	Inert	Inert	light Blue/Green
B5	3.988	1.764	1.772	0.008	Inert	Inert	light Blue/Green
B6	3.942	1.764	1.772	0.008	Inert	Inert	Blue/Green
B7	3.971	1.761	1.774	0.013	Inert	Inert	light Green/Yellow
B8	3.954	1.763	1.771	0.008	Inert	Inert	light Blue/Green
B9	4.068	1.762	1.772	0.010	Inert	Inert	light Blue/Green
B10	3.931	1.765	1.771	0.006	Inert	Inert	light Blue/Green

Table A.1 The gemological properties of sapphires with silky-mineral inclusion before heating (continued).

Sample no.	S.G.	R.I.		Birefringence	Fluorescence		Pleochroism
		n_o	n_e		SWUV	LWUV	
B11	3.974	1.765	1.772	0.007	Inert	Inert	Blue/Green
B12	4.019	1.765	1.773	0.008	Inert	Inert	Blue/Green
B13	3.994	1.762	1.771	0.009	Inert	Inert	Blue/Green
B14	4.05	1.762	1.773	0.011	Inert	Inert	Blue/Green
B15	3.999	1.764	1.771	0.007	Inert	Inert	light Blue/Green
B16	3.951	1.762	1.771	0.009	Inert	Inert	light Blue/Green
B17	3.92	1.763	1.772	0.009	Inert	Inert	Blue/Green
C1	3.823	1.762	1.773	0.011	Inert	Inert	Brown/Brown
C2	3.956	1.763	1.773	0.010	Inert	Inert	Brown/Brown
C3	4.001	1.759	1.771	0.012	Inert	Inert	Brown/Brown
C4	4.039	1.762	1.773	0.011	Inert	Inert	Brown/Brown
C5	3.995	1.763	1.771	0.008	Inert	Inert	Brown/Brown
C6	4.012	1.762	1.772	0.010	Inert	Inert	Brown/Brown
C7	3.978	1.763	1.773	0.010	Inert	Inert	Brown/Brown
C8	4.051	1.763	1.775	0.012	Inert	Inert	Brown/Brown
C9	4.009	1.759	1.770	0.011	Inert	Inert	Brown/Brown
C10	3.973	1.761	1.772	0.011	Inert	Inert	dark Yellow/Green

Table A.2 The gemological properties of sapphires with silky-mineral inclusion after heating.

Sample no.	S.G.	R.I.		Birefringence	Fluorescence		Pleochroism
		n_o	n_e		SWUV	LWUV	
A1	3.947	1.765	1.773	0.008	Inert	Inert	light Blue/Green
A2	3.971	1.763	1.773	0.010	Inert	Inert	light Green/Yellow
A3	3.974	1.766	1.773	0.007	Inert	Inert	light Green/Yellow
A4	4.004	1.764	1.774	0.010	Inert	Inert	light Blue/Green
A5	4.046	1.764	1.773	0.009	Inert	Inert	light Green/Yellow
A6	3.969	1.765	1.772	0.007	Inert	Inert	light Green/Yellow
A7	4.021	1.763	1.771	0.008	Inert	Inert	light Blue/Green
A8	3.954	1.765	1.772	0.007	Inert	Inert	light Blue/light Green
A9	4.068	1.765	1.772	0.007	Inert	Inert	light Green/Yellow
A10	3.931	1.766	1.773	0.007	Inert	Inert	light Blue/light Green
A11	3.974	1.764	1.774	0.010	Inert	Inert	light Green/Yellow
A12	3.973	1.765	1.773	0.008	Inert	Inert	light Green/light Yellow
B1	3.992	1.764	1.771	0.007	Inert	Inert	Green/Yellow
B2	3.94	1.764	1.772	0.008	Inert	Inert	light Blue/Green
B3	3.997	1.763	1.773	0.010	Inert	Inert	light Blue/Green
B4	3.965	1.764	1.771	0.007	Inert	Inert	light Blue/Green
B5	3.918	1.766	1.772	0.006	Inert	Inert	light Blue/Green
B6	4.007	1.766	1.772	0.006	Inert	Inert	light Blue/Green
B7	3.908	1.762	1.772	0.010	Inert	Inert	light Blue/Green
B8	3.933	1.764	1.772	0.008	Inert	Inert	light Blue/Green
B9	3.981	1.761	1.771	0.010	Inert	Inert	light Blue/Green
B10	3.973	1.764	1.772	0.008	Inert	Inert	light Blue/Green

Table A.2 The gemological properties of sapphires with silky-mineral inclusion after heating (continued).

Sample no.	S.G.	R.I.		Birefringence	Fluorescence		Pleochroism
		n_o	n_e		SWUV	LWUV	
B11	4.02	1.764	1.773	0.009	Inert	Inert	Blue/Green
B12	3.974	1.763	1.774	0.011	Inert	Inert	light Blue/Green
B13	3.985	1.761	1.771	0.010	Inert	Inert	light Blue/Green
B14	3.98	1.763	1.773	0.010	Inert	Inert	light Blue/Green
B15	3.952	1.765	1.773	0.008	Inert	Inert	Blue/Green
B16	3.965	1.763	1.772	0.009	Inert	Inert	Green/Yellow
B17	4.038	1.764	1.773	0.009	Inert	Inert	Green/Yellow
C1	3.985	1.761	1.772	0.011	Inert	Inert	Blue/Green
C2	3.849	1.762	1.772	0.010	Inert	Inert	Blue/Green
C3	3.805	1.759	1.773	0.014	Inert	Inert	Blue/Green
C4	3.803	1.764	1.772	0.008	Inert	Inert	Blue/Green
C5	4.018	1.764	1.772	0.008	Inert	Inert	Blue/Green
C6	3.967	1.762	1.773	0.011	Inert	Inert	Blue/Green
C7	4.039	1.763	1.774	0.011	Inert	Inert	Blue/Green
C8	3.937	1.765	1.774	0.009	Inert	Inert	Green/Yellow
C9	3.95	1.760	1.772	0.012	Inert	Inert	Blue/Green
C10	4.038	1.761	1.773	0.012	Inert	Inert	Blue/Green

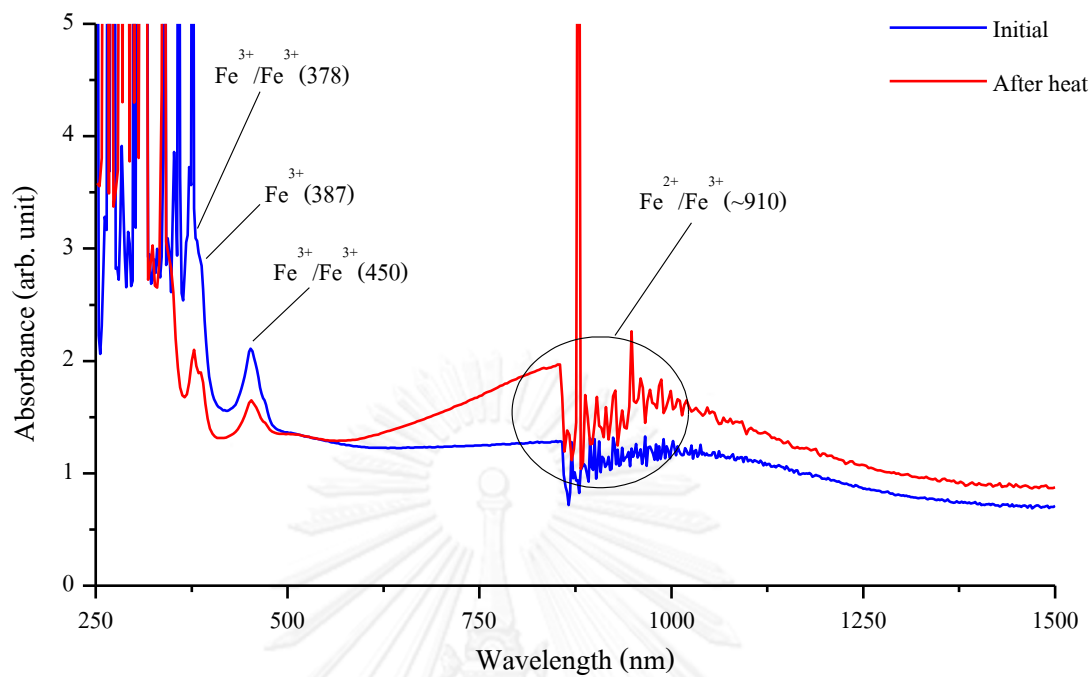


APPENDIX B

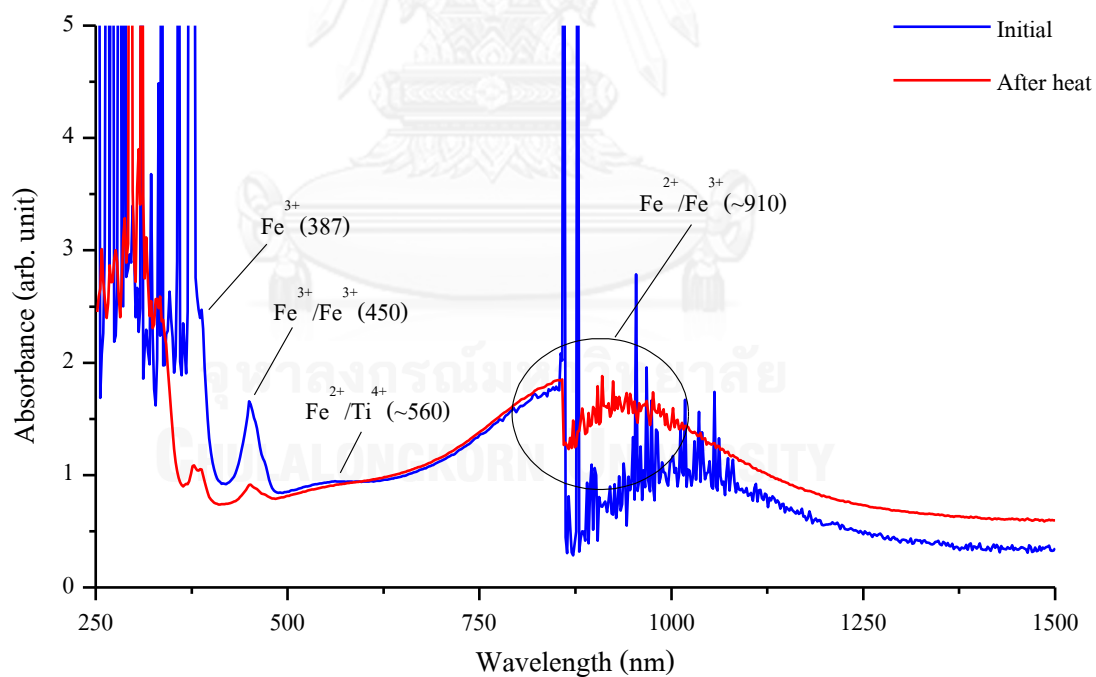
UV-Vis-NIR Spectra of sapphires initial and after heating

A (e-ray):	A1, A2, A3, A4, A5, A6, A7, A8, A9, A10, A11, A12
A (o-ray):	A1, A2, A3, A4, A5, A6, A7, A8, A9, A10, A11, A12
B (e-ray)*:	B1, B3, B5, B6, B7, B9, B10, B12, B16, B17
B (o-ray):	B1, B2, B3, B4, B5, B6, B7, B8, B9, B10, B11, B12, B13, B14, B15, B16, B17
C (e-ray)*:	-
C (o-ray):	C1, C2, C3, C4, C5, C6, C7, C8, C9, C10

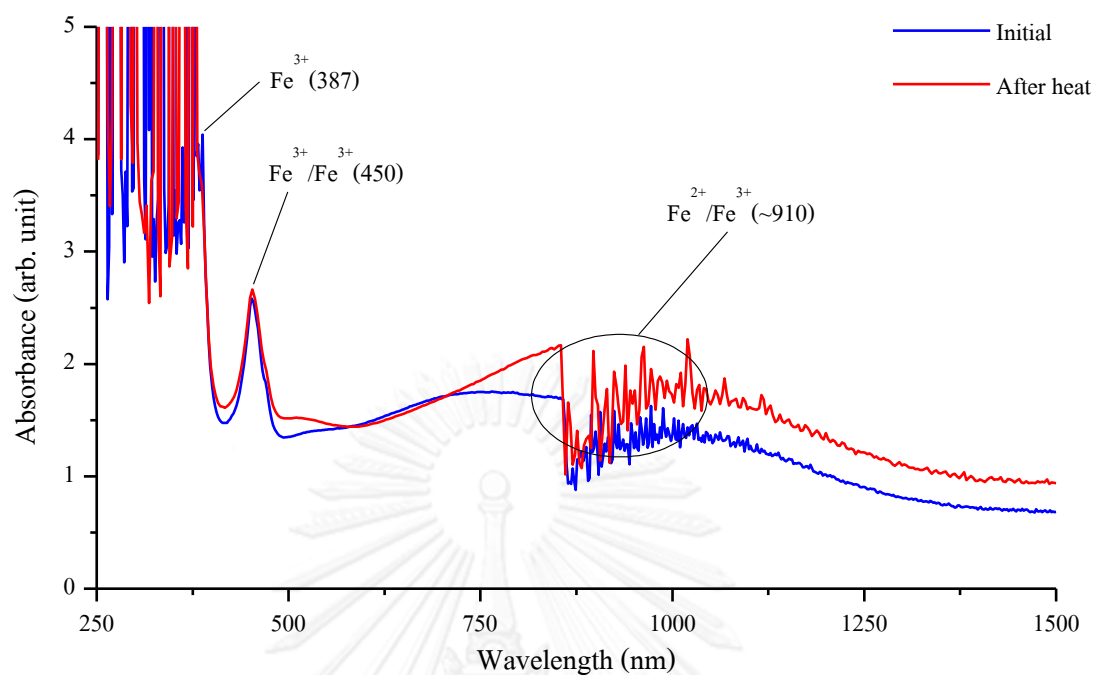
*Limitation of over thickness samples



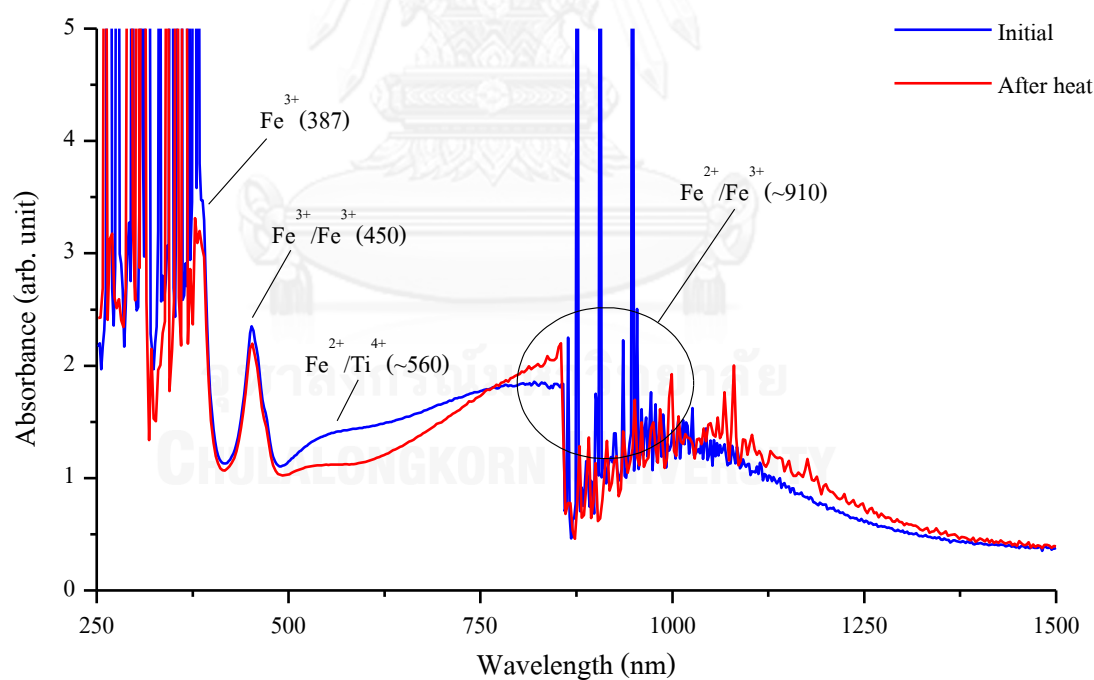
UV-Vis-NIR absorption spectra of sample A1 (e-ray)



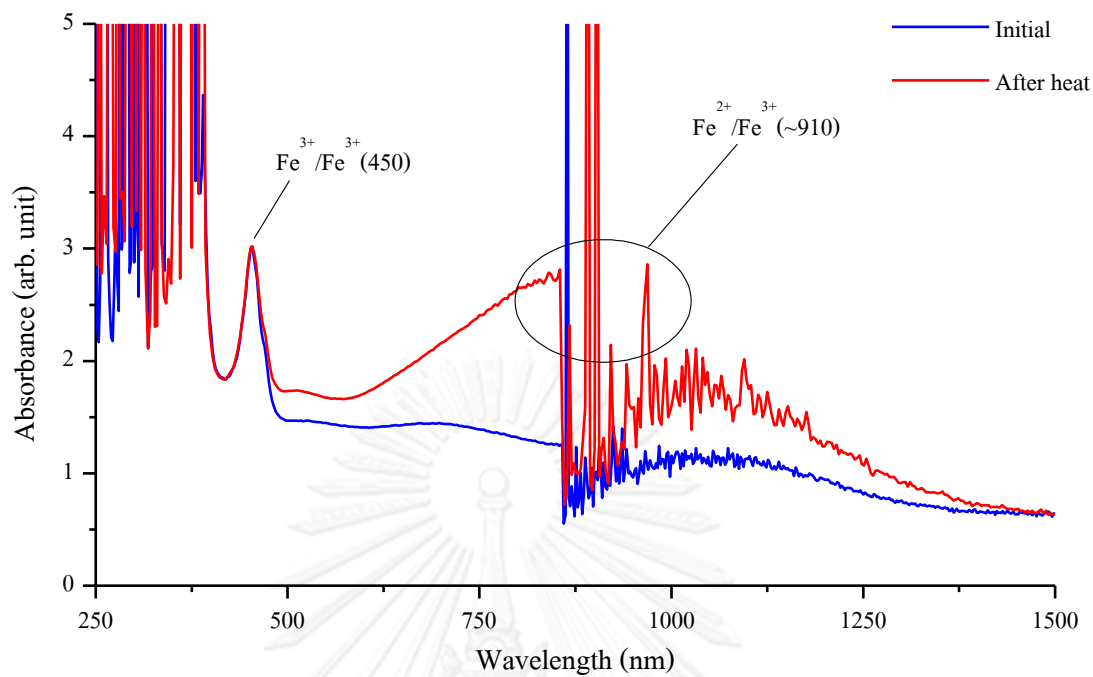
UV-Vis-NIR absorption spectra of sample A1 (o-ray)



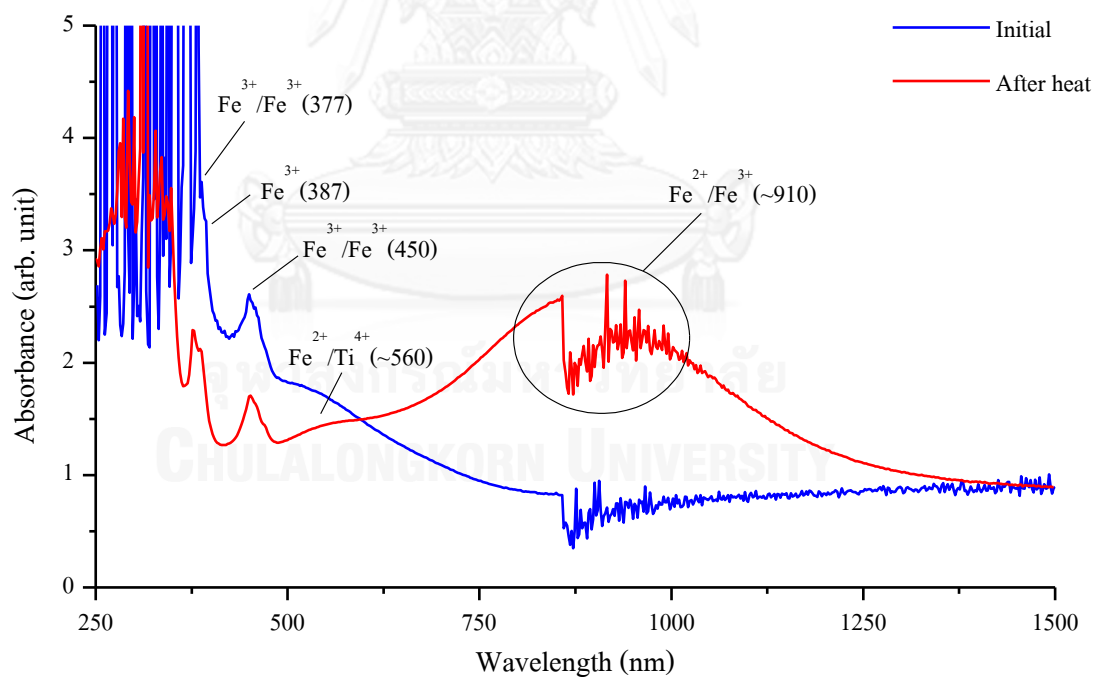
UV-Vis-NIR absorption spectra of sample A2 (e-ray)



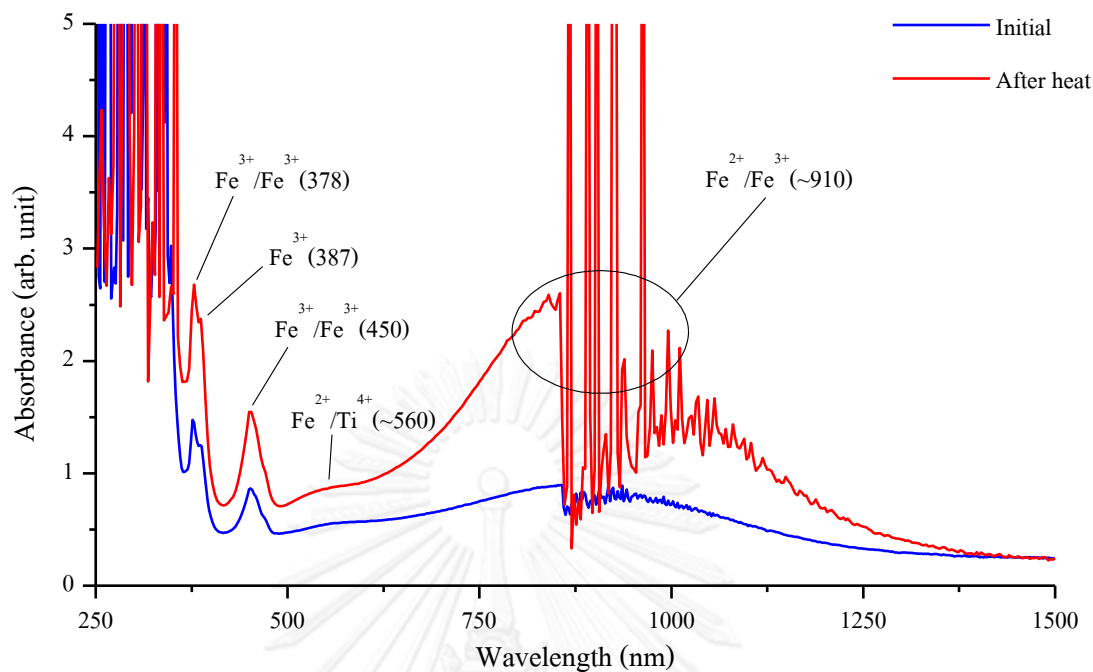
UV-Vis-NIR absorption spectra of sample A2 (o-ray)



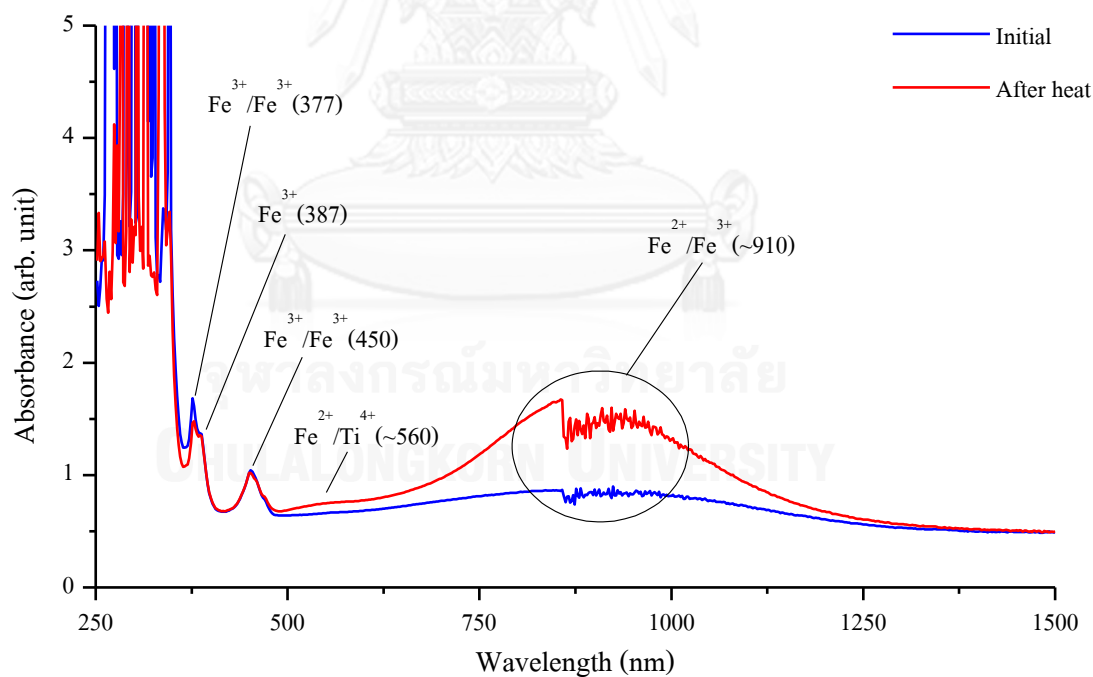
UV-Vis-NIR absorption spectra of sample A3 (e-ray)



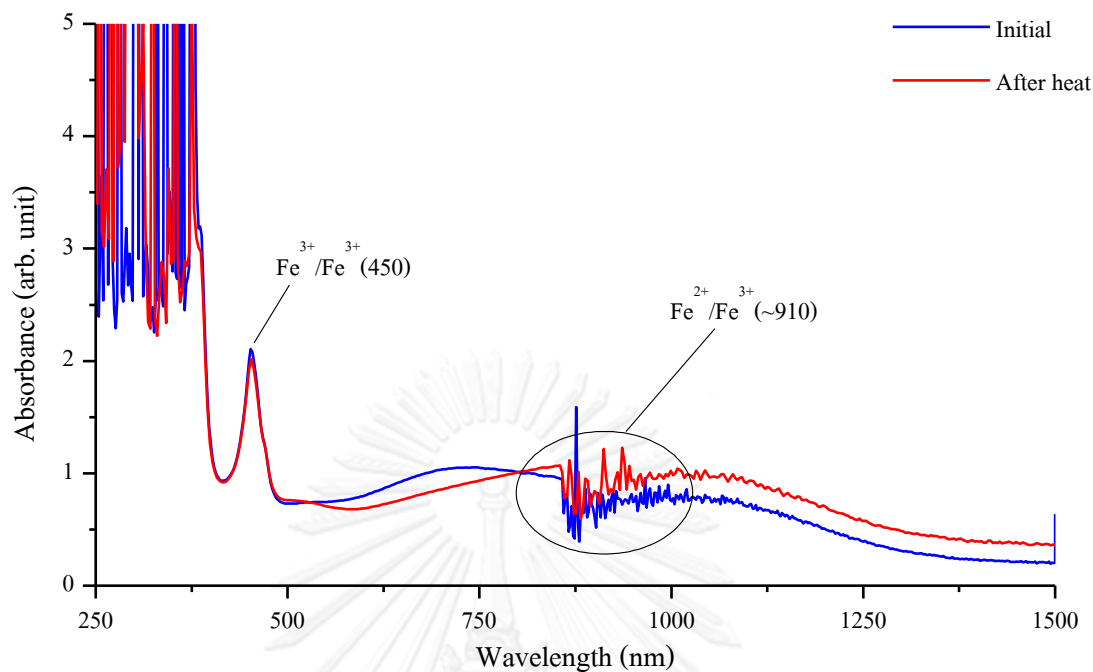
UV-Vis-NIR absorption spectra of sample A3 (o-ray)



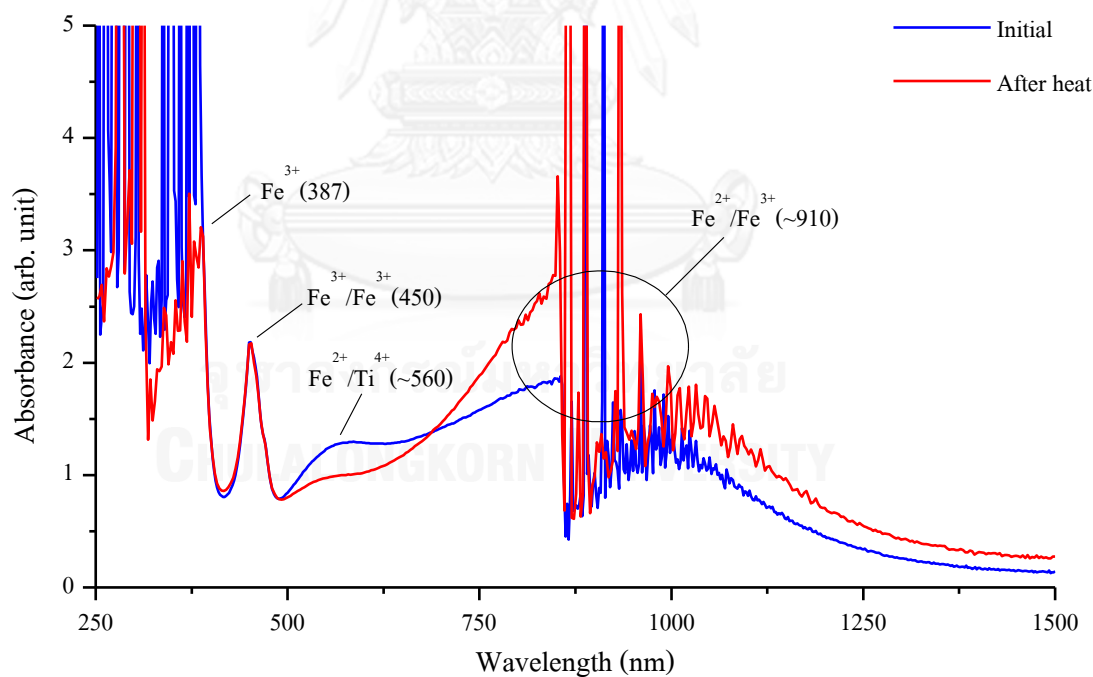
UV-Vis-NIR absorption spectra of sample A4 (e-ray)



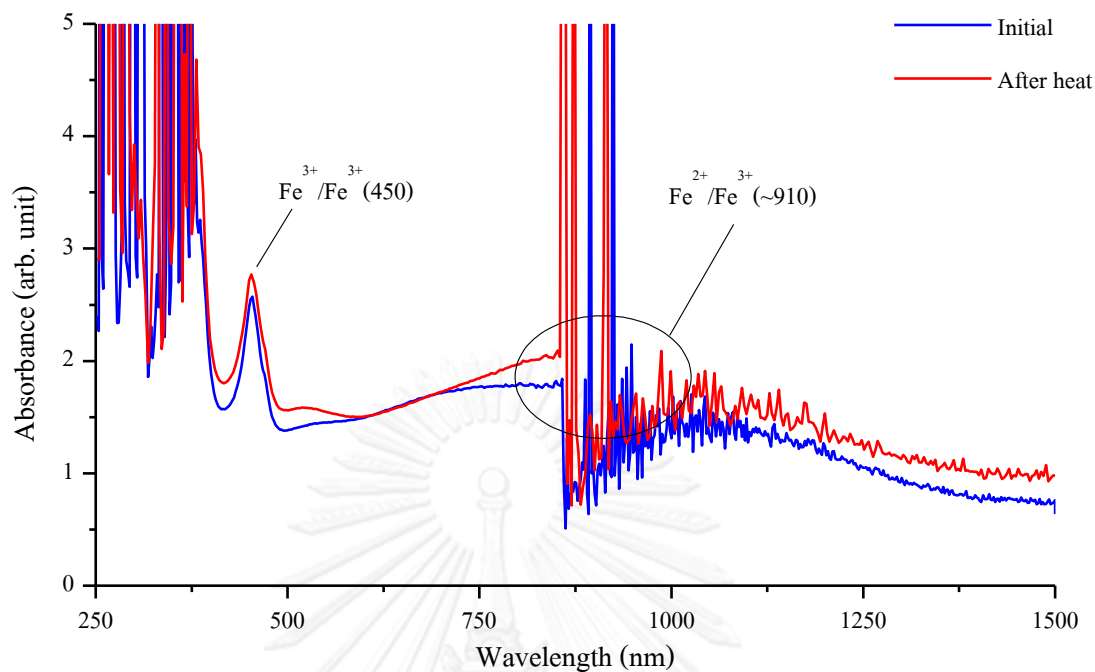
UV-Vis-NIR absorption spectra of sample A4 (o-ray)



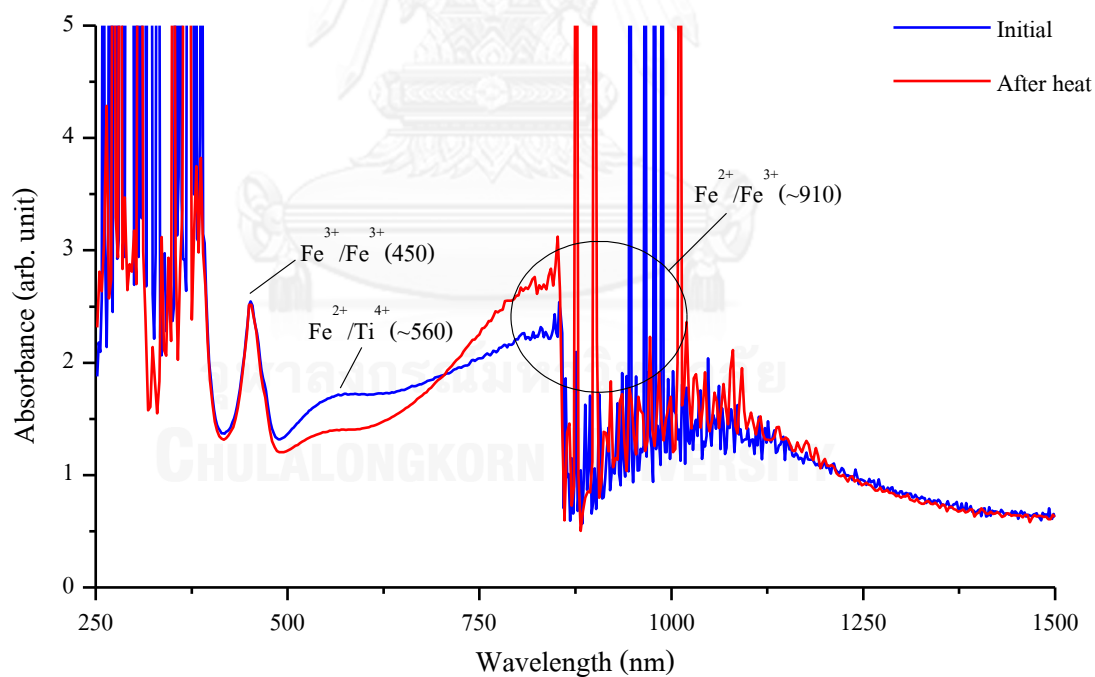
UV-Vis-NIR absorption spectra of sample A5 (e-ray)



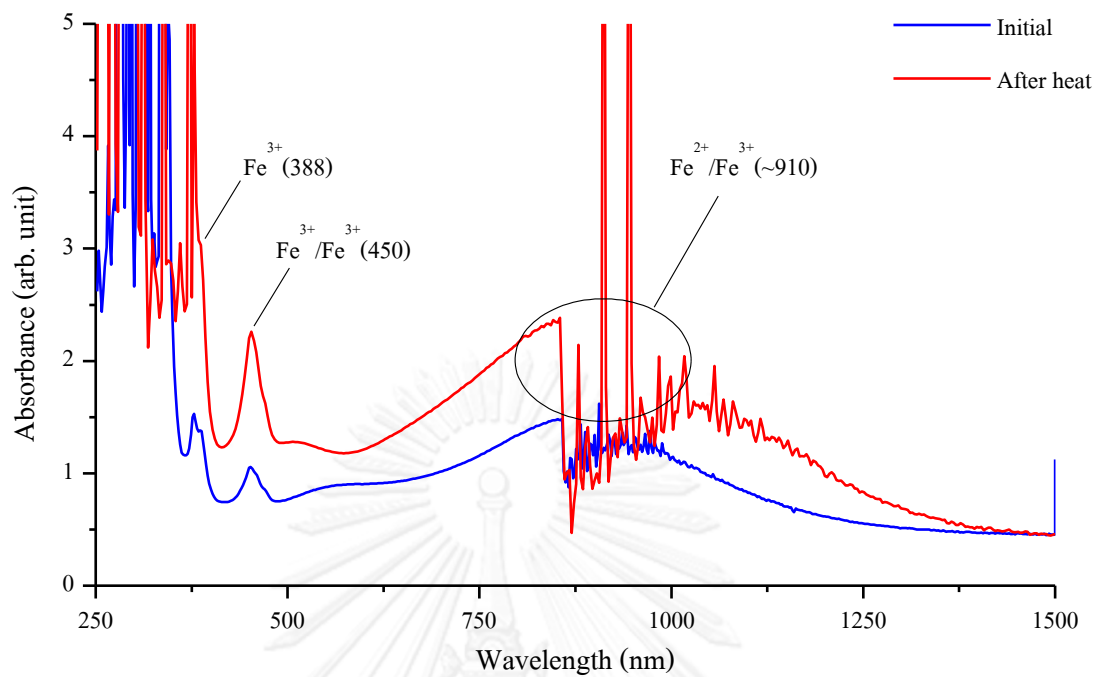
UV-Vis-NIR absorption spectra of sample A5 (o-ray)



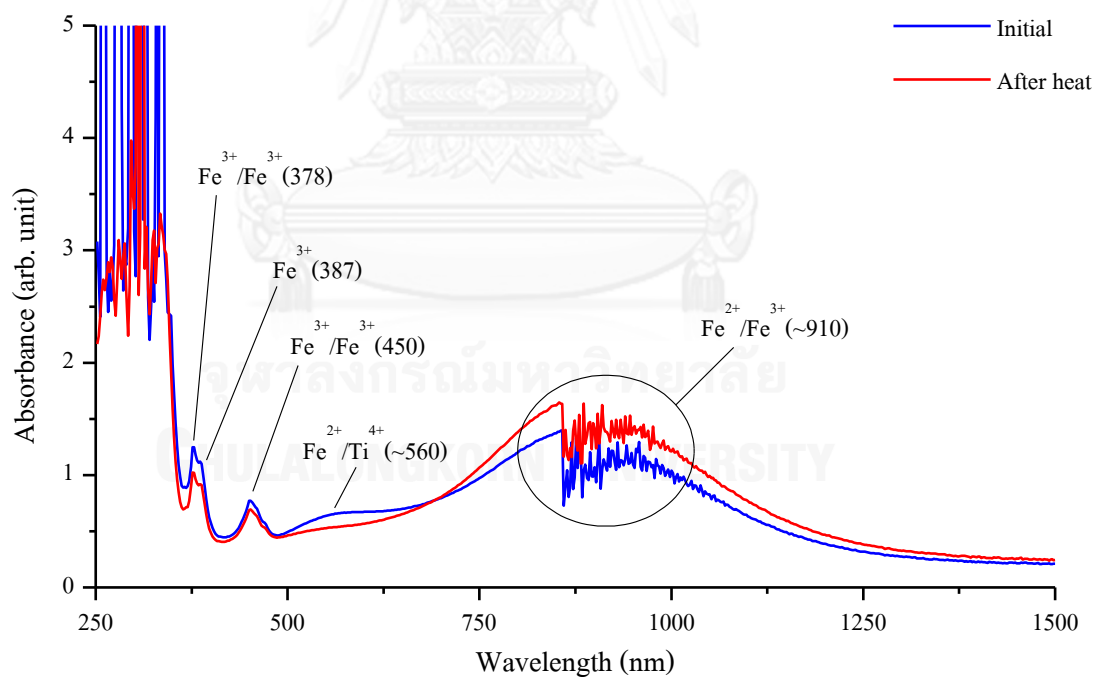
UV-Vis-NIR absorption spectra of sample A6 (e-ray)



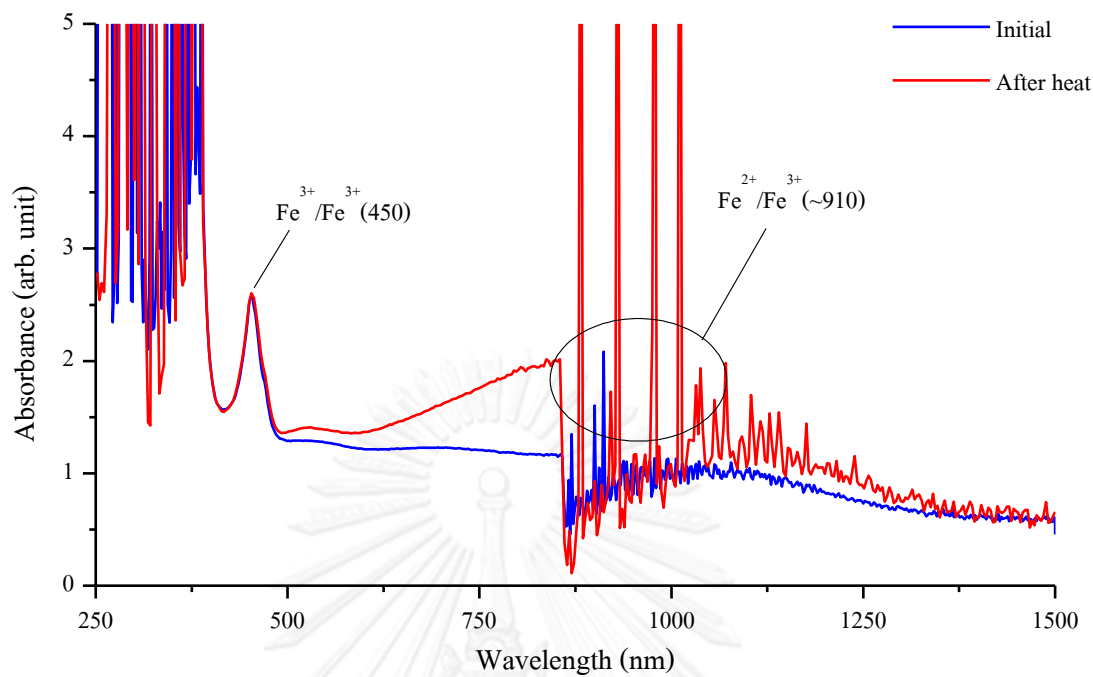
UV-Vis-NIR absorption spectra of sample A6 (o-ray)



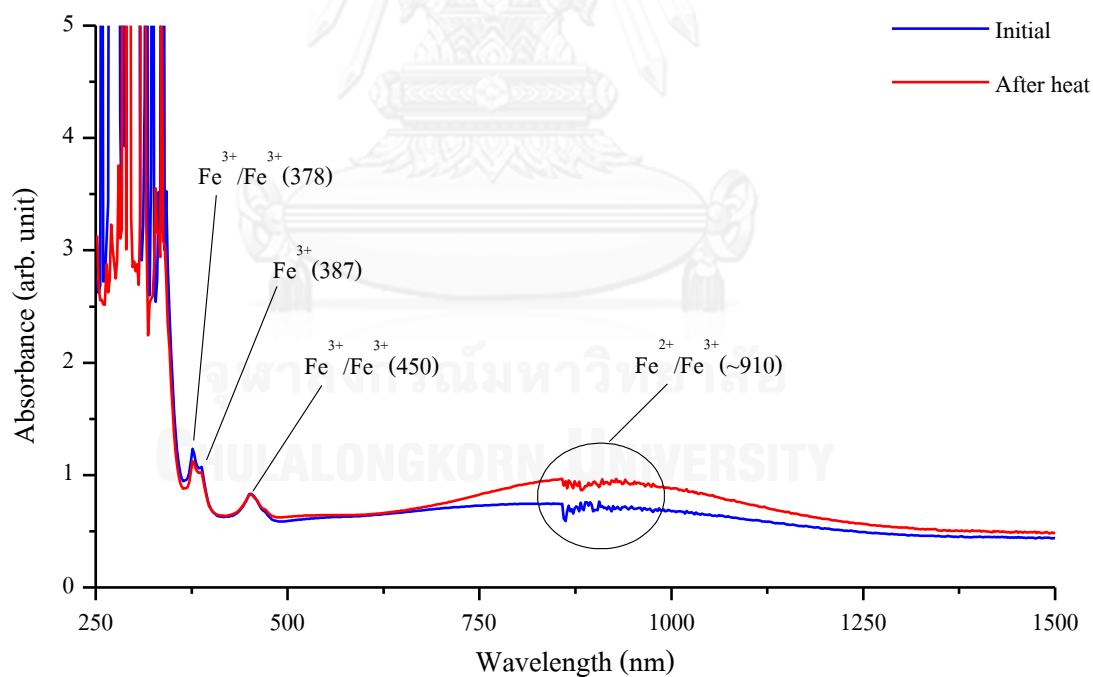
UV-Vis-NIR absorption spectra of sample A7 (e-ray)



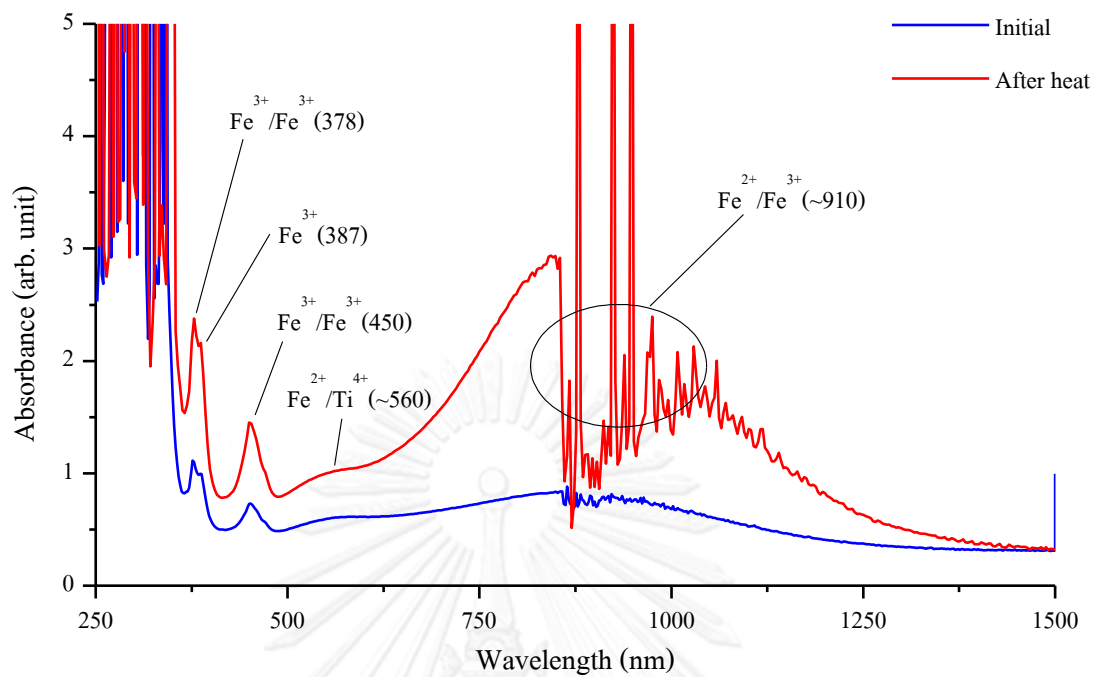
UV-Vis-NIR absorption spectra of sample A7 (o-ray)



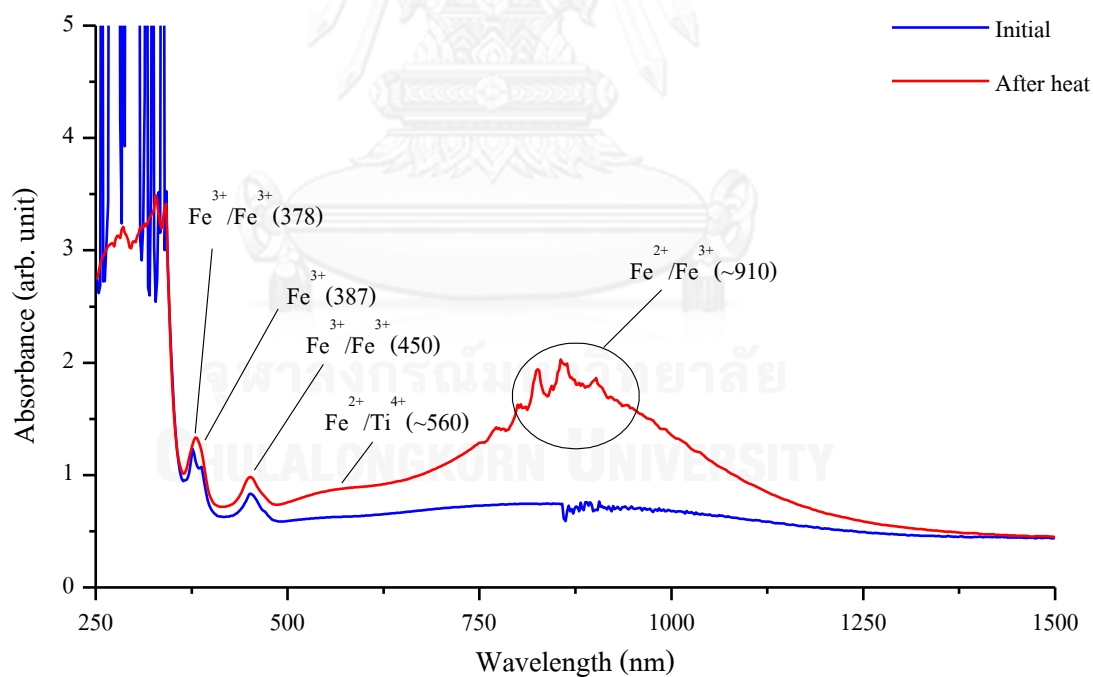
UV-Vis-NIR absorption spectra of sample A8 (e-ray)



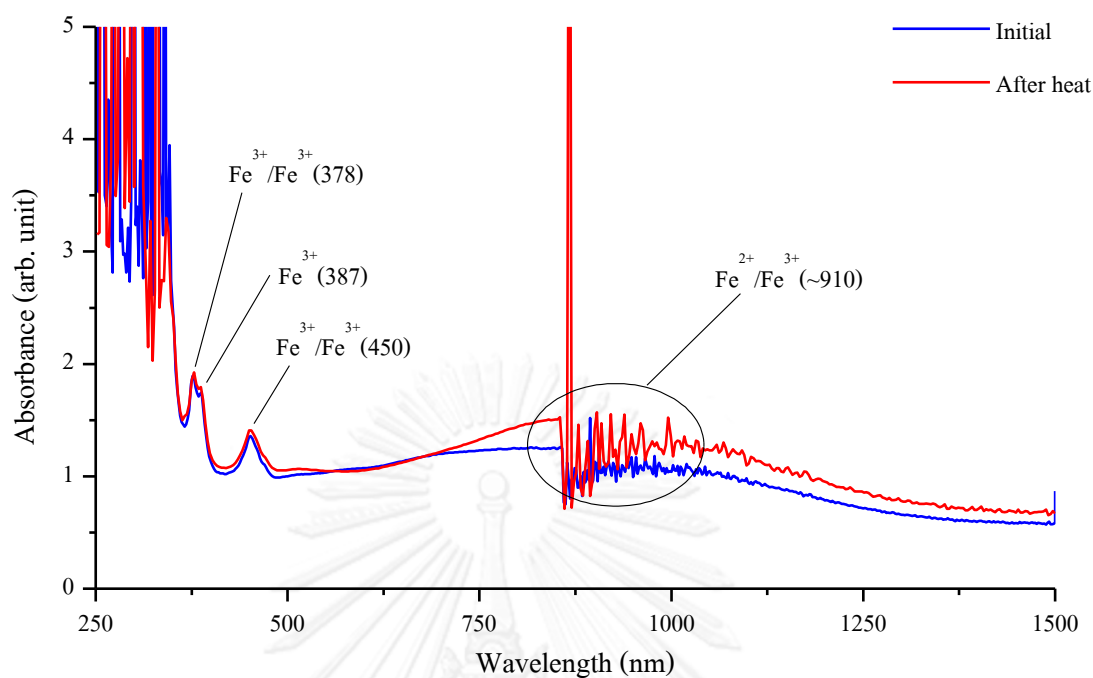
UV-Vis-NIR absorption spectra of sample A8 (o-ray)



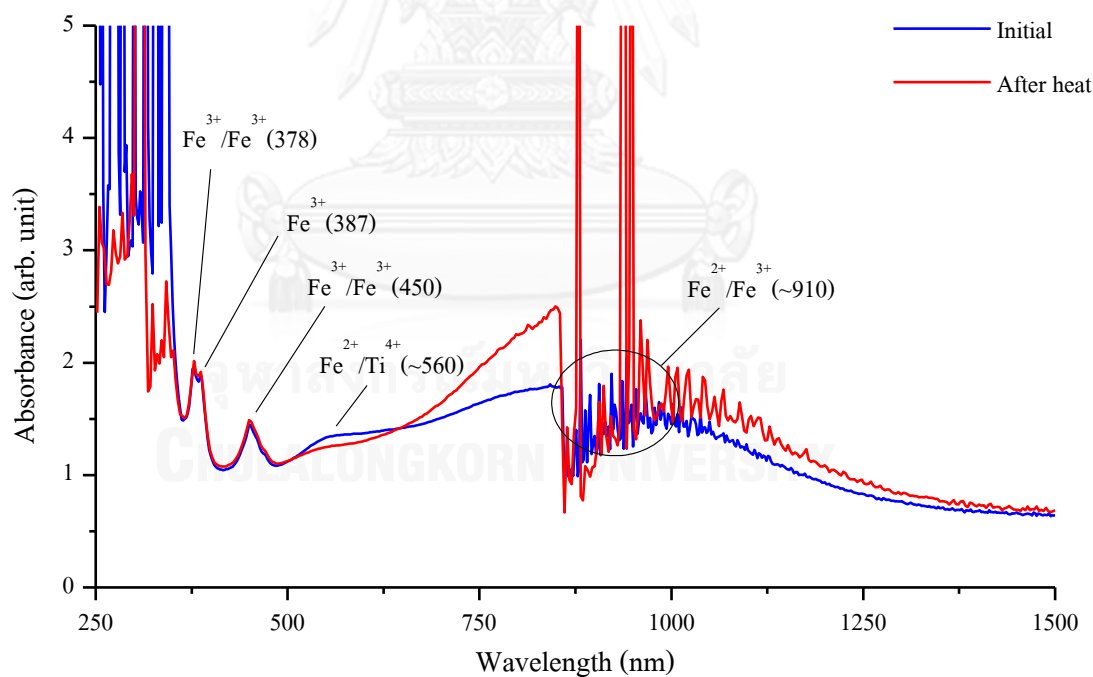
UV-Vis-NIR absorption spectra of sample A9 (e-ray)



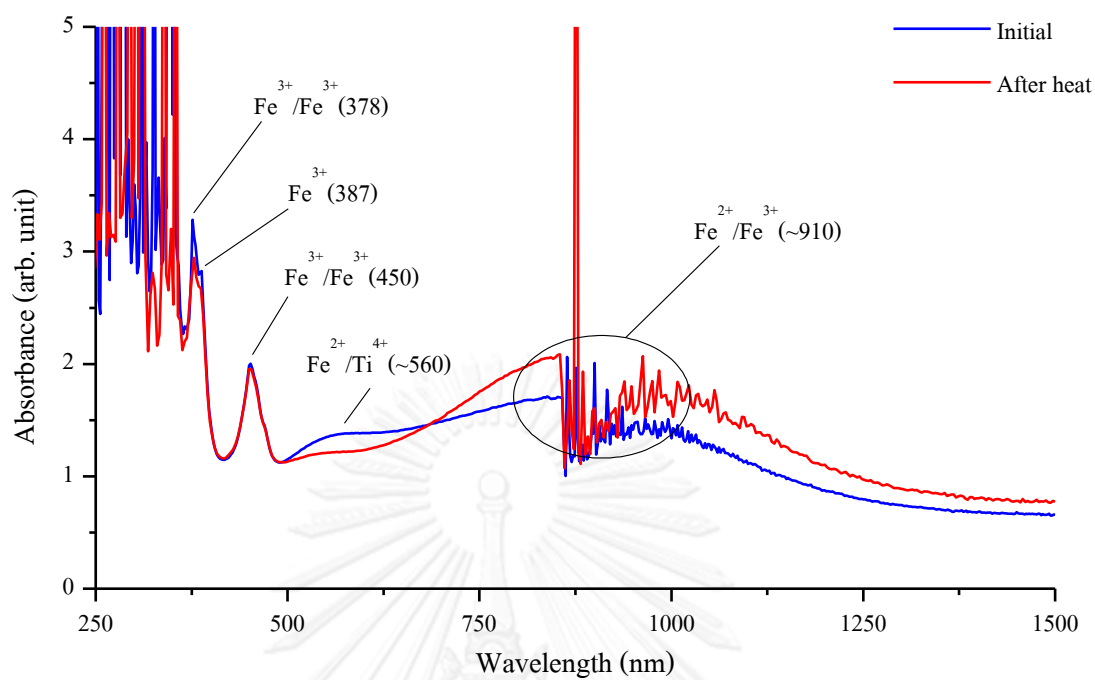
UV-Vis-NIR absorption spectra of sample A9 (o-ray)



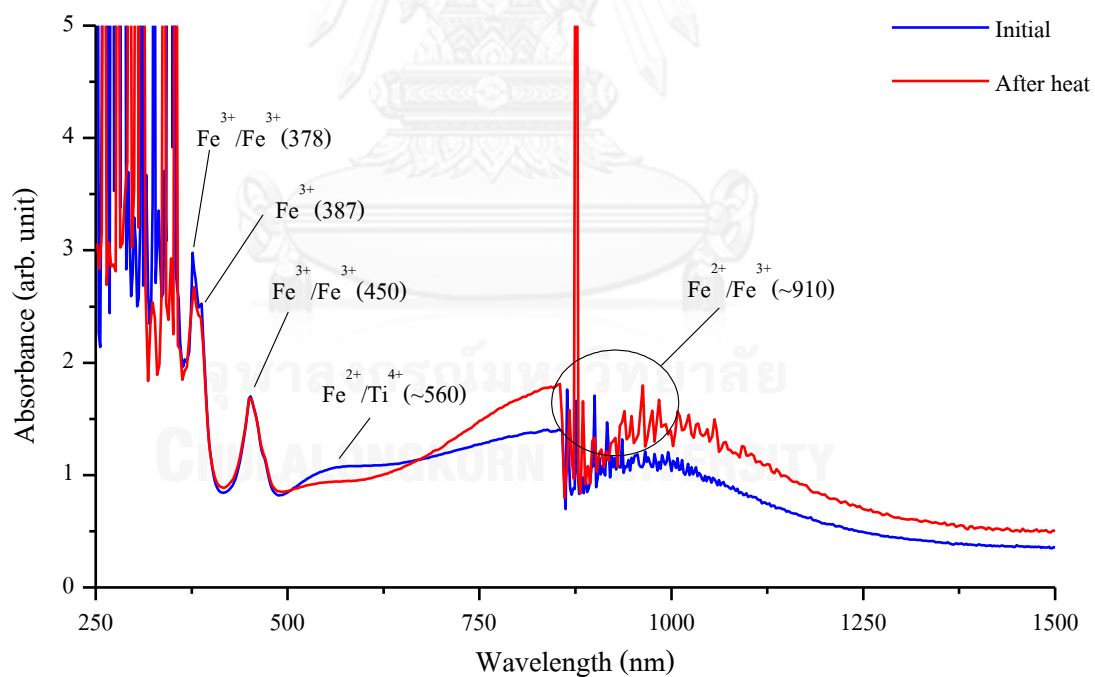
UV-Vis-NIR absorption spectra of sample A10 (e-ray)



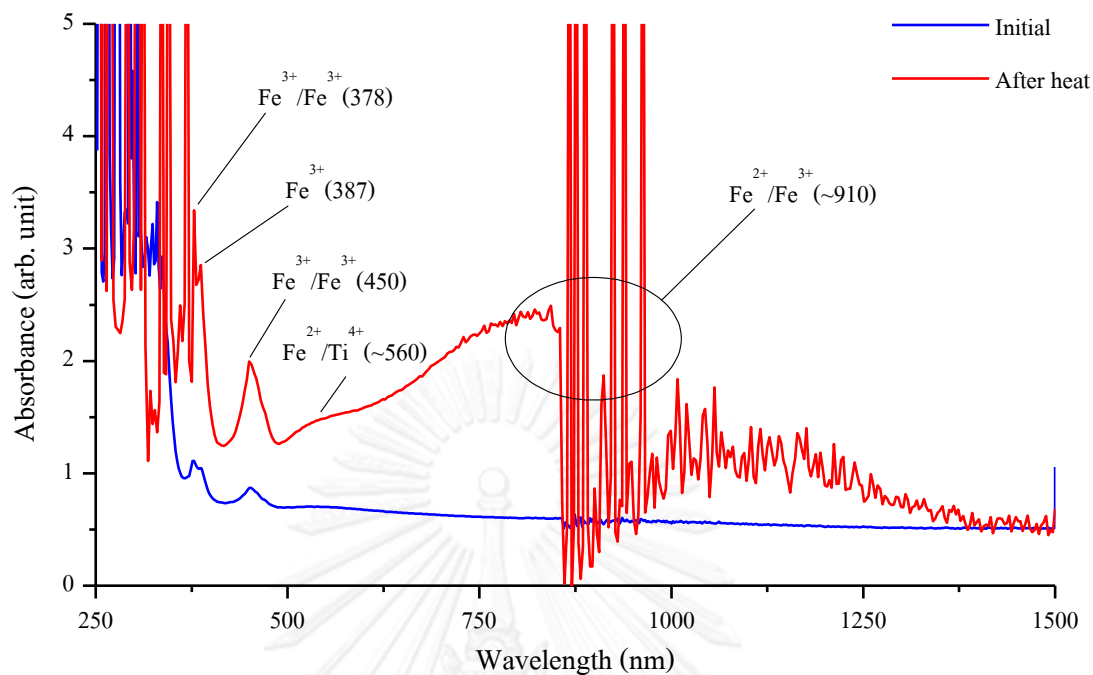
UV-Vis-NIR absorption spectra of sample A10 (o-ray)



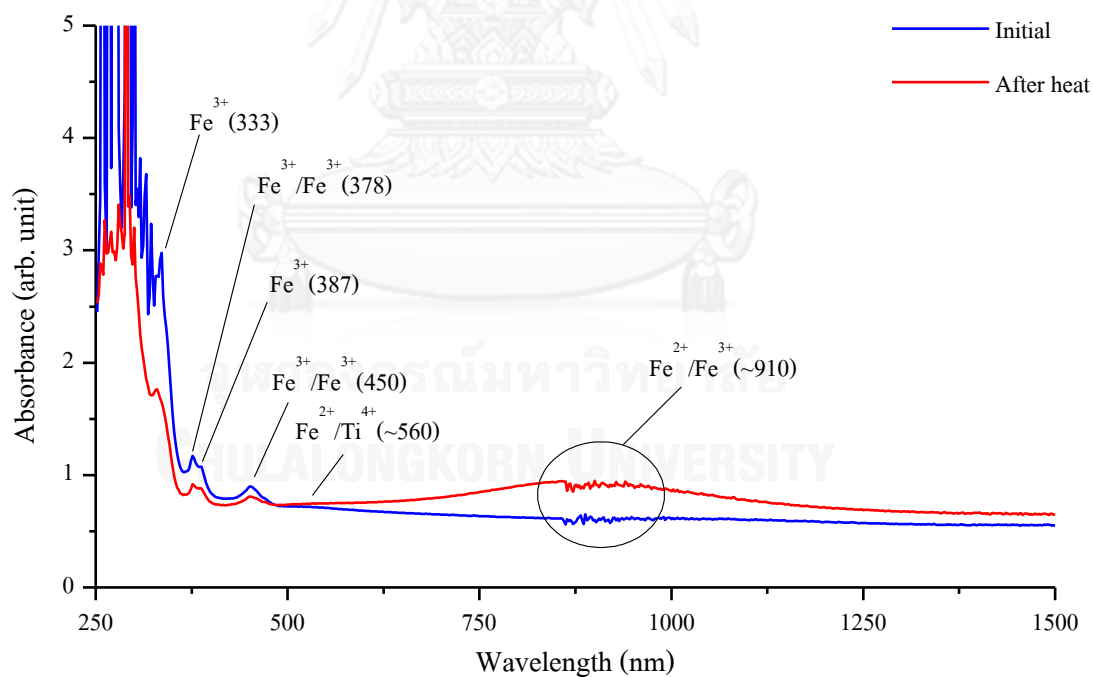
UV-Vis-NIR absorption spectra of sample A11 (e-ray)



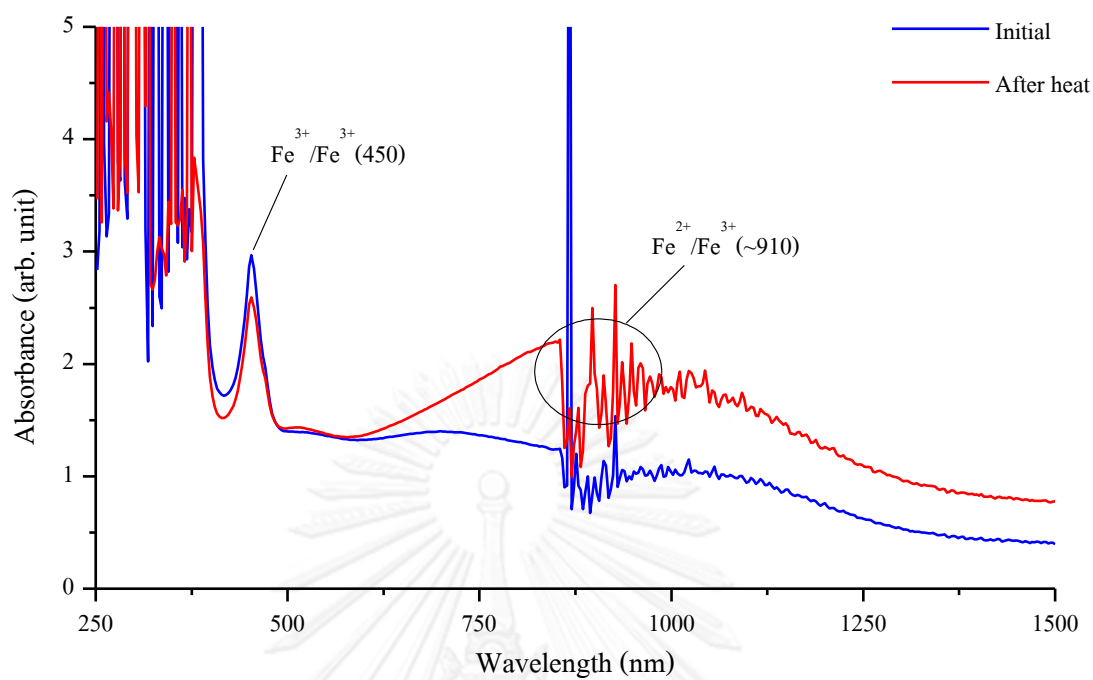
UV-Vis-NIR absorption spectra of sample A11 (o-ray)



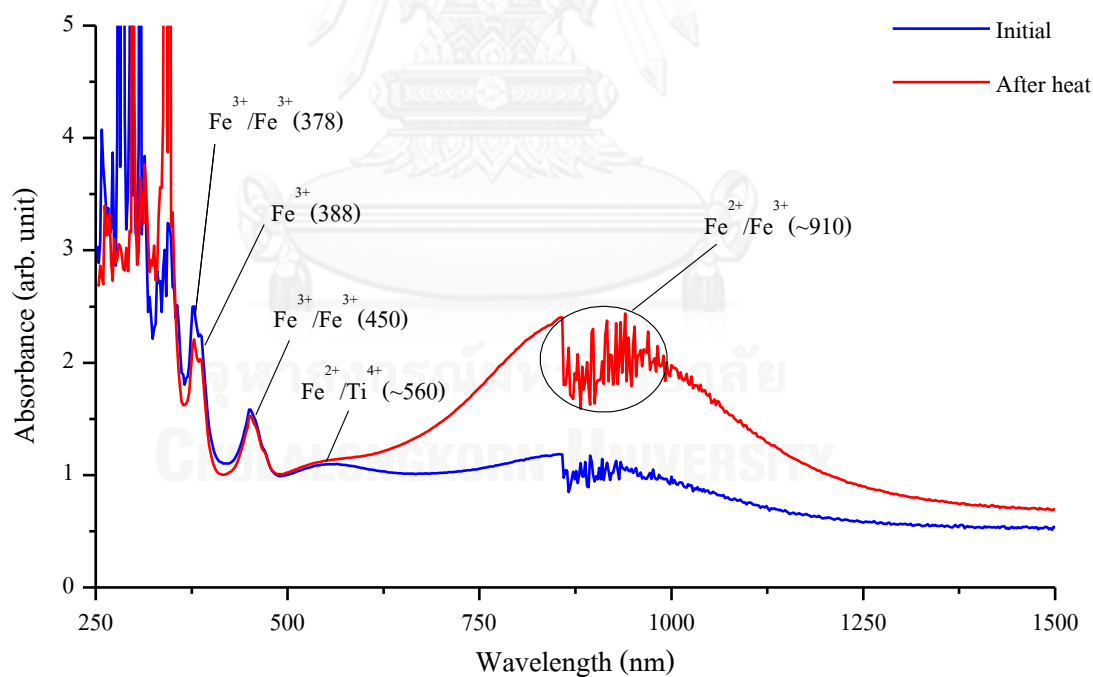
UV-Vis-NIR absorption spectra of sample A12 (e-ray)



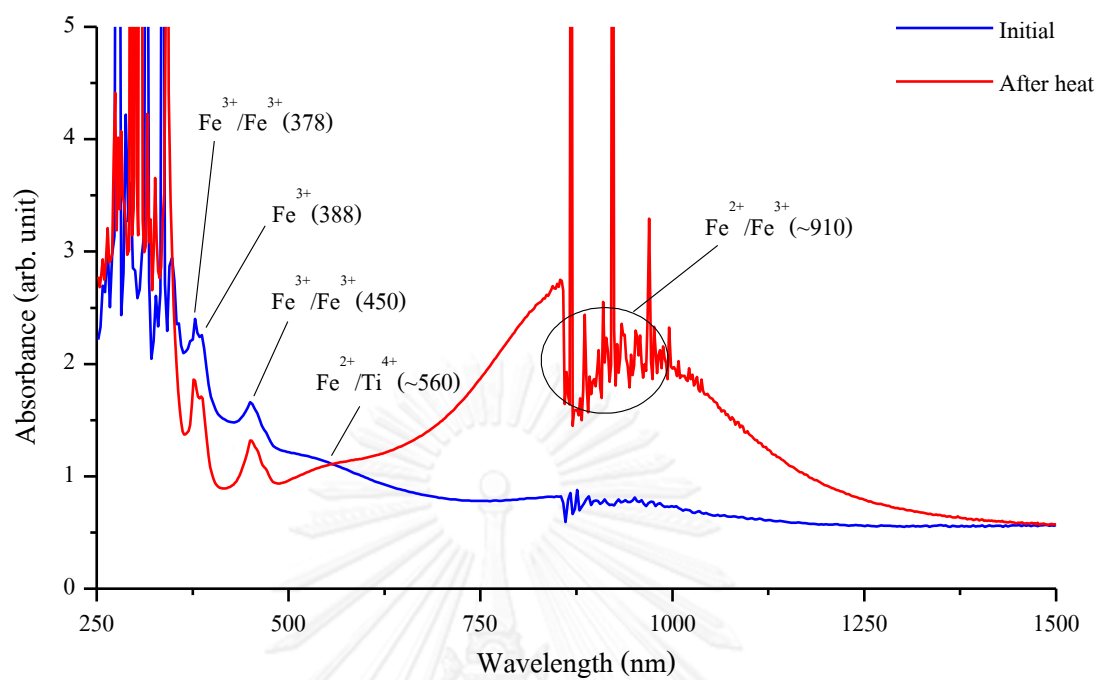
UV-Vis-NIR absorption spectra of sample A12 (o-ray)



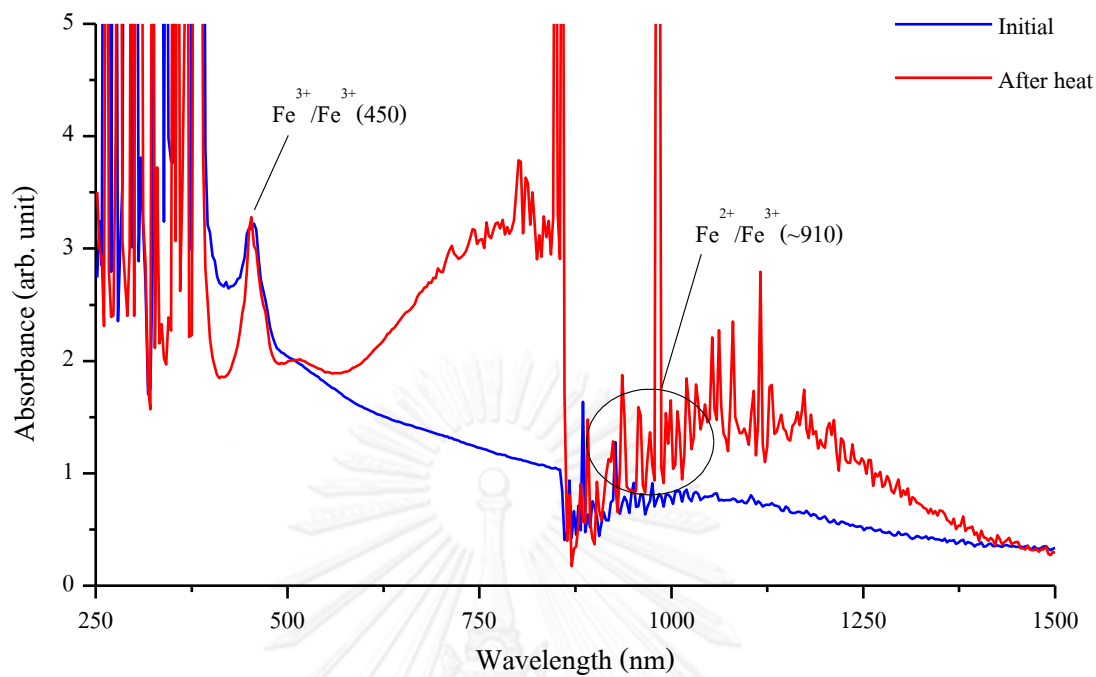
UV-Vis-NIR absorption spectra of sample B1 (e-ray)



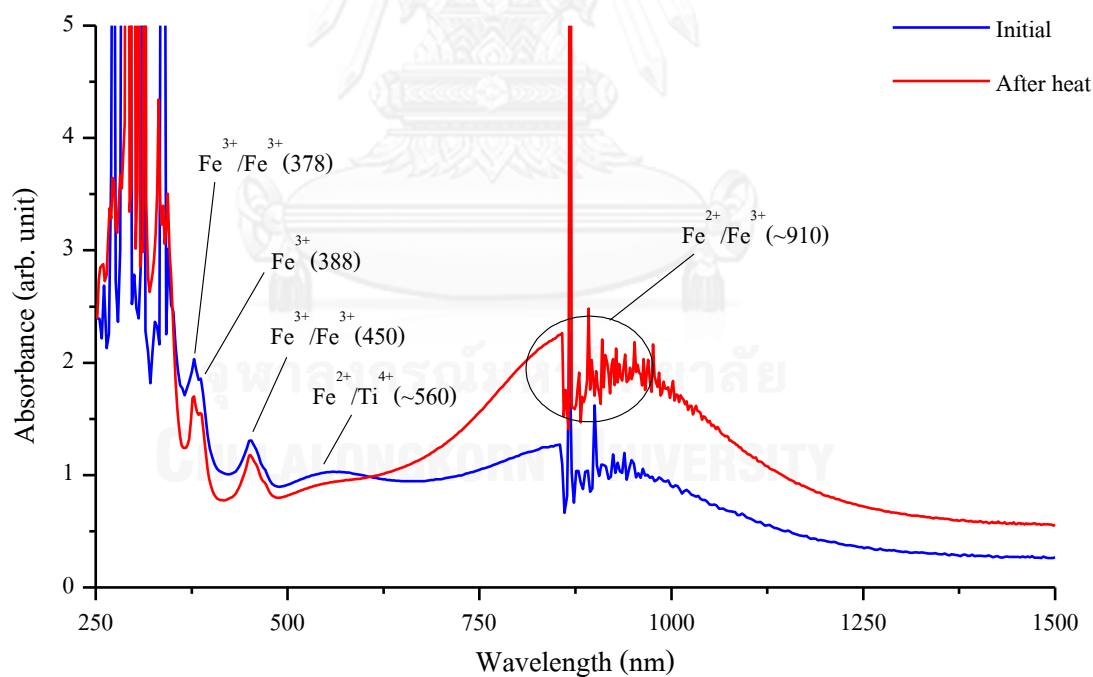
UV-Vis-NIR absorption spectra of sample B1 (o-ray)



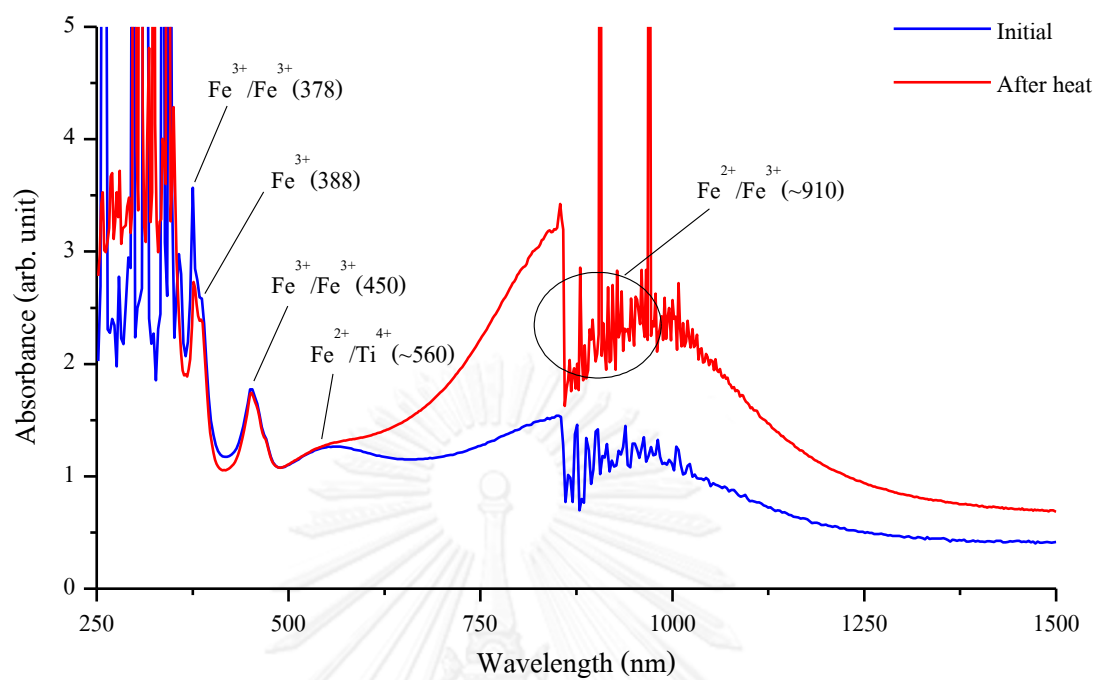
UV-Vis-NIR absorption spectra of sample B2 (o-ray)



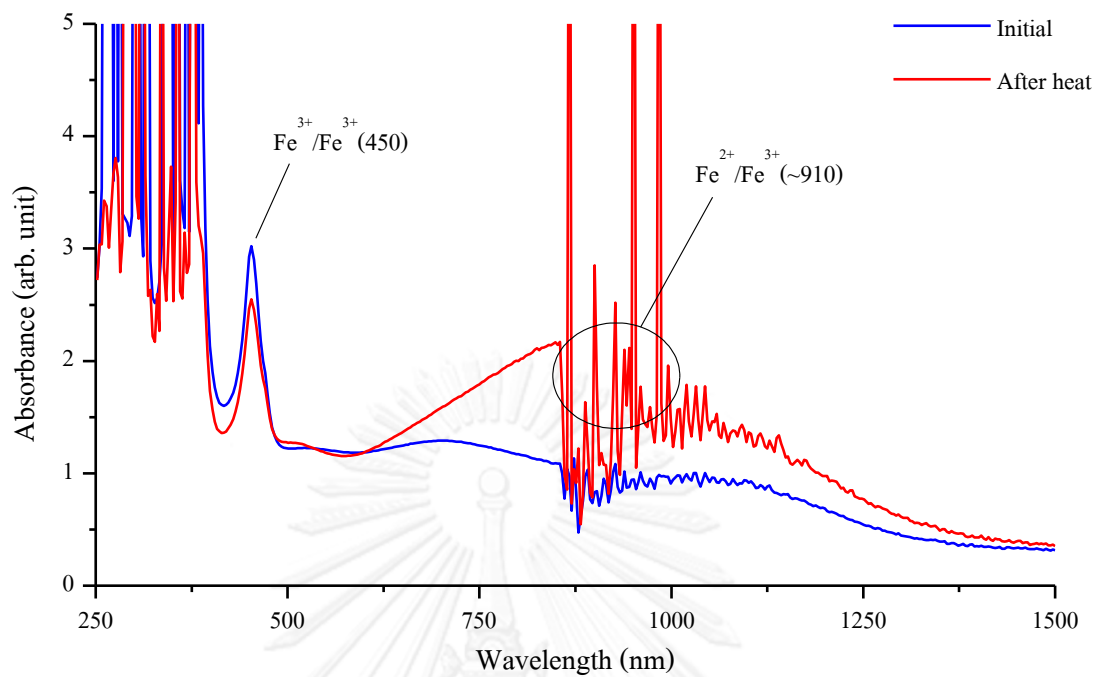
UV-Vis-NIR absorption spectra of sample B3 (e-ray)



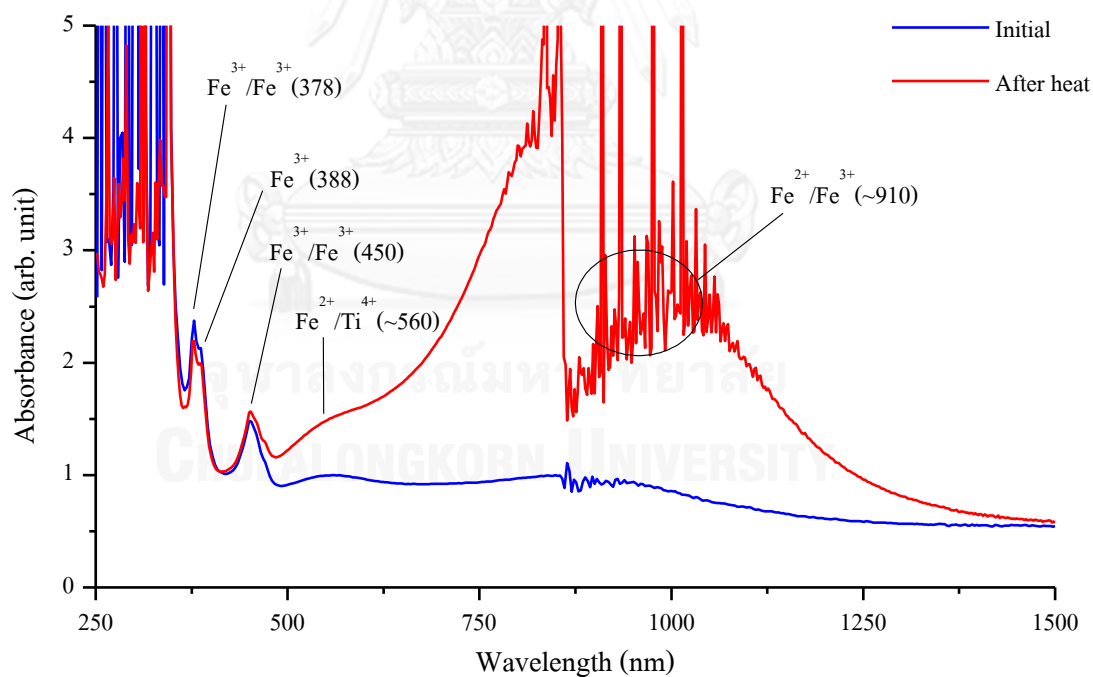
UV-Vis-NIR absorption spectra of sample B3 (o-ray)



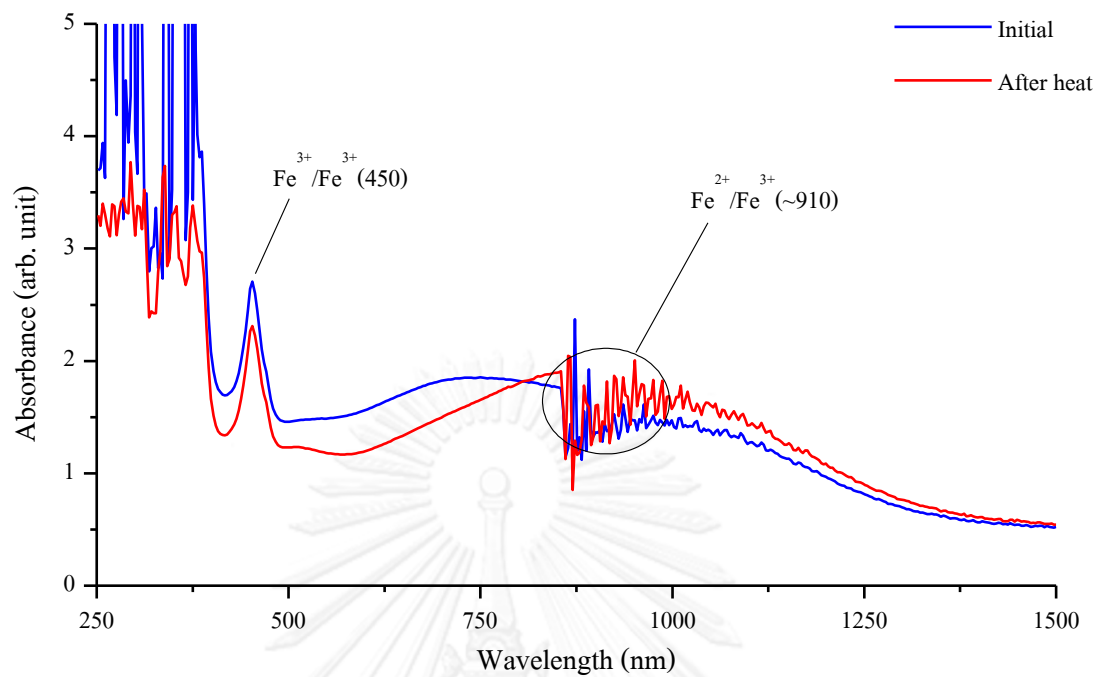
UV-Vis-NIR absorption spectra of sample B4 (o-ray)



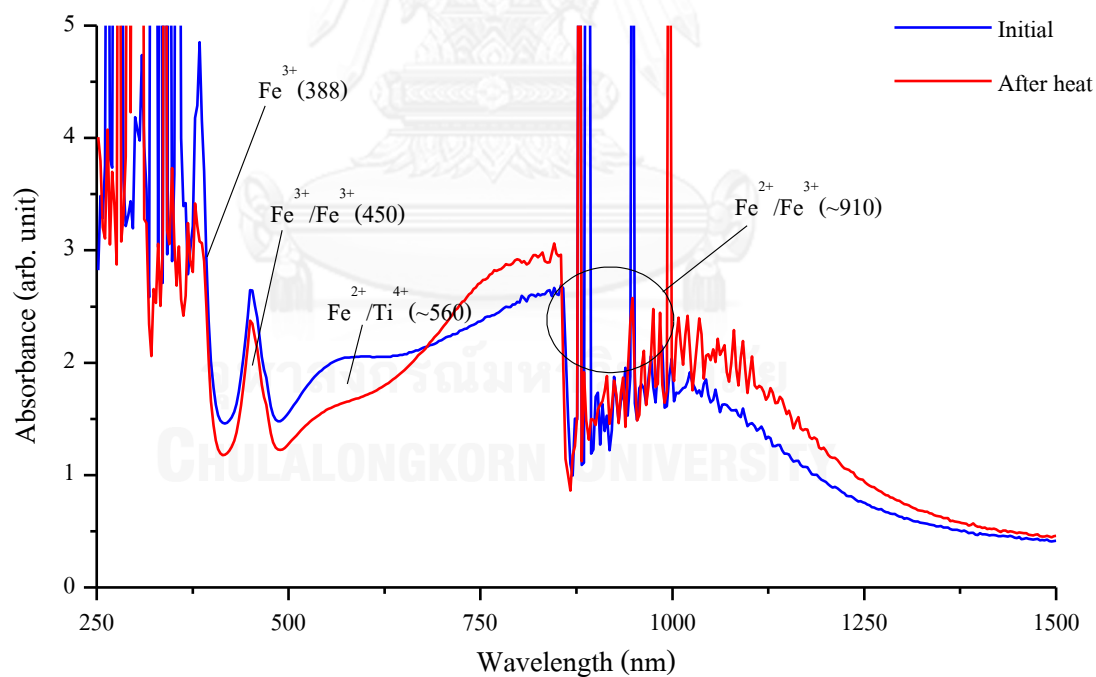
UV-Vis-NIR absorption spectra of sample B5 (e-ray)



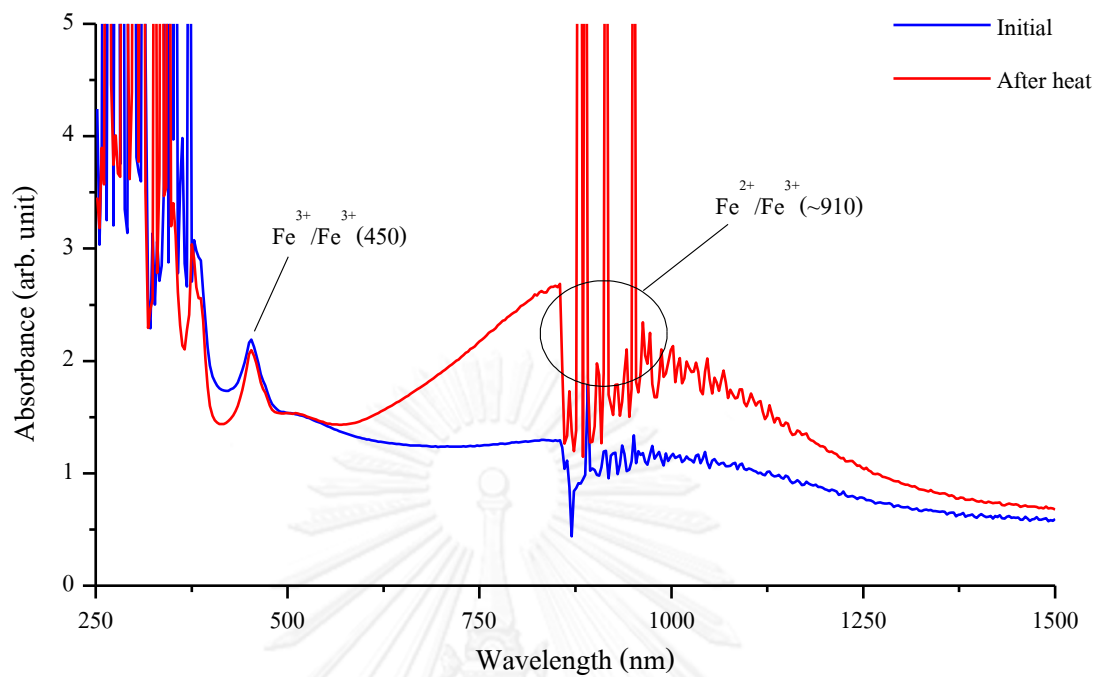
UV-Vis-NIR absorption spectra of sample B5 (o-ray)



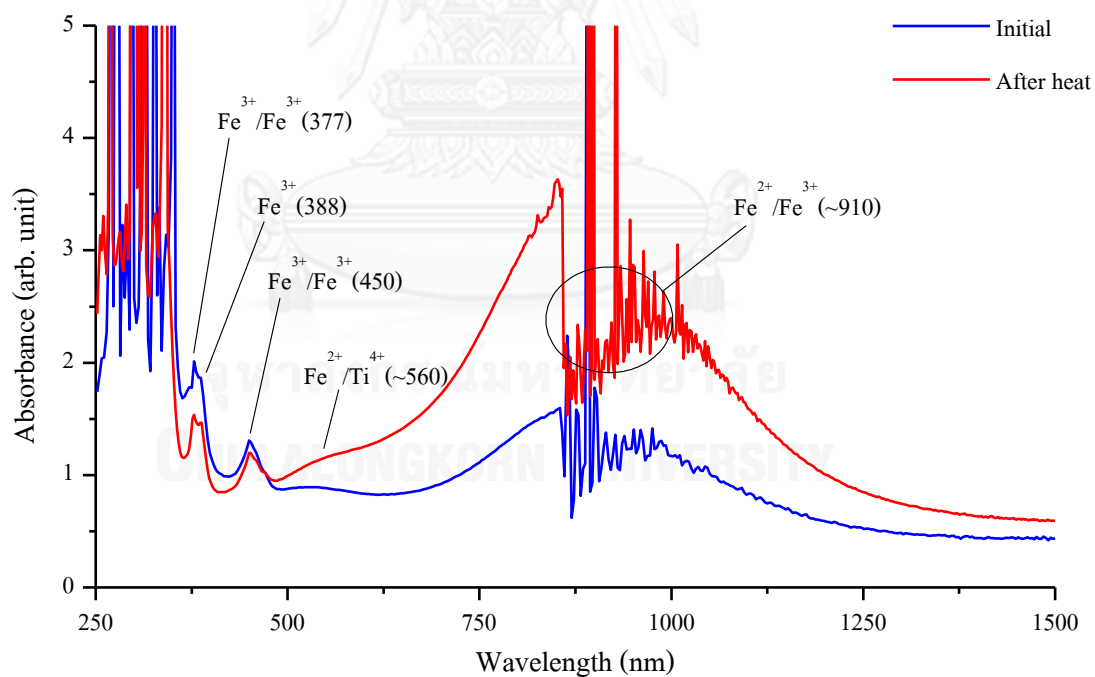
UV-Vis-NIR absorption spectra of sample B6 (e-ray)



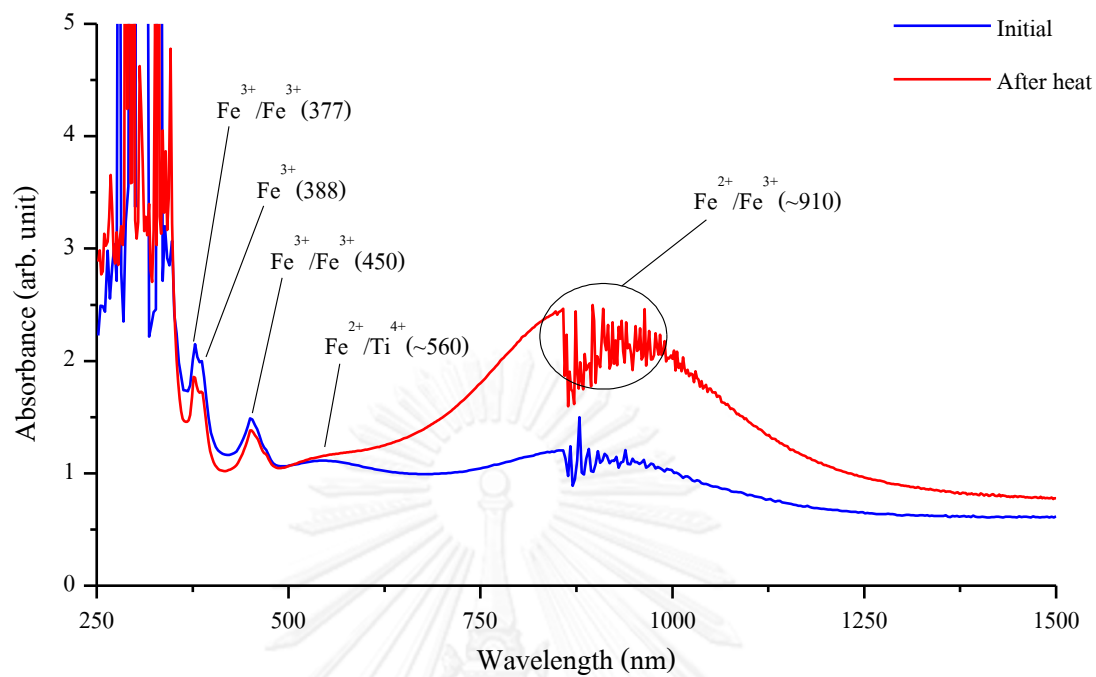
UV-Vis-NIR absorption spectra of sample B6 (o-ray)



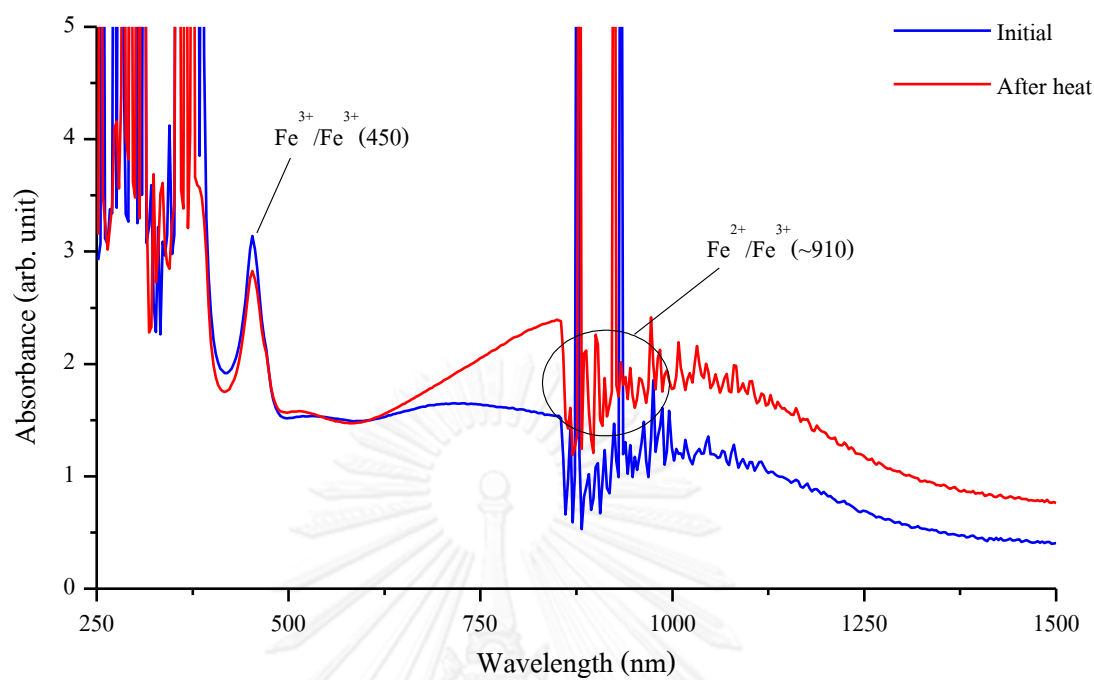
UV-Vis-NIR absorption spectra of sample B7 (e-ray)



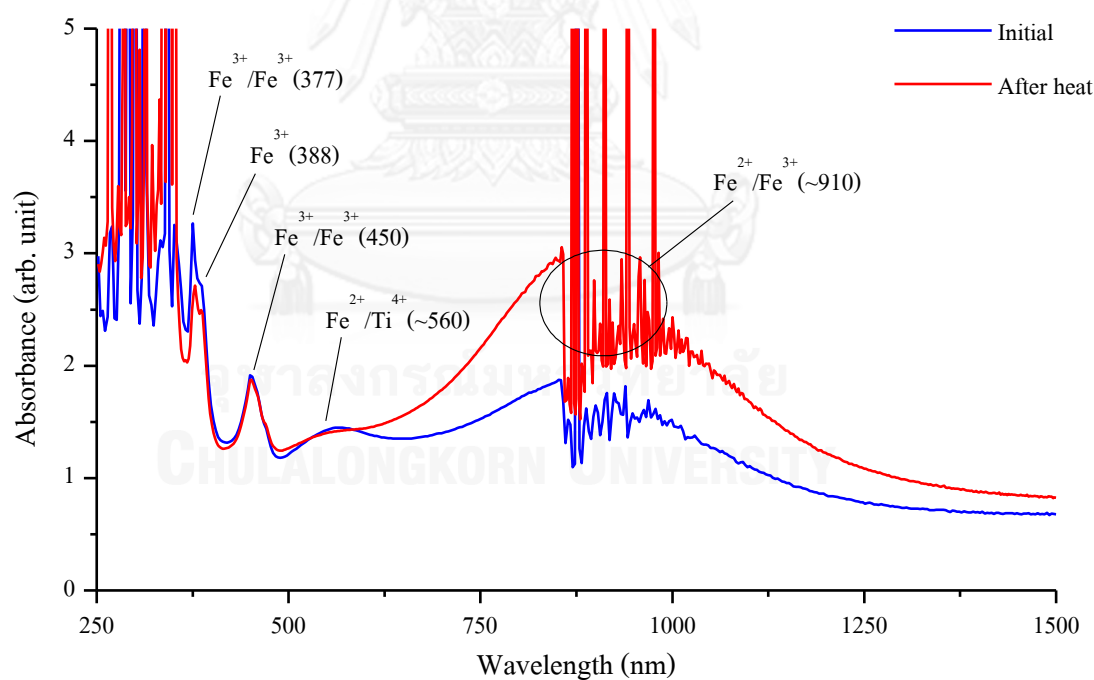
UV-Vis-NIR absorption spectra of sample B7 (o-ray)



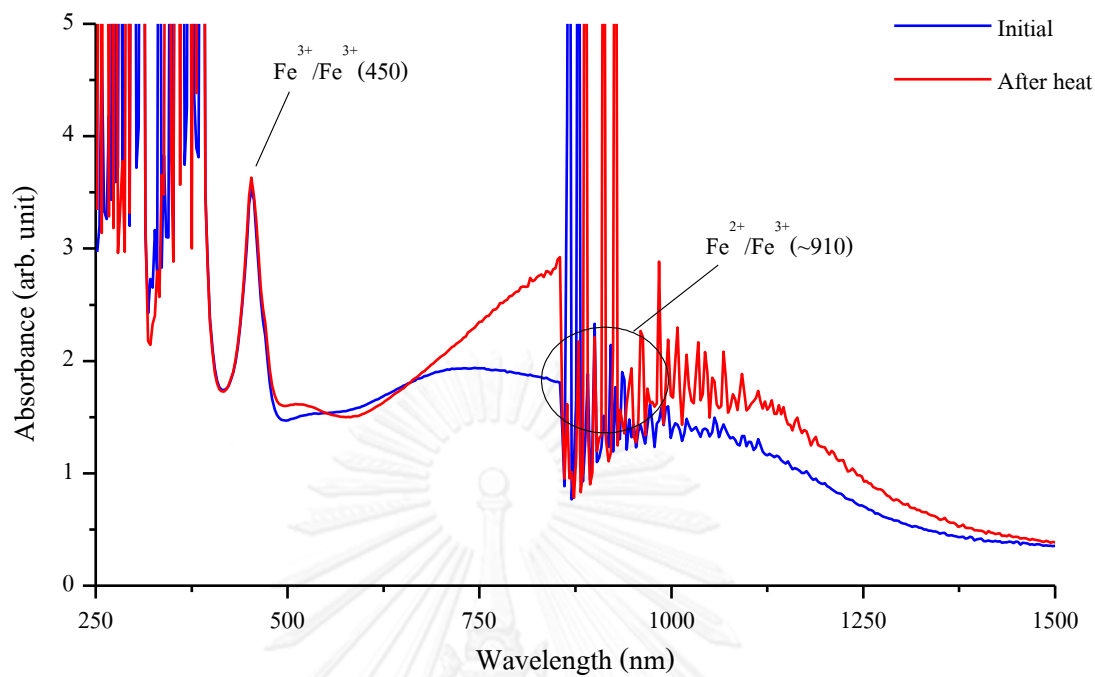
UV-Vis-NIR absorption spectra of sample B8 (o-ray)



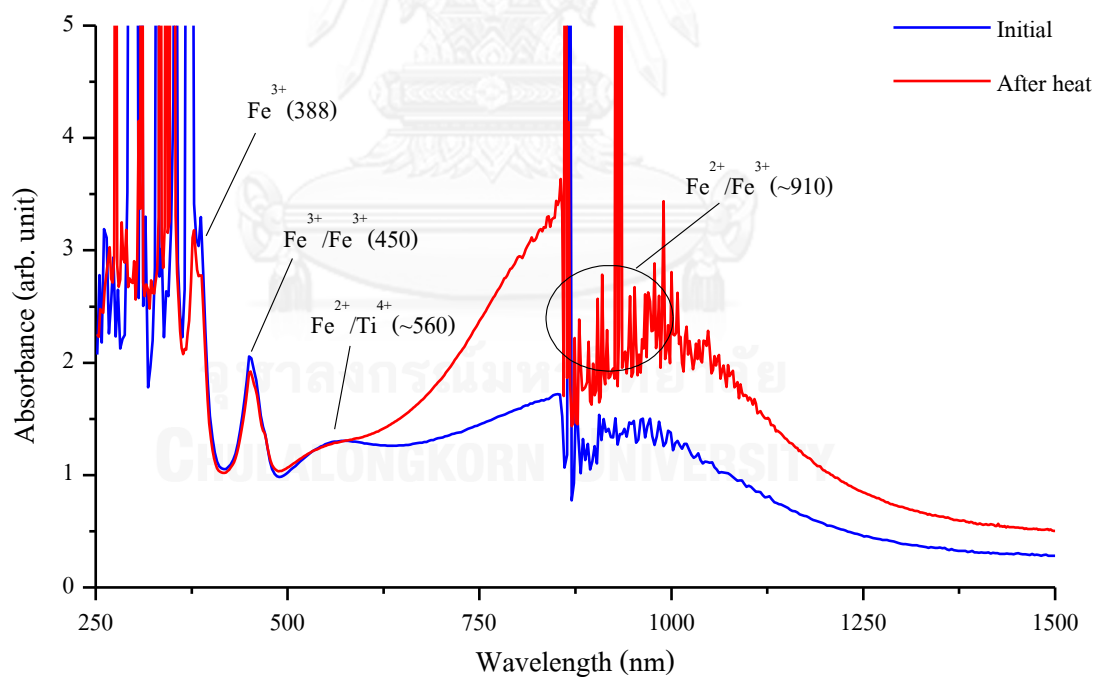
UV-Vis-NIR absorption spectra of sample B9 (e-ray)



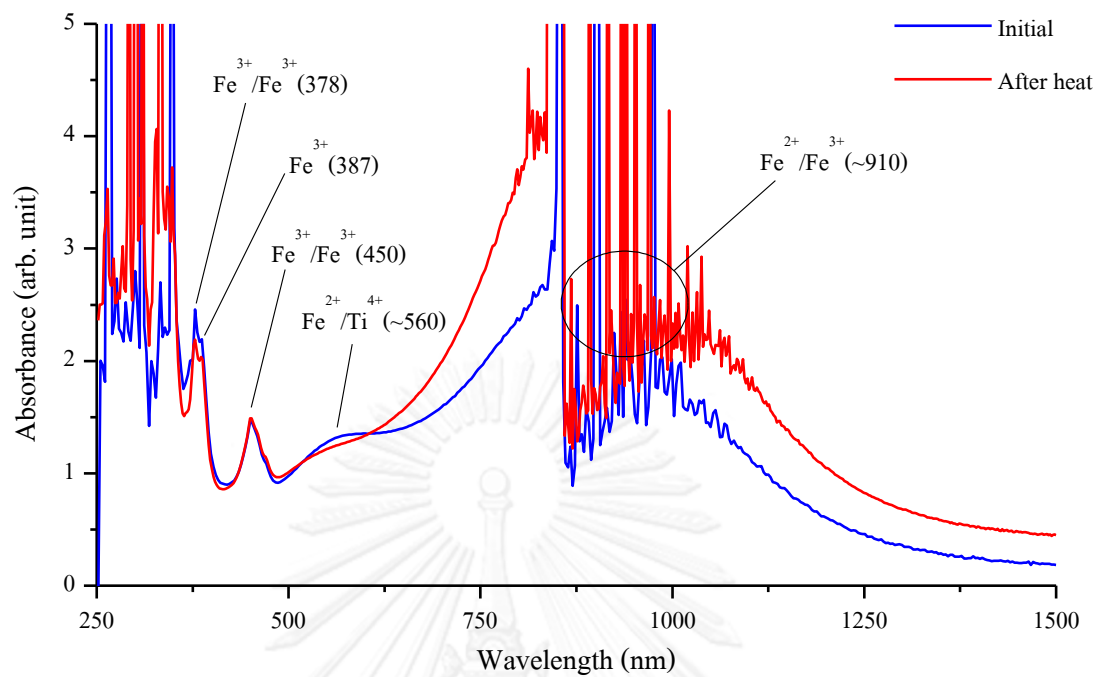
UV-Vis-NIR absorption spectra of sample B9 (o-ray)



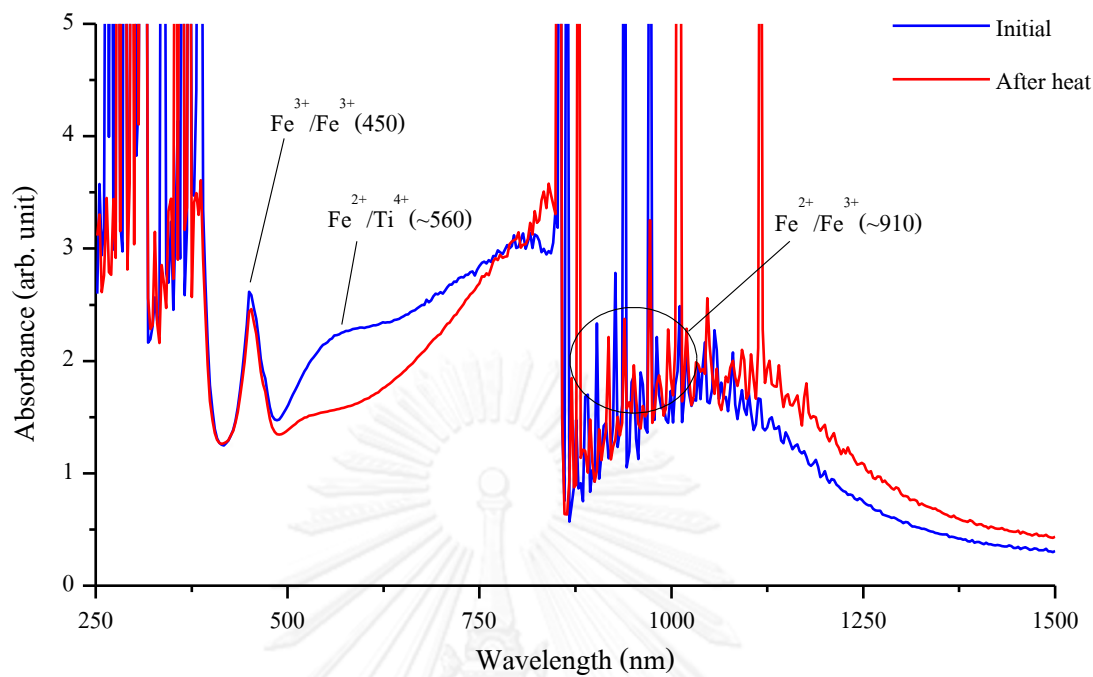
UV-Vis-NIR absorption spectra of sample B10 (e-ray)



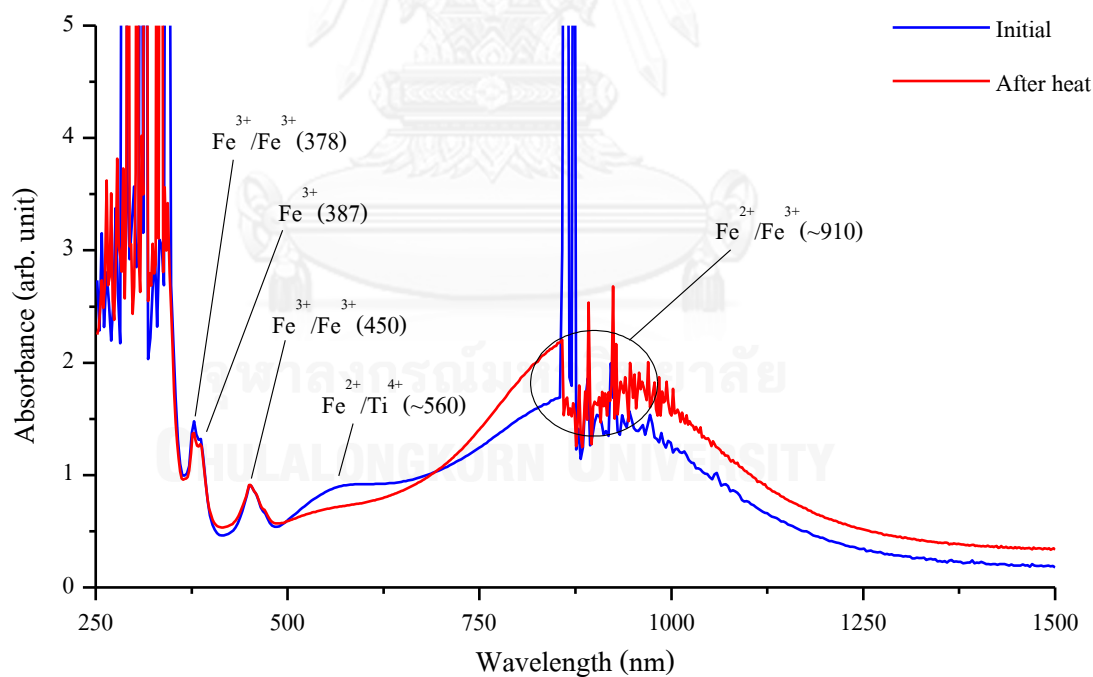
UV-Vis-NIR absorption spectra of sample B10 (o-ray)



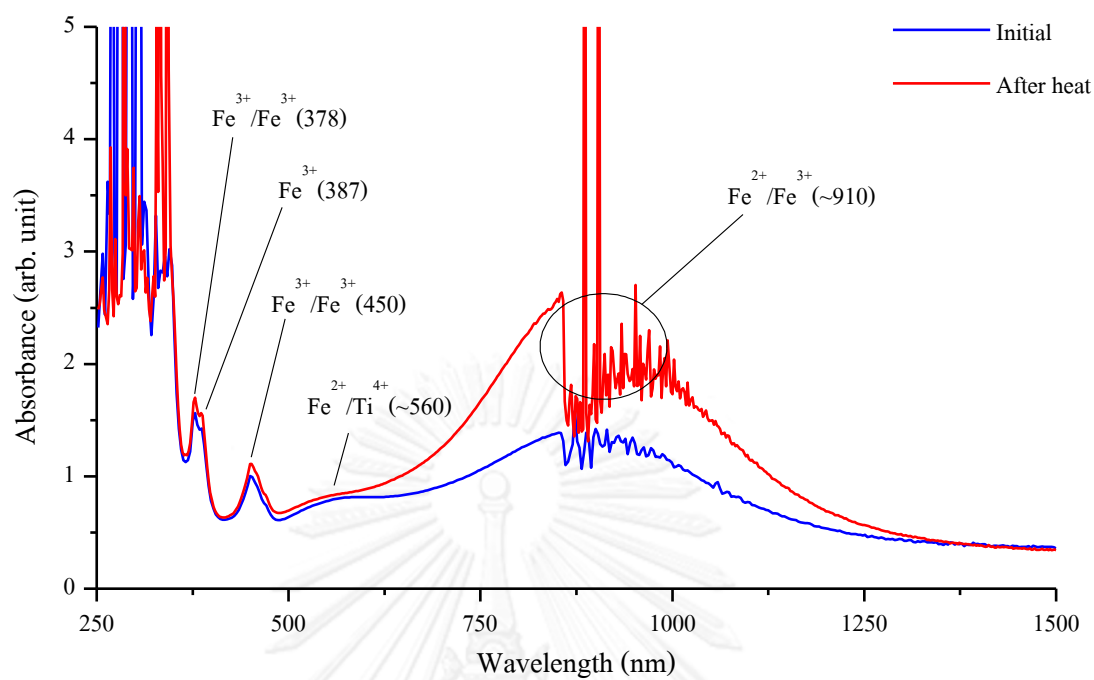
UV-Vis-NIR absorption spectra of sample B11 (o-ray)



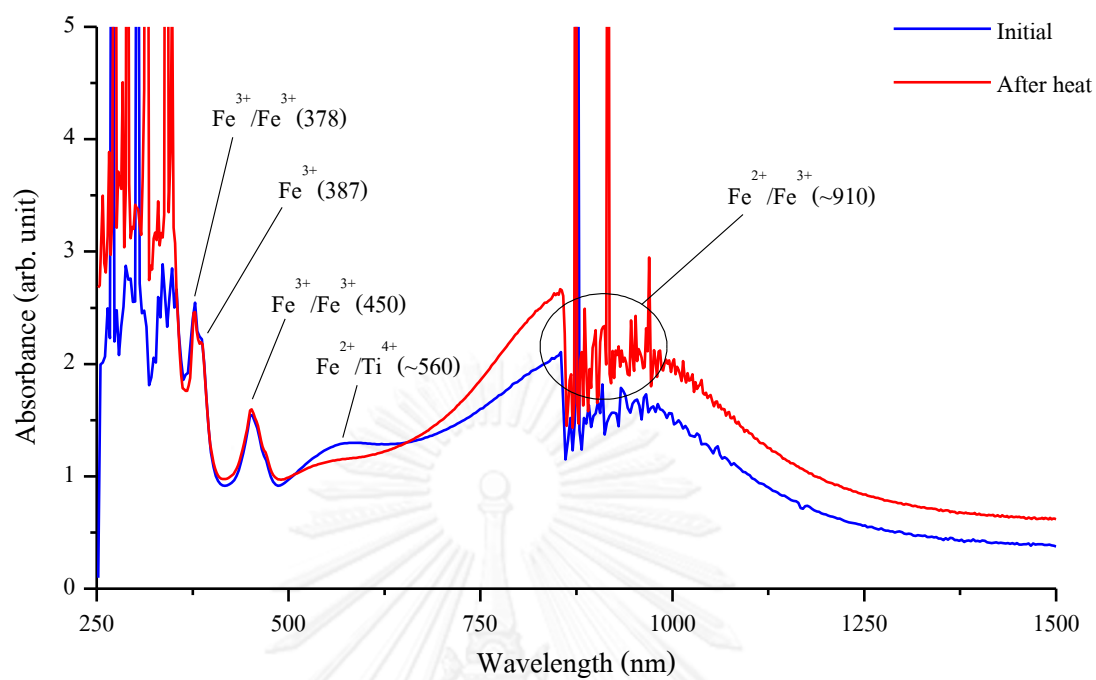
UV-Vis-NIR absorption spectra of sample B12 (e-ray)



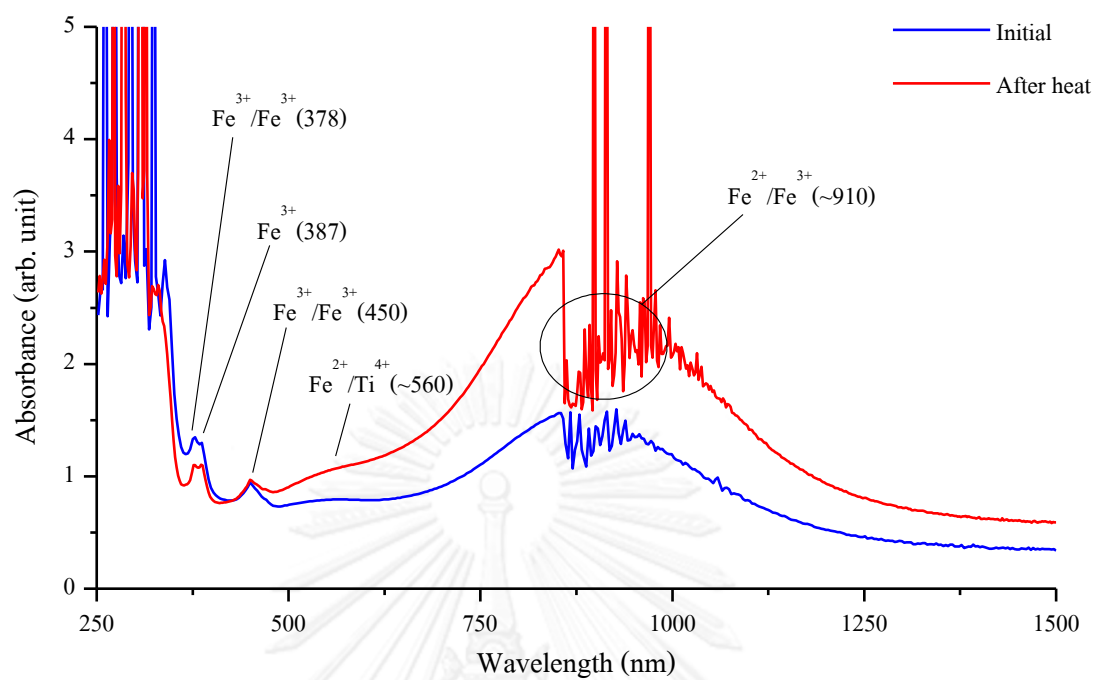
UV-Vis-NIR absorption spectra of sample B12 (o-ray)



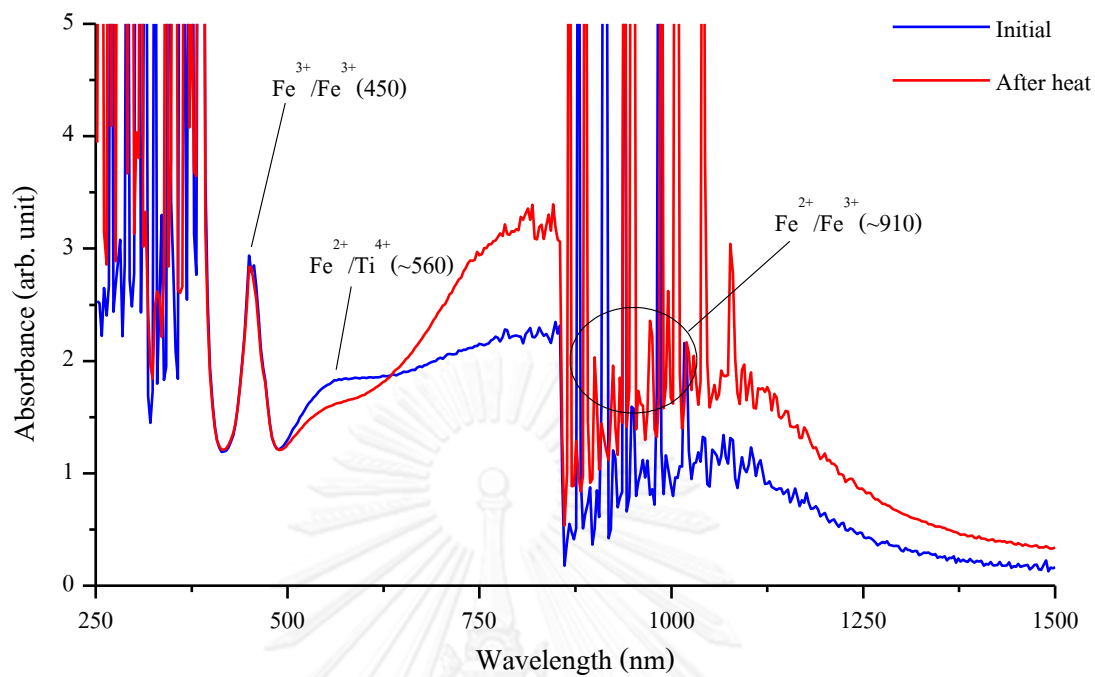
UV-Vis-NIR absorption spectra of sample B13 (o-ray)



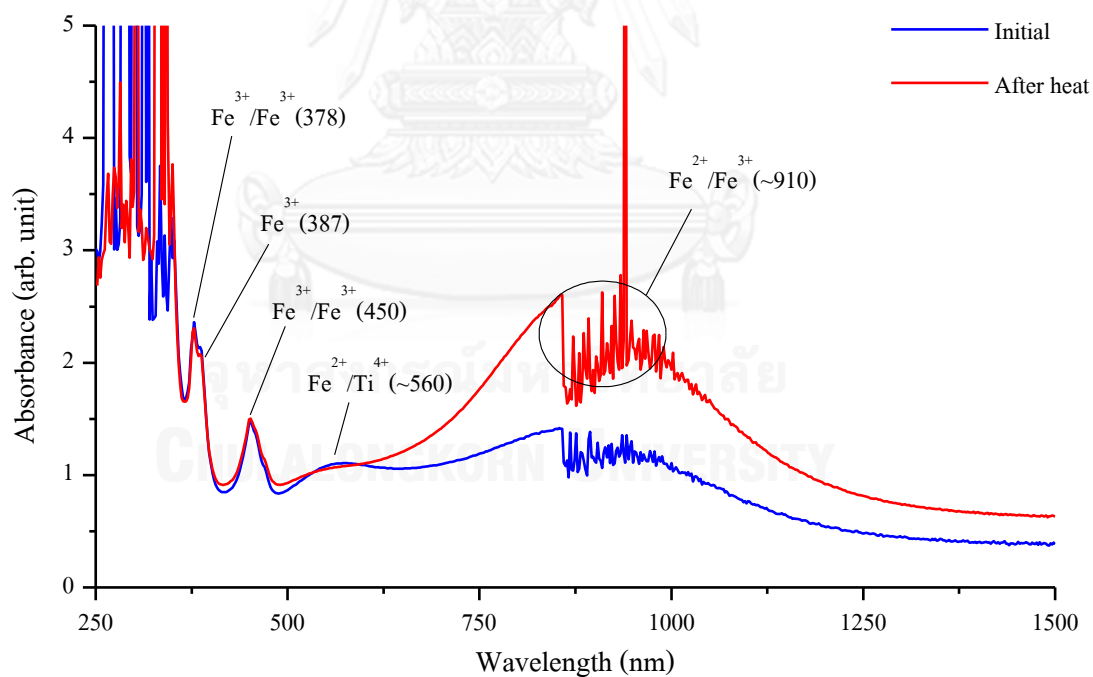
UV-Vis-NIR absorption spectra of sample B14 (o-ray)



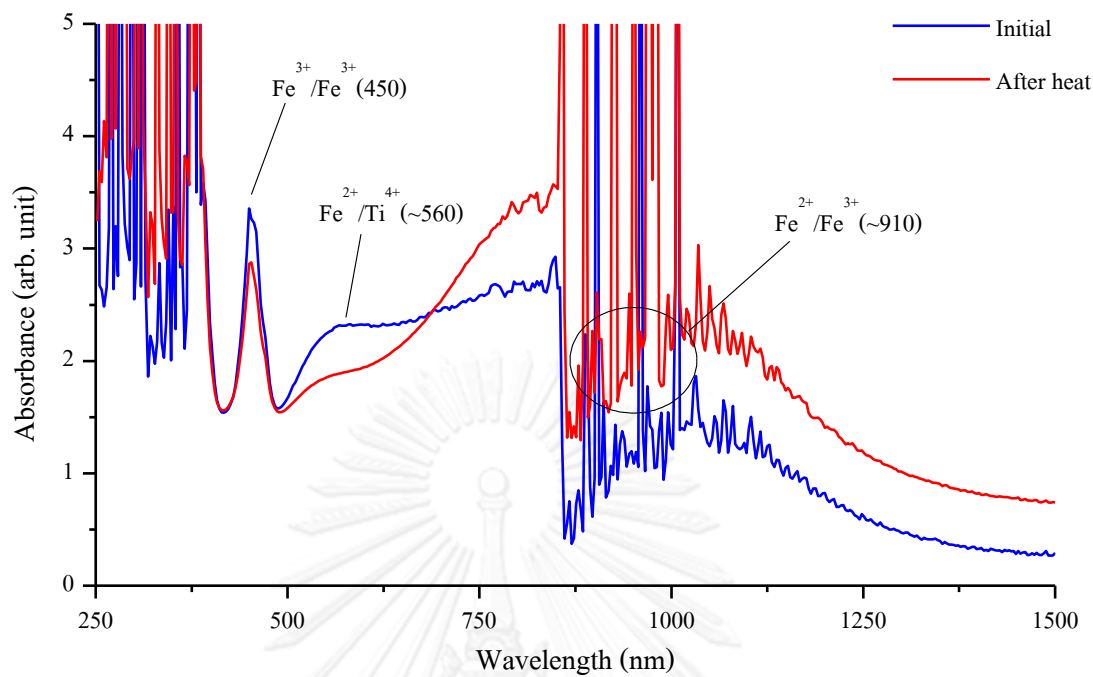
UV-Vis-NIR absorption spectra of sample B15 (o-ray)



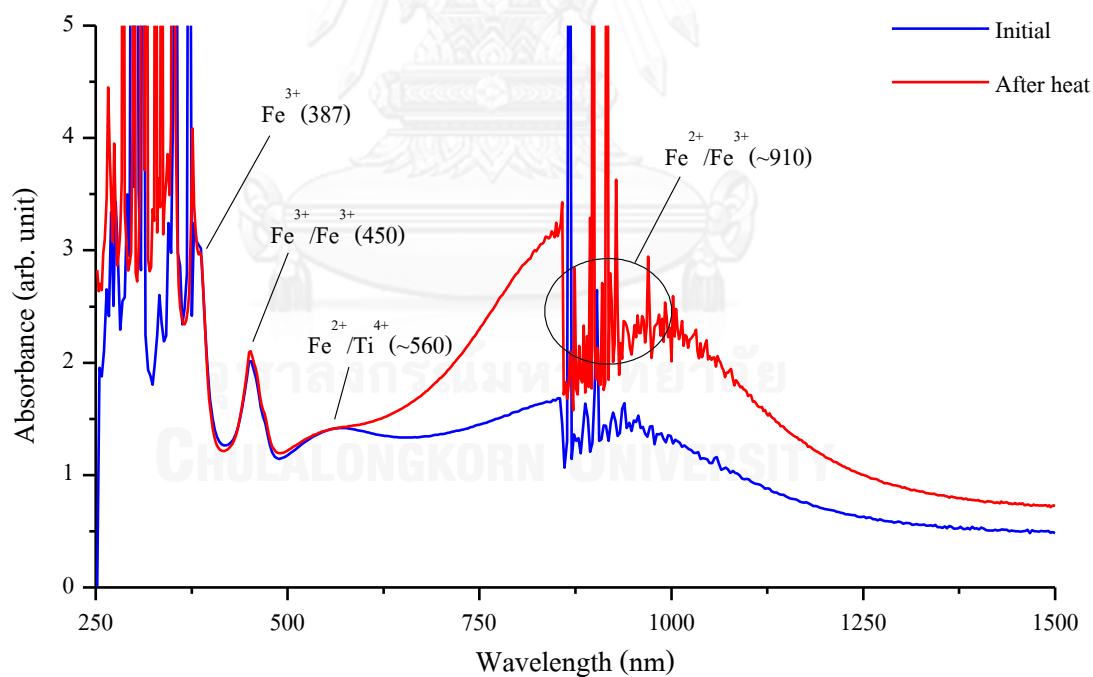
UV-Vis-NIR absorption spectra of sample B16 (e-ray)



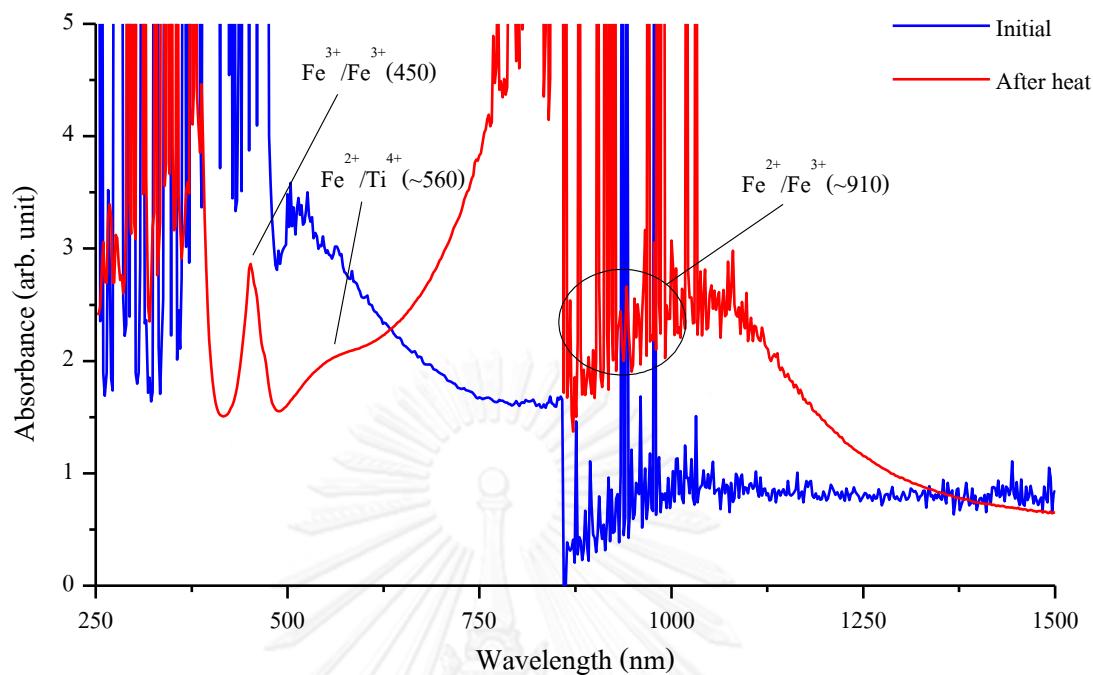
UV-Vis-NIR absorption spectra of sample B16 (o-ray)



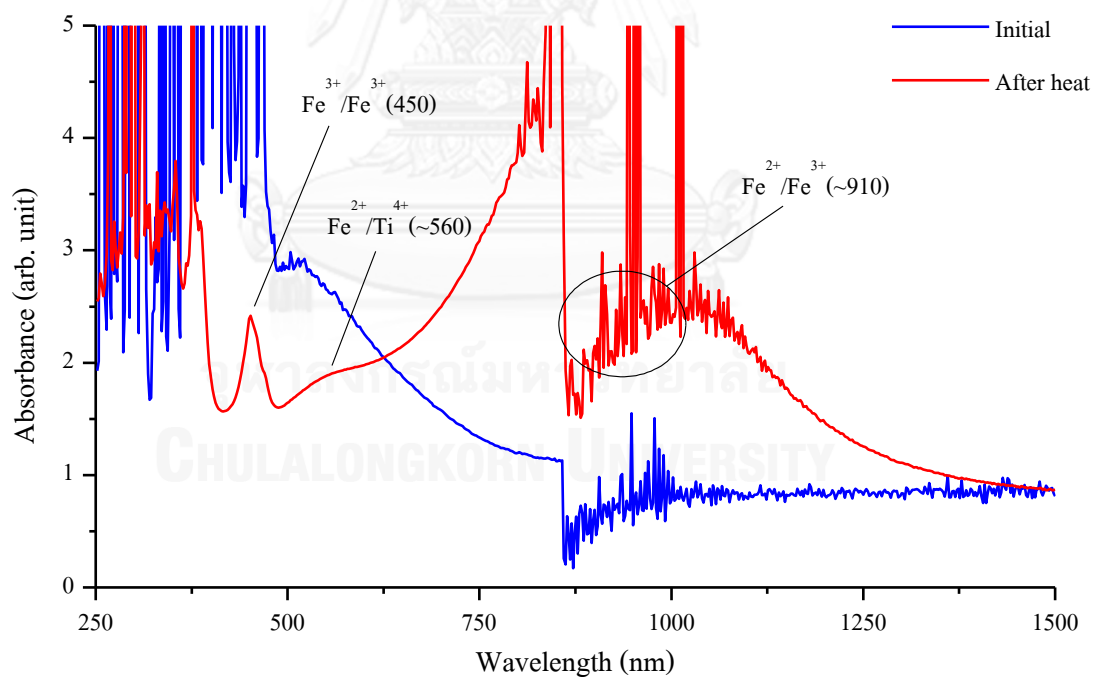
UV-Vis-NIR absorption spectra of sample B17 (e-ray)



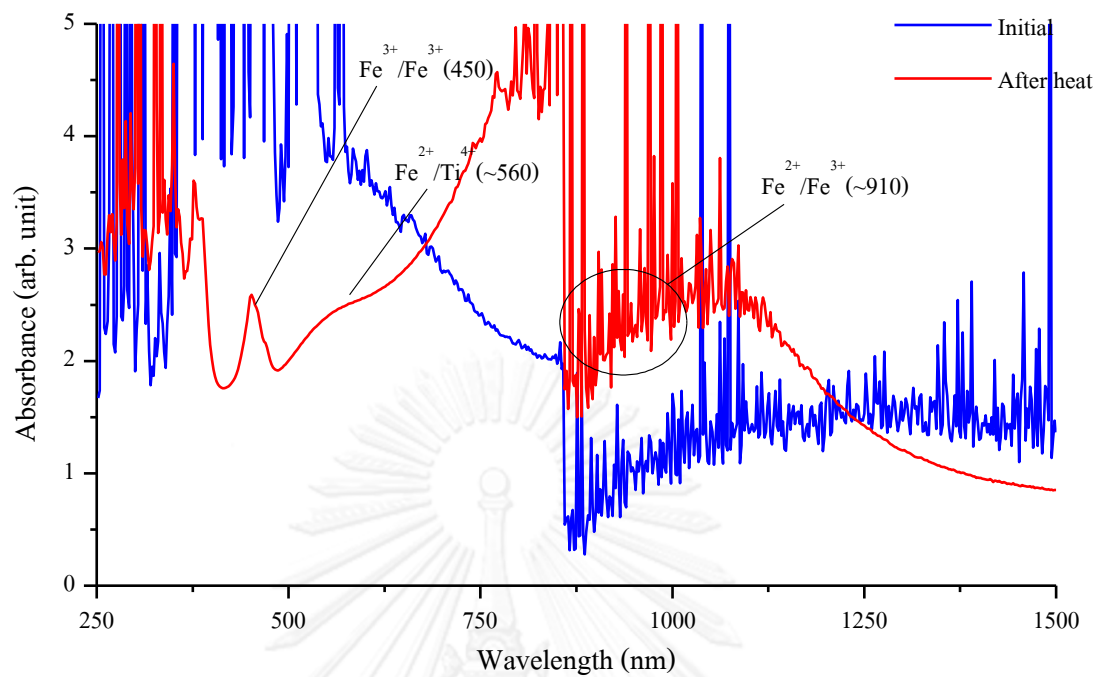
UV-Vis-NIR absorption spectra of sample B17 (o-ray)



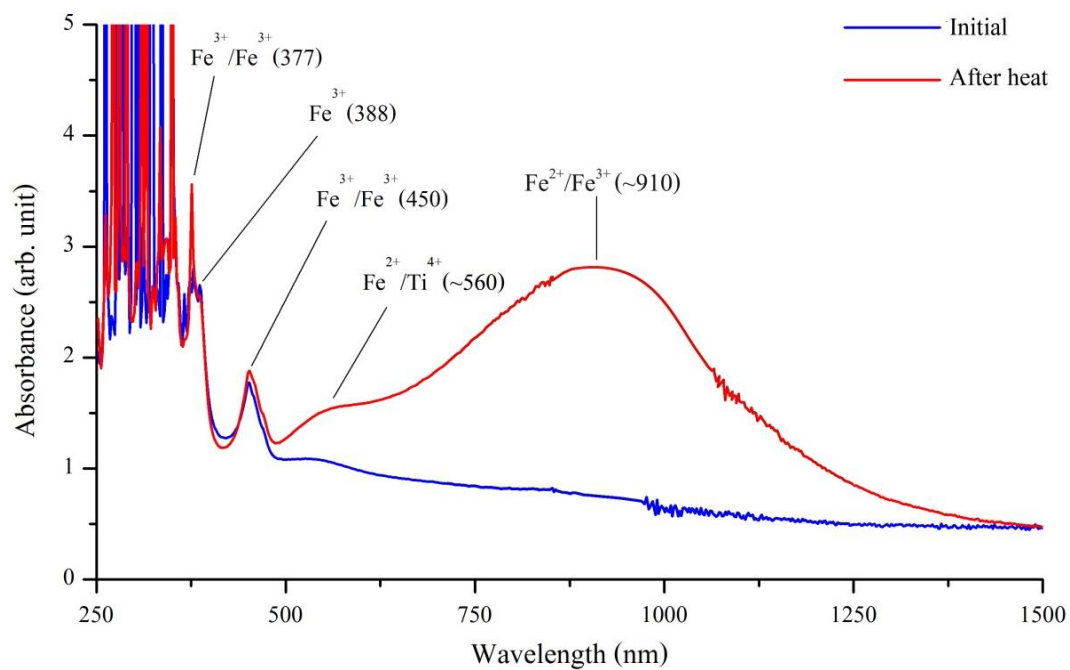
UV-Vis-NIR absorption spectra of sample C1 (o-ray)



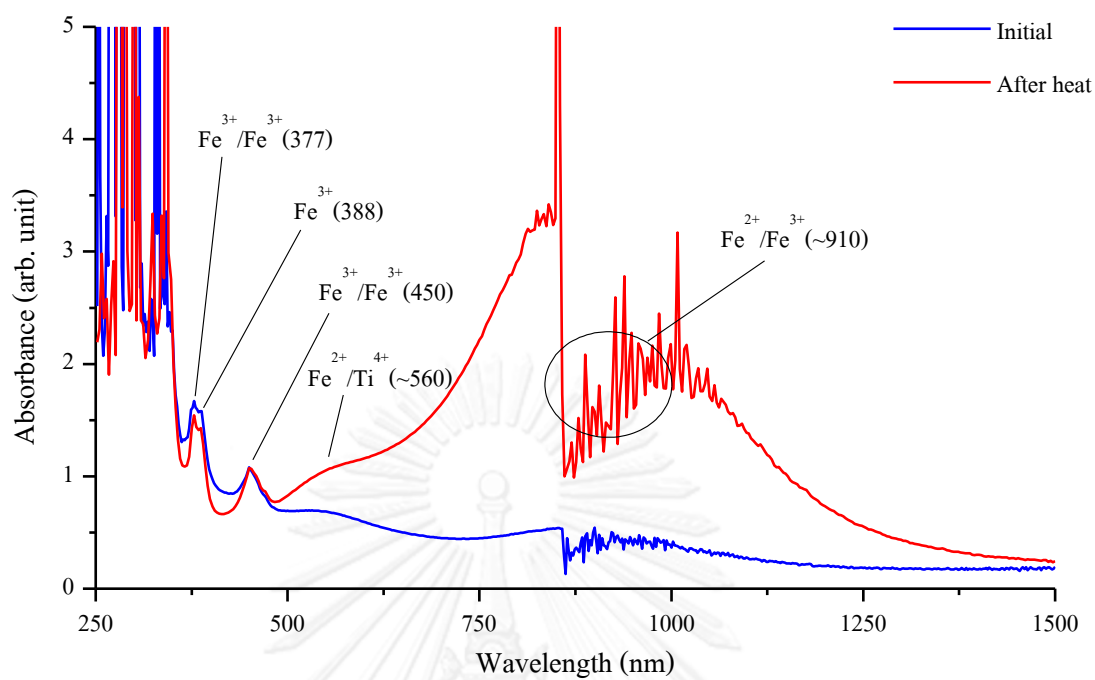
UV-Vis-NIR absorption spectra of sample C2 (o-ray)



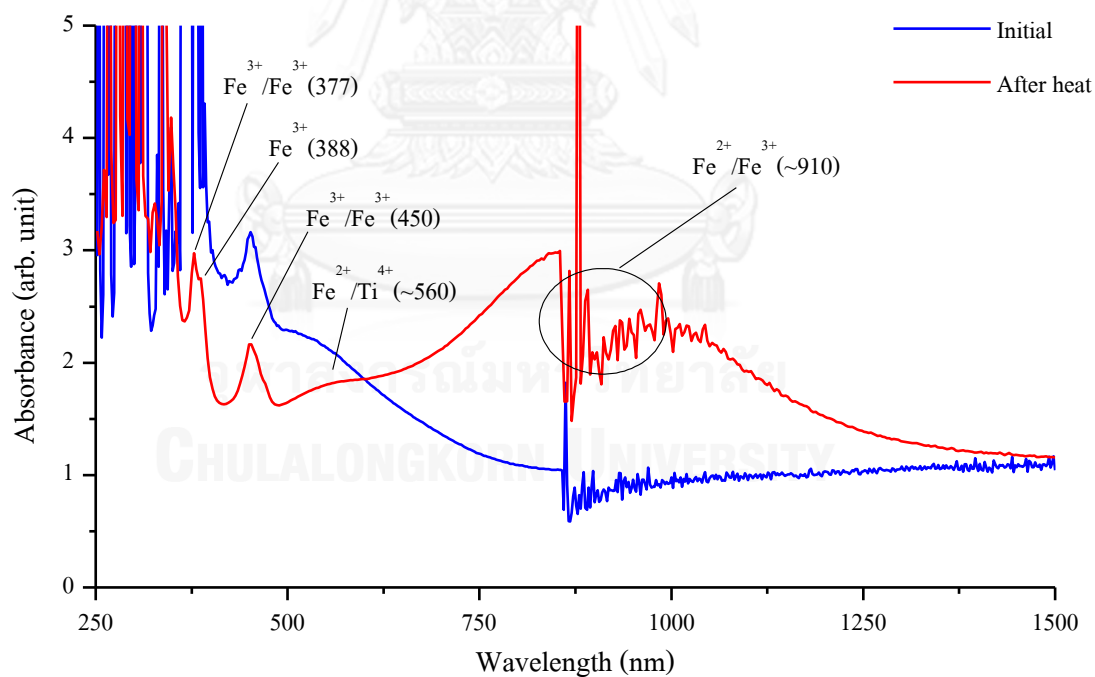
UV-Vis-NIR absorption spectra of sample C3 (o-ray)



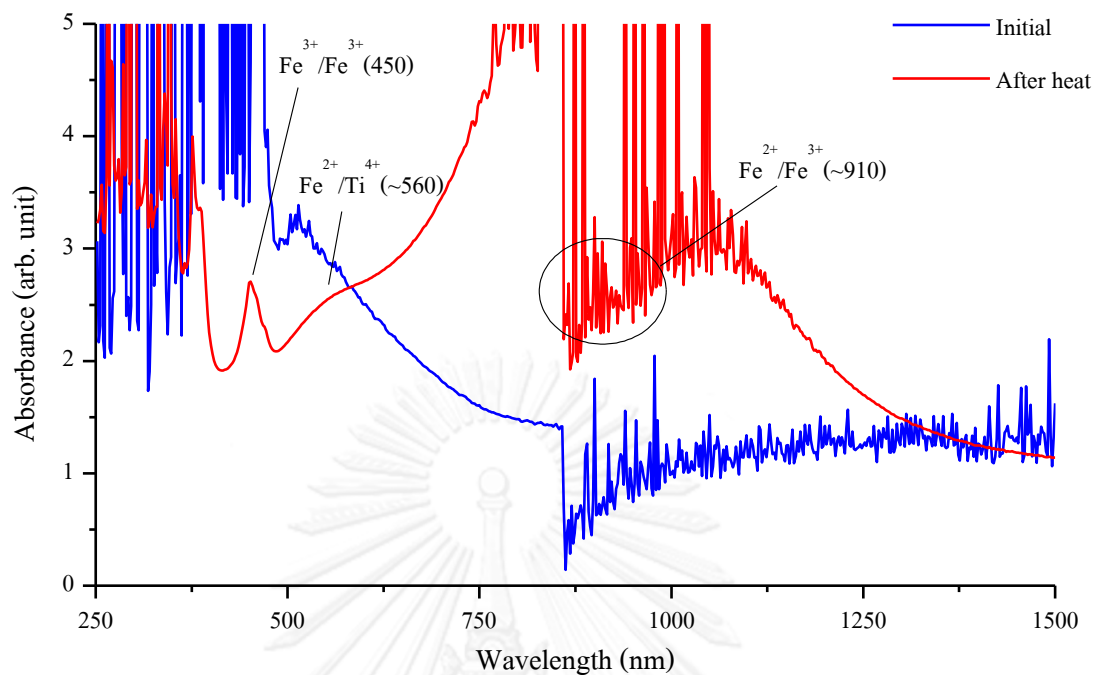
UV-Vis-NIR absorption spectra of sample C4 (o-ray)



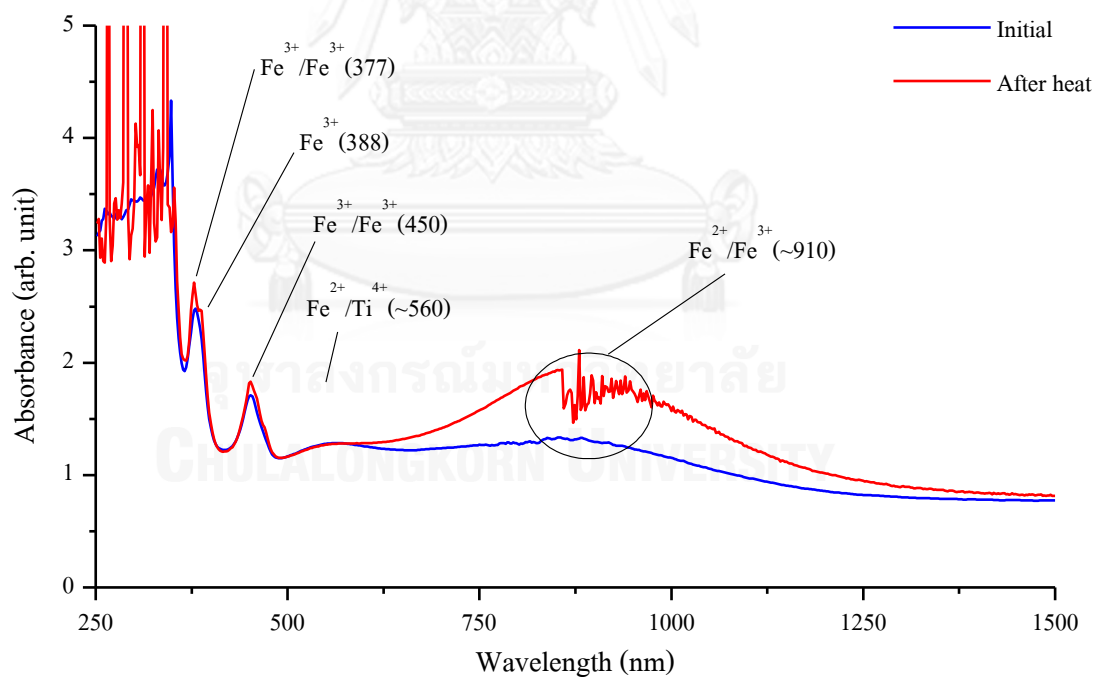
UV-Vis-NIR absorption spectra of sample C5 (o-ray)



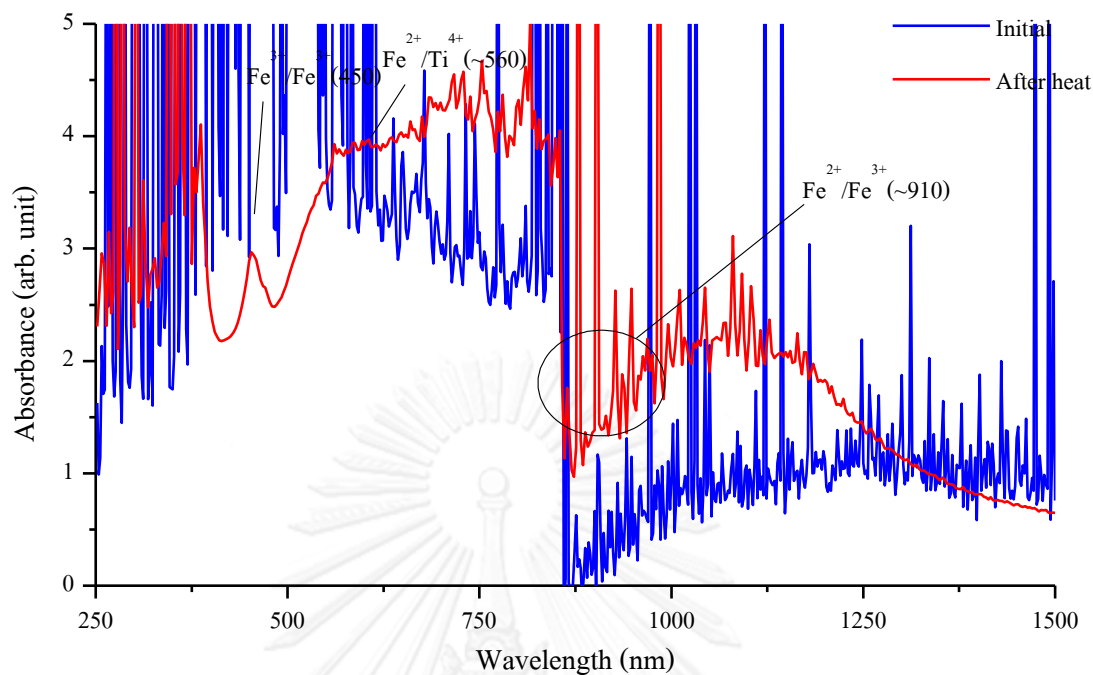
UV-Vis-NIR absorption spectra of sample C6 (o-ray)



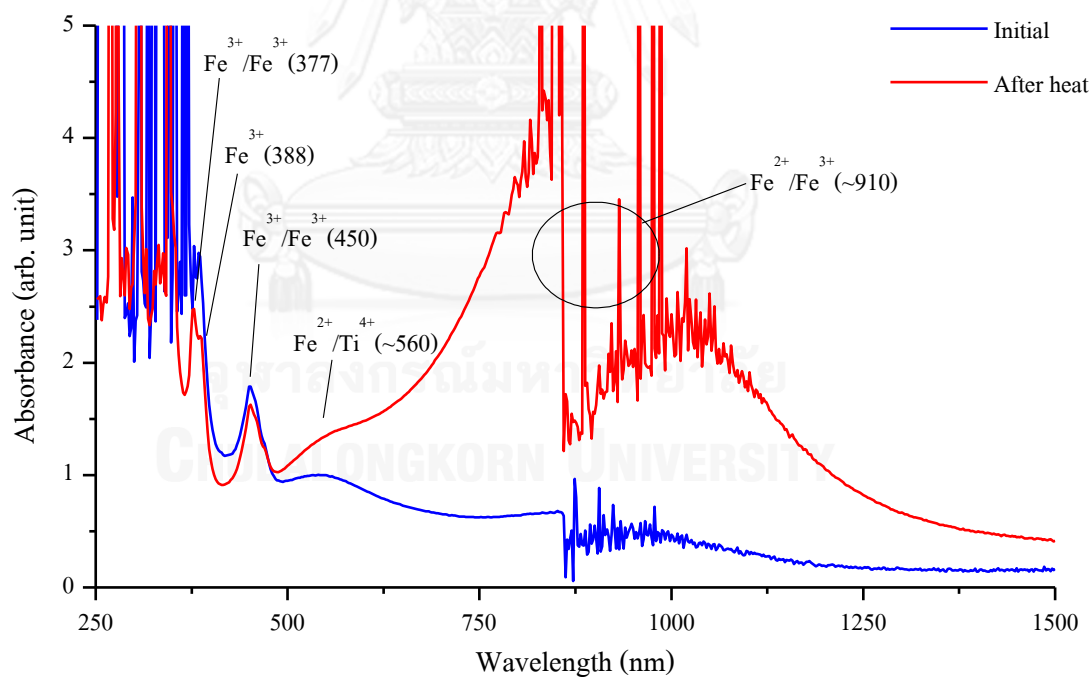
UV-Vis-NIR absorption spectra of sample C7 (o-ray)



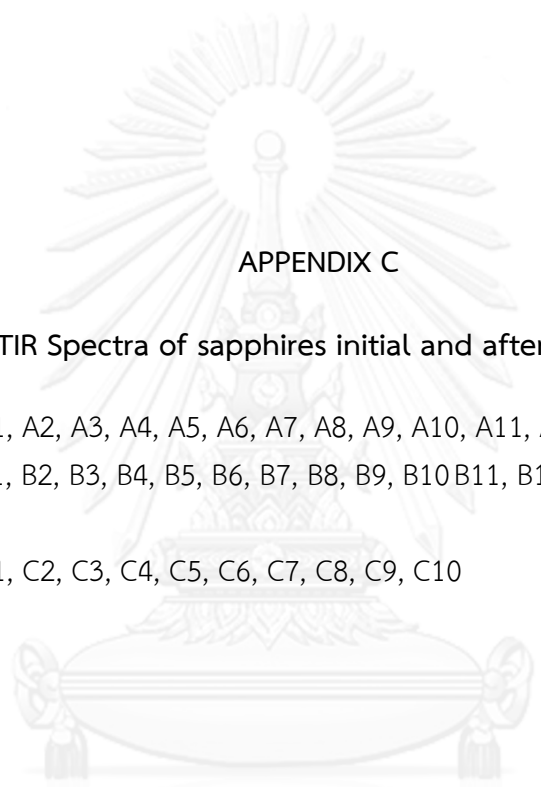
UV-Vis-NIR absorption spectra of sample C8 (o-ray)



UV-Vis-NIR absorption spectra of sample C9 (o-ray)



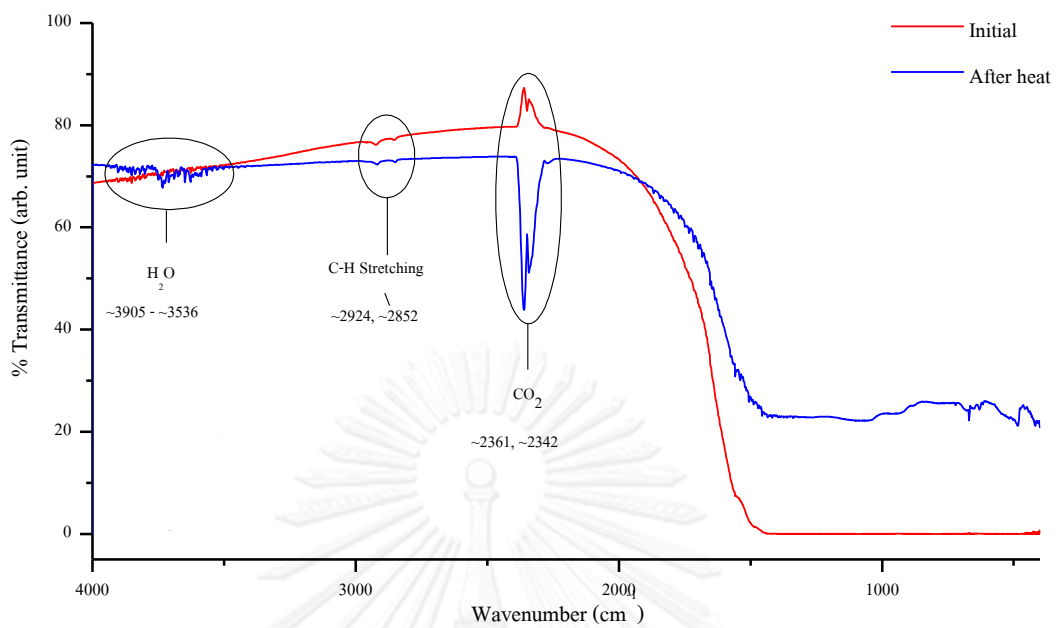
UV-Vis-NIR absorption spectra of sample C10 (o-ray)



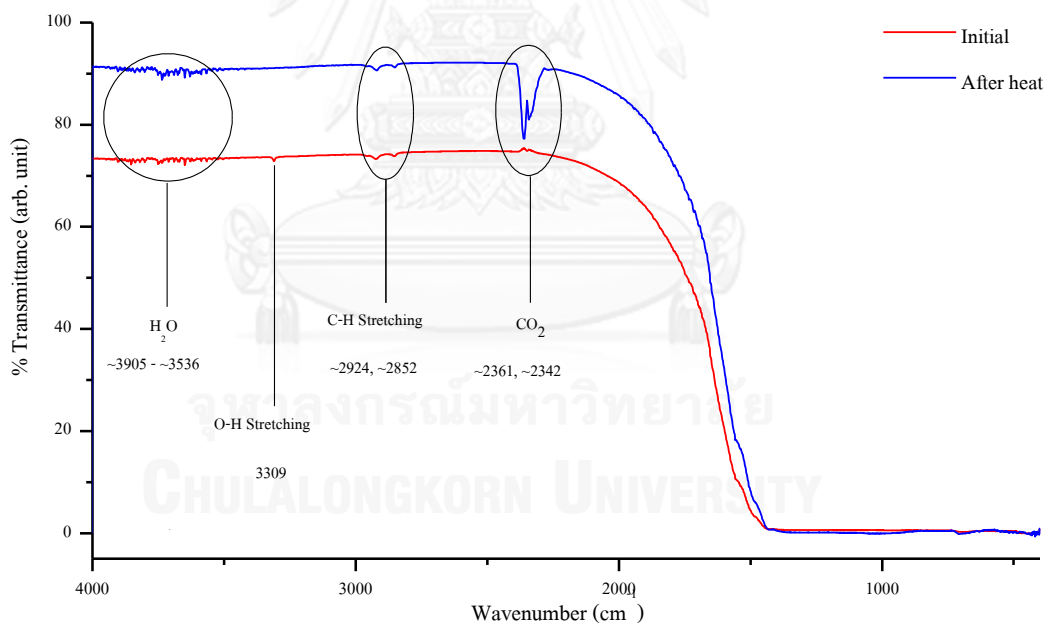
APPENDIX C

FTIR Spectra of sapphires initial and after heating

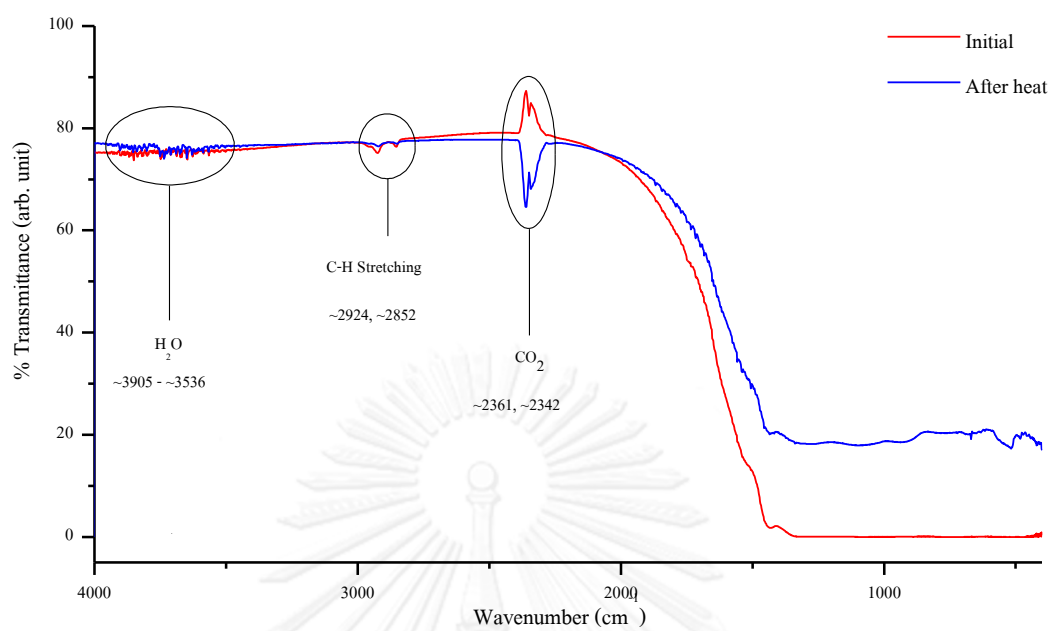
- A: A1, A2, A3, A4, A5, A6, A7, A8, A9, A10, A11, A12
B: B1, B2, B3, B4, B5, B6, B7, B8, B9, B10, B11, B12, B13, B14, B15, B16,
B17
C: C1, C2, C3, C4, C5, C6, C7, C8, C9, C10



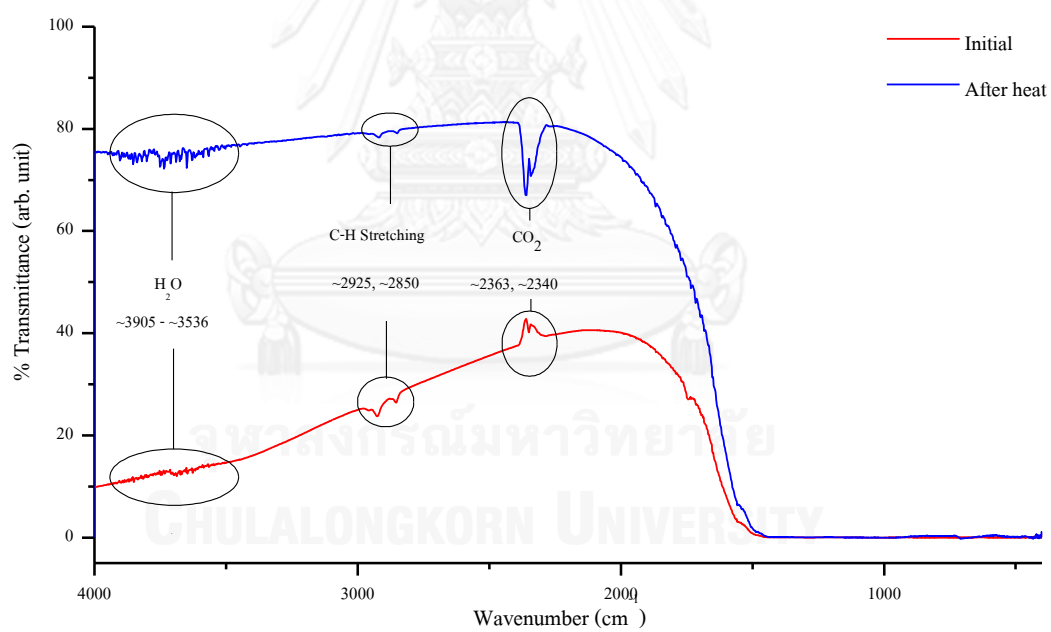
FTIR spectra of sample A1 Initial and after heating



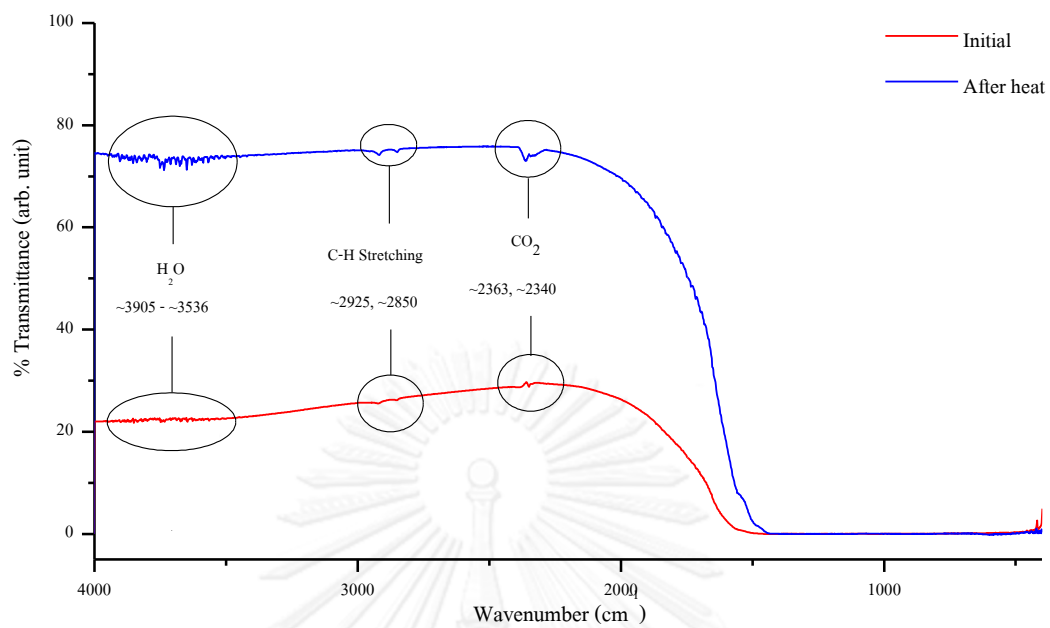
FTIR spectra of sample A2 Initial and after heating



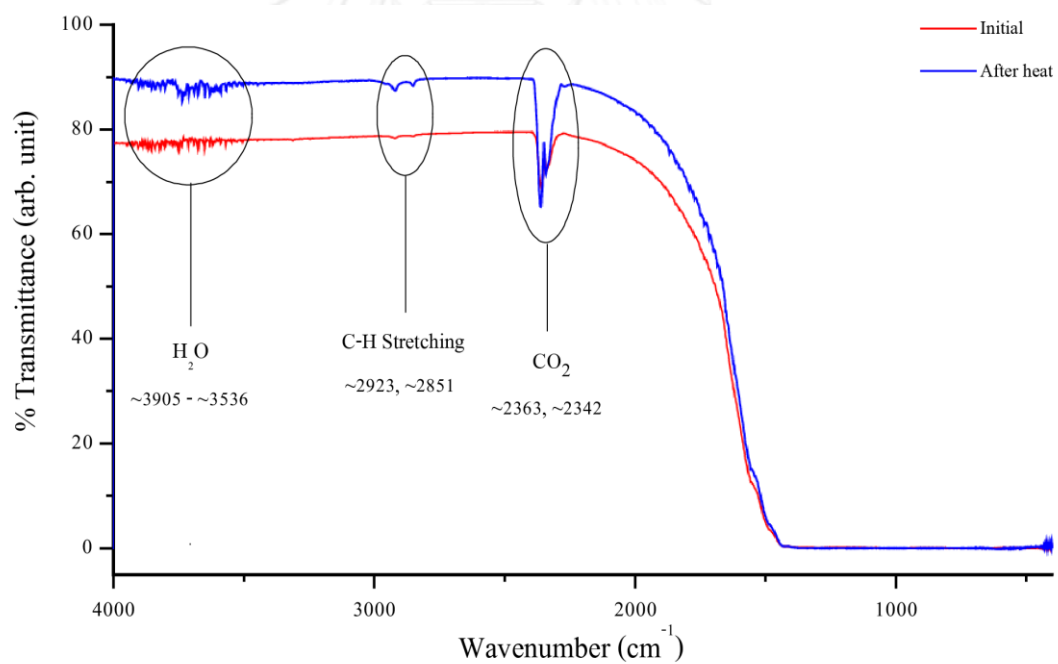
FTIR spectra of sample A3 Initial and after heating



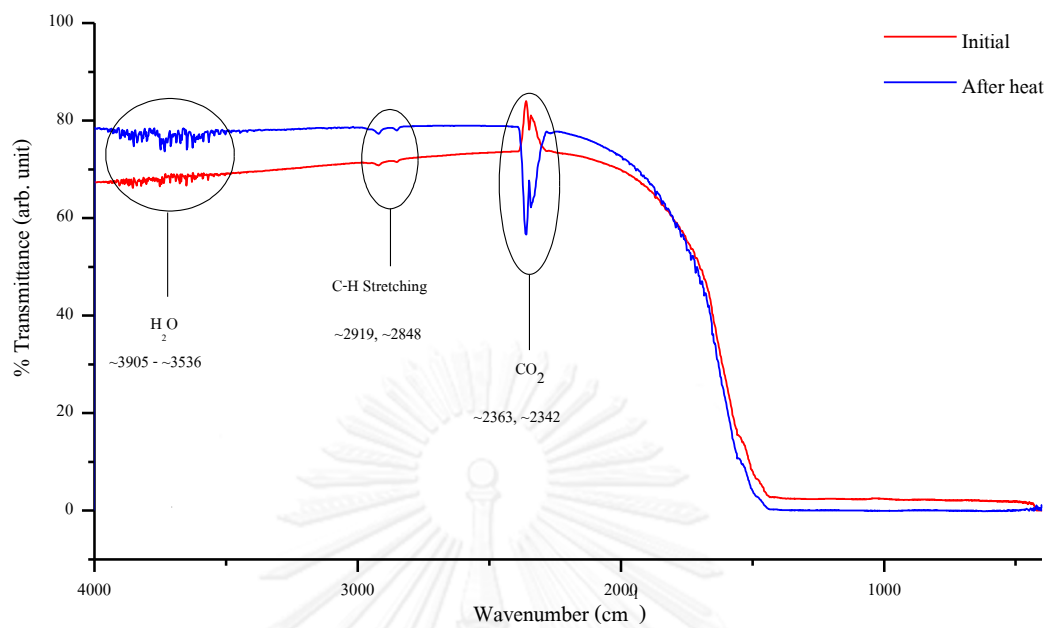
FTIR spectra of sample A4 Initial and after heating



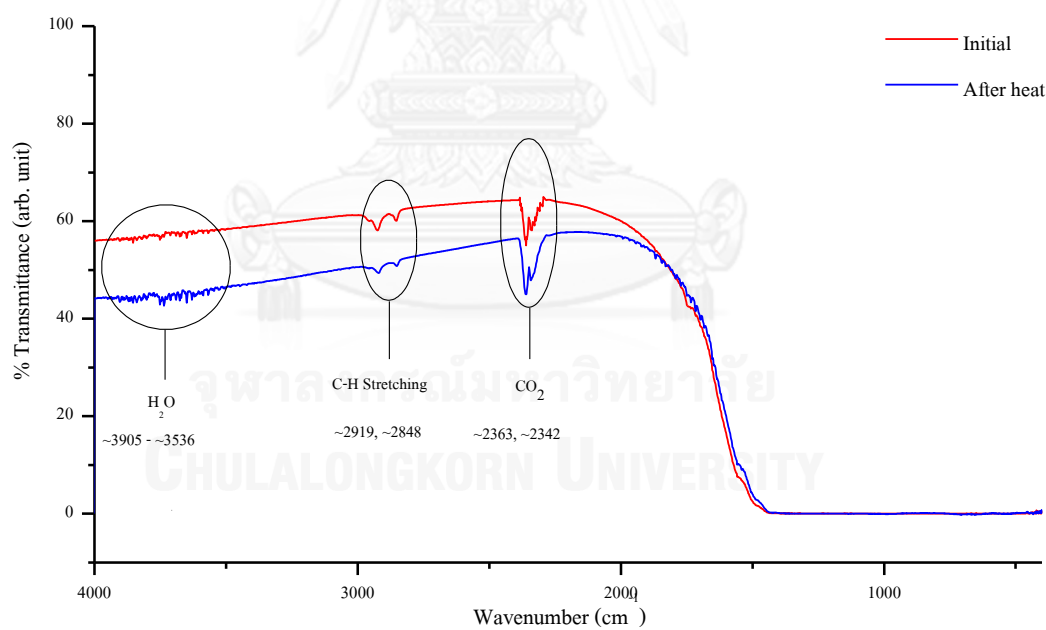
FTIR spectra of sample A5 Initial and after heating



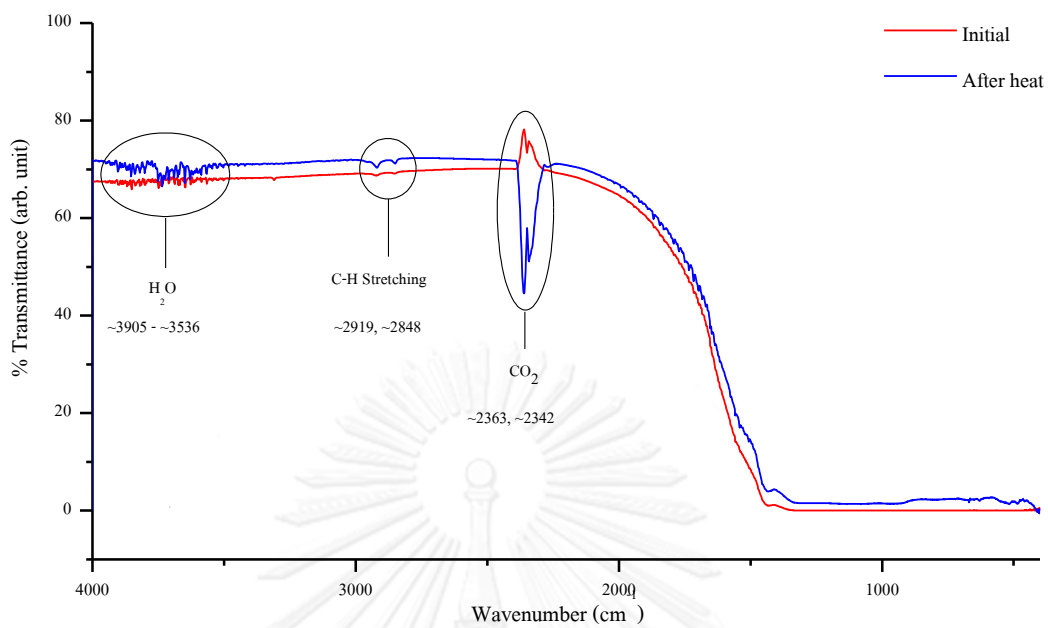
FTIR spectra of sample A6 Initial and after heating



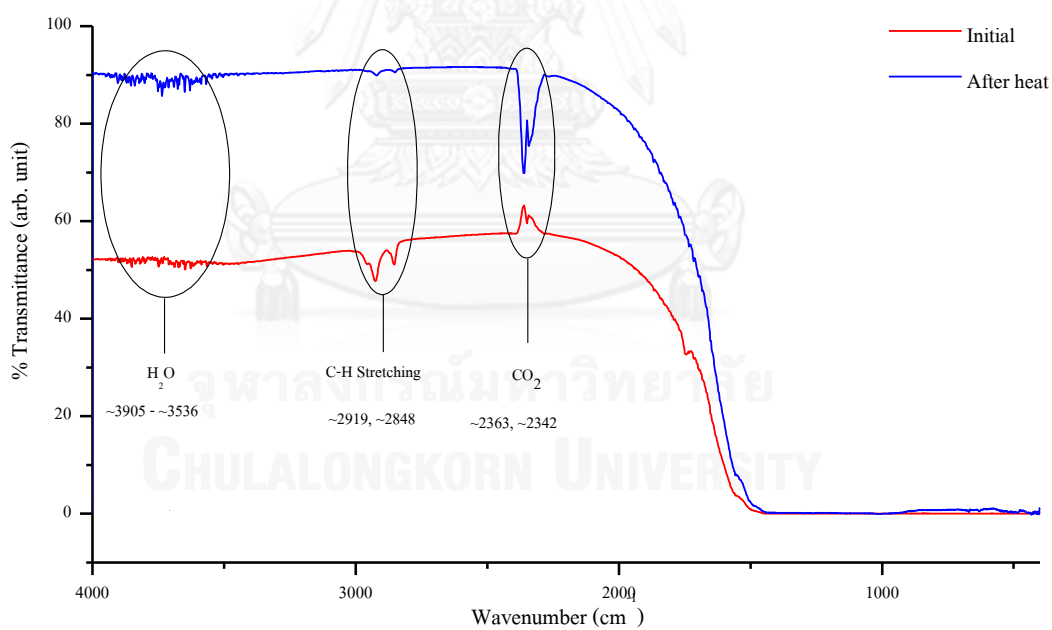
FTIR spectra of sample A7 Initial and after heating



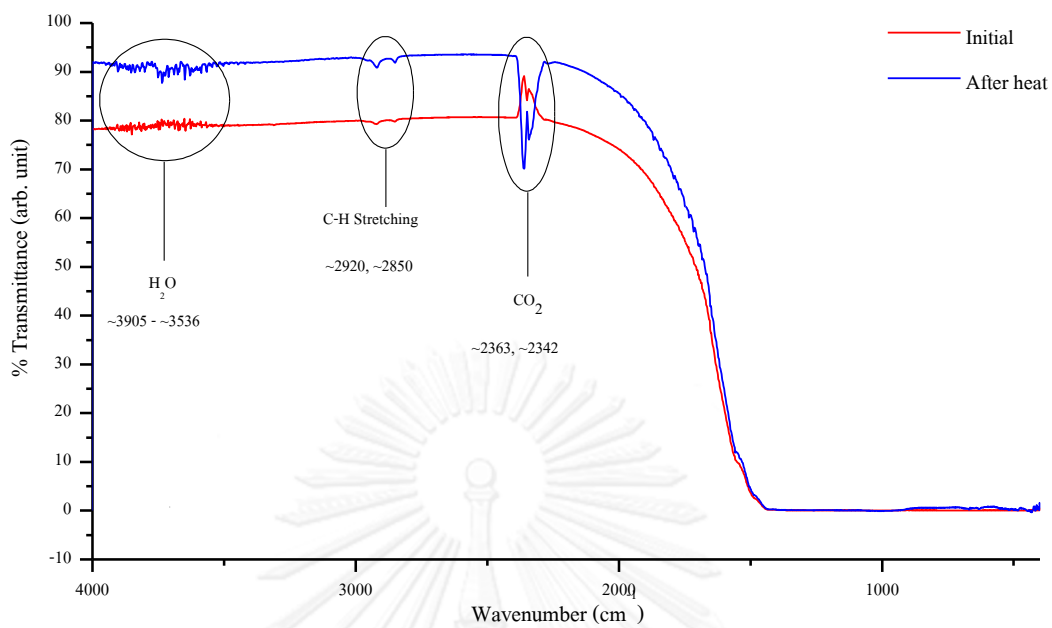
FTIR spectra of sample A8 Initial and after heating



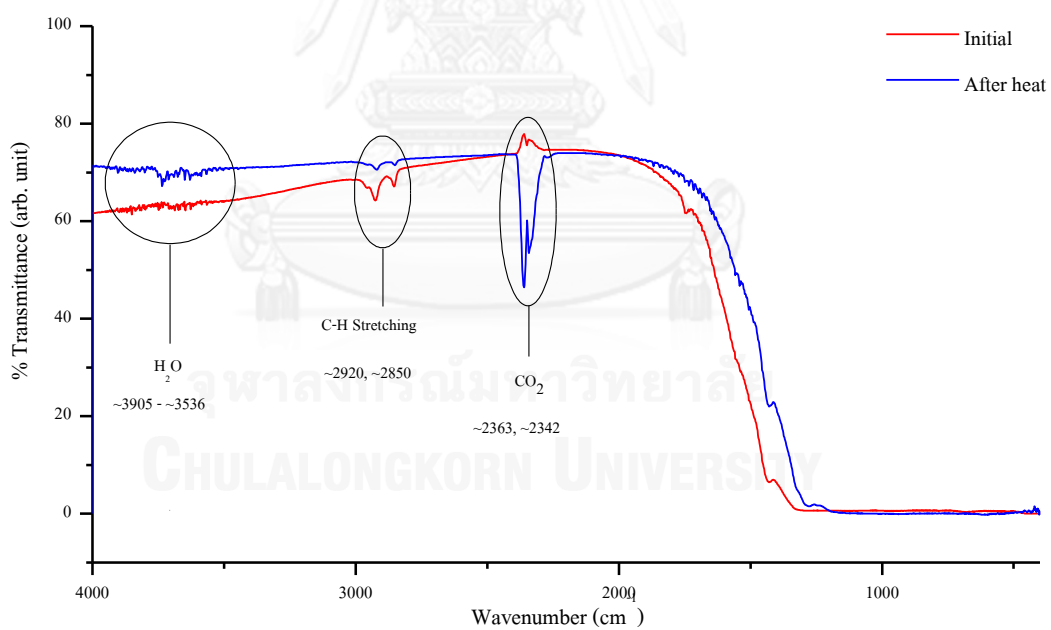
FTIR spectra of sample A9 Initial and after heating



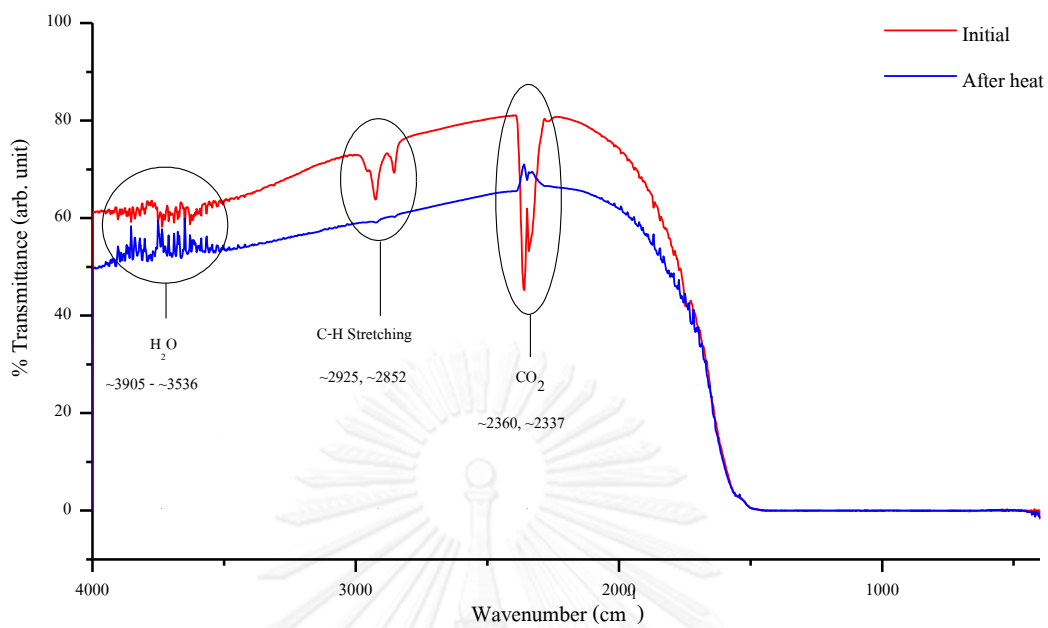
FTIR spectra of sample A10 Initial and after heating



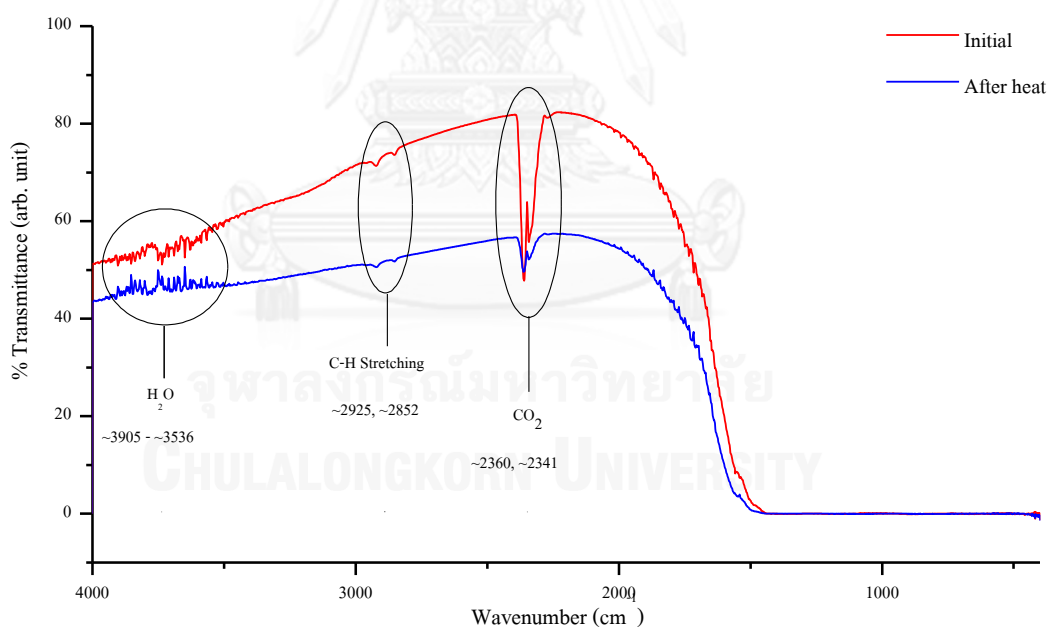
FTIR spectra of sample A11 Initial and after heating



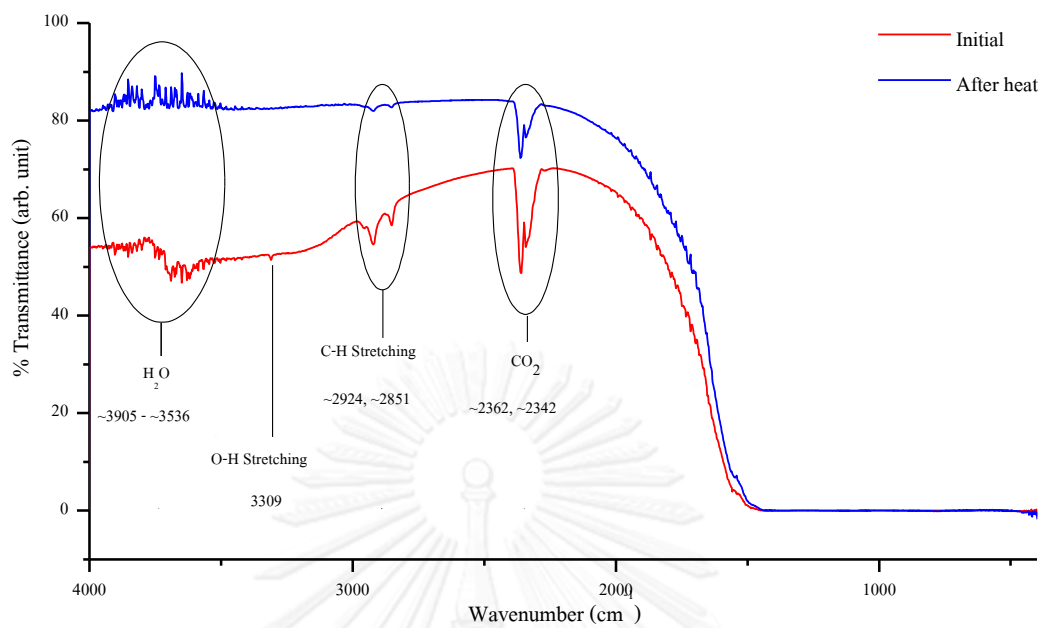
FTIR spectra of sample A12 Initial and after heating



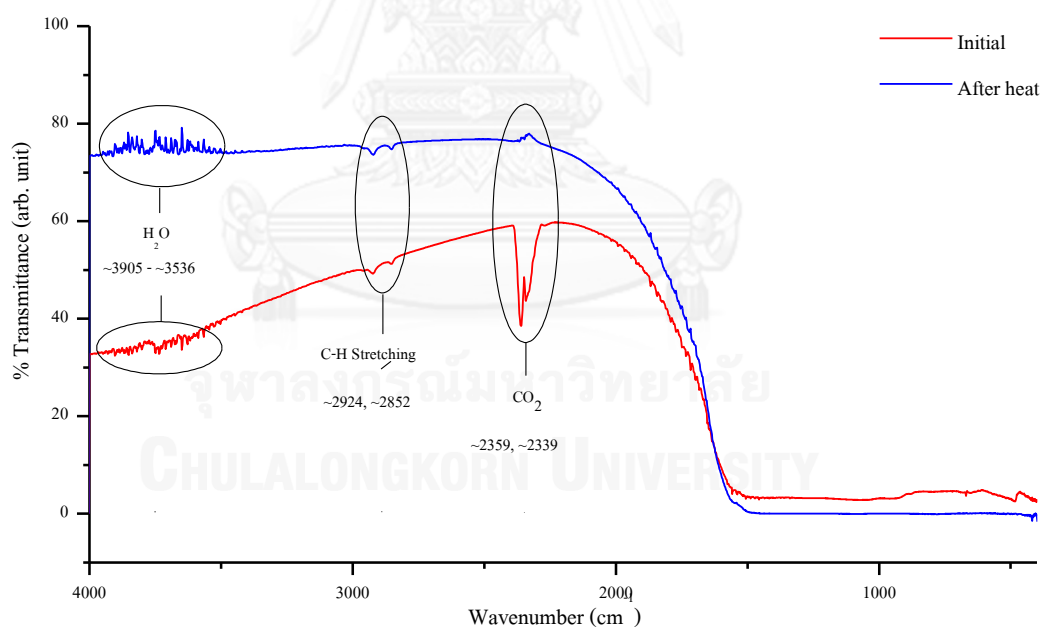
FTIR spectra of sample B1 Initial and after heating



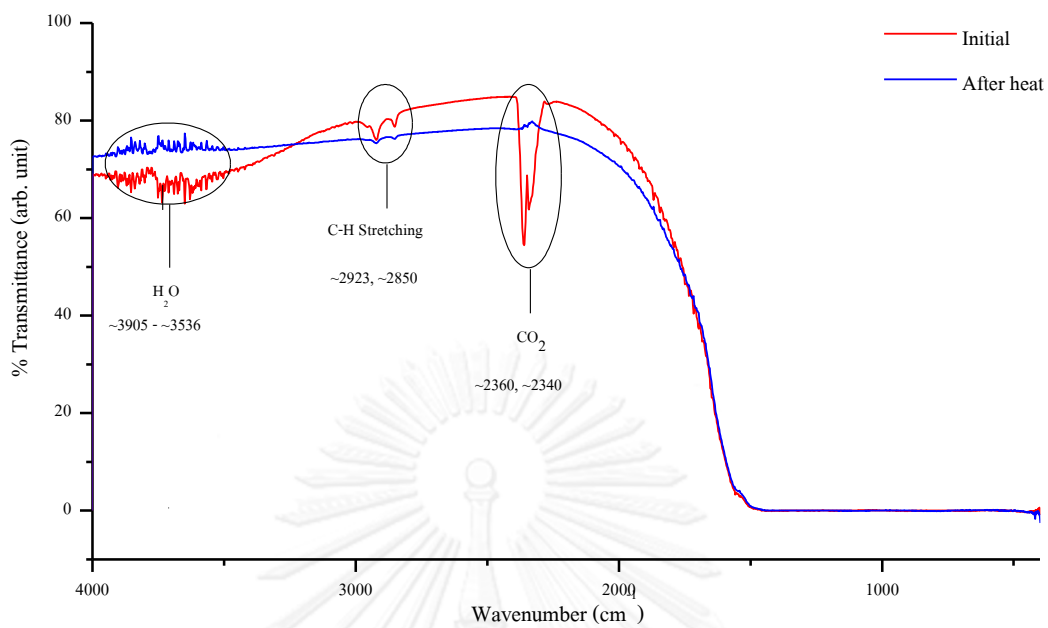
FTIR spectra of sample B2 Initial and after heating



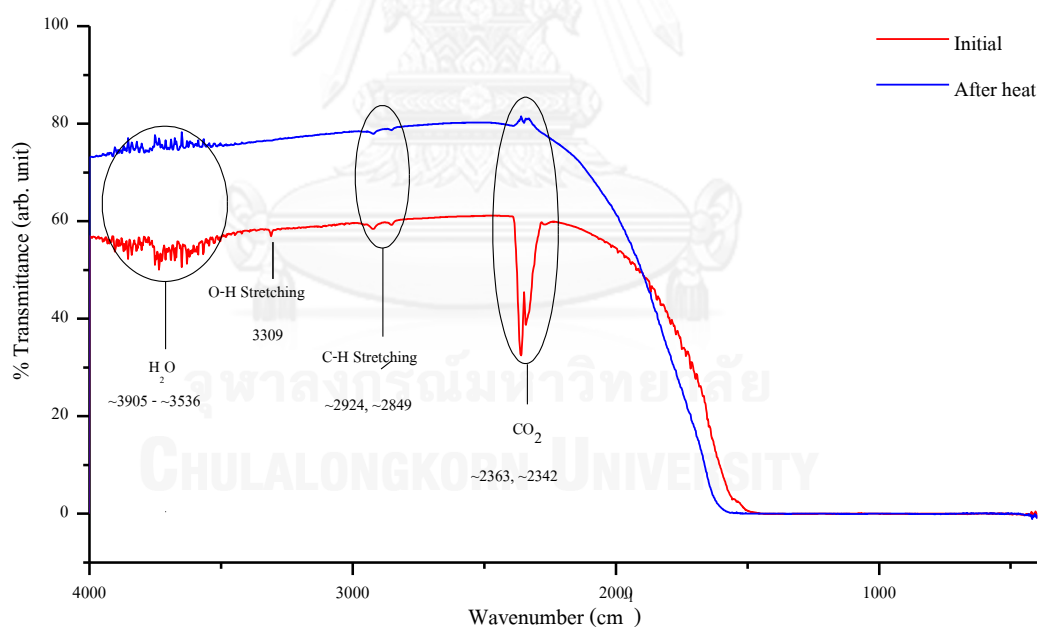
FTIR spectra of sample B3 Initial and after heating



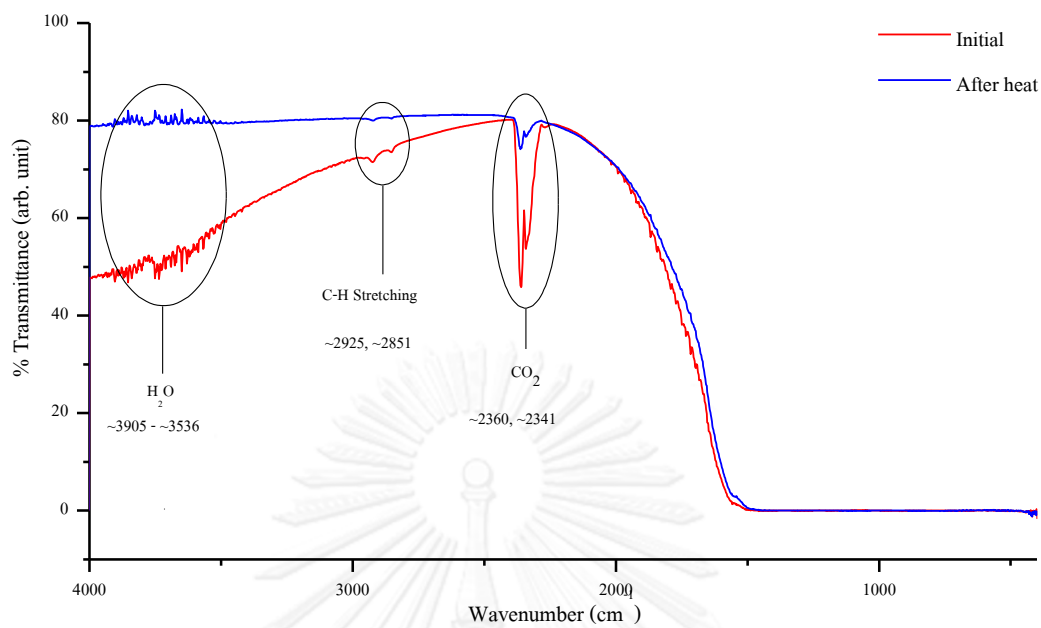
FTIR spectra of sample B4 Initial and after heating



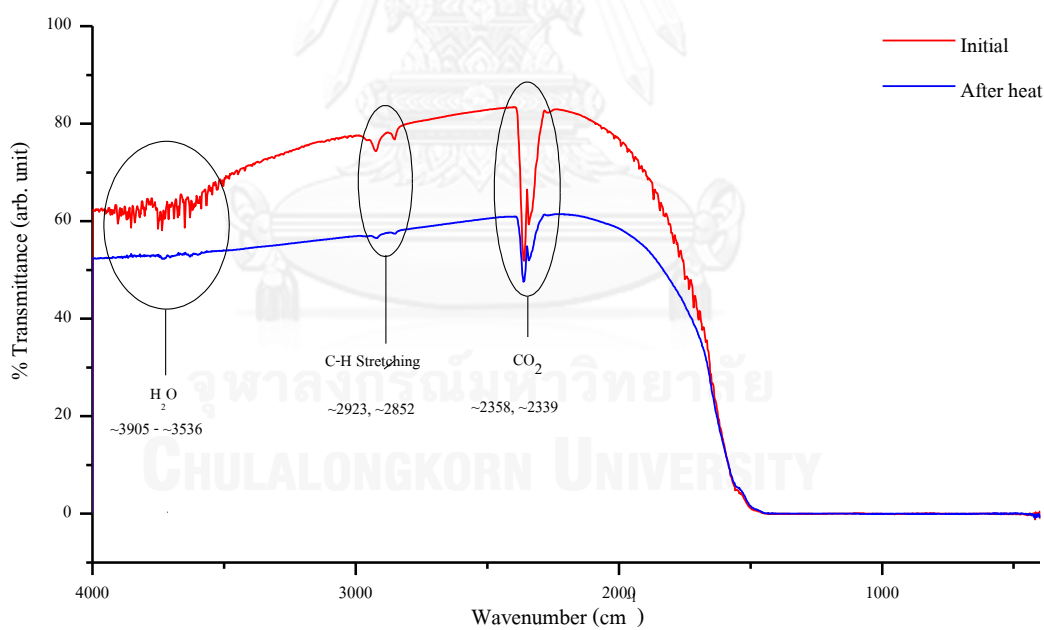
FTIR spectra of sample B5 Initial and after heating



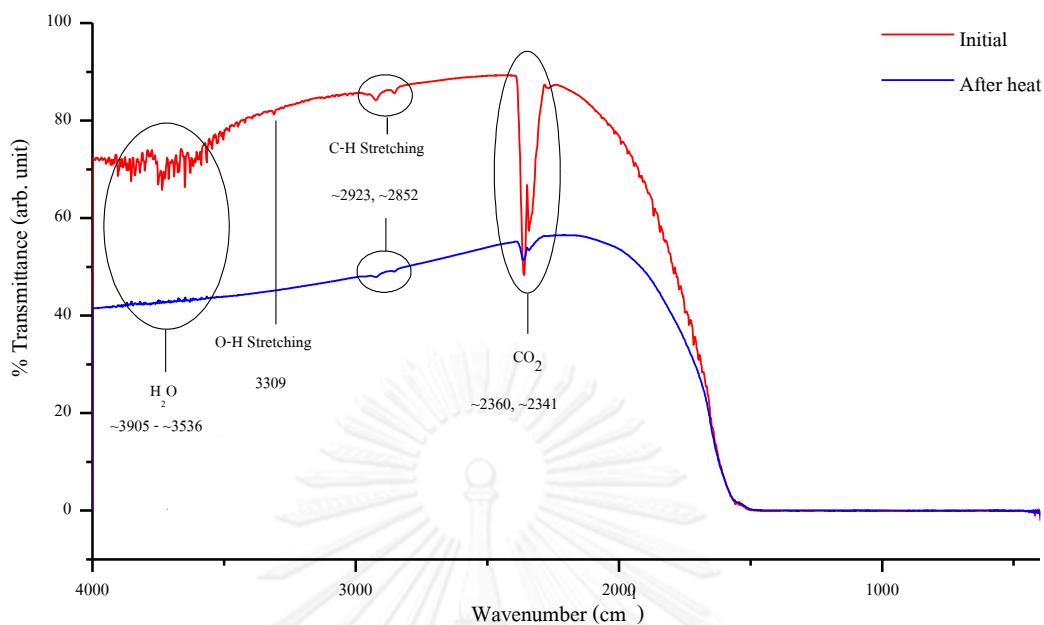
FTIR spectra of sample B6 Initial and after heating



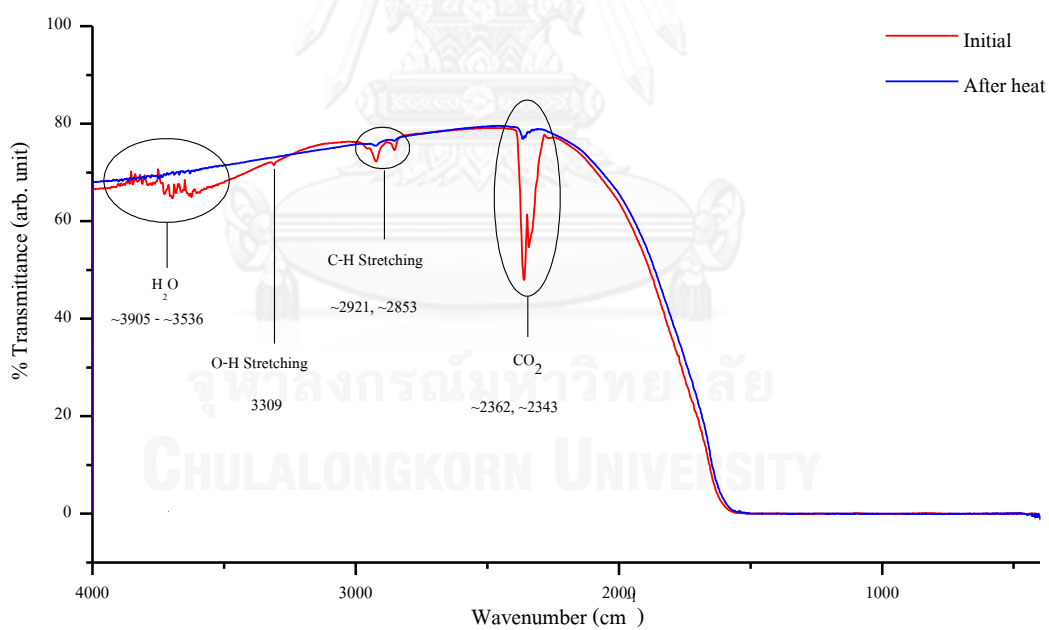
FTIR spectra of sample B7 Initial and after heating



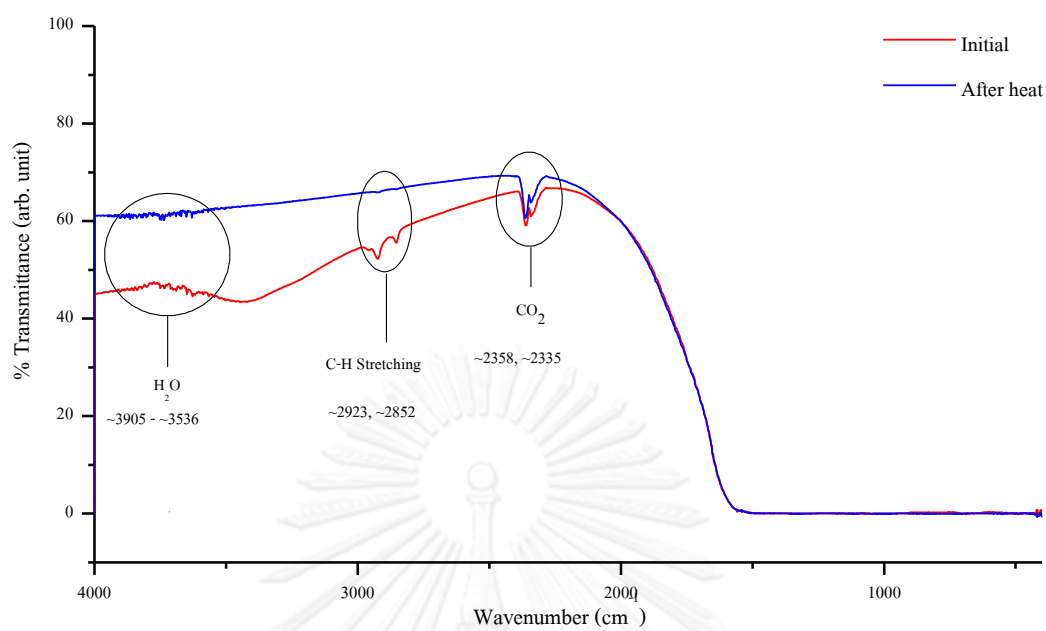
FTIR spectra of sample B8 Initial and after heating



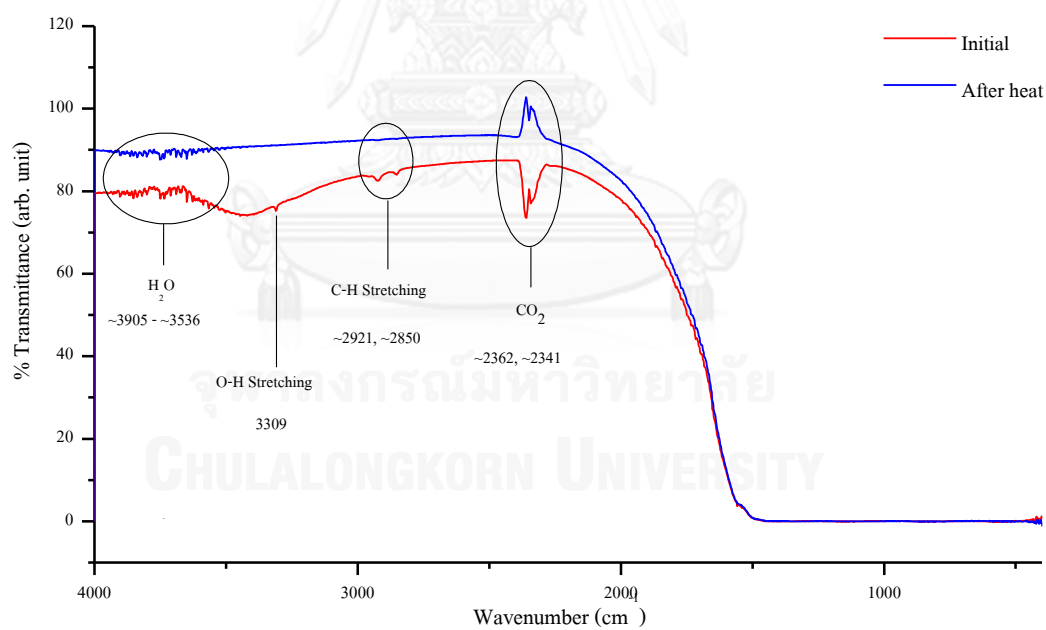
FTIR spectra of sample B9 Initial and after heating



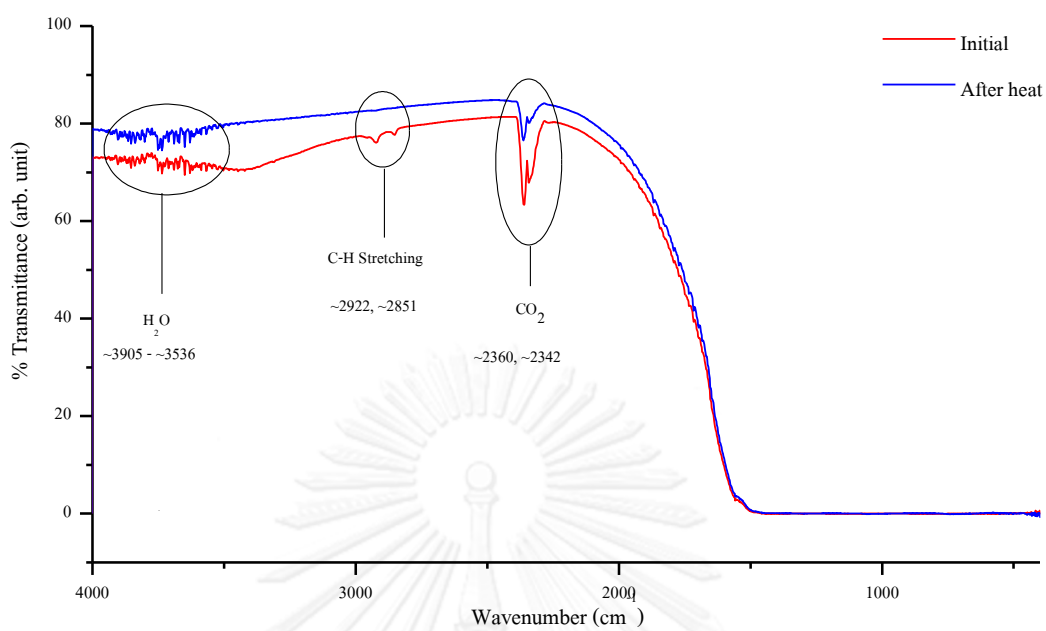
FTIR spectra of sample B10 Initial and after heating



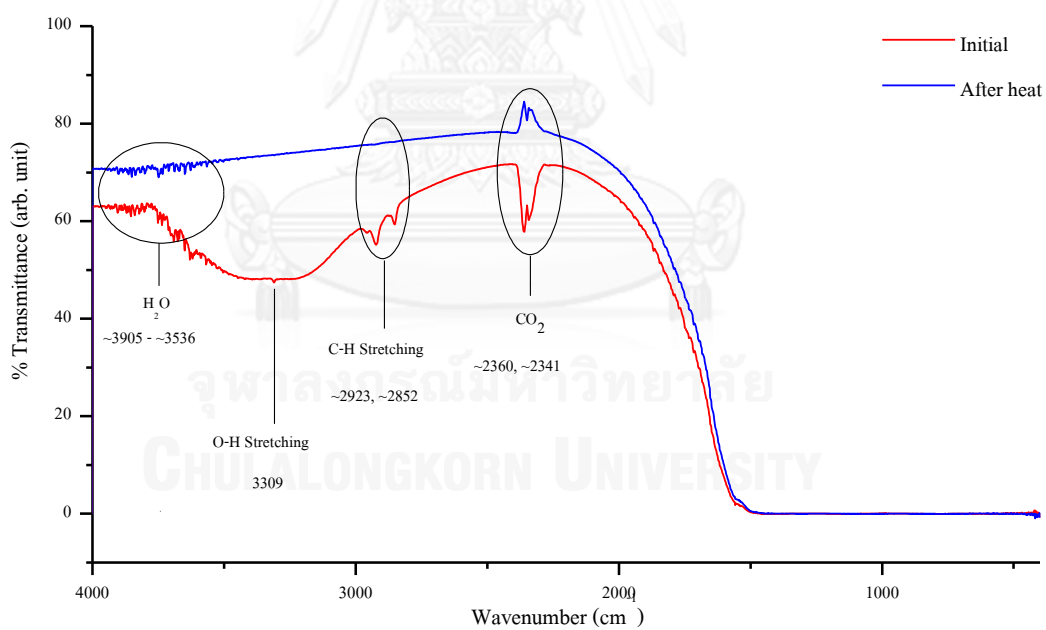
FTIR spectra of sample B11 Initial and after heating



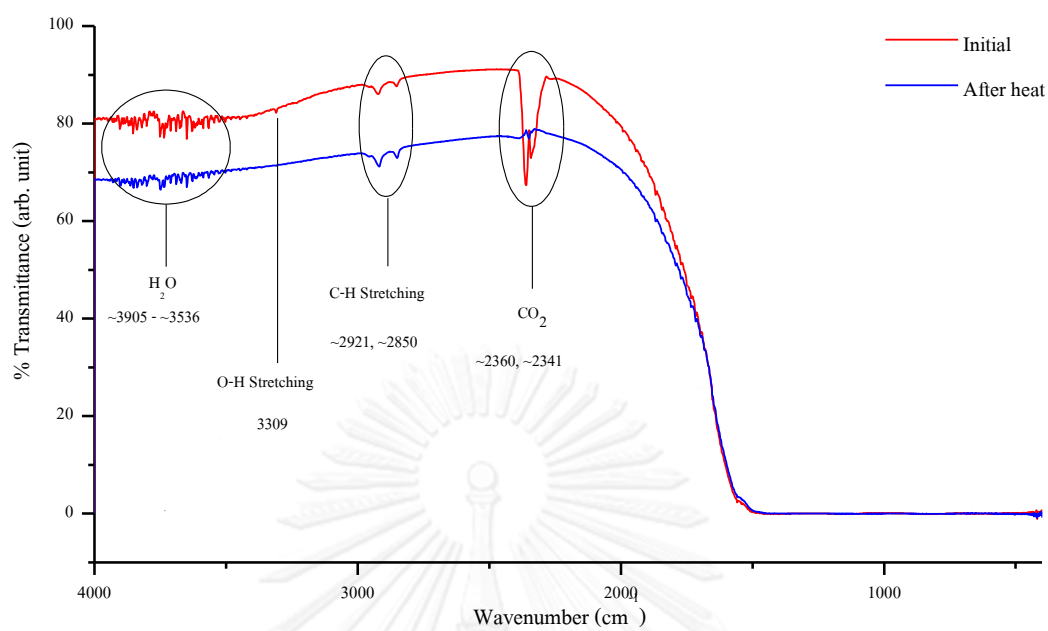
FTIR spectra of sample B12 Initial and after heating



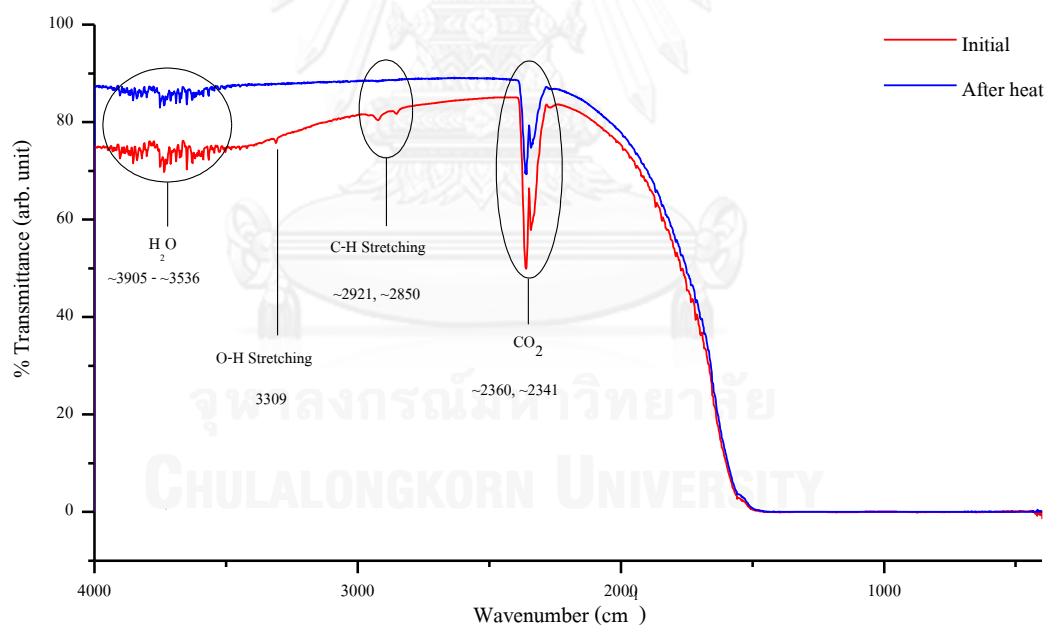
FTIR spectra of sample B13 Initial and after heating



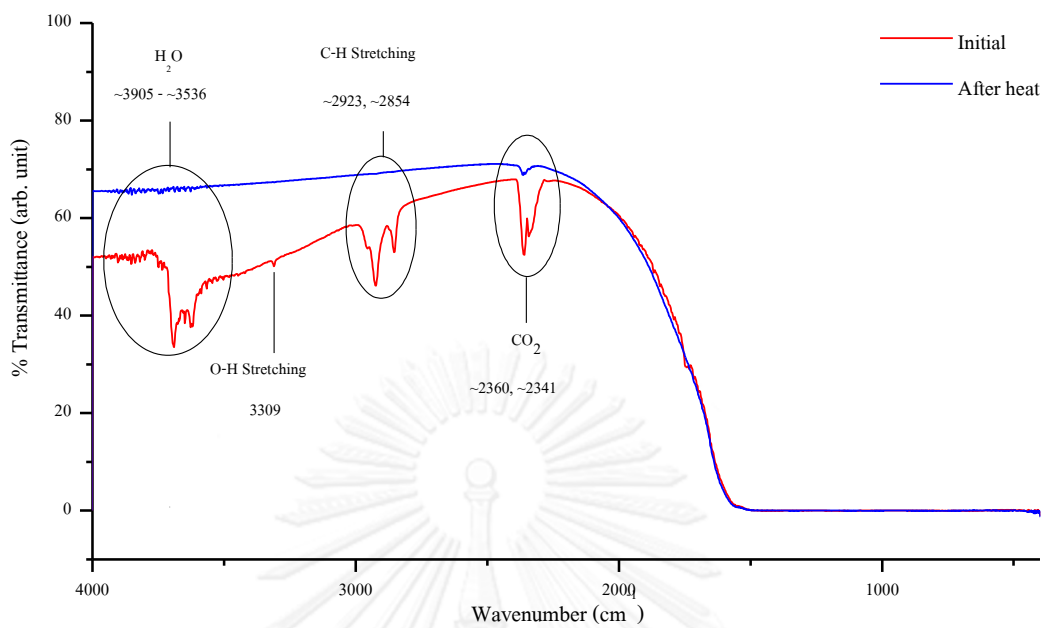
FTIR spectra of sample B14 Initial and after heating



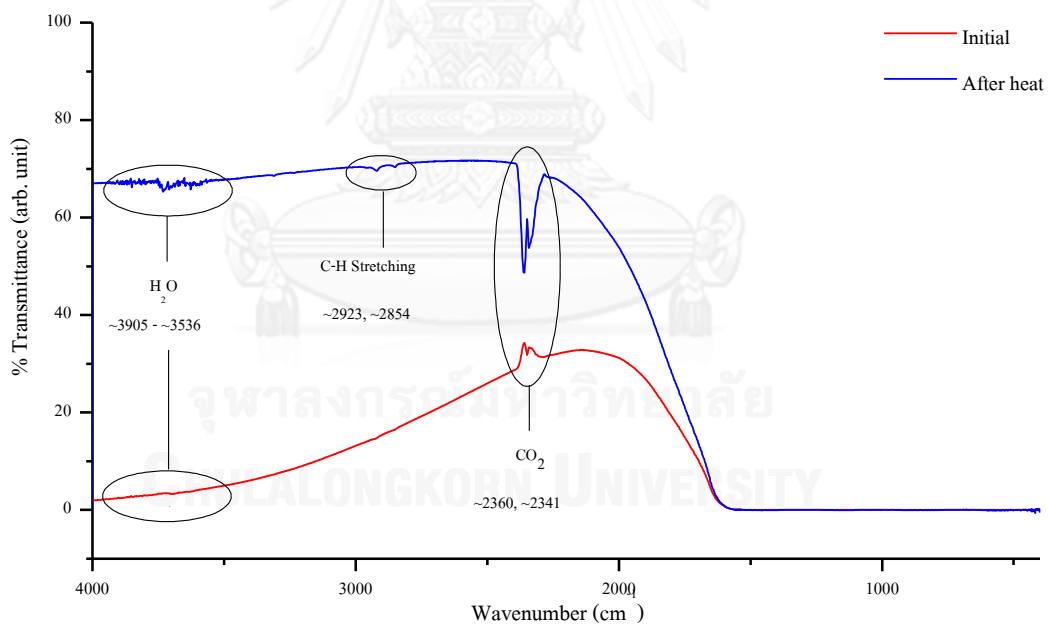
FTIR spectra of sample B15 Initial and after heating



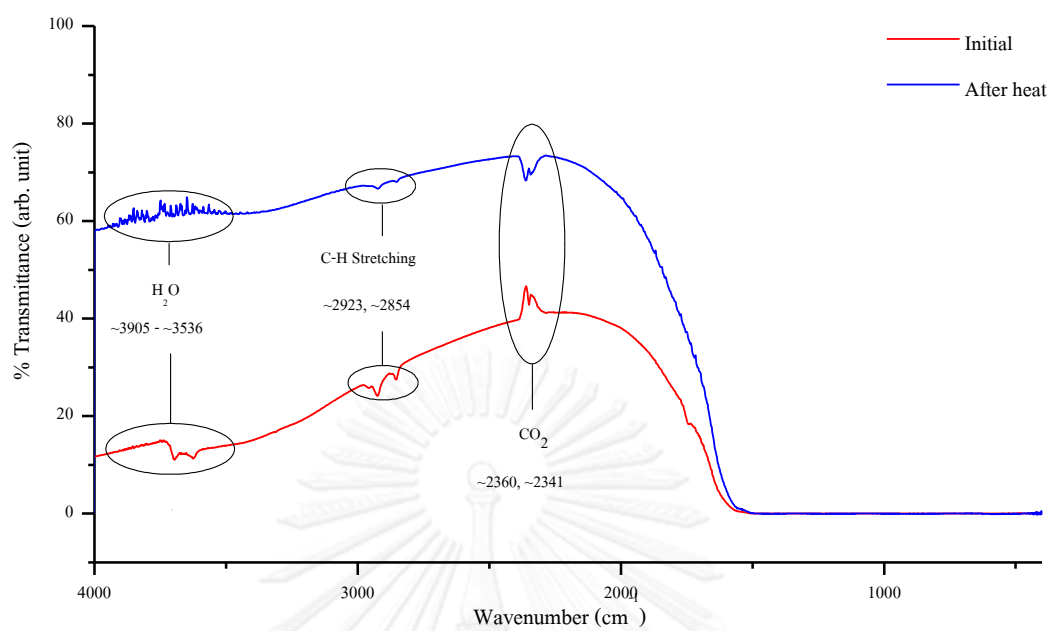
FTIR spectra of sample B16 Initial and after heating



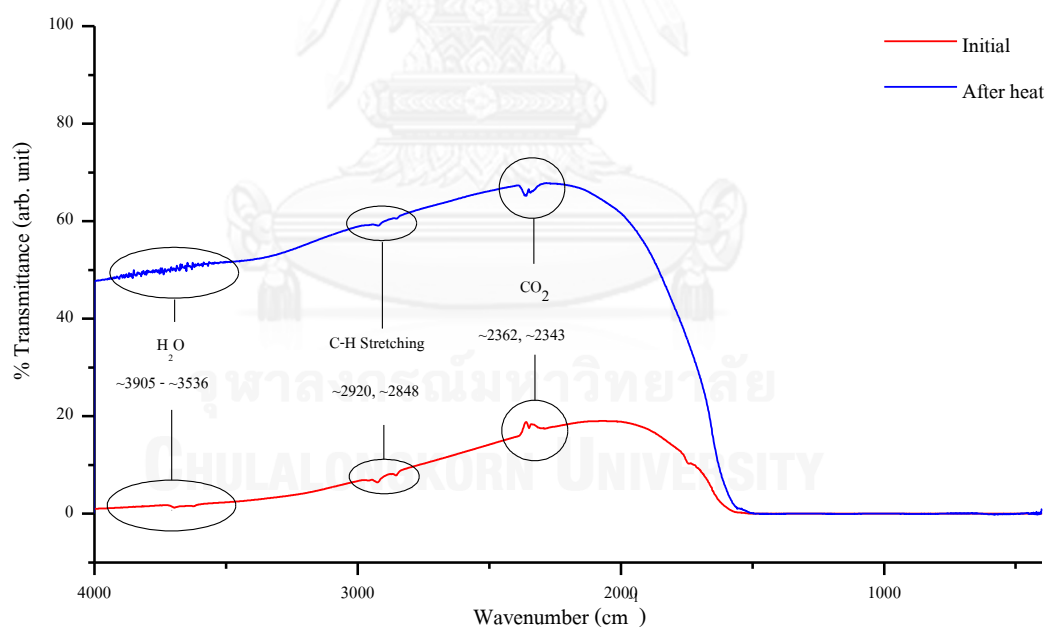
FTIR spectra of sample B17 Initial and after heating



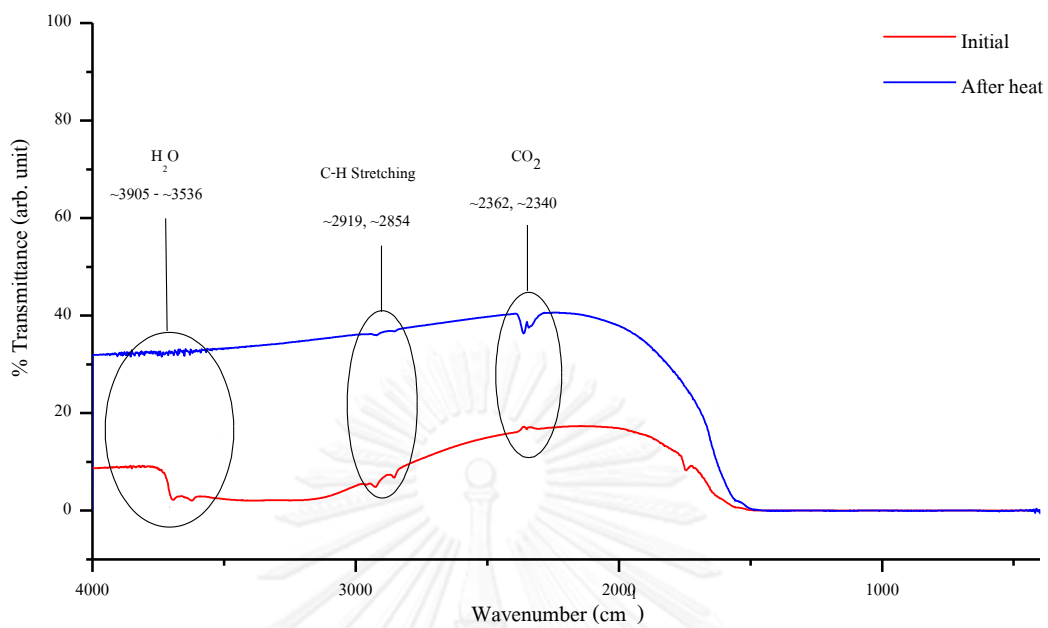
FTIR spectra of sample C1 Initial and after heating



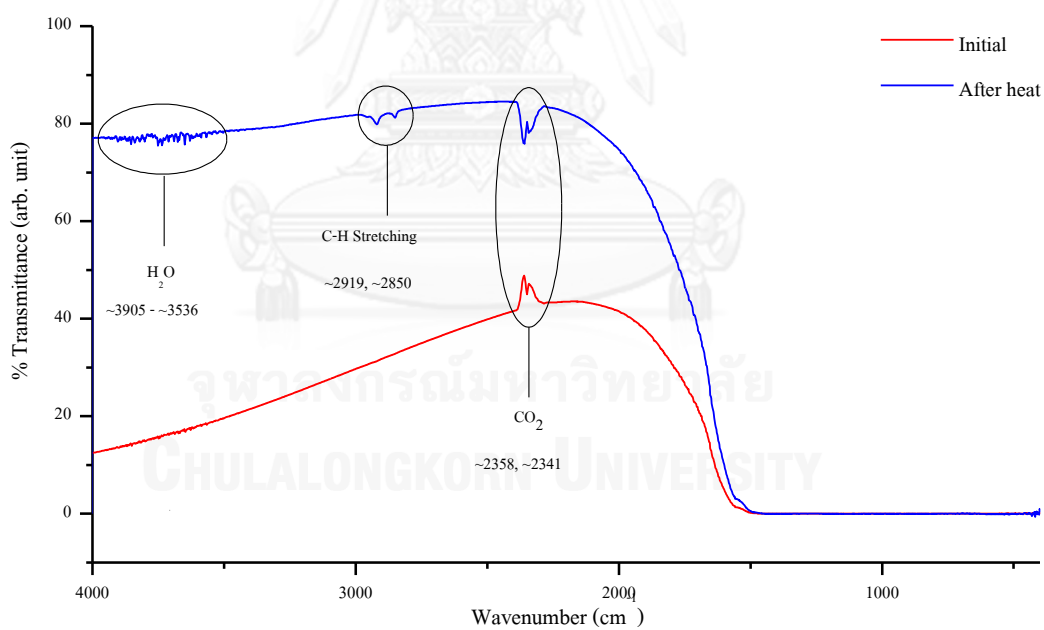
FTIR spectra of sample C2 Initial and after heating



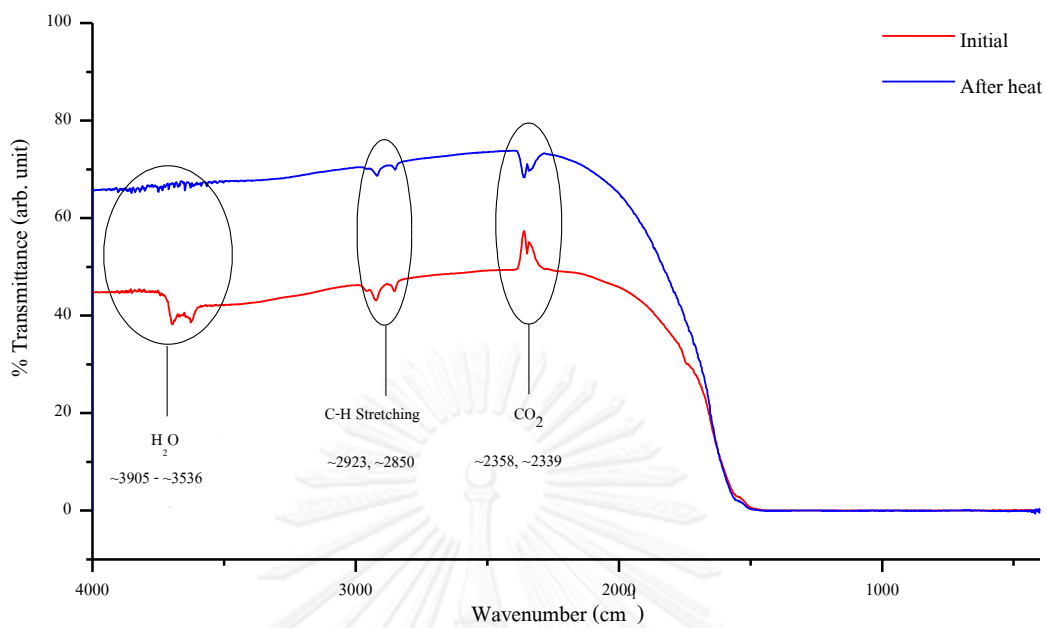
FTIR spectra of sample C3 Initial and after heating



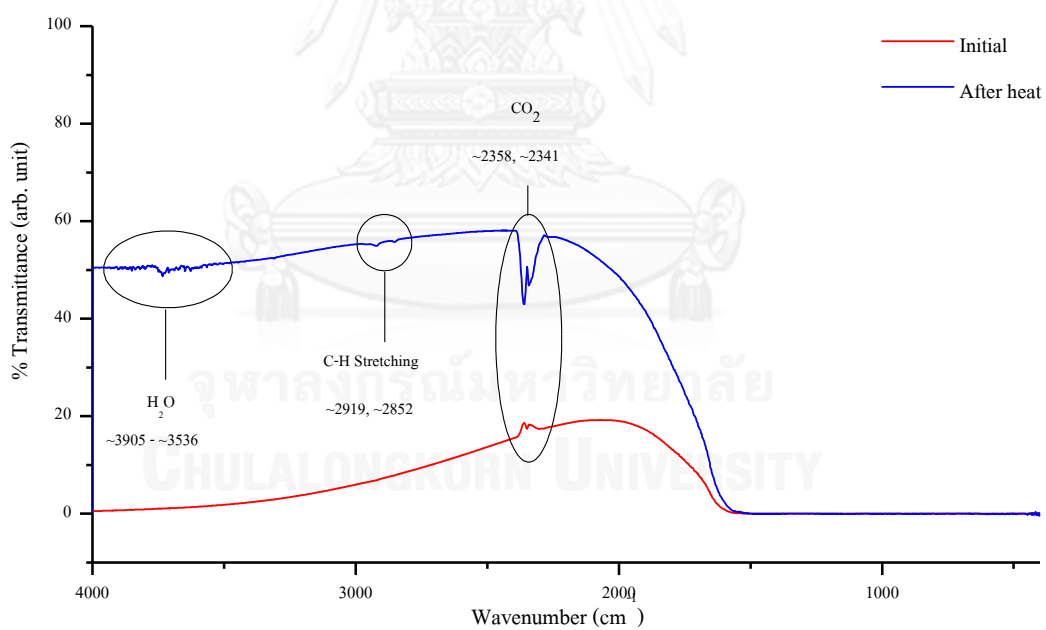
FTIR spectra of sample C4 Initial and after heating



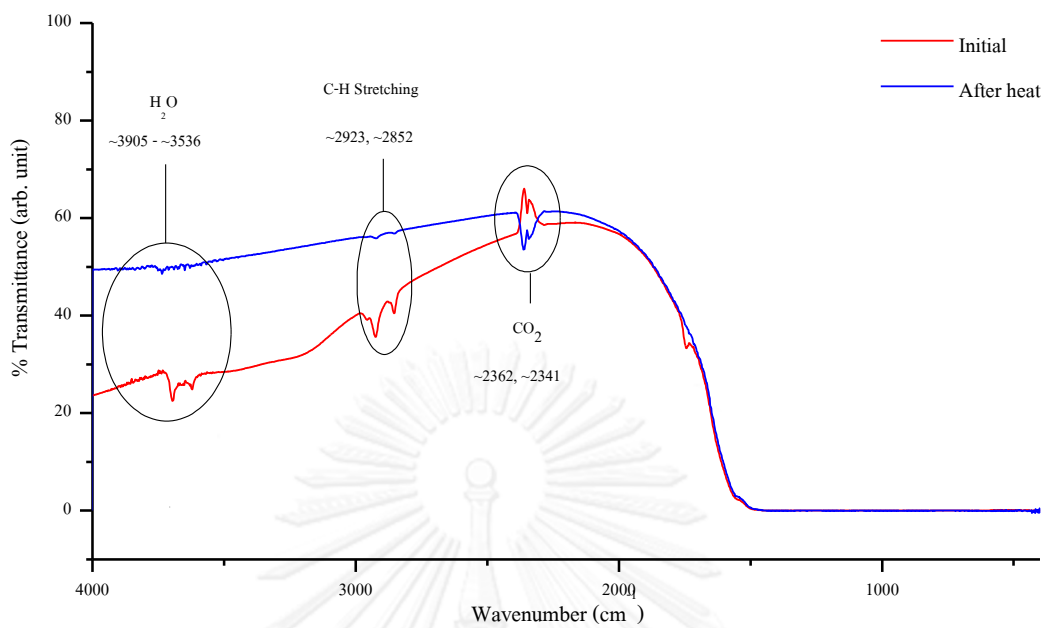
FTIR spectra of sample C5 Initial and after heating



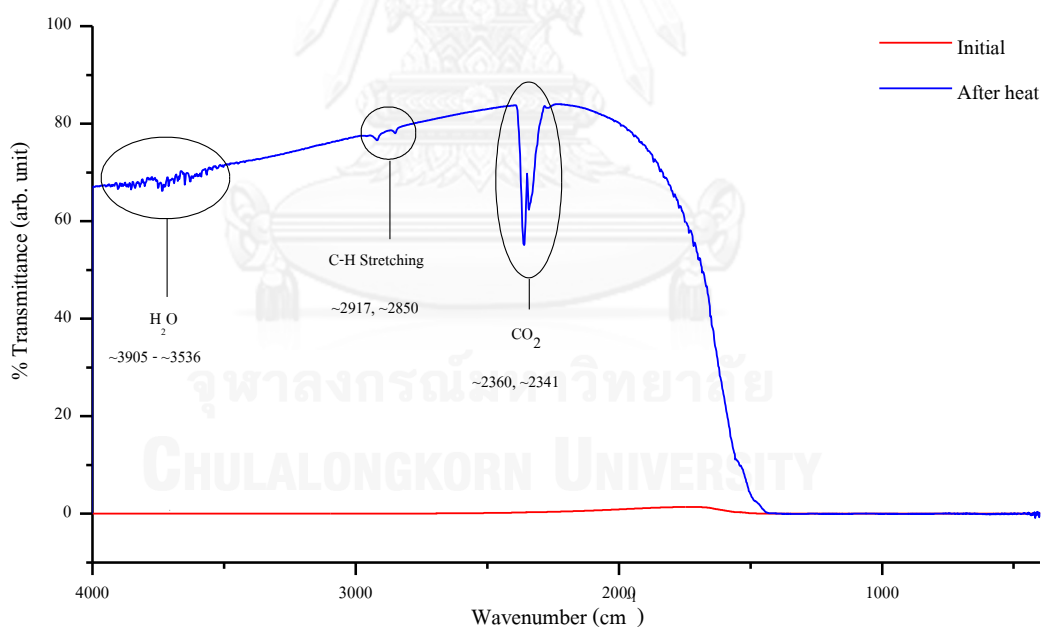
FTIR spectra of sample C6 Initial and after heating



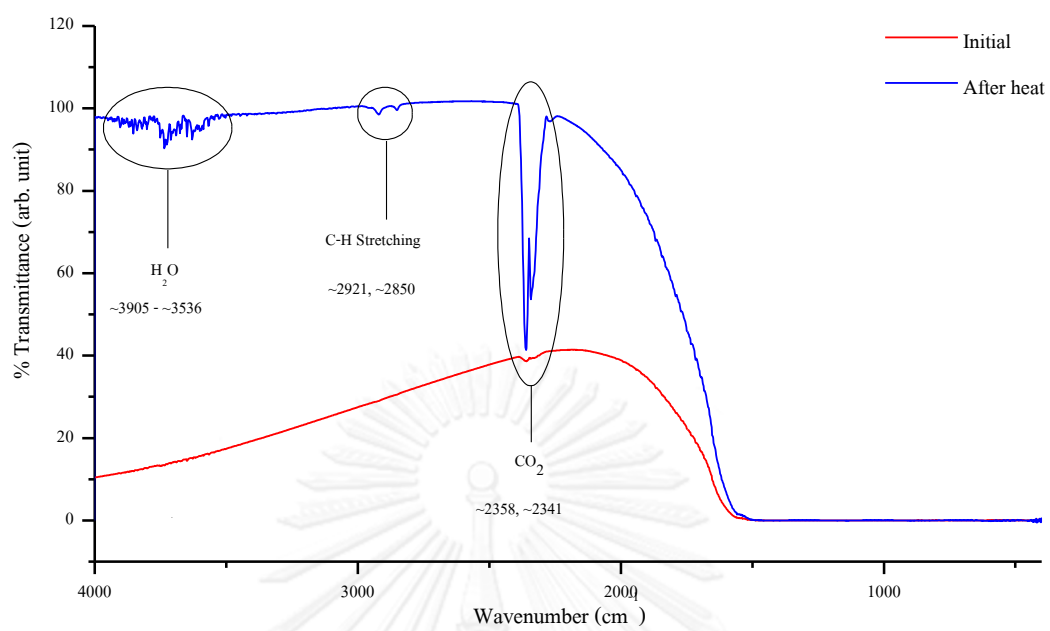
FTIR spectra of sample C7 Initial and after heating



FTIR spectra of sample C8 Initial and after heating



FTIR spectra of sample C9 Initial and after heating



FTIR spectra of sample C10 Initial and after heating

VITA

Mr. Tasnara Sripoonjan was born in June 18, 1989, at Bangkok. He graduated with bachelor degree in major of gemological technology, gems and jewelry from Faculty of Gems, Burapha University in 2010. At the present, he work as gemologist at The Gem and Jewelry Institute of Thailand (Public Organization) and also studies in a Master program in geology at Chulalongkorn University.

